Seismic Evaluation and Retrofit of 230-kV Porcelain Transformer Bushings

Amir S. Gilani
Andrew S. Whittaker
Gregory L. Fenves
University of California, Berkeley

Eric Fujisaki
Pacific Gas & Electric Co.

PEER Report 1999/14
Pacific Earthquake Engineering Research Center
College of Engineering
University of California, Berkeley
December 1999

ABSTRACT

Two identical 230-kV porcelain transformer bushings and two retrofit details were selected for testing and evaluation. The class of the bushing tested was built in the mid-1980s and was known to be vulnerable to earthquake shaking. Resonance-search tests were conducted to determine the dynamic properties of the bushings. Static testing was undertaken to determine the limit states of the bushing and to assess the effectiveness of a retrofit detail. For static testing, the bushing was vertically mounted on a stiff frame and four target displacement orbits were used: unidirectional, unidirectional with offset, bidirectional, and monotonic. During the static tests, oil leaked from the gasket connection, and the porcelain unit immediately above the flange slipped at a displacement of 10 mm. Reduction of the bushing post-tensioning force reduced the uplift displacement at which the bushing leaked oil. The addition of the first retrofit detail (Ring-1) did not prevent the oil leakage or the slip of the porcelain unit. Triaxial earthquake-simulator testing was conducted to evaluate the seismic performance of the bushings mounted on rigid and flexible frames and to evaluate the efficacy of a second retrofit detail (Ring-2). Two sets of spectrum-compatible ground motion records, derived from motions recorded during the 1978 Tabas earthquake in Iran, were used for testing. The fundamental frequency and damping ratio of the bushing were 18 to 20 Hz, and 2 to 3 percent of critical, respectively when mounted on a rigid frame. When subjected to motions compatible with the IEEE 693-1997 spectrum for High Level qualification, there was no structural damage and no oil leakage. The fundamental frequency of the bushing-support system was reduced to approximately 7 Hz when the bushing was installed on a flexible plate. This reduction in frequency substantially increased the response of the bushing. The bushing leaked oil, the porcelain unit immediately above the flange slipped, and the gasket extruded from the porcelain to flange interface when the bushing was subjected to severe shaking. The addition of Ring-2 reduced the slip of the porcelain unit, prevented the extrusion of the gasket, and delayed oil leakage.

ACKNOWLEDGMENTS

The work described in this report was undertaken by the Pacific Earthquake Engineering Research Center (PEER) with funding from the California Energy Commission (CEC), Pacific Gas and Electric (PG&E) Company, Bonneville Power Administration (BPA), Southern California Edison (SCE), and British Columbia Hydro (BC Hydro). This financial support is gratefully acknowledged. The two 230-kV transformer bushings used in the testing program were supplied by BPA.

The authors wish to thank the following individuals for their significant technical contributions to the project: Mr. Ed Matsuda (PG&E), Dr. Anshel Schiff (Precision Measurement Instruments), Dr. Leon Kempner (BPA), Dr. Alan King (BC Hydro), Mr. Jim Kennedy (SCE), and Mr. Lonnie Elder of ABB Power T&D Company, Inc., Components Division (ABB). Thanks are also due to Mr. Don Clyde (PEER), who made significant contributions to the experimental program and Ms. Janine Hannel (PEER), who edited this report. Dr. Schiff designed and installed the two retrofit details described in this report.

This work made use of the Pacific Earthquake Engineering Research Center shared facilities supported by the Earthquake Engineering Research Centers Program of the National Science Foundation under Award Number EEC-9701568.

CONTENTS

Abstract iii

Acknowledgments v

Table of Contents vii

List of Tables xi

List of Figures xiii

1 Introduction 1
- 1.1 Porcelain Transformer Bushings 1
- 1.2 Laboratory Testing of Bushings 2
  - 1.2.1 Introduction 2
  - 1.2.2 Earthquake simulator tests 2
  - 1.2.3 Cantilever tests 2
  - 1.2.4 Static tests 2
- 1.3 Literature Survey 3
  - 1.3.1 Background 3
  - 1.3.2 Laboratory testing of a 500-kV bushing in CERL, 1997 3
  - 1.3.3 Laboratory testing of bushings and transformers by ENEL, 1997-1998 3
  - 1.3.4 Field testing of bushings and transformers, UC Irvine, 1998-1999 4
  - 1.3.5 Laboratory testing of bushings, UC Berkeley, 1997-1999 4
- 1.4 Objectives of the Current Study 5
- 1.5 Report Organization 5

2 Selection Criteria and Properties of Test Bushings 11
- 2.1 Introduction 11
- 2.2 Selection of Candidate Bushing 11
- 2.3 230-kV Type-U Bushing Manufactured by GE 12
- 2.4 Limit States for 230-kV Bushings 15
  - 2.4.1 Background 15
  - 2.4.2 Oil leakage 15
  - 2.4.3 Porcelain slip 16
  - 2.4.4 Gasket extrusion 16
  - 2.4.5 Porcelain fracture 16
- 2.5 Components of Deformation for 230-kV Bushings 16
  - 2.5.1 Introduction 16

3 Qualification and Fragility Testing 23
- 3.1 Introduction 23
- 3.2 IEEE 693-1997 Requirements for Bushing Qualification 23
  - 3.2.1 Resonant-search tests 23
  - 3.2.2 Earthquake test response spectrum 24
  - 3.2.3 Earthquake ground motions 25

4 Fragility Testing of Rigidly Mounted Bushings 39
- 4.1 Introduction 39
- 4.2 Test Setup 39
  - 4.2.1 Overview 39

4.2.2 Earthquake simulator 39
4.2.3 Rigid mounting frame 40
4.2.4 Earthquake ground motions 40
4.2.4.1 Resonant-search tests 40
4.2.4.2 Earthquake test response spectrum 40
4.2.5 Instrumentation 41
4.3 Summary of Experimental Data 41
4.3.1 Overview 41
4.3.2 Dynamic properties of rigidly mounted 230-kV bushings 46
4.3.3 Earthquake testing of Bushing-1 and Bushing-2 46
4.3.3.1 Introduction 46
4.3.3.2 Peak responses 47
4.3.3.3 Response of Bushing-1 47
4.3.3.4 Response of Bushing-2 49
4.3.3.5 Evaluation of seismic response of bushings 50
4.3.4 Response of Bushing-2 to harmonic excitations 50
4.3.4.1 Overview 50
4.3.4.2 Summary of bushing response 51
4.3.4.3 Peak responses 51
4.3.4.4 Response of the simulator platform 52
4.3.4.5 Response of the bushing 53

5 Bushing Retrofit Details 79
5.1 Introduction 79
5.2 Selection of a Candidate Retrofit Detail 79
5.3 Retrofit Rings 80
5.3.1 Introduction 80
5.3.2 Epoxy filler material 80
5.3.2.1 Geometry of Ring-1 81
5.3.3 Retrofit Ring-2 81

6 Static Cyclic Testing of Rigidly Mounted Bushing-1 85
6.1 Overview 85
6.2 Experimental Setup 85
6.2.1 Mounting frame 85
6.2.2 Post-tensioning mechanism 85
6.2.3 Loading collar and joint collar 86
6.2.4 Loading mechanism and test control 86
6.2.5 Instrumentation 86
6.3 Test Protocol 88
6.3.1 Pull-back, quick-release tests 88
6.3.2 Static tests 88
6.4 Experimental Results from Quick-Release Tests 89
6.5 Experimental Results from Static Tests of Bushing-1 without Ring-1 90
6.5.1 Unidirectional tests 90
6.5.2 Unidirectional tests with offset 92
6.5.3 Bidirectional tests 92
6.6 Experimental Results from Static Tests of Bushing-1 with Ring-1 93
6.6.1 Background 93
6.6.2 Unidirectional tests 93
6.6.3 Bidirectional tests 93
6.6.4 Monotonic test 93

6.7 Evaluation of Response of Bushing-1 94
6.7.1 Introduction 94
6.7.2 Modification of recorded data 94
6.7.3 Displacement response of Bushing-1 95
6.7.4 Slip properties of the gasket at the gasket connection 95
6.7.5 Efficacy of Ring-1 96
6.8 Summary 96

7 Fragility Testing of Flexibly Mounted Bushing-2 117
7.1 Overview 117
7.2 Attachment of 230-kV Bushings to Transformers 117
7.3 Test Setup 118
7.3.1 Mounting setup 118
7.3.2 Simulator input motions 118
7.3.2.1 Resonant-search tests 118
7.3.2.2 Earthquake test response spectrum 119
7.3.3 Instrumentation 119
7.3.4 Preparation of Bushing-2 120
7.4 Summary of Experimental Data from Pull-Back, Quick-Release Tests 120
7.4.1 Introduction 120
7.4.2 Test setup 123
7.4.3 Evaluation of the dynamic properties 123
7.4.4 Summary of experimental results 123
7.5 Experimental Results from Seismic Tests 125
7.5.1 Introduction 125
7.5.2 Summary of experimental data 125
7.5.3 Dynamic properties of Bushing-2 mounted on the flexible plate 125
7.5.4 Response of the rigid mounting frame and the flexible plate 128
7.5.5 Response of Bushing-2 without Ring-2 128
7.5.5.1 Peak response 128
7.5.5.2 Bushing response 129
7.5.5.3 Post-test tear-down of Bushing-2 131
7.5.6 Response of Bushing-2 retrofitted with Ring-2 132
7.5.6.1 Peak response 132
7.5.6.2 Bushing response 132
7.5.6.3 Post-test tear-down of Bushing-2 134
7.6 Effect of Support Flexibility and Ring-2 on the Response of Bushing-2 135
7.6.1 Influence of support flexibility 135
7.6.2 Efficacy of Ring-2 136

8 Summary and Conclusions 163
8.1 Summary 163
8.1.1 Overview 163
8.1.2 Test bushings 164
8.1.3 Experimental program 165
8.1.3.1 Introduction 165
8.1.3.2 Mounting frames 165
8.1.3.3 Test program 166
8.1.3.4 Development of ground motions for triaxial earthquake testing 166
8.1.4 Retrofit details 166
8.1.5 Summary of experimental results 167
8.1.5.1 Introduction 167

8.1.5.2 Experimental results from resonant-search tests 167
8.1.5.3 Experimental results from rigidly mounted bushings 167
8.1.5.4 Experimental results from static tests of Bushing-1 169
8.1.5.5 Experimental results from flexibly mounted Bushing-2 169
8.2 Conclusions 171
8.2.1 Seismic response of 230-kV transformer bushings 171
8.2.2 Effect of support flexibility 171
8.2.3 Effect of post-tensioning force 171
8.2.4 Efficacy of retrofit design 172
8.3 Recommendations for future study 172
8.3.1 Procedures for seismic qualification and fragility testing 172
8.3.2 Development of fragility curves for substation equipment 172
8.3.3 Interconnected equipment 173
8.3.4 Behavioral studies of porcelain transformer bushings 173
8.3.5 Mathematical modeling of porcelain transformer bushings 173

References 175

Appendix A IEEE Practice for Earthquake Testing of Transformer Bushings 177
A.1 Introduction 177
A.2 Performance Level and Performance Factor 178
A.3 Performance Level Qualification 178
A.4 Support Frame and Mounting Configuration 179
A.5 Testing Procedures for Transformer Bushings 179
A.5.1 Resonant search tests 179
A.5.2 Earthquake ground motion tests 179
A.6 Instrumentation of Transformer Bushings 180
A.7 Acceptance Criteria for Transformer Bushings 180

LIST OF TABLES

Chapter 2
Characteristics of the GE type-U test bushings 14
Material properties of the bushing components 15

Chapter 3
IEEE earthquake-history testing requirements for Moderate Level qualification 25
High-pass filter frequencies for earthquake histories 27

Chapter 4
Instrumentation for rigidly mounted 230-kV bushings 42
Summary of earthquake testing of Bushing-1 44
Summary of earthquake testing of Bushing-2 45
Modal properties of bushings from resonance-search tests 46
Peak responses of the bushings 48
Peak responses of Bushing-2 to the high-amplitude 5-Hz harmonic tests 51

Chapter 6
Instrumentation for static tests of Bushing-1 87
Protocol for quick-release testing of Bushing-1 88
Protocol for static testing of Bushing-1 90
Modal properties obtained from frequency tests 91

Chapter 7
Instrumentation of Bushing-2 mounted on the flexible plate 121
Modal properties of Bushing-2 along the x-axis 124
Modal properties of Bushing-2 along the y-axis 124
Modal properties of Bushing-2 along the x- axis 124
Summary of earthquake testing of flexibly mounted Bushing-2 without Ring-2 126
Summary of earthquake testing of flexibly mounted Bushing-2 with Ring-2 127
Modal properties of Bushing-2 from resonance-search tests 128
Peak acceleration response of the simulator platform and the mounting frames 129
Peak responses of the Bushing-2 without Ring-2 130
Peak responses of the Bushing-2 retrofitted with Ring-2 133
Response of the UPPER-1 porcelain unit 136

Chapter 8
Characteristics of the 230-kV type-U bushings manufactured by GE 165
Modal properties of 230 kV bushings1 168
Response of flexibly mounted Bushing-2 at the gasket connection 170

LIST OF FIGURES

Chapter 1
Bushing mounted on an oil-filled transformer 7
Cross section of a typical bushing 7
Fracture of an UPPER-1 porcelain unit from severe earthquake shaking 8
Seismic testing of a 500-kV bushing (Courtesy of CERL, Ill) 8
Laboratory testing of a bushing (Courtesy of ENEL and ISMES, Italy) 9
Field testing of a bushing (Courtesy of University of California, Irvine) 9
Laboratory testing of a 550-kV bushing 10

Chapter 2
Typical porcelain-flange interface details for the gasket connection 18
Slip of porcelain in a transformer-mounted 230-kV bushing 19
Bushing-2 prior to testing on the Berkeley simulator 19
Longitudinal section and cross section through a 230-kV type-U bushing, manufactured by General Electric 20
Exploded view of gasket connection detail for a 230-kV type-U bushing 21
Compression stiffness of 6-mm thick nitrile gaskets (Elder, 1999) 21
Deformation modes for components of a 230-kV bushing 22

Chapter 3
Spectra for the Moderate Seismic Performance Level (IEEE, 1998) 28
Test Response Spectra at bushing flange for Moderate PL 28
Normalized acceleration history, power spectrum, and response spectra for the longitudinal (*X*-) component of the original Tabas record 29
Normalized acceleration history, power spectrum, and response spectra for the lateral (*Y*-) component of the Tabas record 30
Normalized acceleration history, power spectrum, and response spectra for the vertical (*Z*-) component of the original Tabas record 31
Acceleration history, power spectrum, and response spectra for the longitudinal (*X*-) component of the Tabas-A record 32
Acceleration history, power spectrum, and response spectra for the lateral (*Y*-) component of the Tabas-A record 33
Acceleration history, power spectrum, and response spectra for the vertical (*Z*-) component of the Tabas-A record 34
Acceleration history, power spectrum, and response spectra for the longitudinal (*X*-) component of the Tabas-B record 35
Acceleration history, power spectrum, and response spectra for the lateral (*Y*-) component of the Tabas-B record 36
Acceleration history, power spectrum, and response spectra for the vertical (*Z*-) component of the Tabas-B record 37

Chapter 4
A rigidly mounted 230-kV bushing on the earthquake simulator 55
IEEE 693-1997 test response spectrum for High Level Qualification 55
Instrumentation for 230-kV bushings 56
Instrumentation at top of Bushing-1 57
Instrumentation of the UPPER-1 porcelain unit 57
Terminal attached to the top of Bushing-2 58

Bushing-2 after Test No 38 showing oil leakage and slip of porcelain 58
Transfer function amplitudes between the top of Bushing-1 and frame 59
Transfer function amplitudes between the top of Bushing-2 and frame 60
Response spectra for Bushing-1; Test No 12, target PGA=1.0g 61
Response spectra for Bushing-1; Test No 17, target PGA=2.0g 62
Vertical displacement versus rocking for Bushing-1; Test No 17, target PGA=2.0g 63
Orbit of motion for Bushing-1; Test No 17, target PGA=2.0g 64
Response spectra for Bushing-2; Test No 19, target PGA=1.0g 65
Response spectra for Bushing-2; Test No 24, target PGA=2.0g 66
Vertical displacement versus rocking for Bushing-2; Test No 24, target PGA=2.0g 67
Orbit of motion for Bushing-1; Test No 24, target PGA=2.0g 68
Simulator x- direction input for the high-amplitude 5-Hz harmonic tests, Test No 37 69
Response spectrum for high-amplitude harmonic tests 70
Acceleration response of Bushing-2 without terminal, Test No 38 71
Acceleration response of Bushing-2 with terminal, Test No 37 72
Displacement history of Bushing-2 relative to support frame, Test No 38 73
Displacement history of Bushing-2 relative to support frame, Test No 37 74
Vertical displacement of the UPPER-1 porcelain unit, Test No 38 75
Vertical displacement of the UPPER-1 porcelain unit, Test No 37 76
Stress history of the UPPER-1 porcelain unit, Test No 38 77
Stress history of the UPPER-1 porcelain unit, Test No 37 78

Chapter 5

Geometry of Ring-1 82
Geometry of Ring-2 83
Ring-1 placed around the gasket connection of Bushing-1 84
Ring-2 prior to installation around the gasket connection of Bushing-2 84

Chapter 6

Bushing-1 and the mounting frame 98
Post-tensioning setup for Bushing-1 98
Joint collar for Bushing-1 99
Bushing-1 prior to cyclic testing 99
Instrumentation for static tests of Bushing-1 100
Instrumentation at the top of Bushing-1 100
Instrumentation of the UPPER-1 porcelain unit 101
Test setup for pull-back, quick-release test 101
Displacement orbits for static tests 102
Displacement history for static cyclic tests 102
Time and frequency response of displacement sensors 103
Effect of preload on the gasket stiffness 104
Bushing-1 at conclusion of Test Set 1 105
Force-displacement response of Bushing-1 (Test No 8, Test Set 1) 105
Displacement histories of Bushing-1 for Test Sets 1, 5, 6, and 7 106
Force-displacement history for Bushing-1, Test No 4, Test Set 3 107
Actuator orbits during bidirectional tests (Test No 6, Test Set 4) 108
Rotation of Ring-1 following Test Set 12 109
Oil leakage from the gasket connection following Test Set 12 109
Separation of Ring-1 from the epoxy filler material, Test Set 13 110
Twist of the UPPER-1 porcelain unit over the flange, Test Set 13 110

Slip of the UPPER-1 porcelain unit following Test Set 14 111
Fracture of the bottom shed of the UPPER-1 porcelain unit, Test Set 14 111
Torn portion of gasket at the gasket connection, Test Set 14 112
Fracture of cast aluminum flange following Test Set 14 112
Response of Bushing-1 during the monotonic test (Test Set 14) 113
Force-displacement response of Bushing-1 at the gasket connection 114
Response of Bushing 1 at the gasket connection (Test Sets 1 and 12) 115

Chapter 7

Details for flexible plate 137
230 kV-bushing installed atop the flexible plate 138
View of the flange connection showing the mounting gasket and bolts 138
Gasket connection showing Ring-2 retrofit detail 139
IEEE 693-1997 test response spectrum for High Level Qualification 139
Acceleration history, power spectrum, and response spectrum for the longitudinal (*X*- component of the CERL record 140
Acceleration history, power spectrum, and response spectrum for the transverse (*Y*- component of the CERL record 141
Acceleration history, power spectrum, and response spectrum for the vertical (*Z*- component of the CERL record 142
Instrumentation for seismic testing of Bushing-2 mounted on a flexible plate 143
Instrumentation at the top of Bushing-2 144
Instrumentation of the UPPER-1 porcelain unit and the flexible mounting plate 144
Bushing-2 after Test No 15 (target PGA=1.4g) showing oil leakage 145
Bushing-2 after Test No 17 (target PGA=1.8g) showing slip of porcelain 145
Bushing-2 after Test No 18 (target PGA=2.0g) showing extruded gasket 146
Retrofitted Bushing-2 after Test No 23 (target PGA=2.8g) showing oil leakage 146
Transfer function amplitudes between the top of Bushing-2 and the flexible plate 147
Transfer function amplitudes between the flexible plate and the rigid support 148
Response spectrum for Bushing-2 without Ring-2; Test No 13, Tabas-A, target PGA=1.0g 149
Response spectrum for Bushing-2 without Ring-2; Test No 18, Tabas-A, target PGA=2.0g 150
Components of vertical motion for Bushing-2 without Ring-2; Test No 18, Tabas-B, target PGA=2.0g 151
Components of horizontal motion for Bushing-2 without Ring-2; Test No 18, Tabas-B, target PGA=2.0g 152
Bushing-2 after earthquake testing showing the largest tear in the gasket 153
Drawing of the gasket locating tears 153
Response spectrum for Bushing-2 retrofitted with Ring-2; Test No 13, Tabas-A, target PGA=1.0g 154
Response spectrum for Bushing-2 retrofitted with Ring-2; Test No 18, Tabas-B, target PGA=2.0g 155
Response spectrum for Bushing-2 retrofitted with Ring-2; Test No 19, CERL, target PGA=1.0g 156
Response spectrum for Bushing-2 retrofitted with Ring-2; Test No 24, Tabas-B, target PGA=3.0g 157
Components of vertical motion for Bushing-2 retrofitted with Ring-2; Test No 24, Tabas-B, target PGA=3.0g 158
Components of horizontal motion for Bushing-2 retrofitted with Ring-2; Test No 24, Tabas-B, target PGA=3.0g 159
Post-test photograph of gasket locating tears and lacerations 160

Effects of support flexibility on the spectral acceleration response of a bushing 161
Displacement response of flexible plate in *z*- direction; Test No 24,
Tabas-B, target PGA=3.0g 162

Appendix A

Spectra for High Seismic Performance Level (IEEE 1998) 181
Spectra for Moderate Seismic Performance Level (IEEE 1998) 181
Spectra for High Level Required Response Spectrum (IEEE 1998) 182
Spectra for Moderate Level Required Response Spectrum (IEEE 1998) 183
Test Response Spectrum for Moderate Level qualification of a transformer-mounted bushing 184

1 Introduction

1.1 Porcelain Transformer Bushings

Porcelain transformer bushings are a key component of power transmission and distribution (T&D) systems. They are insulated conductors used to provide electrical connectivity between a high-voltage line and an oil-filled transformer, and are typically mounted on the top of a transformer or on a turret attached to the transformer (see Figure 1-1) using a bolted flange connection. A section through a typical bushing at its connection to a transformer is shown in Figure 1-2. The bushing flange, the porcelain stack immediately above the flange (referred to as UPPER-1 porcelain unit herein), and the gasket between the bushing flange and the UPPER-1 porcelain unit are shown in Figure 1-2.

Recent major earthquakes (Northridge, 1994; Kobe, 1995; Izmit, 1999; and Southern California, 1999) have demonstrated that porcelain transformer bushings, especially the high-voltage bushings rated at 196 kV and above, are susceptible to damage during severe ground shaking. For these bushings, it has been postulated that the inertia forces produce large shear forces and bending moments at the connection between the UPPER-1 porcelain unit and the bushing flange (termed the gasket connection herein, see Figure 1-2), and that these forces can cause failure. Four types of failure have been documented (Schiff, 1997): (a) oil leakage at the gasket connection, (b) slip of the UPPER-1 porcelain unit relative to the bushing flange, (c) gasket extrusion from the gasket connection, and (d) cracking of porcelain. Figure 1-3 shows a bushing with cracked porcelain mounted atop a turret (Schiff, 1997).

Since transformer bushings form an integral part of power T&D systems, their structural and electrical integrity are critical to maintaining power transmission. To mitigate the vulnerability of new bushings and other electrical substation equipment, representatives from electrical utilities and equipment manufacturers, together with consulting engineers and members of the academic community jointly developed a new national standard, IEEE 693-1997 (IEEE 1998). These requirements are expected to improve the seismic capability of substation equipment. However, electrical utilities will continue to maintain substantial inventories of the older equipment procured prior to the development of the current standard. The investigation reported herein was motivated by the need to develop retrofit methods to improve the seismic performance of older, vulnerable transformer bushings.

Section 1.2 describes the experimental methods used in this study, Section 1.3 summarizes previous research on bushings, Section 1.4 lists the objectives of the current study, and Section 1.5 describe the organization of this report.

1.2 Laboratory Testing of Bushings

1.2.1 Introduction

In the current study, three types of tests were used to characterize the performance of transformer bushings: earthquake simulator tests, pull-back quick-release tests, and static tests. Summary information on these tests follow.

1.2.2 Earthquake simulator tests

In the United States, the Institute for Electrical and Electronics Engineers, (IEEE) has developed guidelines for seismic testing and qualification of bushings. These guidelines are described in *IEEE Recommended Practice for Seismic Design of Substations*, IEEE 693-1997. According to these standards, transformer bushings rated at 161 kV and above need to be qualified by means of triaxial simulator testing. The key IEEE 693-1997 requirements for seismic qualification tests are identified in Appendix A. Three types of simulator testing are typically undertaken: resonance-search tests, seismic qualification tests, and seismic fragility tests.

Resonant-search tests are conducted at low levels of shaking and are used to determine the dynamic properties (fundamental frequency and damping ratio) of the equipment. Seismic *qualification* tests are intended to demonstrate (through experimentation) that a piece of equipment is able to perform its function during and after an earthquake. Seismic *fragility* tests are experiments that test to failure and are intended to obtain data points correlating a particular limit state (or failure) with a representative ground motion parameter (typically selected as the peak ground acceleration, PGA). This information is then used to develop fragility curves that plot the cumulative probability of reaching a limit state as a function of the chosen ground motion parameter.

1.2.3 Cantilever tests

Cantilever tests are mechanical tests performed by the bushing manufacturers to determine the static lateral load capacity of a bushing. Elastic (stiffness) and dynamic (frequency) properties of the bushing may also be derived from such tests. The bushing is typically mounted vertically on a stiff frame and a static concentrated force is applied at the top of the bushing. The rated cantilever strength of the bushing is a conservative estimate of the maximum load that may be applied before structural or functional failure. Oil leakage is the typical failure mode.

1.2.4 Static tests

Static (cyclic and monotonic) tests have been extensively and successfully used to test many structures and structural components (steel beam-column connections, concrete structures, supplementary dampers, and isolation bearings). Quasi-static cyclic tests are cost efficient and the slow rate of testing allows the investigator to observe and document the response during the

testing. The testing program described in this report is the first to use this method of testing to evaluate the response of transformer bushings and to supplement earthquake simulator tests.

1.3 Literature Survey

1.3.1 Background

In the past five years, a number of seismic tests of transformer bushings have been completed. A summary of selected tests and some of the key findings are presented in this section.

1.3.2 Laboratory testing of a 500-kV bushing in CERL, 1997

Wilcoski and Smith (1997) conducted triaxial seismic qualification and fragility testing of a 500-kV bushing supplied by the Tennessee Valley Authority (TVA), and manufactured by the General Electric Company (GE). The objectives of the tests were to determine the dynamic characteristics of the bushing, to qualify the bushing to the IEEE 693-1997 spectrum anchored at 0.5g, and to investigate the application of the CERL equipment fragility and protection procedure (CEFAPP) to electrical equipment.

The bushing was mounted on a small braced frame (see Figure 1-4) and tested using input motions generated from random signal. The motions consisted of a set of narrow-banded input signals whose amplitudes at the prescribed center frequency were adjusted to equal the IEEE 693-1997 acceleration spectrum ordinates. A fundamental frequency of approximately 6 Hz and a damping ratio of between 2 to 3 percent of critical were reported. During the qualification test (matched to the 2-percent IEEE 693-1997 response spectrum with a PGA of 0.5g), the bushing sustained no damage. During the fragility tests, (matched to the 2-percent IEEE 693-1997 response spectrum with a PGA of 1.0g), the bushing leaked oil.

1.3.3 Laboratory testing of bushings and transformers by ENEL, 1997-1998

Bellorini et al., (1997, 1998) conducted experimental and analytical studies of 230-kV bushings and transformers. The objectives of the tests were to determine the dynamic characteristics of the transformer-bushing system, to develop a finite element model of the transformer, to evaluate the amplification factor between the accelerations at the bushing flange and the transformer base, and to test a bushing to failure.

Forced vibration tests were used to determine the natural frequency of the transformer-bushing system. For the transformer-mounted bushing, a fundamental frequency and a damping ratio of 11 Hz and 2 percent of critical were reported. A linear three-dimensional finite element model of the transformer-bushing system was prepared and was calibrated using the experimental data. Utilizing the calibrated finite element model, the authors conducted response-history analysis of the transformer-bushing system. Two types of input motions were used: (1) a synthetic history derived from IEC-61463 (IEC 1996) matched to a 2-percent response spectrum with a PGA of 0.5g, and (2) two recorded ground motion histories (Friuli 1976 and Irpinia 1980) scaled to a PGA of 0.5g. The results of the dynamic analyses indicated an amplification factor of approximately 1.0 between the top of the transformer and the transformer base, and an amplification factor of approximately 2.2 between the bushing flange (top of turret) and the base of the transformer;

therefore the accelerations at the bushing flange were nearly 2.2 times greater than the transformer-base acceleration due to the flexibility of the transformer-turret support. For the earthquake simulator tests, the 230-kV bushing was attached to a rigid supporting frame (Figure 1-5). The bushing was subjected to (1) a synthetic history compatible with the IEC 61463-1996 (IEC 1996) 2-percent damped response spectrum with a PGA of 0.5g and (2) recorded ground motion histories. Oil leakage, large deformations, or breakage were not observed in any of these tests.

1.3.4 Field testing of bushings and transformers, UC Irvine, 1998-1999

Villaverde et al., (1999) conducted field testing and analytical studies of 230-kV and 500-kV bushings mounted on transformers. The objectives of the studies were to evaluate the dynamic characteristics of the transformer-bushing systems and to compute the amplification between the accelerations at the bushing flange and the ground as a result of the flexibility of the transformer tank and the turrets to which the bushings were attached.

Figure 1-6 shows part of the instrumentation used during the field testing of a 230-kV bushing. The tests were conducted by placing a vibrating shaker on the top of the transformer tank and laterally exciting the transformer. A fundamental frequency of approximately 6 Hz, and a damping ratio of 2 percent of critical for the 230-kV transformer-mounted bushings and a fundamental frequency of between 3 to 4 Hz, and a damping ratio of between 2 and 4 percent of critical for the 500-kV transformer-mounted bushings were reported. Linear three-dimensional finite element models of the transformer-bushing systems were prepared and calibrated using the experimental data. Using the calibrated finite element model, the authors conducted response-history analysis of the transformer-bushing systems. Two types of input motions were used: synthetic histories compatible with the IEEE 693-1997 (IEEE 1998) 2-percent damped response spectrum with a PGA of 0.5g, and recorded ground motion histories from 1989 Loma Prieta, and 1994 Northridge earthquakes.

1.3.5 Laboratory testing of bushings, UC Berkeley, 1997-1999

As part of a cooperative effort between the Pacific Earthquake Engineering Research (PEER) Center, the Pacific Gas and Electric (PG&E) Company, and the California Energy Commission (CEC), seismic testing and evaluation of two 196-kV and three 550-kV bushings was recently completed at the University of California at Berkeley. These bushings were manufactured by ABB Power T&D Company, Inc., Components Division of Alamo, Tennessee (ABB). The objectives of the studies were to compute the dynamic properties of the bushings, to qualify the bushings to either the IEEE 693-1997 moderate- or high-level spectrum, and to characterize the seismic performance of the bushings.

The bushings were mounted on a stiff braced frame and subjected to IEEE 693-1997 spectrum-compatible triaxial earthquake histories. The motions were developed from recorded near-field accelerations, using a time-domain spectrum matching technique. For the 196-kV bushings (Gilani et. al, 1998), fundamental frequencies of between 14 and 16 Hz and damping ratios of between 2 to 4 percent of critical were measured. One 196-kV bushing was qualified to the IEEE 693-1997 moderate-level spectrum (target PGA equal to 1.0g) and the second 196-kV bushing

was qualified to the IEEE 693-1997 high-level spectrum (target PGA equal to 2.0g). For the 550-kV bushings (Gilani et. al, 1999), a fundamental frequency of approximately 8 Hz and damping ratio of between 3 to 4 percent of critical were measured. None of the three 550-kV bushings met the IEEE 693-1997 requirements for the moderate-level qualification (target PGA equal to 1.0g) and when subjected to severe shaking, all three bushings experienced oil leakage at the gasket connection and slip of the UPPER-1 porcelain unit over the flange, (see Figure 1-7).

1.4 Objectives of the Current Study

In this study, PEER researchers, representatives from electrical utilities and transformer-bushing equipment manufacturers collaborated to develop new information on the response of bushings and to improve the seismic performance of *in-service* transformer bushings. This research program addressed three issues not explored in the previous studies, namely: (1) retrofit of (existing) in-service bushings; (2) the influence of support flexibility and bushing preload on bushing response; and (3) the utility of static testing as a complement to triaxial earthquake simulator seismic tests.

The five objectives of the study were to:

1. Identify bushings that were susceptible to severe earthquake shaking and select a vulnerable bushing type for further investigation.

2. Conduct fragility tests of bushings mounted on a rigid base (termed hereafter as a *rigidly* mounted bushing) to identify dynamic properties and limit states of the bushings.

3. Develop a retrofit procedure for a sample bushing that was cost effective, could be implemented simply, and met the electrical requirements specified by the manufacturers.

4. Conduct static tests of a bushing to identify its limit states of response (e.g., oil leakage and slip of porcelain) and to evaluate the efficacy of the retrofit detail.

5. Conduct fragility tests of a bushing mounted on a flexible base (termed hereafter as a *flexibly* mounted bushing) to investigate the influence of support flexibility on bushing response and to assess the efficacy of the retrofit detail.

1.5 Report Organization

This report comprises into eight chapters, references, and one appendix. Chapter 2 provides information on the two bushings used for testing. Chapter 3 discusses the simulator motions developed for the seismic tests. Chapter 4 describes the test setup (including the rigid mounting frame and a list of the transducers used to monitor the response of the bushings) and results from the earthquake testing of *rigidly* mounted bushings. Chapter 5 provides information on the retrofit details. Chapter 6 describes the test setup (including the stiff mounting frame and a list of the transducers used to monitor the response of the bushing) and the results from the static testing of a bushing. Chapter 7 describes the test setup (including the flexible mounting attachment and a list of the transducers used to monitor the response of the bushing) and the results from the earthquake testing of a *flexibly* mounted bushing. Chapter 8 includes a summary of the key

findings and conclusions drawn from the research project. References are listed following Chapter 8. The IEEE 693-1997 Recommended Practice for earthquake testing of transformer bushings is summarized in Appendix A. Raw data and video images from all earthquake tests were supplied to Pacific Gas & Electric under separate cover.

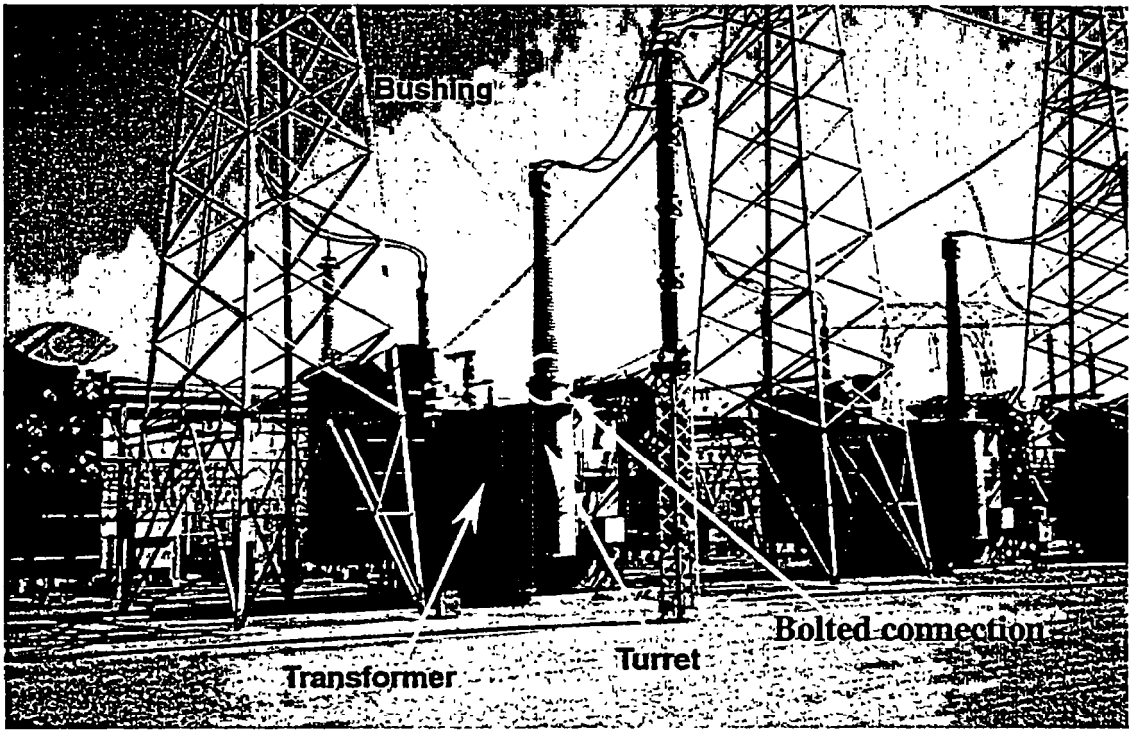

Figure 1-1 Bushing mounted on an oil-filled transformer

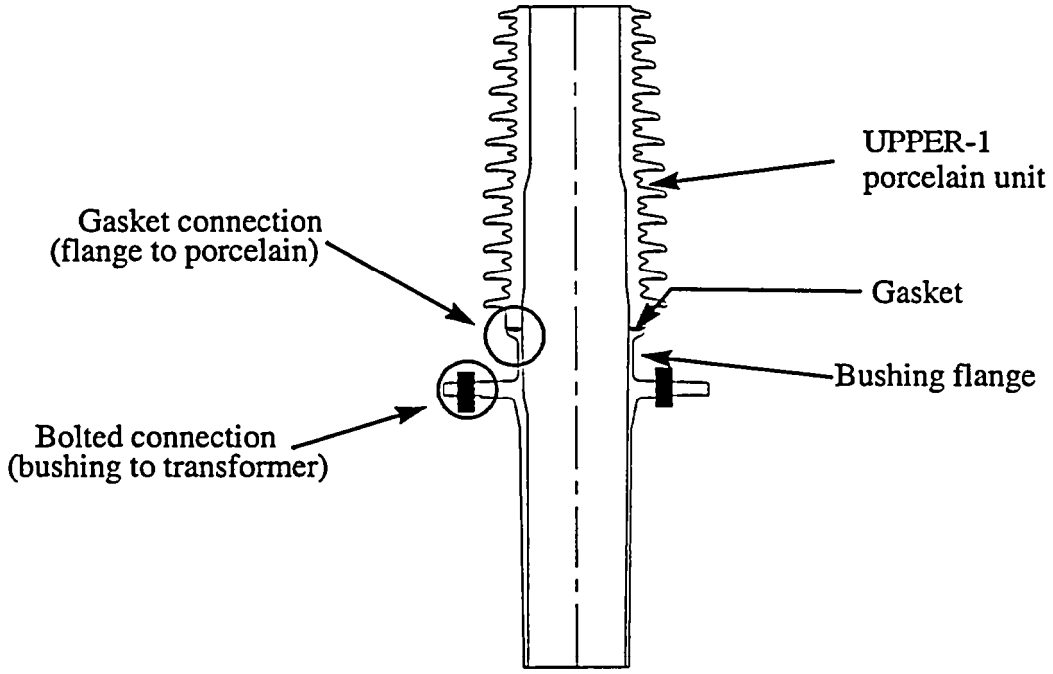

Figure 1-2 Cross section of a typical bushing

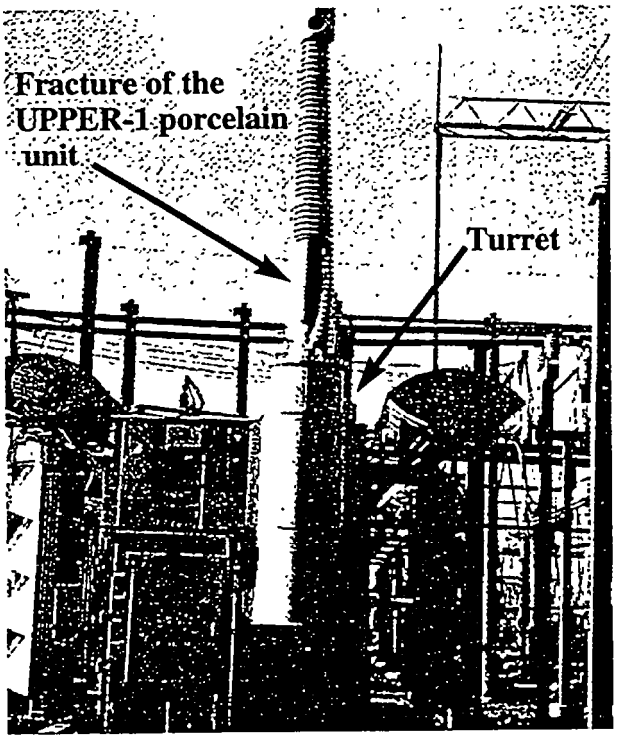

Figure 1-3 Fracture of an UPPER-1 porcelain unit from severe earthquake shaking

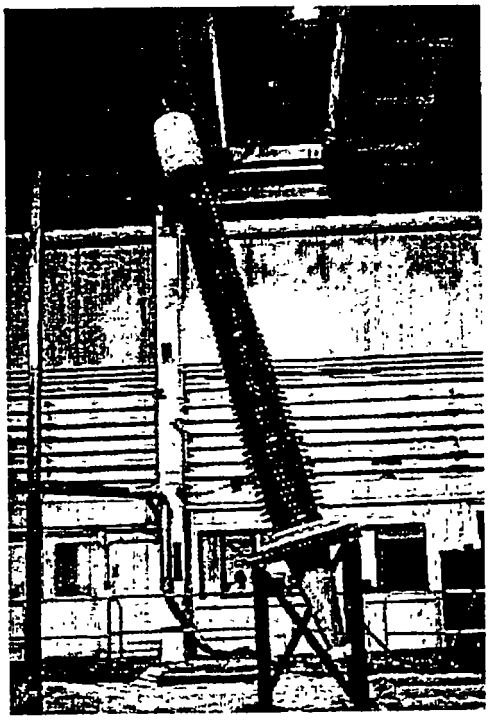

Figure 1-4 Seismic testing of a 500-kV bushing (Courtesy of CERL, Ill)

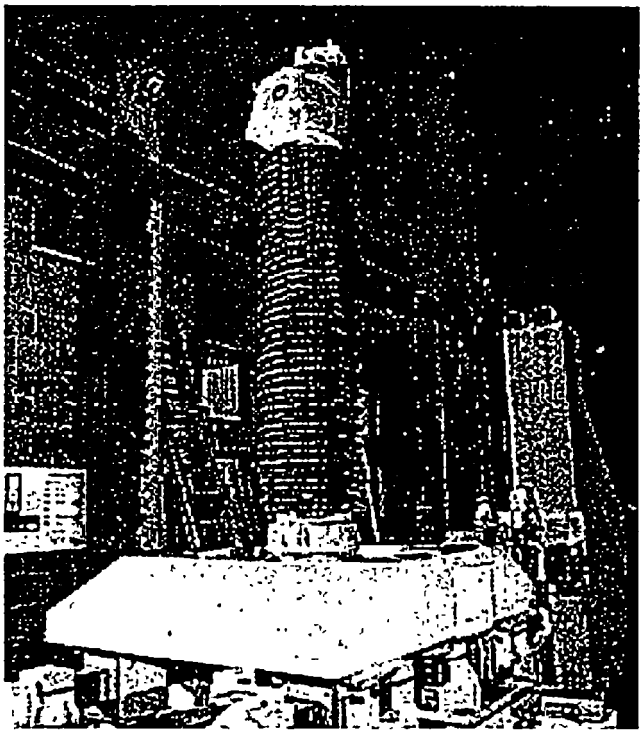

Figure 1-5 Laboratory testing of a bushing (Courtesy of ENEL and ISMES, Italy)

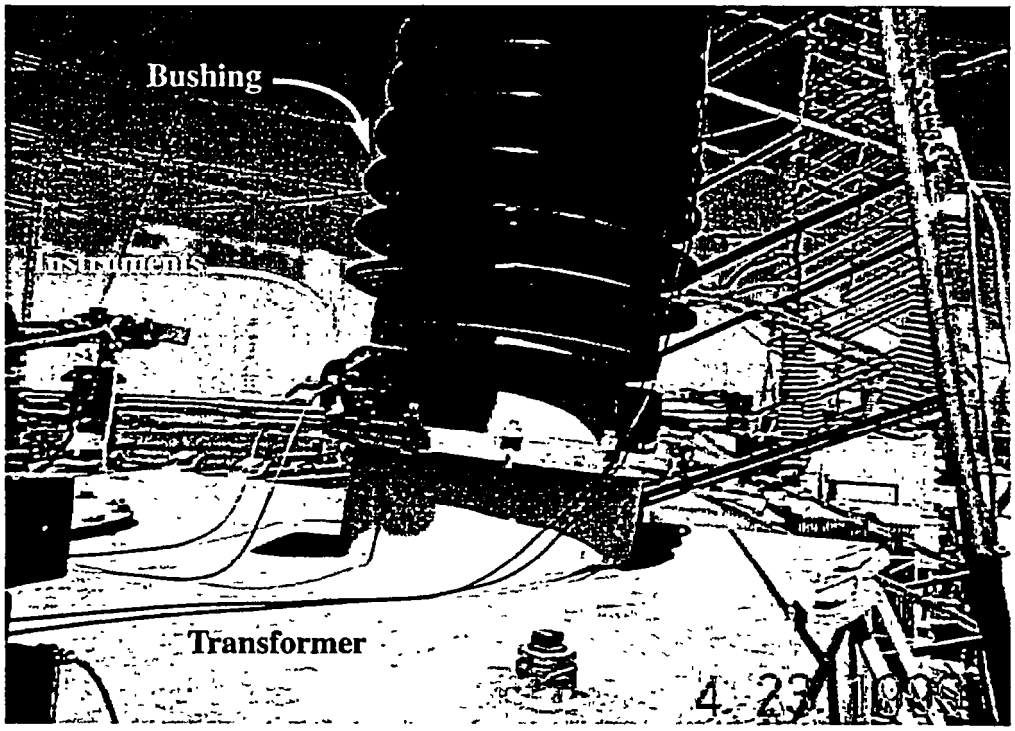

Figure 1-6 Field testing of a bushing (Courtesy of University of California, Irvine)

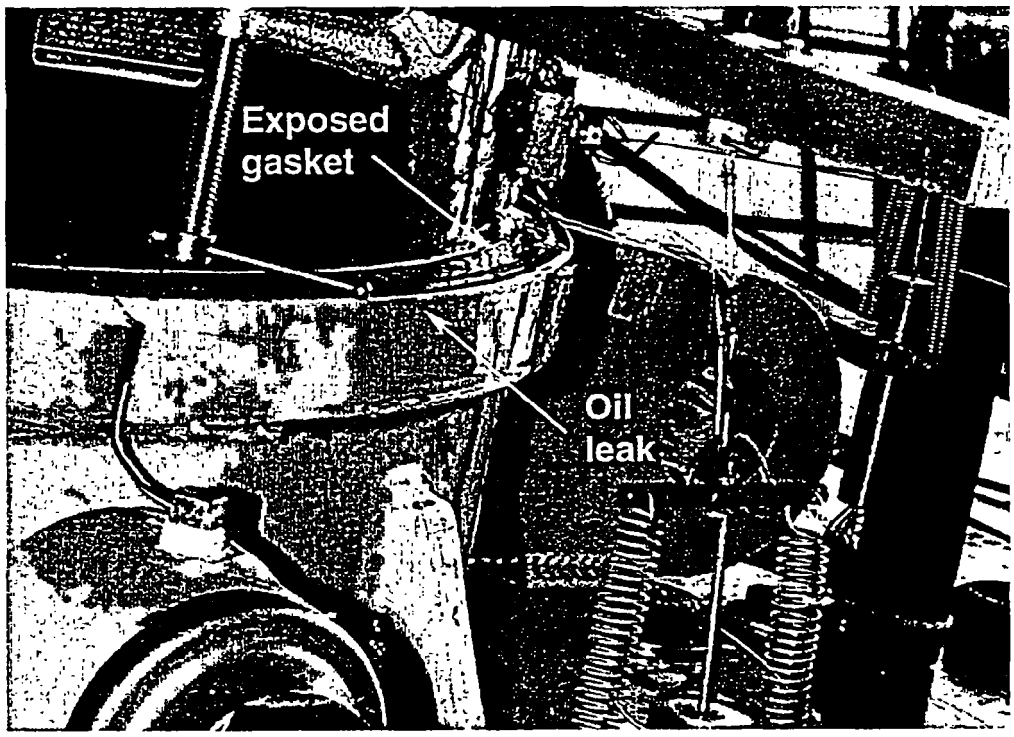

Figure 1-7 Laboratory testing of a 550-kV bushing

2 Selection Criteria and Properties of Test Bushings

2.1 Introduction

Review of reconnaissance reports from past earthquakes provides one source of information on the performance of electrical substation equipment. Electrical substations are often widely distributed and are unmanned. As a result, there are few witnesses to damage sustained during earthquakes, and evidence of failures is often disturbed because utility maintenance crews must quickly repair damaged equipment to restore service. Nonetheless, post-earthquake reconnaissance has shown that higher-voltage porcelain substation equipment, and in particular high-voltage porcelain transformer bushings, tend to be vulnerable to earthquake-induced damage due to their size, mass, and height.

The following sections list the evaluation criteria used to select the high-voltage bushing for testing and evaluation, describe the test bushing, and discuss the limit states and components of deformation of the test bushing.

2.2 Selection of Candidate Bushing

It is impractical to evaluate the seismic performance of all types and designs of higher voltage bushings. In general, documentation of bushing failures due to earthquake shaking by manufacturer, model, and key construction details are not available. Two criteria were used to select the test bushing. First, the bushing was to be widely used in practice and second, there was to be evidence that the candidate bushing had sustained earthquake-induced damage. A survey of electrical substations by the utilities indicated that 230-kV porcelain bushings (or similar bushings de-rated to 196 kV) were widely used, and that this class of bushing had sustained damage in past earthquakes. Two hundred and thirty kV bushings were selected for study and the utilities identified a number of spare 230-kV bushings of an older design for laboratory testing.

Porcelain bushings are composed of an inner core (used for electrical conduction and post-tensioning) and a number of outer stacks of unconnected porcelain (used for insulation). Most porcelain bushings are post-tensioned through the core to hold the stacks (units) of porcelain and the flange assembly together. The critical joint for the 230-kV transformer bushings is the

interface between the bushing flange and the porcelain stack immediately above it (hereafter referred to as the gasket connection), shown in Figure 1.2. Most bushing failure modes (oil leakage, porcelain slip, gasket extrusion, and porcelain fracture) have been linked to this connection.

Bushing manufacturers use a number of design details and geometries for this connection. Four of the more widely used gasket connections are shown in Figure 2-1. In the Type-A connection, the bushing flange is cast with a shallow groove or pocket, the porcelain unit is placed in the groove above a gasket, and the annular gaps between the flange groove and the porcelain are sealed using a flexible grout. In the Type-B connection, the bushing flange has an annular lip that extends above the connection and overlaps the inner face of the porcelain unit, and is cast with a shallow groove to accept the gasket. An O-ring seals the gap between the inside face of the porcelain unit and the outside face of the annular lip: An annular gasket is placed in the shallow groove and the porcelain is placed atop the gasket. In the Type-C connection, the bushing flange is cast with a groove, a gasket is placed in the groove and the porcelain unit is placed on the gasket. In the Type-D connection, the bushing flange has an annular lip that extends above the connection and overlaps the outer face of porcelain. The gap between the flange and porcelain is grouted using Portland cement. An O-ring gasket is placed in a specifically designed groove and the porcelain is placed on the O-ring gasket.

One of the predominant modes of failure of porcelain bushings is slip of the porcelain unit above the flange (see Figure 2-2). Since three of the gasket connections (Type-A, Type-B, and Type-D) are only moderately susceptible to this type of failure, only transformer bushings with Type-C gasket connection were considered for further investigation.

2.3 230-kV Type-U Bushing Manufactured by GE

Two identical 230-kV, 3000-A, type-U transformer bushings, manufactured in the mid-1980s by the General Electric (GE) Company, were supplied by BPA for testing and evaluation. These bushings are widely used in electrical substations and use a Type-C gasket connection, which does not prevent slip of porcelain over the bushing flange. Figure 2-3 shows one of the bushings prior to testing. The two bushings were identified by Serial Numbers 1795450 and 1795451, and were designated Bushing-1 and Bushing-2, respectively.

A longitudinal section and a cross section through one of the test bushings is shown in Figure 2-4. Also shown in the same figure are the coordinate system and designations for selected bushing elevations (top, midheight, and bottom) used in this report. The overall length of the transformer bushing is 144.5 in. (3.7 m). The segment of the bushing above the cast aluminum flange, which protrudes above the top of the transformer as seen in Figure 1.1, is 85 in. (2.2 m) long and this segment includes two porcelain insulator units or stacks (hereafter referred to as UPPER-1 and UPPER-2), and a metallic dome at the top of the bushing above porcelain unit UPPER-2. The porcelain units, the cast aluminum flange, and the metallic dome are separated by gaskets made of nitrile rubber. The gasket between the bushing flange and UPPER-1 porcelain unit is a flat annular strip of rubber; details of the gasket and the flange at the gasket connection are shown in Figure 2-5. The segment of the bushing below the flange, which is immersed in oil in the transformer tank, includes an extension of the cast aluminum flange, one porcelain insulator, and a cast aluminum

lower support. Flat annular gaskets separate these components. The flange plate, which is used to connect the bushing to the transformer, is cast with two lifting lugs (set 180 degrees apart, along the x-axis of the bushing as defined in Figure 2-4) to facilitate movement and installation of the bushing.

In cross section, the bushing has an aluminum core that provides the electrical connection; a multilayered, oil-impregnated, kraft paper condenser wrapped around the core; an annular gap between the porcelain and condenser that is filled with oil to provide electrical insulation; and a porcelain insulator. The weight of the bushing is approximately 920 lbs (4.1 kN), and its center of mass is located approximately 18 in. (0.45 m) above the flange plate. The portion of the bushing extending from the top of flange to the top of the bushing, weighs approximately 560 lbs (2.5 kN), with its center of mass located 44 in. (1.1 m) above the flange plate.

The bushing is post-tensioned along its longitudinal axis through its core. Twenty-seven springs in the metallic dome provide a uniform distribution of compression force around the perimeter of the porcelain units and the gaskets.

Prior to shipment for testing, the bushing post-tensioning (PT) force was set at approximately at 22 kips (98 kN) by PBA. This value was determined by subtracting 5 kips (22 kN) from the manufacturer recommended PT value of 27 kips (120 kN) to account for the PT loss due to elevated operating temperatures.

The key physical and electrical characteristics of the bushings are summarized in Table 2-1.

Table 2-2 lists material properties for the key components of the bushing. The manufacturer (Elder, 1999) provided the material data for the porcelain, bushing flange, transformer oil, condenser, and core tube.

Test data for 1/4-in. (6-mm) thick nitrile rubber gaskets were supplied by Elder (Elder, 1999). Tests were performed by GE on 3/4-in. (19-mm) and 1-in. (25-mm) wide gaskets. Test specimens were 6-in. (152-mm) long samples with a Durometer hardness of 65. The test setup involved compression loading of unconfined rubber strips between plates having F6 finished surfaces. Test data are reproduced in Figure 2-6. The dashed line at 6.2 MPa corresponds to the gasket pressure (stress) for a post-tensioning force of 27 kips (120 kN). A gasket elastic modulus of approximately 7 ksi (48 MPa) is computed from averaging the two tangent moduli shown as dashed lines in the figure. This computed compression modulus value is substantially larger than the value of 6 MPa listed by Roberts (Roberts, 1988) and Lindley (Lindley, 1978) for a 65-Durometer hardness rubber. This discrepancy is likely due to the different rubber types tested and variations in the test setup. The compression modulus of rubber is highly dependent on the confinement of rubber.

The compression modulus of confined rubber (E_c) can be computed from the elastic modulus of rubber (E_0) as:

$$E_c = E_0(1 + 2kS^2) \tag{2-1}$$

Table 2-1 Characteristics of the GE type-U test bushings

Property	*Parameter*	*Value*
Electrical	Voltage rating	230 kV
	Amperage	3,000 A
	BIL[1]	900 kV
	Conductor core	Aluminum
	Electrical connection type (draw lead or bottom connect)	Bottom connect
Physical	Weight	4.1 kN
	Total length	3.7 m
	Length above flange	2.2 m
	Length below flange	1.5 m
	Initial post-tensioning force	98 kN
	No. of porcelain stacks above flange	2
Gasket connection	Porcelain-flange interface	Type-C (see Section 2.2)
	Gasket material	Nitrile rubber
	Gasket geometry	Annular ring (OD = 300 mm, ID = 250 mm)
		Thickness: 6.4-mm nominal and 5.6-mm compressed
	Flange material	Cast aluminum
	Flange groove	Annular, 24-mm wide, 4.8-mm deep
	Separation[2]	13 mm
Identification plate	Model No.	11B802BB G10
	Serial No.: Bushing-1, Bushing-2	1795450, 1795451

1. Basic Impulse level (BIL) designates the impulse voltage the bushing can withstand.
2. Denotes distance between UPPER- inner surface and the voltage tap electrical wire, adjacent to the kraft paper.

In Equation 2.1, k denotes a hardness-dependent numerical factor and S designates the shape factor (defined as the ratio of the one loaded area to the total force-free area). For the annular gasket with a Durometer hardness of 65, an outside diameter of 11.75 in. (298 mm), an inside diameter of 10 in. (254 mm), and a thickness of 0.25 in. (6 mm), the k factor equals 0.54 (Roberts, 1988) and S equals 1.75. As such, the compression modulus of confined rubber (E_c) is nearly four times the elastic modulus (E_0).

In the Type-C gasket connection, the gasket is placed in an annular groove in the bushing flange and can be considered to be confined. If the gasket is so confined, then the value of E_c should be used as its effective compression modulus.

Table 2-2 Material properties of the bushing components

Component	*Material*	*Unit weight (kN / m[1])*	*E (MPa)*[1]
porcelain	porcelain	24	97,000
flange assembly	cast aluminum	27	69,000
transformer oil	mineral oil	9	-
condenser	kraft paper	12	10,000
core tube	aluminum	27	69,000
gasket	nitrile rubber	-	48[2]

1. Material properties for all components except the gasket was provided by the manufacturer (Elder, 1999).
2. Elastic modulus, E_0, was estimated from available test data (Elder, 1999).

2.4 Limit States for 230-kV Bushings

2.4.1 Background

As noted in Chapter 1, inspection of failed bushings following major earthquakes has identified four distinct and related failure modes at the gasket connection. The following subsections give a brief description of these limit states and their likely causes.

Although no previous test data was available for the 230-kV bushings tested at PEER, prior cantilever laboratory tests conducted on a similar bushing, a 196-kV bushing that has replaced the 230-kV type-U bushing provided some insight into the response of the test bushing. Examination of such test data by the manufacturer (Elder, 1999) indicated that the bushing leaked oil when the porcelain uplift at the gasket connection exceeded a threshold value of 0.03 to 0.04 in. (0.8 to 1 mm) and that the bushing withstood the application of a concentrated static force of 1.4 kips (6.3 kN) at the top without failure.

2.4.2 Oil leakage

The gasket, seated in the annular flange groove, provides a barrier against oil leakage. When unprestressed, the gasket protrudes approximately 1/16 in. (1.6 mm) above the upper surface of the pocket or groove. The application of the nominal post-tensioning force of 27 kips (120 kN), compresses the gasket, and reduces the gasket protrusion above the flange groove to approximately 0.04 in. (0.8 mm).

Under the application of lateral forces above the gasket connection, an overturning moment is produced at the gasket connection. This moment is resisted by the stabilizing post-tensioning moment equal to Nr, where N is the applied post-tensioning force, and r is the bushing radius measured the center of the bushing to the centerline of the gasket. When the value of the overturning moment exceeds the value of the stabilizing moment, the porcelain will uplift at a discrete location. When the maximum uplifts exceeds the threshold value of approximately 0.03 in. (0.8 mm), oil will leak from the bushing.

2.4.3 Porcelain slip

In the absence of uplift, the gasket is in contact with the UPPER-1 porcelain unit; the lateral force required to initiate porcelain slip is μN, where N is the applied post-tensioning force and μ is a slip coefficient. The core kraft paper assembly provides resistance to the slip and as such, the slip coefficient is larger than the friction coefficient between porcelain and rubber. The value of the friction coefficient is reduced if the gasket surface is coated with oil (lubricated).

2.4.4 Gasket extrusion

The gasket is seated in the bushing flange groove or pocket and can not extrude from the groove under the application of lateral loading. However, once the UPPER-1 porcelain unit slips or uplifts over the gasket connection, it can bear down unevenly on the gasket and force a portion of the gasket out of the flange groove.

2.4.5 Porcelain fracture

The porcelain is under nearly uniform compressive force from post-tensioning of the inner core and bears uniformly over the gasket. There is little stress concentration and there is no direct contact between the UPPER-1 porcelain unit and bushing flange. However, once the UPPER-1 porcelain unit slips or uplifts over the gasket connection, comes into direct contact with the bushing flange and is subjected to concentrated compressive axial forces and tensile circumferential stresses that can fracture brittle porcelain.

2.5 Components of Deformation for 230-kV Bushings

2.5.1 Introduction

Four modes of deformation contribute to the displaced shape of the segment of the bushing extending from the flange to the top of the bushing under the application of a concentrated horizontal load or horizontal inertial loads. The four modes of deformation are bending of the porcelain, rigid rotation of the UPPER-1 porcelain unit over the flange, translation of UPPER-1 porcelain unit over the gasket in the gasket connection, and slip of the UPPER-1 porcelain unit over the flange. The horizontal motion of a point at elevation z above the gasket connection can be written as:

$$u(z) = u(z)_{porcelain} + u(z)_{uplift} + u(z)_{gasket} + u(z)_{slip} \qquad (2\text{-}2)$$

The first term, $u_{porcelain}$, denotes the cubic (cantilever) deformation of the porcelain above the gasket connection (see Figure 2-7a). Porcelain has high stiffness and this component is assumed to be zero.

The second term, u_{uplift}, designates the rigid rotation of the porcelain above the gasket connection due to the axial (flexural) flexibility of the gasket in the gasket connection (see Figure 2-7b). Under the application of a lateral load, P, at a point z_0 above the gasket connection, the linear deformation of the porcelain can be written as:

$$u(z)_{uplift} = \theta_{base} z = \frac{P z_0}{k_{\theta gasket}} z = \frac{t_g}{E_g I_g} P z_0 z \qquad (2\text{-}3)$$

In this equation, θ_{base} denotes the concentrated rotation at the gasket connection due to the flexibility of the gasket. The stiffness of the gasket ($k_{\theta gasket}$) is approximately equal to the product of the gasket compression modulus (E_g) and gasket moment of inertia (I_g) about the vertical (z-) axis, divided by the gasket thickness (t_g).

The third term, u_{gasket}, corresponds to the height-independent (constant) translation of the porcelain above the gasket connection due to the shear flexibility of the gasket in the gasket connection (see Figure 2-7c). Under the application of a lateral load, P, at a point z_0 above the gasket connection, the constant displacement of the porcelain can be written as:

$$u_{gasket} = \frac{P}{k_{vgasket}} = \frac{\tau_g}{G_g A_g} P \qquad (2\text{-}4)$$

In this equation, ($k_{vgasket}$) denotes the shear stiffness of the gasket and is computed as equal to the gasket effective thickness (τ_g) divided by the product of the gasket shear modulus (G_g) and the gasket plan area (A_g) in the horizontal (x-y) plane. Because the gasket is placed in a groove at the gasket connection, the value of the effective gasket thickness τ_g is smaller than the nominal thickness (t_g), and can be assumed to be approximately equal 0.02 in. (0.8 mm) — amount by which the compressed gasket projects above the flange groove.

The fourth term (u_{slip}) corresponds to the height-independent (constant) motion of the bushing above the gasket connection due to the slip of UPPER-1 porcelain unit over the gasket (see Figure 2-7d). Under the application of a lateral load, P, at a point z_0 above the gasket connection, this displacement is non-zero when the value of the applied load, P, exceeds the slip resistance at the gasket connection. The friction between the nitrile gasket and the porcelain, and the restraint provided by the core kraft paper assembly contribute to the slip resistance at the gasket connection. The friction component depends on the value of normal (post-tensioning) load, N, and the friction coefficient, f, between porcelain and nitrile rubber. This friction coefficient depends on the surface condition of the gasket (dry or coated with oil).

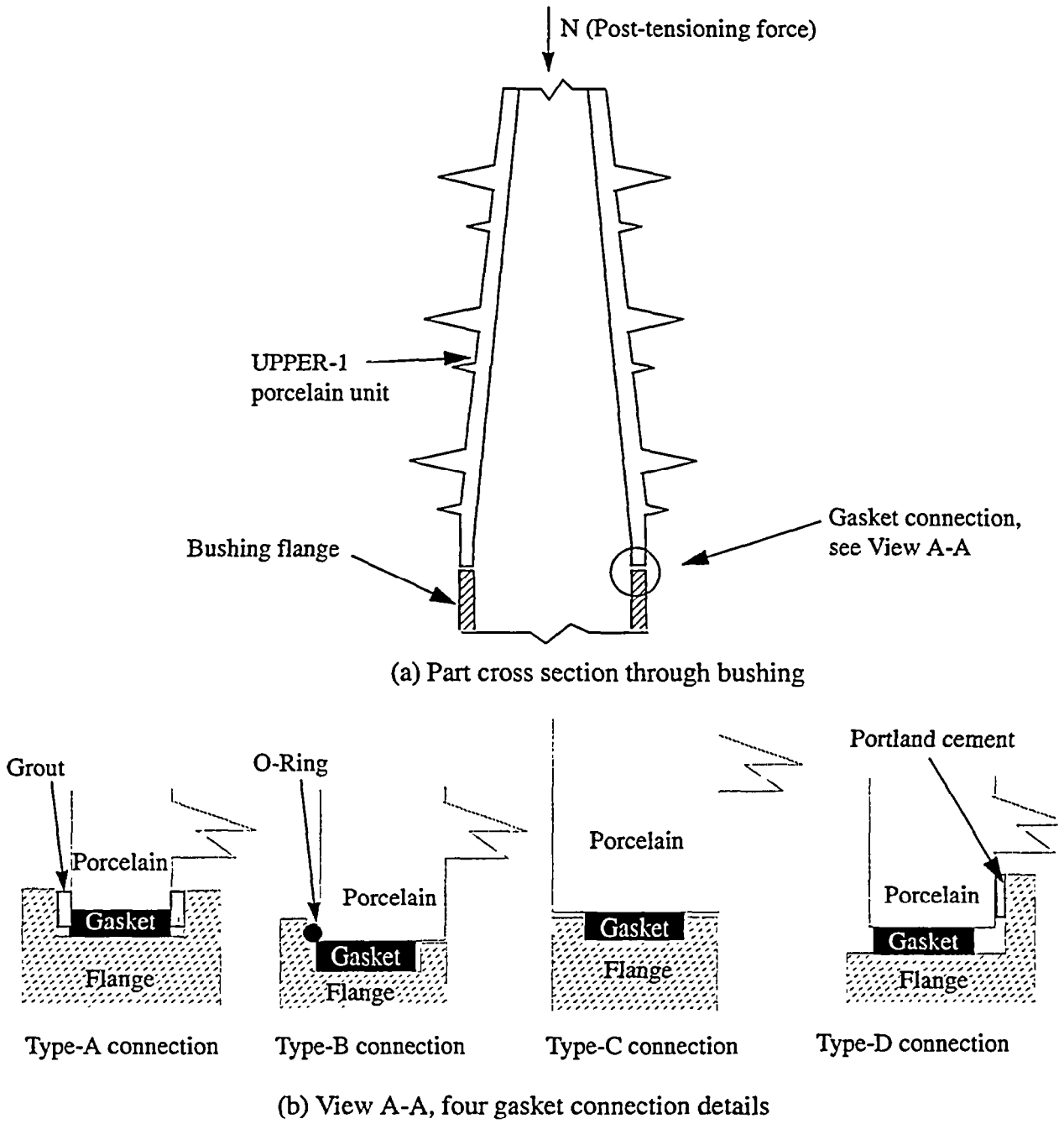

Figure 2-1 Typical porcelain-flange interface details for the gasket connection

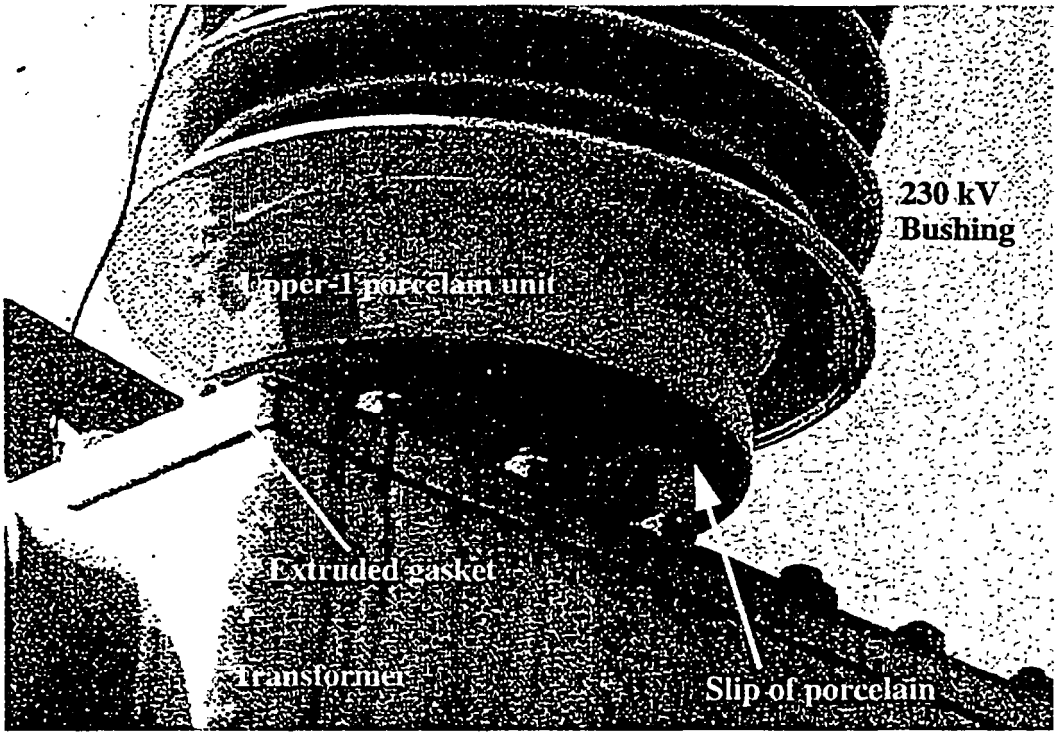

Figure 2-2 Slip of porcelain in a transformer-mounted 230-kV bushing

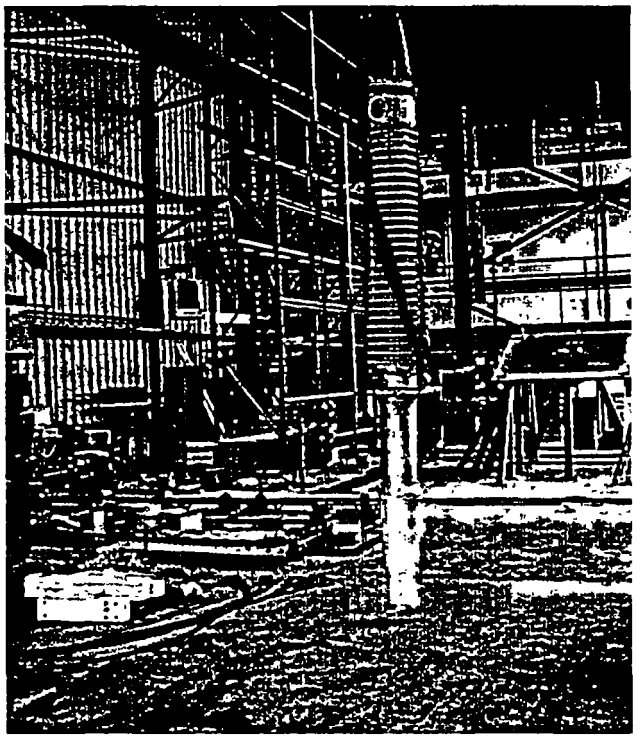

Figure 2-3 Bushing-2 prior to testing on the Berkeley simulator

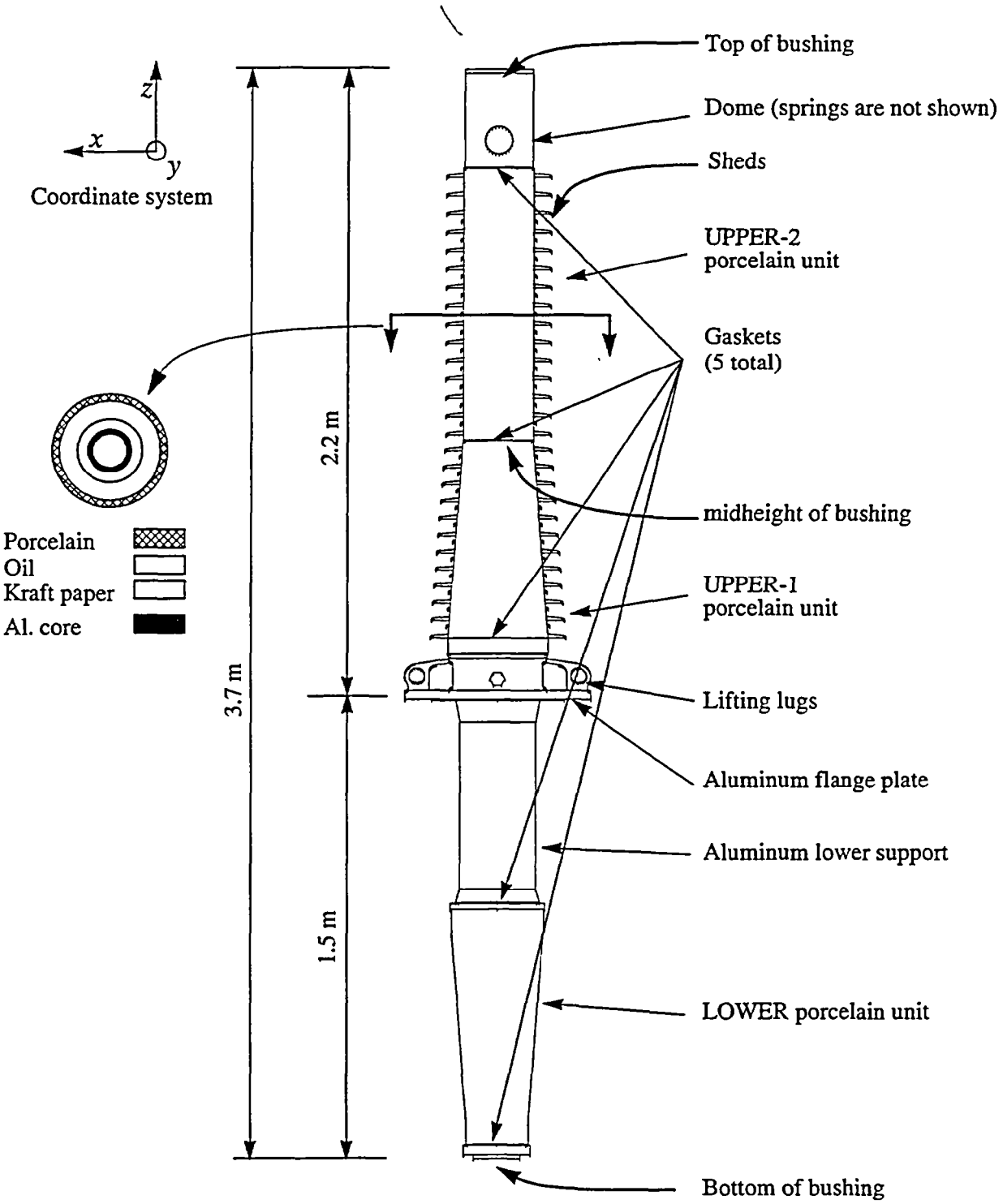

Figure 2-4 Longitudinal section and cross section through a 230-kV type-U bushing, manufactured by General Electric

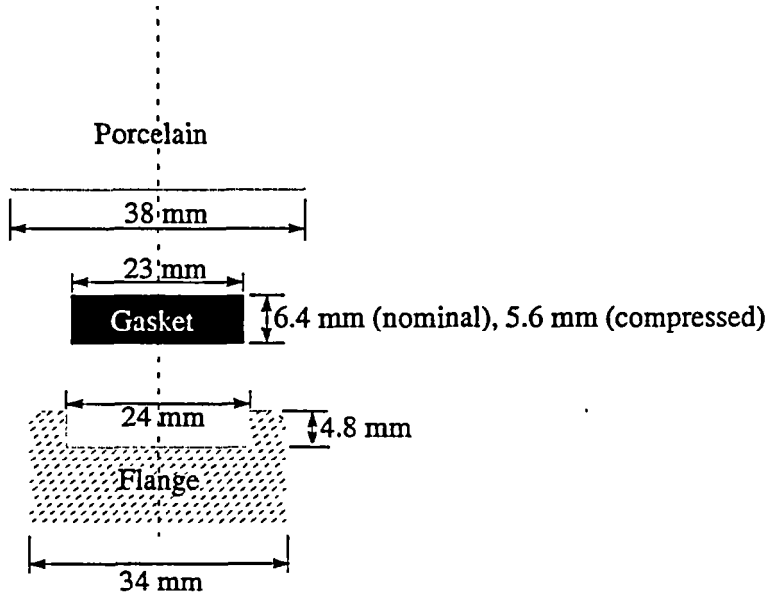

Figure 2-5 Exploded view of gasket connection detail for a 230-kV type-U bushing

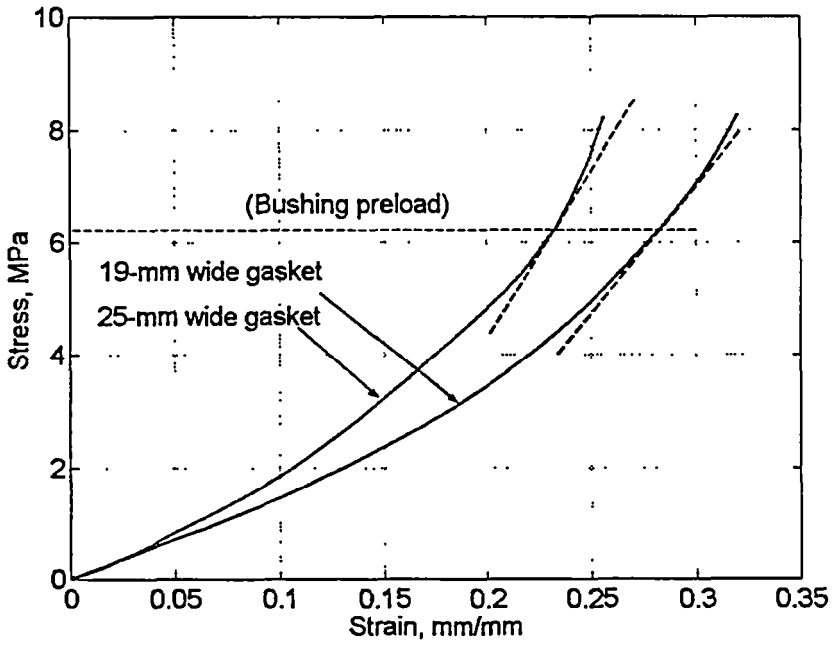

Figure 2-6 Compression stiffness of 6-mm thick nitrile gaskets (Elder, 1999)

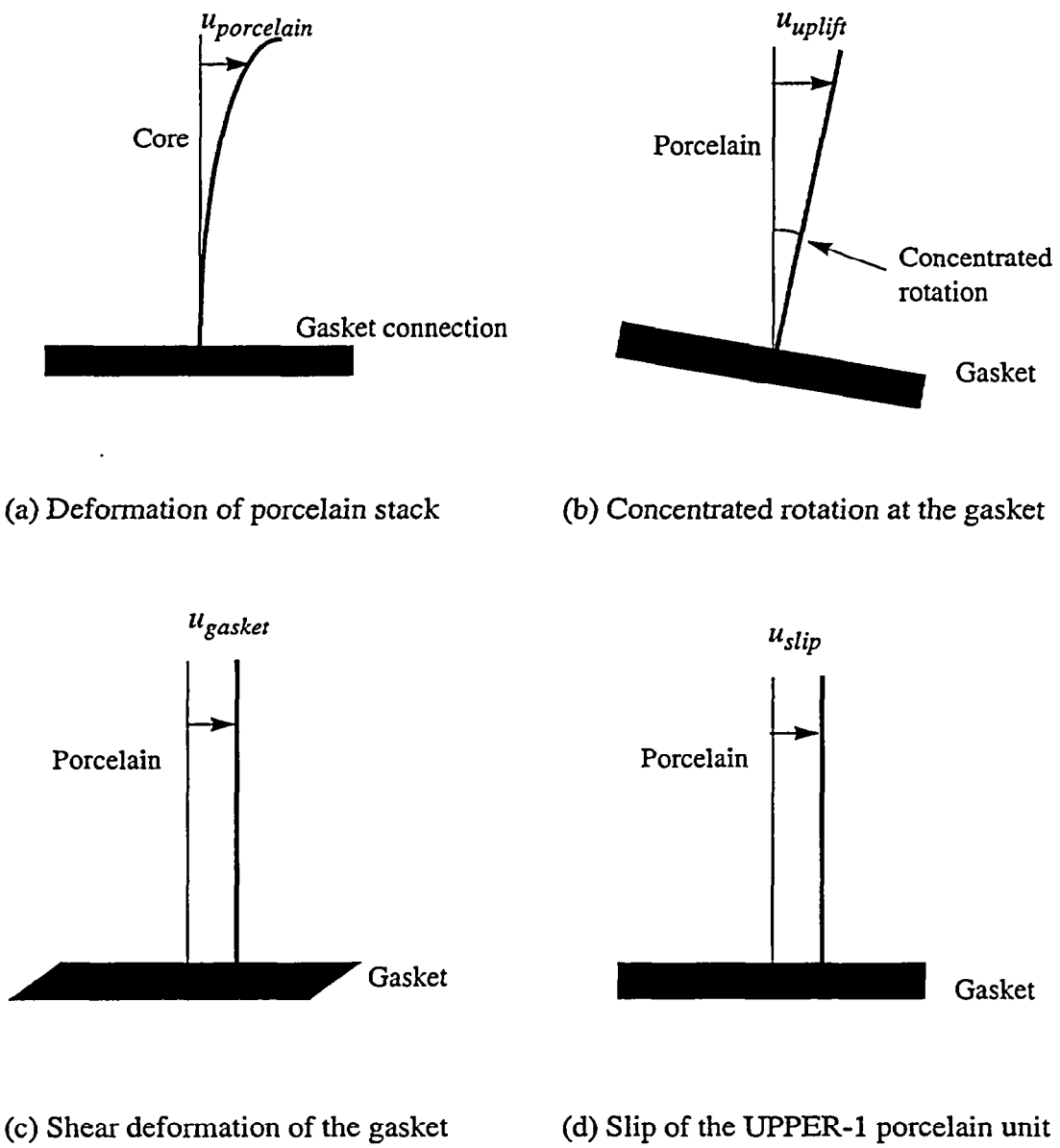

(a) Deformation of porcelain stack

(b) Concentrated rotation at the gasket

(c) Shear deformation of the gasket

(d) Slip of the UPPER-1 porcelain unit

Figure 2-7 Deformation modes for components of a 230-kV bushing

3 Qualification and Fragility Testing

3.1 Introduction

Recorded earthquake ground motion histories were used to evaluate the seismic response of the two 230-kV transformer bushings: Bushing-1 and Bushing-2. The following section describes the requirements of IEEE 693-1997 (IEEE, 1998) for the qualification of transformer bushings and the procedures used to develop earthquake histories for testing.

3.2 IEEE 693-1997 Requirements for Bushing Qualification

Three types of earthquake-simulator testing are identified in IEEE 693-1997 for the seismic qualification of transformer bushings: (a) earthquake ground motions, (b) resonant frequency search, and (c) sine-beat testing. Earthquake ground motion tests (termed *time-history shake table tests* in IEEE) and resonant frequency tests are mandatory. Information on these two types of tests follows.

3.2.1 Resonant-search tests

Sine-sweep or broadband white-noise tests are used to establish the dynamic characteristics (natural frequencies and damping ratios) of a bushing. These so-called *resonant-search* tests are undertaken using unidirectional excitation along each global axis of the earthquake simulator platform. If only broadband white-noise tests are performed, the amplitude of the white-noise must not be less than 0.25g. If only sine-sweep tests are used, IEEE 693-1997 specifies that the resonant-search be conducted at a rate not exceeding one octave per minute in the range for which the equipment has resonant frequencies but at least 1 Hz. Frequency searching above 33 Hz is not required. Because both sine-sweep and white-noise tests were used in this testing program to identify the modal properties of the transformer bushings, the recommendations of IEEE 693-1997 were not followed exactly.

The history for the banded white-noise tests was prepared using a random signal generator. The sine-sweep history was developed using a rate of two octaves per minute. (At two octaves per minute, the input frequency doubles every 30 seconds.) A continuous frequency function was used to develop the sine-sweep function

$$x(t) = x_0 \sin\left(2\pi\left[\frac{30}{\log 2}\right]2^{t/30}\right) \tag{3-1}$$

where x is the displacement, and x_0 is the maximum displacement. For both sine-sweep and white-noise tests, a simulator input acceleration amplitude of 0.1g was used.

3.2.2 Earthquake test response spectrum

IEEE 693-1997 identifies several response spectra of identical shape but different amplitudes for the qualification of transformer bushings. These spectra are described below; a more detailed description is presented in Appendix A.

Test Response Spectrum (TRS). For earthquake simulator testing, IEEE 693-1997 states that the TRS for each horizontal earthquake motion must match or exceed the target spectrum and that the TRS for vertical earthquake motion be no less than 80 percent of target spectrum. IEEE 693-1997 recommends that 2-percent damping be used for spectral matching and requires at least 20 seconds of strong motion shaking be present in each earthquake record. Earthquake motions can be established using either synthetic or recorded histories. Recorded motions formed the basis of the earthquake histories used to test the 230-kV bushings.

Performance Level (PL). IEEE 693-1997 represents a PL for substation equipment by a response spectrum. The PL represents the expected level of performance when a piece of equipment is qualified to the RRS and meets the requirements for allowable stress design. The two PLs relevant to California are *Moderate* and *High*. For reference, the Moderate Level ground motion spectra are shown in Figure 3-1.

Required Response Spectrum (RRS). It is often neither practical nor cost effective to test components to the Moderate PL. As such, IEEE 693-1997 permits equipment to be tested using a reduced level of shaking called the RRS. The shapes of the RRS and the PL are identical, but the ordinates of the PL are twice that (referred to as performance factor in IEEE 693-1997) of the RRS. Equipment tested or analyzed using the RRS is expected to have acceptable performance at the PL. This assumption is checked by measuring the stresses obtained from testing at the RRS, and (a) comparing the stresses to 50 percent (equal to the inverse of the performance factor) of the ultimate strength of the porcelain (assumed to be brittle) or cast aluminum components and (b) using a factor of safety against yield combined with an allowance for ductility of steel and other ductile materials.

Test Response Spectra for Mounted Equipment (TRSME). To account for the possible amplification of earthquake motion due to the influence of the transformer body and local flexibility of the transformer near the bushing mount, IEEE 693-1997 states that the input motion *as measured at the bushing flange* shall match a spectrum with ordinates twice that of the RRS, termed herein as the TRSME. For this level of shaking, IEEE 693-1997 states that the stresses in the porcelain components must be less than 50 percent of the ultimate stress, and the factor of safety against oil leakage must be greater than or equal to 2.0.

An alternate approach that is identified in Annex D5.1(d) of IEEE 693-1997 was used for the studies reported herein. Namely, earthquake histories with spectral ordinates twice those of the TRSME were used for testing: the target peak horizontal acceleration at the bushing flange was 1.0g. Porcelain stresses at this level of earthquake shaking were required to be less than or equal to the ultimate value, and there was to be no evidence of oil leakage. The spectrum for this motion is shown in Figure 3-2 and is the same as the Moderate PL spectrum.

The key requirements of IEEE 693-1997 for qualification and fragility testing of bushings are summarized in Table 3-1.

Table 3-1 IEEE earthquake-history testing requirements for Moderate Level qualification

Peak Ground Acceleration	*Comments*
0.5g	Moderate Seismic Performance Level (PL) for substation equipment
0.25g	Required Response Spectrum (RRS) for Moderate Seismic Performance Level for substation equipment
0.5g	Test Response Spectrum for Mounted Equipment (TRSME) for Moderate Seismic Performance Level.
1.0g	Response spectrum for checking porcelain stresses and oil leakage for bushings mounted on transformers.

3.2.3 Earthquake ground motions

The earthquake histories used for the qualification and fragility testing of the 230-kV bushings were developed using the three-component set of near-fault earthquake motions recorded during the 1978 Tabas earthquake. Figures 3-3 through 3-5 present the acceleration history, power spectrum, and pseudo-acceleration response spectra for the three components of the Tabas record. The amplitude of each history (*X*-, *Y*-, and *Z*-) record was normalized to a peak acceleration of 1.0g. The power spectrum for each history has moderate bandwidth. The 2-percent and 5-percent damped IEEE spectra for Moderate Level qualification, anchored to a peak ground acceleration of 1.0g, are also shown in the figures. The response-spectrum ordinates for each normalized earthquake history exceed the target IEEE values for frequencies greater than 2 to 3 Hz and drop below the target values for frequencies less than 2 Hz.

To obtain IEEE 693-1997 spectrum-compatible normalized histories, the original Tabas acceleration records were modified using a non-stationary response-spectrum matching technique developed by Abrahamson (Abrahamson, 1996). In traditional spectrum-matching routines, adjustments are performed in the frequency domain. Specifically, the original acceleration record is transformed into the frequency domain, the amplitude of the Fourier spectrum is adjusted at each frequency to match the target value, and the record is then transformed back into the time domain. Two key disadvantages of the frequency-domain method are that the modified earthquake history rarely resembles the original earthquake history, and that frequency leakage often makes convergence to the target spectrum difficult. Abrahamson's time-domain method is

based on the algorithm proposed by Lilhanand and Tseng (1988) wherein short-duration wavelets are added to the original earthquake history at optimal times in the history to match the spectral amplitude at each frequency to the target value. The modified history generally resembles the original earthquake history and frequency leakage is negligible.

The testing of 196-kV ABB bushings (Gilani, et al., 1998) at Berkeley utilized spectrum-compatible earthquake histories developed using the Abrahamson technique. The resulting spectra matched the target spectra across a broad frequency range (0.1 Hz to 100 Hz). Because the maximum displacement and velocity of the Berkeley simulator platform are 5 in. (127 mm) and 25 in./sec (635 mm/sec), respectively, the spectrum-compatible motions were high-pass filtered (removal of low-frequency content) to reduce the peak displacements and velocities of the simulator platform. However, the resulting power spectra of the filtered histories were narrow banded, and not particularly representative of strong earthquake ground motion.

A different strategy was used to develop earthquake histories for the studies reported herein. This strategy combined the Abrahamson spectrum-matching algorithm and frequency-domain trapezoidal high-pass filters. Input ground motions to the simulator were developed in a three-step process as follows. First, the original earthquake history was high-pass filtered to remove low-frequency content (see Table 3-2) such that the maximum displacement and velocity of the filtered history were approximately equal to 5 in. (127 mm) and 25 in./sec (635 mm/sec), respectively. (All content below the cut-off frequency was eliminated; all content above the corner frequency was retained; and content between these frequencies was multiplied by a linearly increasing value that ranged from zero at the cut-off frequency to unity at the corner frequency. The cut-off frequencies were much smaller than the resonant frequency of the 230-kV bushings (known to range between 16 to 20 Hz for *rigidly* mounted bushings and estimated to range between 6 to 8 Hz for *flexibly* mounted bushings). Removal of such low-frequency components from the input signals to the simulator is known to have a negligible impact on the dynamic response of the bushings. Second, the filtered earthquake history was matched to the target spectrum for frequencies greater than the corner frequency of the trapezoidal filter using the Abrahamson algorithm. Third, the spectrum-compatible motions from step two were high-pass filtered to exactly limit the maximum displacement and velocity to 5 in. (127 mm) and 25 in./sec (635 mm/sec), respectively.

Two independent sets of three earthquake histories (Tabas-A and Tabas-B) were generated using the above procedure. Tabas-A was used for all simulations up to and including the Moderate Level qualification for which the target simulator acceleration was 1.0g (see Figure 3-2). Tabas-B was used for all other tests up to those corresponding to High Level qualification for which the target acceleration was 2.0g. Table 3-2 summarizes the step-one filter frequencies used to generate the Tabas-A and Tabas-B histories. Figures 3-6 through 3-8 present the acceleration history, power spectrum, and response spectra for the three spectrum-compatible Tabas-A records. Figures 3-9 through 3-11 present the same information for the three spectrum-compatible Tabas-B records.

Table 3-2 High-pass filter frequencies for earthquake histories

		Filter frequencies (Hz)	
Set	*Component*	*Cut-off*	*Corner*
Tabas-A	*X*	1.0	1.5
	Y	1.0	1.5
	Z	1.0	1.5
Tabas-B	*X*	2.0	2.5
	Y	2.2	2.5
	Z	2.2	2.5

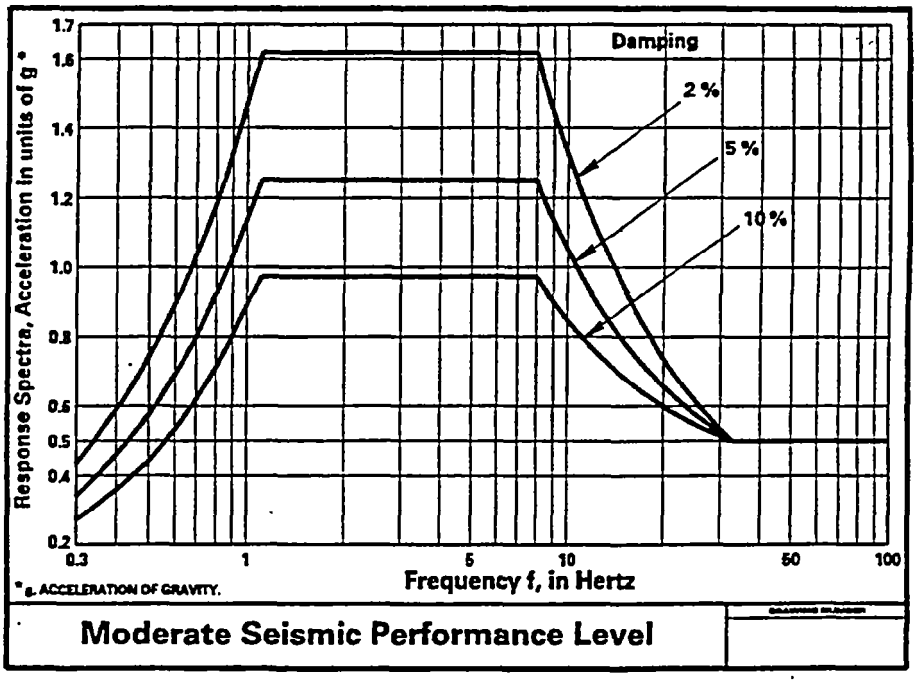

Figure 3-1 Spectra for the Moderate Seismic Performance Level (IEEE, 1998)

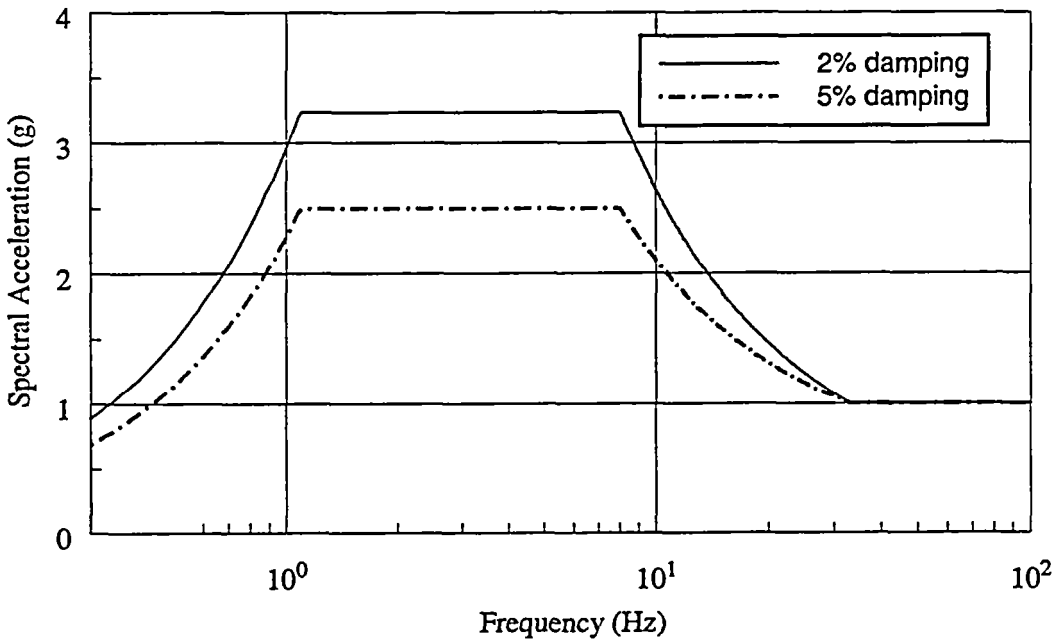

Figure 3-2 Test Response Spectra at bushing flange for Moderate PL

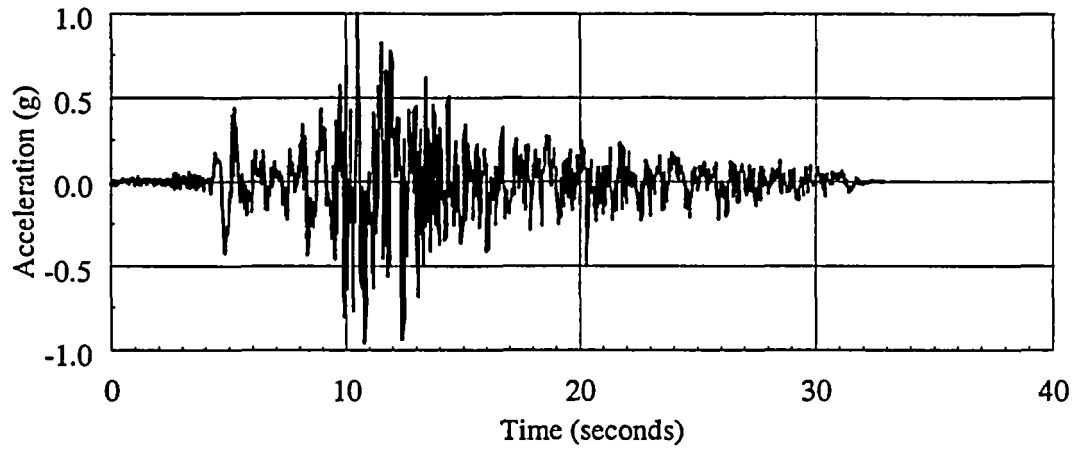

(a) Normalized acceleration history

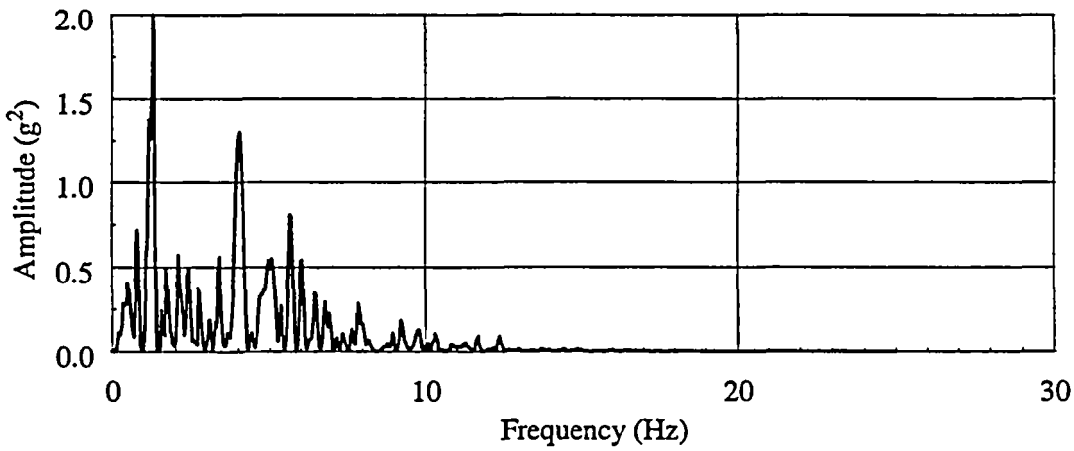

(b) Power spectrum

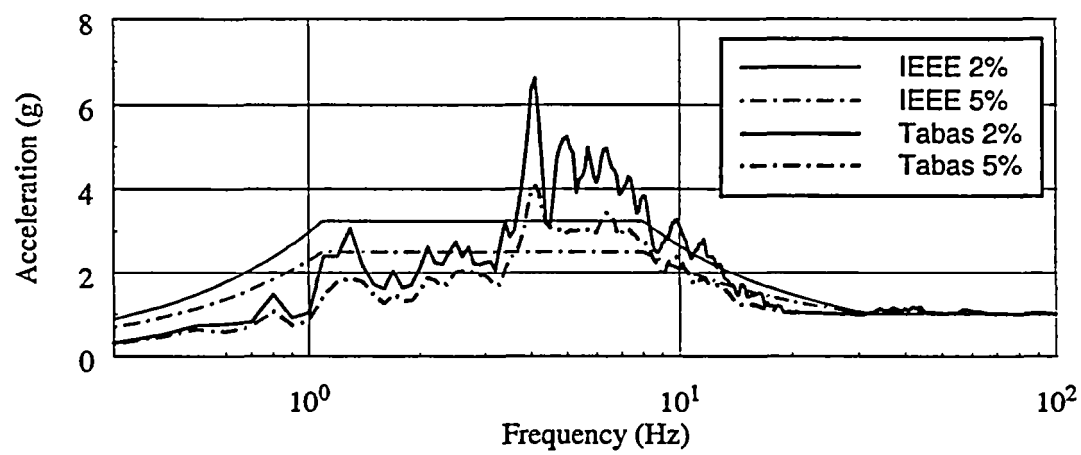

(c) Response spectrum

Figure 3-3 Normalized acceleration history, power spectrum, and response spectra for the longitudinal (*X*-) component of the original Tabas record

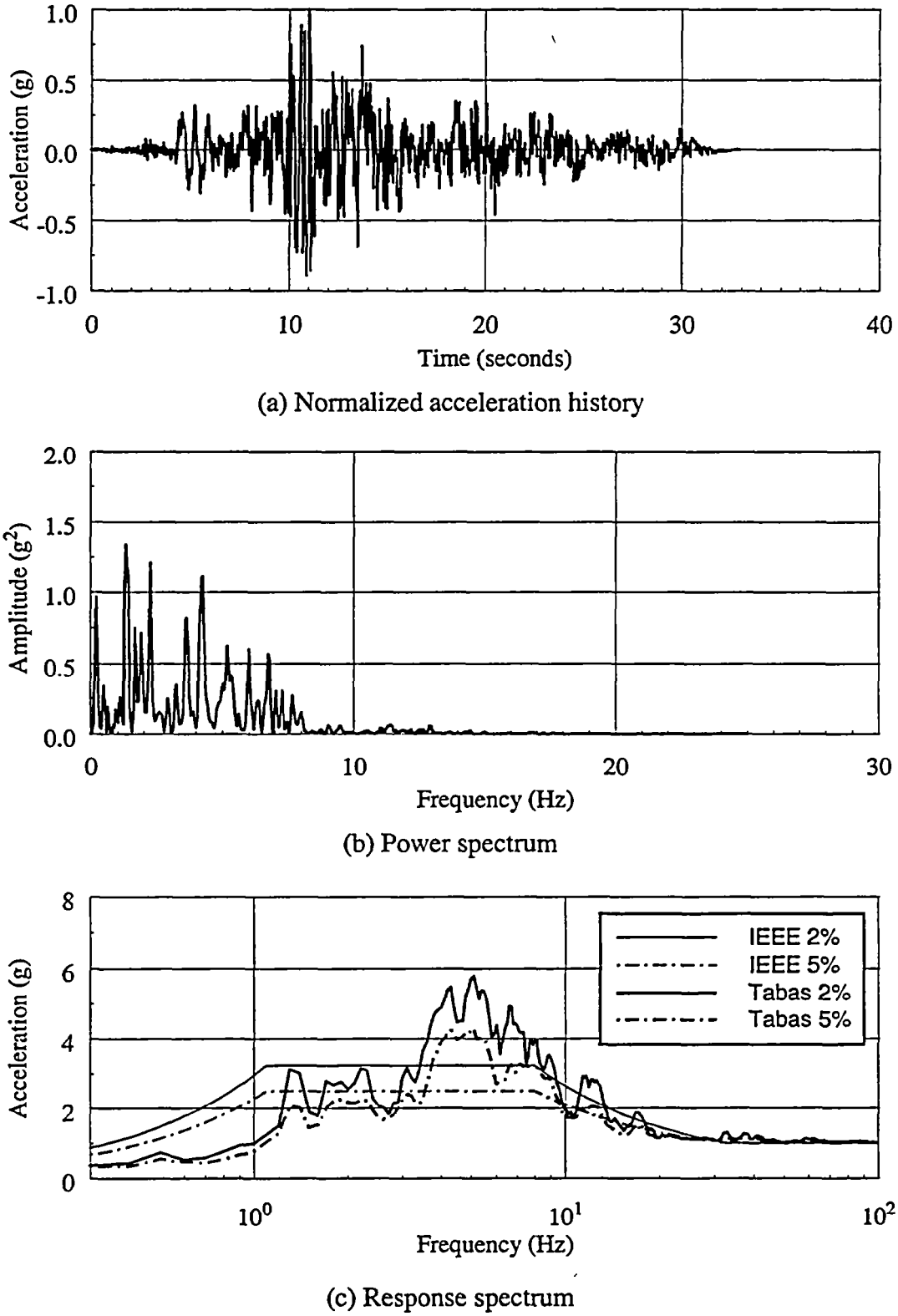

Figure 3-4 Normalized acceleration history, power spectrum, and response spectra for the lateral (*Y*-) component of the Tabas record

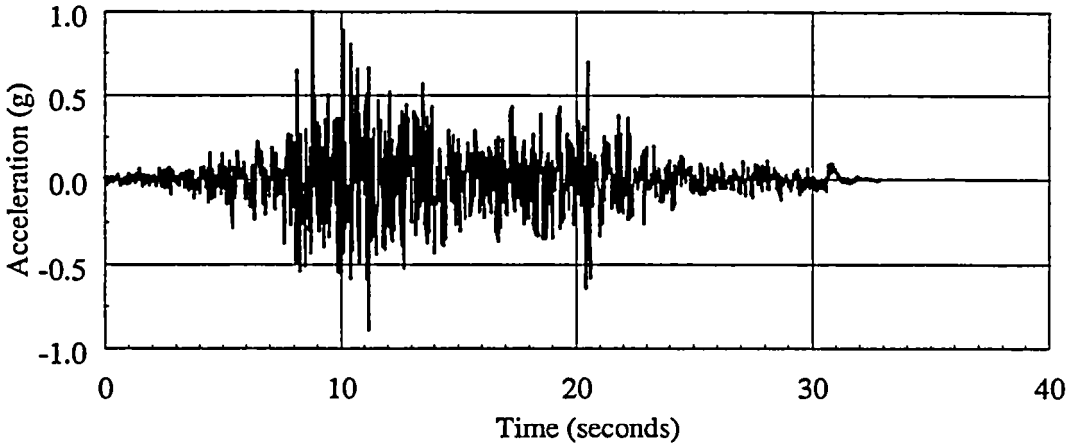

(a) Normalized acceleration history

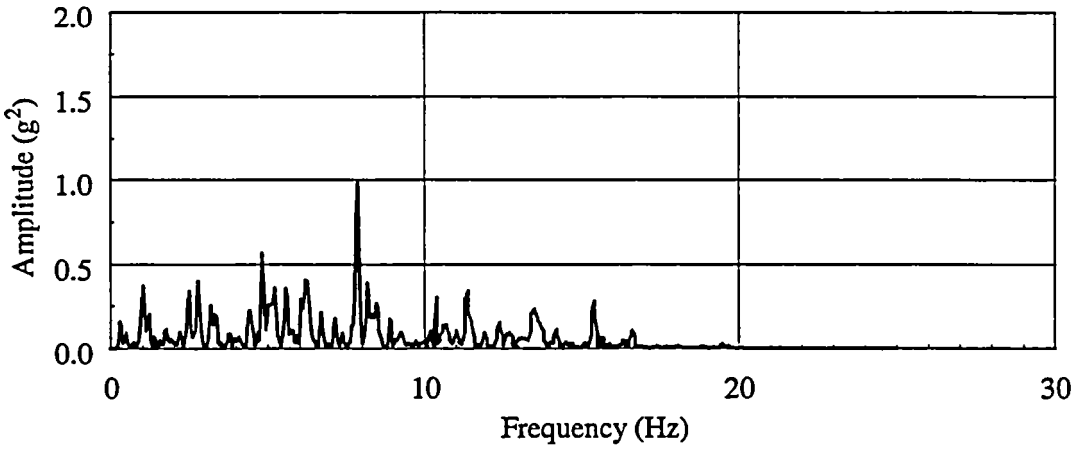

(b) Power spectrum

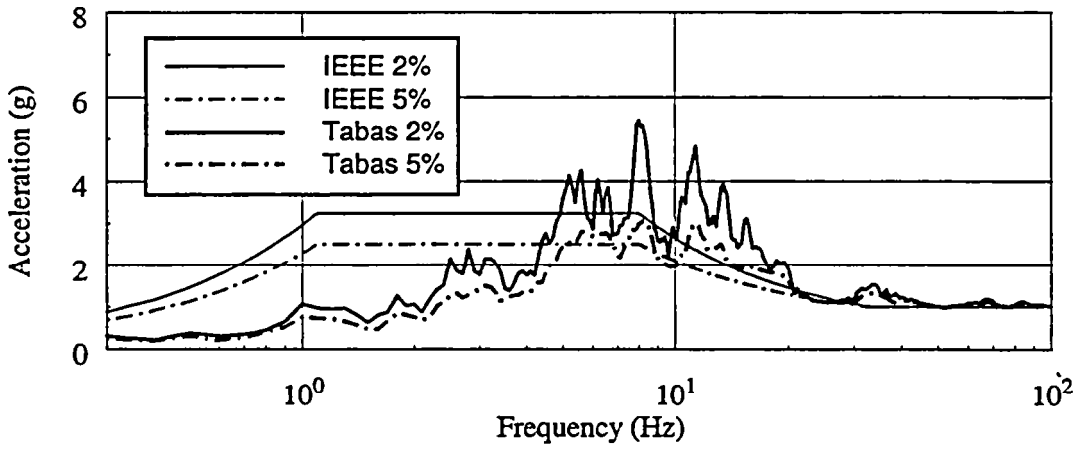

(c) Response spectrum

Figure 3-5 Normalized acceleration history, power spectrum, and response spectra for the vertical (Z-) component of the original Tabas record

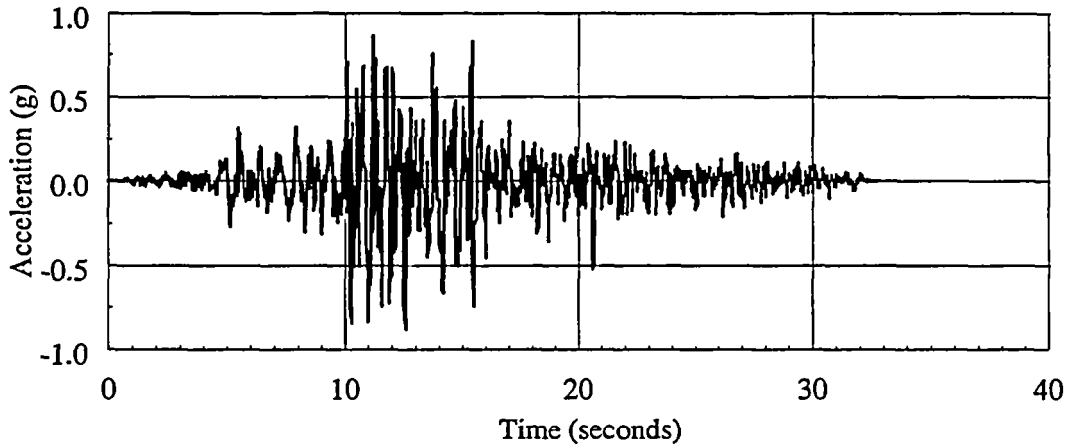

(a) Acceleration history

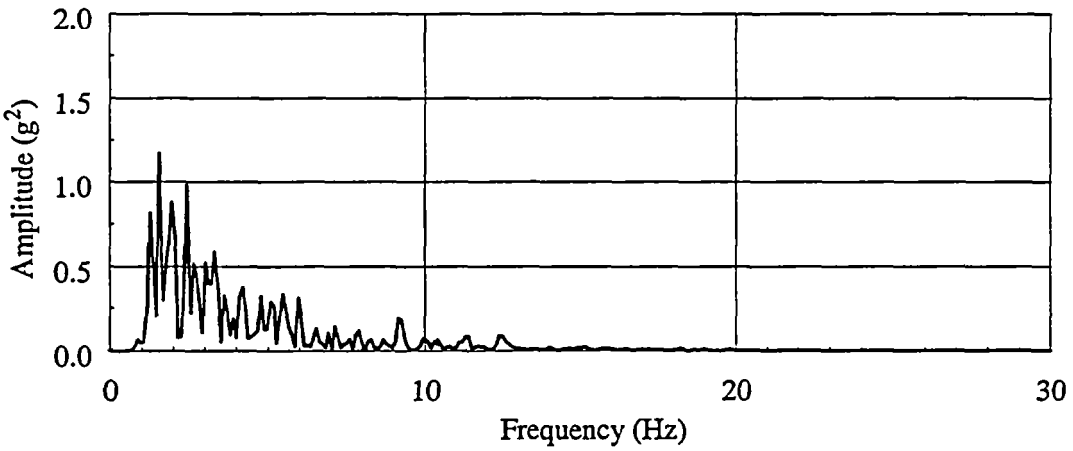

(b) Power spectrum

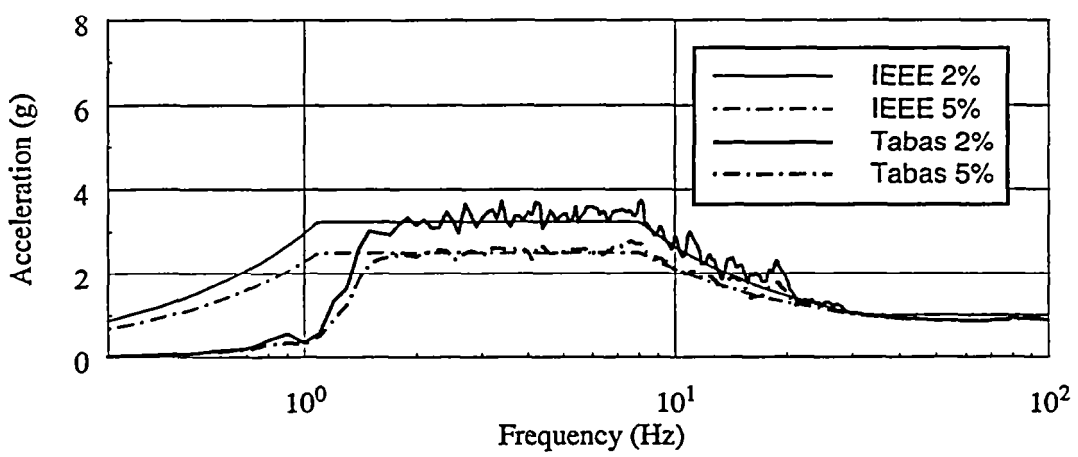

(c) Response spectrum

Figure 3-6 Acceleration history, power spectrum, and response spectra for the longitudinal (*X*-) component of the Tabas-A record

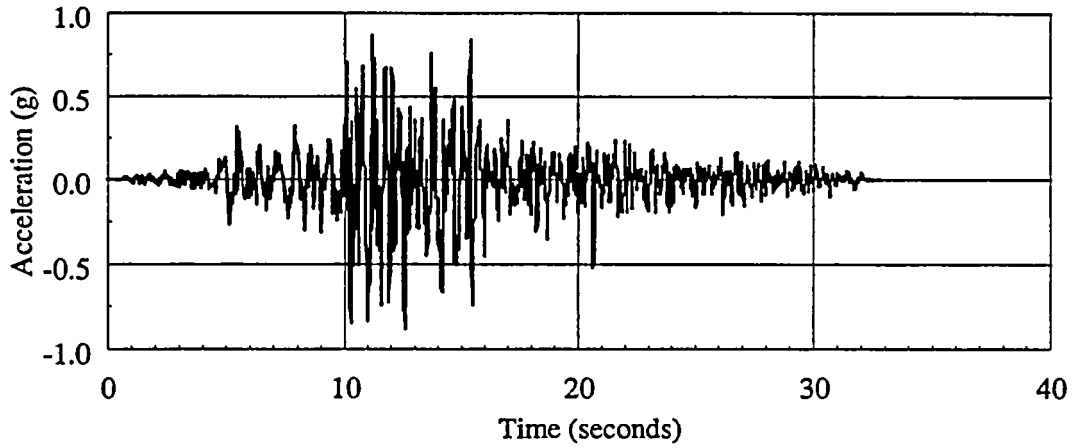

(a) Acceleration history

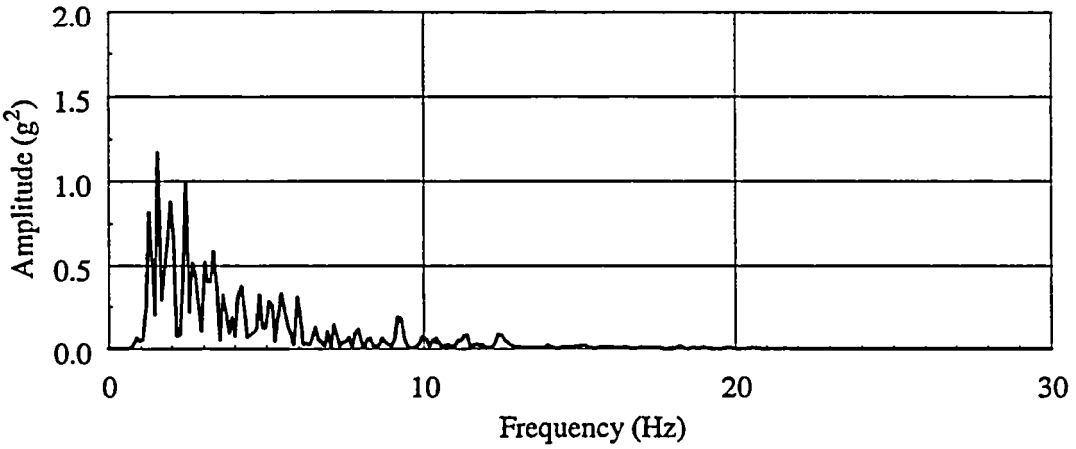

(b) Power spectrum

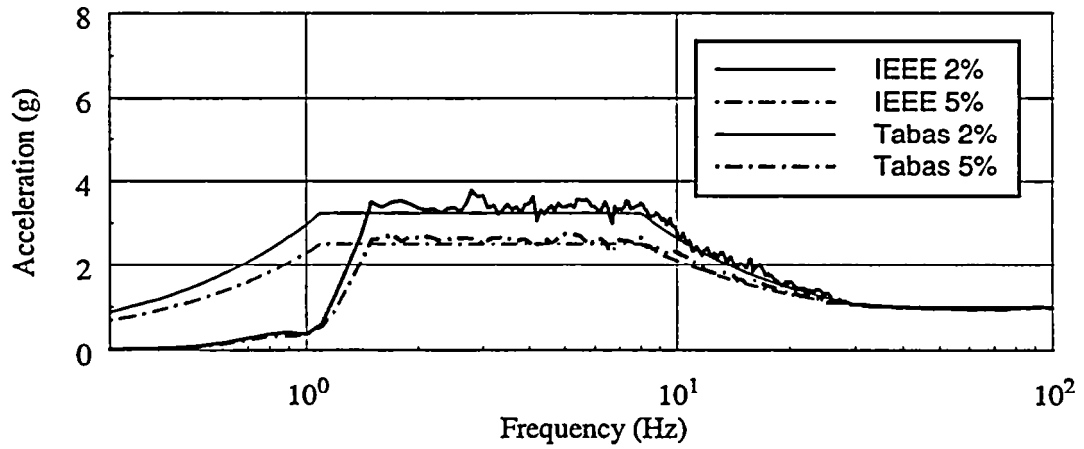

(c) Response spectrum

Figure 3-7 Acceleration history, power spectrum, and response spectra for the lateral (*Y*-) component of the Tabas-A record

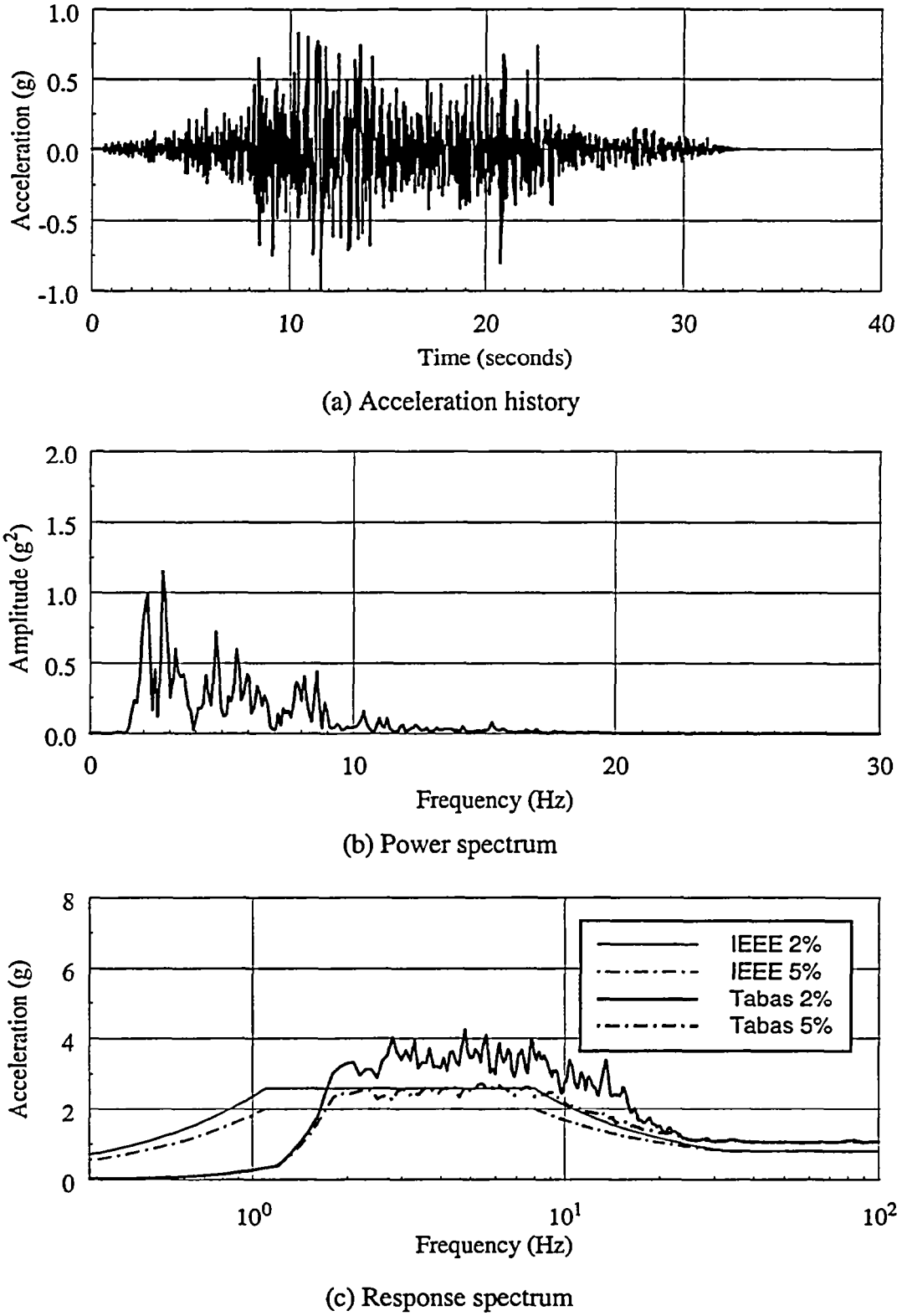

Figure 3-8 Acceleration history, power spectrum, and response spectra for the vertical (Z-) component of the Tabas-A record

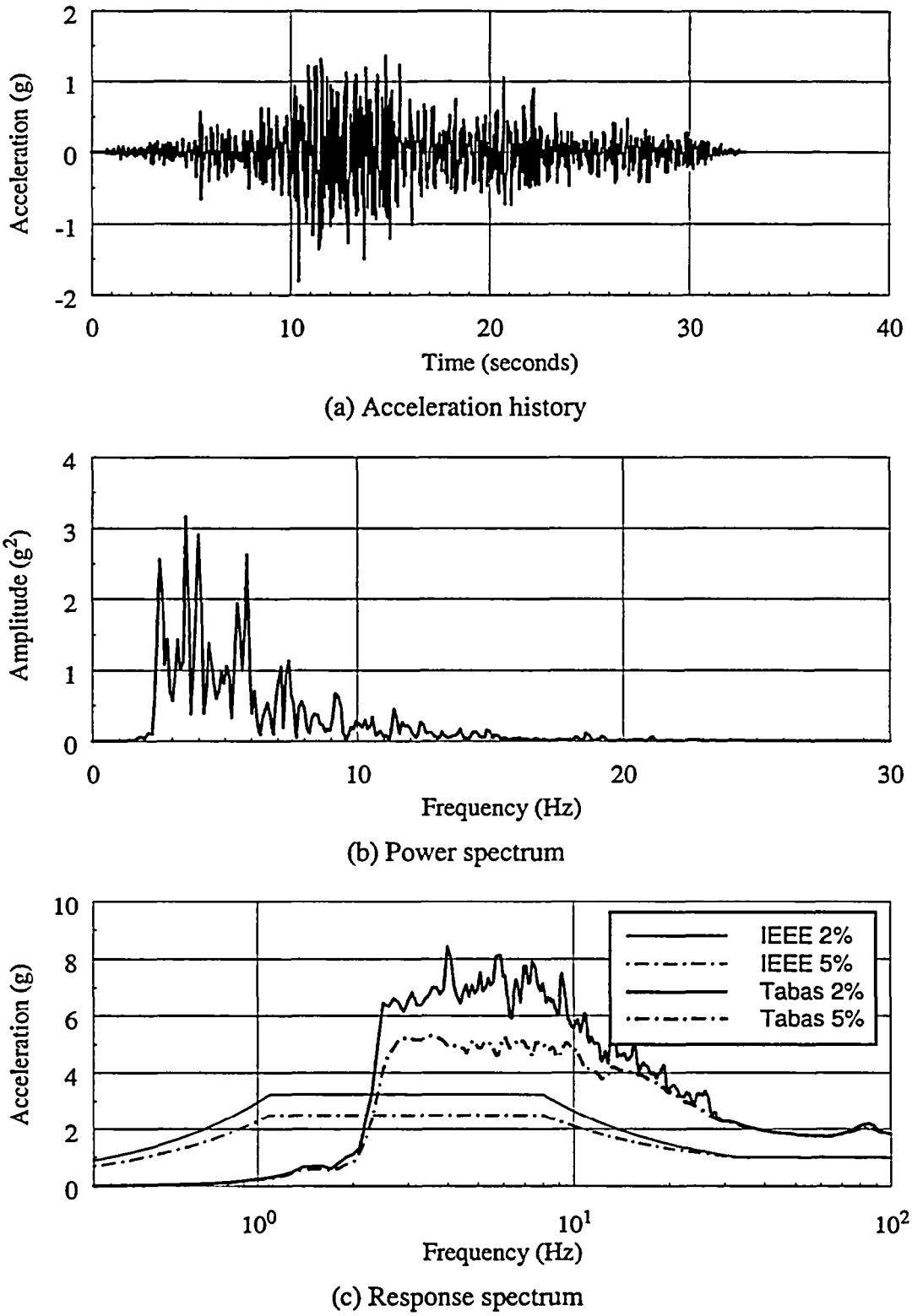

Figure 3-9 Acceleration history, power spectrum, and response spectra for the longitudinal (*X*-) component of the Tabas-B record

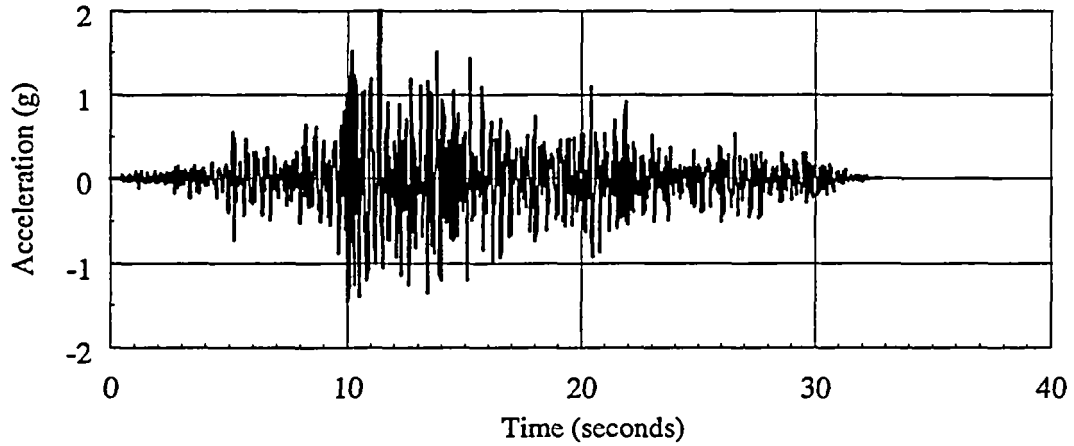

(a) Acceleration history

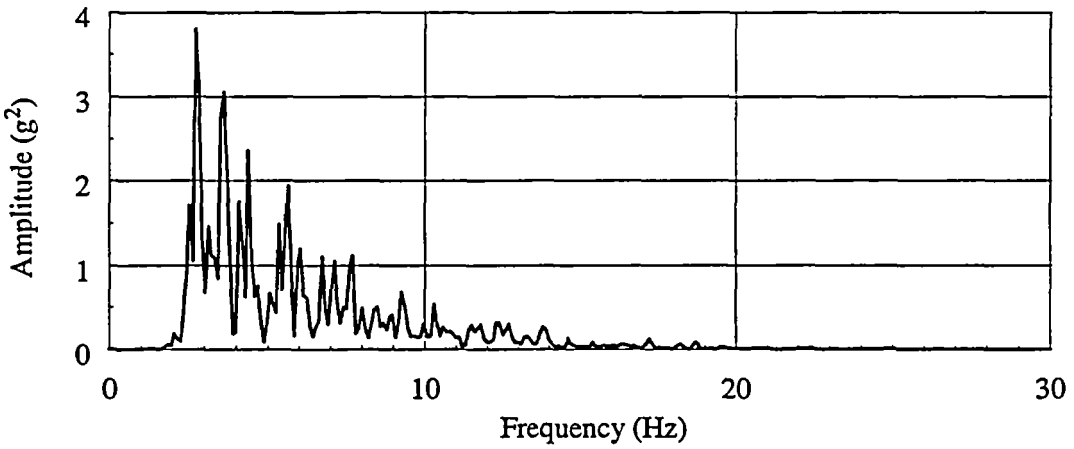

(b) Power spectrum

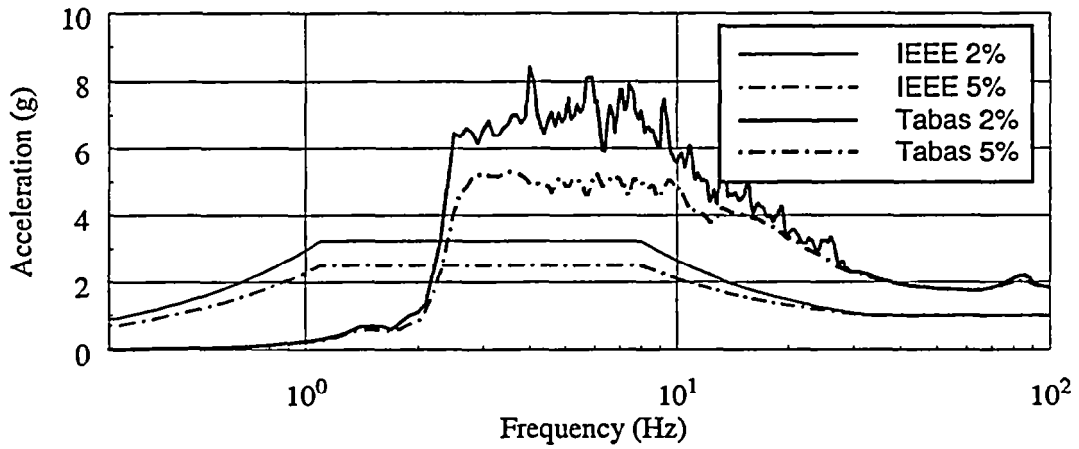

(c) Response spectrum

Figure 3-10 Acceleration history, power spectrum, and response spectra for the lateral (*Y*-) component of the Tabas-B record

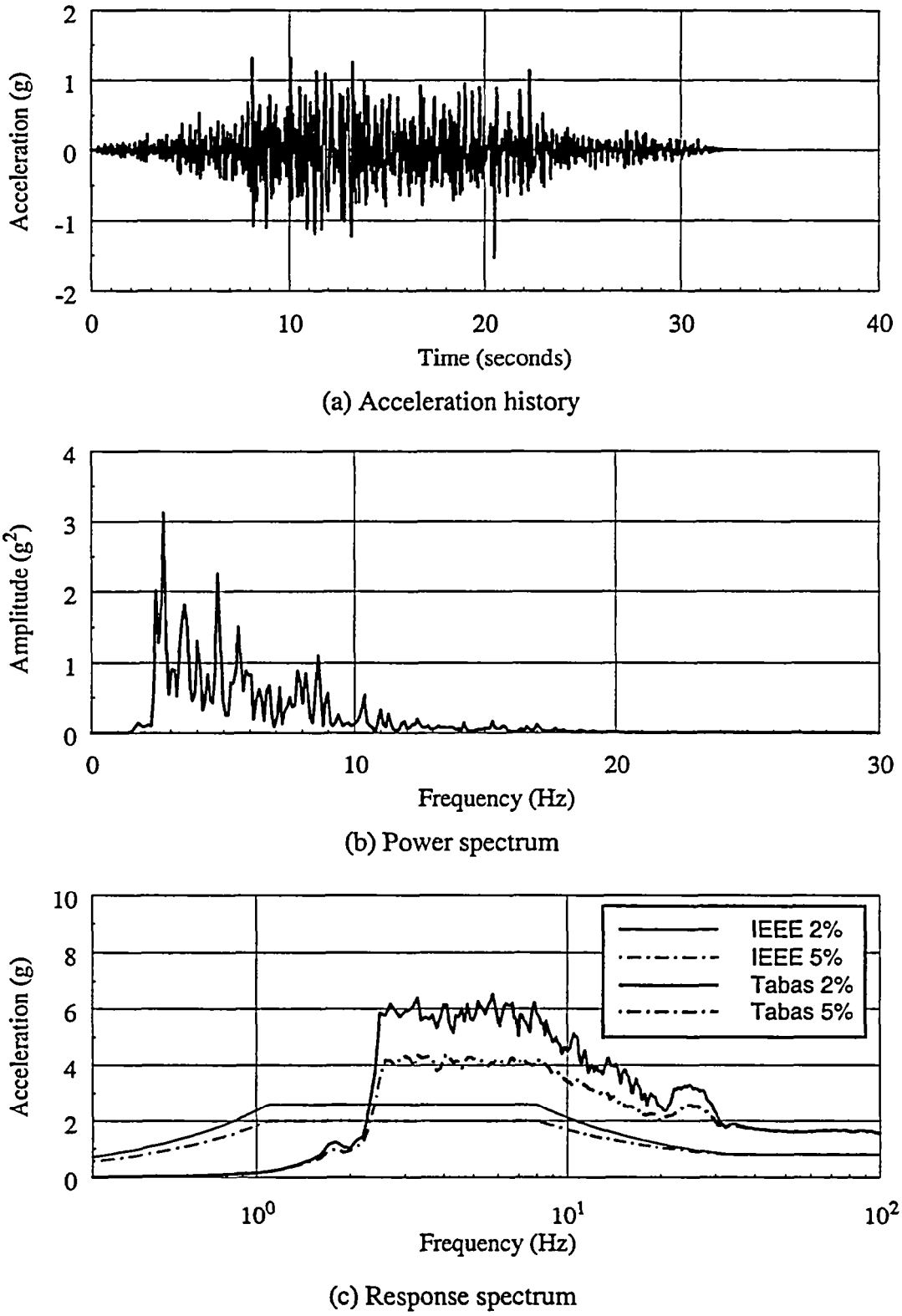

Figure 3-11 Acceleration history, power spectrum, and response spectra for the vertical (Z-) component of the Tabas-B record

4 Fragility Testing of Rigidly Mounted Bushings

4.1 Introduction

Triaxial earthquake simulator testing was used to evaluate the seismic response of the two 230-kV transformer bushings mounted on a *rigid* frame. The following sections describe the test setup, the earthquake motions used for the fragility tests, the instrumentation of the bushings, and selected test results.

4.2 Test Setup

4.2.1 Overview

The fragility tests of the two 230-kV bushings were conducted using the earthquake simulator. For testing, the bushings were placed in a *rigid* mounting frame, designed for the testing of bushings of sizes varying between 196 kV and 550 kV. Two sets of three-component spectrum-compatible input motions were developed for the fragility tests. For seismic testing, IEEE 693-1997 (see Appendix A) states that porcelain bushings must be instrumented to record (a) maximum vertical and horizontal accelerations at the top of the bushing, at the bushing flange, and at the top of the earthquake simulator platform, (b) maximum displacement of the top of the bushing relative to the flange, and (c) maximum porcelain stresses at the base of the bushing near the flange. The instrumentation scheme developed for the tests described in this chapter exceeded the IEEE 693-1997 requirements. The following sections provide a brief review of the test setup.

4.2.2 Earthquake simulator

The earthquake simulator at the Pacific Earthquake Engineering Research (PEER) Center at the University of California at Berkeley was used for the seismic evaluation of the bushings. The 20 ft by 20 ft (6.1 by 6.1 m) simulator has a maximum payload of 140 kips (623 kN) and can accommodate models up to 40 ft (12.2 m) in height. The six-degree-of-freedom simulator (three translations and three rotations) can be programmed to reproduce any waveform (e.g., sinusoidal, white-noise, earthquake history). The maximum horizontal displacement and velocity of the simulator are ±5 in. (±127 mm) and 25 in./sec (635 mm/sec), respectively.

4.2.3 Rigid mounting frame

IEEE 693-1997 (see Appendix A) states that bushings rated at 161 kV and above must be qualified using three-component earthquake-simulator testing. Because it is impractical to test bushings mounted on a transformer, IEEE 693-1997 specifies that bushings must be mounted on a rigid stand for earthquake testing and qualification. IEEE 693-1997 also recommends that a transformer bushing be tested at 20 degrees measured from the vertical because a bushing, if so tested and qualified, is assumed to be qualified for use on all transformers with angles from vertical to 20 degrees.

The mounting frame used for the fragility tests was a fully welded steel frame consisting of TS 5x5x3/8" (127x127x10 mm) columns, L 5x5x3/4" (127x127x19 mm) braces, and a 2.0-in. (51-mm) thick steel mounting plate (sloping at 20 degrees to the horizontal). The mounting frame was post-tensioned to the earthquake simulator platform using fifteen 1-in. (25-mm) diameter high-strength threaded rods. A special 1.5-in. (38-mm) adaptor plate was designed and fabricated to connect the flange plate of the 230-kV bushings to the support frame. Twelve 1-1/4 in. (32 mm) diameter high-strength (Grade 8, equivalent to A490 steel) bolts were used for the adaptor plate-to-mounting plate connection The flange of the bushing was joined to the adaptor plate with twelve 3/4 in. (19 mm) diameter Grade 2 steel bolts (equivalent to A307 steel) torqued to 100 ft-lb (136 N-m) per the field installation specification supplied by Elder (Elder, 1999). The support frame was designed to be extremely stiff to minimize the amplification of the simulator input to the bushing. Figure 4-1 shows one of the 230-kV bushings installed in the mounting frame atop the earthquake simulator.

4.2.4 Earthquake ground motions

IEEE 693-1997 requires that experimental testing of bushings include: (a) resonant-search tests to identify the dynamic properties of the bushings and (b) triaxial earthquake ground motions tests for bushing qualification and fragility testing.

4.2.4.1 Resonant-search tests

Sine-sweep and broad band white-noise tests were used to establish the dynamic characteristics (natural frequencies and damping ratios) of the bushings. These so-called *resonant-search* tests were undertaken using unidirectional excitation along each global axis of the earthquake simulator platform. For both sine-sweep and white-noise tests, a simulator input acceleration amplitude of 0.1g was used.

4.2.4.2 Earthquake test response spectrum

IEEE 693-1997 identifies several response spectra of identical shape but different amplitudes for the qualification of transformer bushings. For a detailed description of these spectra, the reader is referred to Appendix A. Figure 4-2 shows an IEEE 693-1997 High Level qualification response spectrum used for checking porcelain stresses and oil leakage. The spectrum is anchored to a peak ground acceleration (PGA) equal to 2.0g. Spectrum-compatible earthquake histories were generated using the procedures set forth in Section 3.2.3.

Two separate and independent three-component records were utilized for fragility testing. The Tabas-A motion was used for all the tests up to and including motions with target PGAs of 1.0g. The Tabas-B motion was used for all tests with a target PGA exceeding 1.0g but less than 2.0g.

4.2.5 Instrumentation

The instrumentation scheme developed for the tests described in this chapter included 52 transducers and 54 channels of data. Table 4-1 lists the channel number, instrument type, response quantity, coordinate system, and location for each transducer. Figure 4-3 presents information on the instrumentation of the earthquake simulator platform (Figure 4-3a), the bushing and the mounting frame (Figure 4-3b), and the porcelain unit immediately above the flange (UPPER-1) of the bushing (Figure 4-3c). The global *(X, Y, Z)* and local *(x, y, z)* coordinate systems adopted for the testing program are shown in the figure. Figure 4-4 shows the instrumentation at the top of Bushing-1. Figure 4-5 is a photograph of the instrumentation immediately above the flange plate for this bushing.

Sixteen channels (channels 3 through 18) recorded the acceleration and displacement of the earthquake simulator platform in the global coordinate system. The accelerations of the mounting frame in the local coordinate system (channels 28, 29, and 30) and the absolute displacements of the mounting frame in the global coordinate system (channels 37 and 38) were recorded. The accelerations of the bushing in the local coordinate system (channels 19 through 27) and the absolute displacements of the bushing in the global coordinate system (channels 31 through 36) were measured at the top, midheight, and bottom of the bushing. Four strain gages (channels 39 through 42) monitored the axial strains in the UPPER-1 porcelain unit immediately above the gasket. Four displacement transducers (channels 43 through 46), located immediately below the gasket, measured the radial slip of the flange plate relative to the support frame. Another four displacement transducers (channels 47 through 50), located immediately above the gasket, measured radial slip of the UPPER-1 porcelain unit relative to the support frame. The relative slip of the porcelain over the flange plate was computed using these eight transducers. Four displacement transducers (channels 51 through 54) recorded vertical displacements of the UPPER-1 porcelain unit across the gasket, parallel to the local *z*- axis of the bushing.

4.3 Summary of Experimental Data

4.3.1 Overview

The objective of the testing program described in this chapter was to evaluate the seismic behavior of *rigidly* mounted 230-kV transformer bushings by testing Bushing-1 and Bushing-2 to motions with target PGAs of up to 2.0g. The list of earthquake tests and key observations for Bushing-1 and Bushing-2 are presented in Table 4-2 and Table 4-3, respectively. After each earthquake test, the response data were analyzed, the bushing was inspected for damage and oil leakage, and the bolts joining the bushing flange plate to the adaptor plate, and the adaptor plate to the mounting plate, were checked for tightness. All bolts were found to be tight for all tests. The

following sections summarize the dynamic properties and the seismic response of the bushings. Section 4.3.2 discusses the dynamic properties of the two bushings and Section 4.3.3 presents fragility data for Bushing-1 and Bushing-2. Section 4.3.4 describes the response of Bushing-2 to harmonic excitation.

Table 4-1 Instrumentation for rigidly mounted 230-kV bushings

Channel Number	*Transducer*[1]	*Response Quantity*	*Coordinate System and Orientation*[2]	*Transducer Location*[3]
1	-	date	-	-
2	-	time	-	-
3	LVDT	platform displacement	global *X*	simulator platform
4	LVDT	platform displacement	global *Y*	simulator platform
5	LVDT	platform displacement	global *X*	simulator platform
6	LVDT	platform displacement	global *Y*	simulator platform
7	LVDT	platform displacement	global *Z*	simulator platform
8	LVDT	platform displacement	global *Z*	simulator platform
9	LVDT	platform displacement	global *Z*	simulator platform
10	LVDT	platform displacement	global Z	simulator platform
11	A	platform acceleration	global *X*	simulator platform
12	A	platform acceleration	global *X*	simulator platform
13	A	platform acceleration	global *Y*	simulator platform
14	A	platform acceleration	global *Y*	simulator platform
15	A	platform acceleration	global *Z*	simulator platform
16	A	platform acceleration	global *Z*	simulator platform
17	A	platform acceleration	global *Z*	simulator platform
18	A	platform acceleration	global Z	simulator platform
19	A	bushing acceleration	local *x*	bottom of bushing
20	A	bushing acceleration	local *y*	bottom of bushing
21	A	bushing acceleration	local *z*	bottom of bushing
22	A	bushing acceleration	local *x*	midheight of bushing
23	A	bushing acceleration	local *y*	midheight of bushing
24	A	bushing acceleration	local *z*	midheight of bushing
25	A	bushing acceleration	local *x*	top of bushing
26	A	bushing acceleration	local *y*	top of bushing
27	A	bushing acceleration	local *z*	top of bushing

Table 4-1 Instrumentation for rigidly mounted 230-kV bushings

Channel Number	*Transducer*[1]	*Response Quantity*	*Coordinate System and Orientation*[2]	*Transducer Location*[3]
28	A	frame acceleration	local *x*	top of mounting frame
29	A	frame acceleration	local *y*	top of mounting frame
30	A	frame acceleration	local *z*	top of mounting frame
31	LP	bushing displacement	global *X*	bottom of bushing
32	LP	bushing displacement	global *Y*	bottom of bushing
33	LP	bushing displacement	global *X*	midheight of bushing
34	LP	bushing displacement	global *Y*	midheight of bushing
35	LP	bushing displacement	global *X*	top of bushing
36	LP	bushing displacement	global *Y*	top of bushing
37	LP	frame displacement	global *X*	top of mounting frame
38	LP	frame displacement	global *Y*	top of mounting frame
39	SG	porcelain strain	local *z*	gasket connection
40	SG	porcelain strain	local *z*	gasket connection
41	SG	porcelain strain	local *z*	gasket connection
42	SG	porcelain strain	local *z*	gasket connection
43	DCDT	flange plate slip	relative to frame	gasket connection
44	DCDT	flange plate slip	relative to frame	gasket connection
45	DCDT	flange plate slip	relative to frame	gasket connection
46	DCDT	flange plate slip	relative to frame	gasket connection
47	DCDT	UPPER-1 slip	relative to frame	gasket connection
48	DCDT	UPPER-1 slip	relative to frame	gasket connection
49	DCDT	UPPER-1 slip	relative to frame	gasket connection
50	DCDT	UPPER-1 slip	relative to frame	gasket connection
51	DCDT	UPPER-1 uplift	relative to frame	gasket connection
52	DCDT	UPPER-1 uplift	relative to frame	gasket connection
53	DCDT	UPPER-1 uplift	relative to frame	gasket connection
54	DCDT	UPPER-1 uplift	relative to frame	gasket connection

1. A = accelerometer; LVDT = displacement transducer; LP = linear potentiometer; SG = strain gage; DCDT = displacement transducer.
2. For the local (*x*-, *y*-, *z*-) and global (*X*- *Y*- *Z*-) coordinate systems see Figure 4-3.
3. For transducer locations on the bushings see Figure 4-3.

Table 4-2 Summary of earthquake testing of Bushing-1

Test No.	*Test Date*	*Identification*[1]	*PGA*[2]	*Comments*
1	4/6/99	WN-X	0.1g	Data scanned at 100 Hz.
2	4/6/99	WN-Y	0.1g	
3	4/6/99	WN-Z	0.1g	
4	4/6/99	SS-X	0.1g	
5	4/6/99	SS-Y	0.1g	
6	4/6/99	SS-Z	0.1g	
7	4/6/99	Tabas-A	0.1g	
8	4/7/99	Tabas-A	0.2g	Scan rate increased to 200 Hz.
9	4/7/99	Tabas-A	0.3g	
10	4/7/99	Tabas-A	0.5g	
11	4/7/99	Tabas-A	0.7g	
12	4/7/99	Tabas-A	1.0g	Spectrum equivalent to moderate-level qualification.
13	4/7/99	Tabas-B	1.2g	
14	4/7/99	Tabas-B	1.4g	
15	4/7/99	Tabas-B	1.6g	
16	4/7/99	Tabas-B	1.8g	
17	4/7/99	Tabas-B	2.0g	Spectrum equivalent to high-level qualification.
18	4/7/99	SS-X	0.1g	
19	4/7/99	SS-Y	0.1g	
20	4/7/99	SS-Z	0.1g	

1. WN = white-noise, SS = sine-sweep; *-X*, *-Y*, and *-Z* denote direction of testing in global coordinate system; Tabas-A = spectrum-compatible Tabas-A earthquake histories; Tabas-B = spectrum-compatible Tabas-B earthquake histories.

2. PGA = target peak acceleration of the simulator platform.

For all tests, the transducer response histories were processed using the computer program Matlab (Mathworks, 1999). Experimental histories were low-passed filtered using a rectangular filter with a cut-off frequency of 40 Hz and then zero-corrected.

Table 4-3 Summary of earthquake testing of Bushing-2

Test No.	*Test Date*	*Identification*[1]	*PGA*[2]	*Comments*
1	5/10/99	WN-X	0.1g	Data scanned at 200 Hz.
12	5/11/99	WN-Y	0.1g	Data scanned at 100 Hz.
13	5/11/99	WN-Z	0.1g	
14	5/11/99	SS-X	0.1g	
15	5/11/99	SS-Y	0.1g	
16	5/11/99	SS-Z	0.1g	
18	5/11/99	Tabas-A	0.5g	
19	5/11/99	Tabas-A	1.0g	Spectrum equivalent to moderate-level qualification.
20	5/11/99	Tabas-B	1.2g	
21	5/11/99	Tabas-B	1.4g	
22	5/11/99	Tabas-B	1.6g	
23	5/11/99	Tabas-B	1.8g	
24	5/11/99	Tabas-B	2.0g	Spectrum equivalent to high-level qualification.
25	5/11/99	5 Hz-X	2.0g	Bushing leaked oil at the gasket connection.
26	5/11/99	WN-X	0.1g	
27	5/11/99	WN-Y	0.1g	
28	5/11/99	WN-Z	0.1g	
29	5/11/99	Tabas-A	1.0g	Spectrum equivalent to moderate-level qualification, no oil leakage.
30	5/11/99	Tabas-B	2.0g	Spectrum equivalent to high-level qualification, no oil leakage.
31	5/11/99	WN-X	0.1g	Added terminal to top of bushing, see Figure 4-6.
32	5/11/99	WN-Y	0.1g	
33	5/11/99	WN-Z	0.1g	
34	5/11/99	Tabas-A	1.0g	Spectrum equivalent to moderate-level qualification, no oil leakage.
35	5/11/99	Tabas-B	2.0g	Spectrum equivalent to high-level qualification, no oil leakage.
36	5/11/99	5 Hz-X	1.0g	
37	5/11/99	5 Hz-X	2.0g	No oil leakage.
38	5/11/99	5 Hz-X	2.0g	Removed terminal prior to testing; bushing leaked oil and porcelain slipped noticeably, see Figure 4-7.

1. WN = white-noise, SS = sine-sweep; *-X*, *-Y*, and *-Z* denote direction of testing in global coordinate system; Tabas-A = spectrum-compatible Tabas-A earthquake histories; Tabas-B = spectrum- compatible Tabas-B earthquake histories; 5 Hz = 20-cycle constant-amplitude harmonic input.

2. PGA = target peak acceleration of the simulator platform.

4.3.2 Dynamic properties of rigidly mounted 230-kV bushings

Sine-sweep and white-noise tests were used to calculate the modal frequencies and damping ratios for the bushings. Figure 4-8 and Figure 4-9 show the transfer functions between the top of the bushing and the mounting frame in the three local directions (*x, y, z*) for Bushing-1 and Bushing-2, respectively. These tests were conducted prior to the earthquake tests. The resonant frequency in the local *x*- and *y*-directions were approximately 20 Hz and 18 Hz, respectively. Damping ratios of between 2 to 3 percent of critical were obtained using the half-power bandwidth method.

Table 4-4 summarizes the measured dynamic properties of the bushings in the *x*- and *y*-directions. Modal data could not be determined for the local *z*-direction. Three key observations are: (1) the modal frequencies differ slightly in the *x*- and *y*- directions due to the unsymmetrical distribution of lifting lugs immediately above the flange plate; (2) although Bushing-2 leaked oil during Test Number 25, the modal properties of the bushing measured immediately after leakage (Test Set 26-31) do not differ from the properties measured prior to earthquake simulator testing (Test Set 1 and 12-16); and (3) the addition of the 64-lb (280-N) terminal and its 11-lb (50-N) attachment to the top of the bushing introduced a second vibration frequency to the bushing response and reduced the first mode frequencies of the bushing in the *x*- and *y*- directions significantly.

Table 4-4 Modal properties of bushings from resonance-search tests

		Frequency (Hz)		*Damping Ratio (% critical)*	
Bushing	*Test Set*	*x-direction*	*y-direction*	*x-direction*	*y-direction*
1	1-6	20	18	2	2
1	18-20	20	18	3	2
2	1, 12-16	20	18	3	2
2	26-28	20	18	3	2
2	31-33	14[1]	13[1]	3	3

1. During the tests with the terminal attached to the top of bushing, a second mode frequency of 26.5 Hz was evident in the *x*- and *y*- directions.

4.3.3 Earthquake testing of Bushing-1 and Bushing-2

4.3.3.1 Introduction

The following subsections present peak responses of Bushing-1 and Bushing-2 and local response characteristics of the bushings measured at the junction of the UPPER-1 porcelain unit and the flange plate.

4.3.3.2 Peak responses

The peak acceleration, relative displacements, and strain responses of the bushings are presented in Table 4-5. Only the peak responses at the top of bushings are reported; the maximum acceleration responses at the bottom of the bushings were of the same order as than those at the top and the accelerations at midheight were smaller than the values measured at either the top or the bottom of bushings. The values of peak absolute accelerations are defined as the maximum of the vector sum of acceleration components in the local *x*- and local *y*- directions, evaluated from acceleration histories. Similarly, the values of peak relative displacements (relative to the mounting frame) are defined as the maximum of the vector sum of relative displacement components in the global *X*- and local *Y*- directions, evaluated from displacement histories. The values of maximum strain were computed from measured porcelain strains (channels 39 through 42); the largest maximum value is tabulated.

Although, the target PGAs are listed in increasing order in Table 4-5, the tabulated response values do not necessarily increase in a corresponding manner. Among the factors contributing to this variation are the temperature-dependent dynamics of the simulator's hydraulic system, interaction between the simulator platform and bushing-support system, simulator rotational accelerations, and the phase difference between the *x*- (or *X-)* and *y*- (or *Y-*) components of response used to compute the vector sum of the response.

4.3.3.3 Response of Bushing-1

The global response of Bushing-1 was assessed by analysis of data from Test Number 12 (Tabas-A, target PGA equal to 1.0g) and Test Number 17 (Tabas-B, target PGA equal to 2.0g).

During Test Number 12, a maximum acceleration and relative displacement of 3.9g and 0.17 in. (4 mm) were recorded at the top of the bushing, respectively. (see Table 4-5). Acceleration response spectra for Bushing-1 in the local coordinate system, generated using measured acceleration histories at the flange are shown in Figure 4-10. For information, the 2-percent and 5-percent damped IEEE 693-1997 response spectra for Moderate Level qualification are also shown in this figure. In the range of the fundamental frequency of the bushing (18-20 Hz), the computed spectral accelerations exceed the IEEE 693-1997 ordinates for Moderate Level qualification.

During Test Number 17, a maximum acceleration and relative displacement of 6.0g and 0.40 in. (10 mm) were recorded at the top of the bushing, respectively. (see Table 4-5). Acceleration response spectra for Bushing-1 in the local coordinate system, generated using measured acceleration histories at the flange are shown in Figure 4-11. For information, the 2-percent and 5-percent damped IEEE 693-1997 response spectra for High Level qualification are also shown in this figure. In the range of the fundamental frequency of the bushing, the computed spectral accelerations exceed the IEEE 693-1997 ordinates for High Level qualification.

Table 4-5 Peak responses of the bushings

Bushing	*Test No.*	*Identification*[1]	*PGA*[2]	*Peak Acceleration (g)*	*Peak Relative Displacement (mm)*	*Peak Porcelain Strain (με)*
1	7	Tabas-A	0.1g	1.2	1.3	3
1	8	Tabas-A	0.2g	2.0	2.3	4
1	9	Tabas-A	0.3g	3.0	2.6	7
1	10	Tabas-A	0.5g	3.3	3.6	7
1	11	Tabas-A	0.7g	3.2	3.3	8
1	12	Tabas-A	1.0g	3.9	4.3	9
1	13	Tabas-B	1.2g	3.9	5.3	8
1	14	Tabas-B	1.4g	4.5	7.6	9
1	15	Tabas-B	1.6g	4.5	8.9	8
1	16	Tabas-B	1.8g	4.5	9.7	8
1	17	Tabas-B	2.0g	6.0	10.2	11
2	18	Tabas-A	0.5g	3.8	3.0	8
2	19	Tabas-A	1.0g	3.9	4.1	10
2	20	Tabas-B	1.2g	4.3	5.8	12
2	21	Tabas-B	1.4g	3.9	7.1	13
2	22	Tabas-B	1.6g	4.6	8.9	11
2	23	Tabas-B	1.8g	5.1	9.9	10
2	24	Tabas-B	2.0g	5.7	9.8	12
2	29	Tabas-A	1.0g	3.6	4.3	11
2	30	Tabas-B	2.0g	5.4	9.7	19
2	34	Tabas-A	1.0g	2.8	5.8	12
2	35	Tabas-B	2.0g	4.6	14.0	29

1. Tabas-A = spectrum-compatible Tabas-A earthquake histories; Tabas-B = spectrum-compatible Tabas-B earthquake histories

2. PGA = target peak acceleration of the simulator platform

Figure 4-12a shows the relation between the average vertical displacement in the local z-direction and rocking about the local y-axis. The average vertical displacement in the z-direction was calculated as one-half of the corrected, to the face of the bushing, sum of the channel 51 and channel 53 displacements. Rocking about the local y-axis was calculated as the difference between the channel 51 and 53 displacements divided by the 25-in. (635-mm) distance between these transducers. Figure 4-12b shows the relation between the average vertical displacement in the local z-direction and rocking about the local x-axis. The average vertical displacement in the z-direction was calculated as one half of the sum of the channel 52 and channel 54 displacements; the rocking about the local x-axis was calculated as the difference between the channel 52 and 54 displacements divided by the 25-in. (635-mm) distance between these transducers. The maximum uplift at the edge of porcelain unit can be computed by adding the product of the rocking angle and the radius of the UPPER-1 porcelain unit, at the flange plate, to the average longitudinal displacement.

Figure 4-13 presents the zero-corrected displacement orbit of the center of the bushing, measured at the height of the radial displacement transducers, relative to the flange plate. Shear deformation in the gasket and slip of UPPER-1 porcelain over the gasket contribute to the measured displacement. The maximum value of this displacement is approximately 0.02 in. (0.5 mm).

4.3.3.4 Response of Bushing-2

The global response of Bushing-2 was assessed by analysis of data from Test No 19 (Tabas-A, target PGA equal to 1.0g) and Test No 24 (Tabas-B, target PGA equal to 2.0g).

During Test No 19, a maximum acceleration and relative displacement of 3.9g and 0.16 in. (4 mm) were recorded at the top of the bushing, respectively. (see Table 4-5). Acceleration response spectra for Bushing-2 in the local coordinate system, generated using measured acceleration histories at the flange are shown in Figure 4-14. For information, the 2-percent and 5-percent damped IEEE 693-1997 response spectra for Moderate Level qualification are also shown in this figure. In the range of the fundamental frequency of the bushing (18-20 Hz), the computed spectral accelerations exceed the IEEE 693-1997 ordinates for Moderate Level qualification.

During Test No 24, a maximum acceleration and relative displacement of 6.0g and 0.38 in. (10 mm) were recorded at the top of the bushing, respectively. (see Table 4-5). Acceleration response spectra for Bushing-2 in the local coordinate system, generated using measured acceleration histories at the flange are shown in Figure 4-15. For information, the 2-percent and 5-percent damped IEEE 693-1997 response spectra for High Level qualification are also shown in this figure. In the range of the fundamental frequency of the bushing, the computed spectral accelerations exceed the IEEE 693-1997 ordinates for High Level qualification.

Figure 4-16a shows the relation between the average vertical displacement in the local z-direction and rocking about the local y-axis. Values of displacement and rocking were computed per Section 4.3.3.3.

Figure 4-17 presents the zero-corrected displacement orbit of the center of the bushing, measured at the height of the radial displacement transducers, relative to the flange plate. Shear deformation in the gasket and slip of UPPER-1 porcelain over the gasket contribute to the measured displacement. The maximum value of this displacement is less than 0.02 in. (0.4 mm).

4.3.3.5 Evaluation of seismic response of bushings

Neither bushing was designated for seismic qualification as part of this study. However, when mounted on a stiff frame, both bushings withstood severe shaking compatible with IEEE 693-1997 spectrum for High Level qualification. In the range of the fundamental frequency of the bushings (18-20 Hz), the computed spectral accelerations exceeded the recommended IEEE 693-1997 ordinates for High Level qualification (see Figures 4-11 and 4-15). For these tests, there was no structural damage and no oil leakage, and the recorded stresses in the UPPER-1 porcelain unit were substantially smaller than the ultimate values (see Table 4-5). Bushing-1 and Bushing-2 were therefore qualified by test to the High Level.

4.3.4 Response of Bushing-2 to harmonic excitations

4.3.4.1 Overview

At the request of the utilities, Bushing-2 was subjected to four constant-amplitude unidirectional (*X*-direction) harmonic motions. Although such input is neither representative of earthquake shaking nor the type of motion typically used for qualification and fragility testing of bushings, these tests were undertaken to complement the triaxial earthquake tests, because the IEEE-required High Level qualification time history tests for the *rigidly* mounted bushing were not severe enough to reproduce the bushing failures observed in the field during moderate to severe earthquakes.

The input displacement for the harmonic tests took the form:

$$d(t) = d_o \sin(2\pi f t) \tag{4-1}$$

where, $d(t)$ is the time-dependent simulator platform displacement, d_o is the simulator platform displacement amplitude, and f is the frequency (= 5 Hz) of the harmonic signal.

For the three high-amplitude harmonic tests (Test Nos 25, 37, and 38), the maximum target velocity of the harmonic signal was set at 25 in./sec (635 mm/sec) to avoid exceeding the velocity limits of the earthquake simulator. The corresponding target displacement and acceleration amplitudes were 0.8 in. (20 mm) and 2.0g, respectively. Each test was four seconds (20 cycles) long.

For the low-amplitude harmonic test (Test No 36), the amplitude of input signal was one half of the amplitude of the high-level tests.

4.3.4.2 Summary of bushing response

Bushing-2 was subjected to three identical, 5-Hz harmonics with a target peak simulator acceleration of 2.0g (Test Nos 25, 37, and 38). For one of these tests (Test No 37) a terminal was attached to the top of the bushing. For the other two tests (Test Nos 25 and 38), the terminal was not attached. Oil leakage was observed during Test No 25. Oil leakage and significant slip of the UPPER-1 porcelain unit were observed during Test No 38. When the terminal was not attached to the bushing, the fundamental frequency of the bushing in the x- direction (as measured at the top of the bushing) was approximately 20 Hz. When the terminal was attached to the bushing dome, the fundamental frequency of the bushing in the x-direction (as measured at the top of the bushing) dropped to approximately 14 Hz and an additional mode with a frequency of 26.5 Hz was identified (see Table 4-4).

4.3.4.3 Peak responses

The recorded test data were used to compute the peak acceleration and displacement responses of Bushing-2 relative to the mounting frame and peak values of slip, uplift, and stress for the UPPER-1 porcelain unit. These values are presented in Table 4-6. The values of peak absolute accelerations are defined as the maximum of the vector sum of acceleration components in the local x- and local y- directions, evaluated from the acceleration histories. Similarly, the values of peak relative displacements (relative to the mounting frame) are defined as the maximum of the vector sum of the relative displacement components in the global X- and local Y- directions, evaluated from the displacement histories. The peak values for porcelain slip, uplift, and strain were computed as the largest value of porcelain slip (channels 47 through 50), porcelain uplift (channels 51 through 54), and porcelain stress (channels 39 through 42).

Table 4-6 Peak responses of Bushing-2 to the high-amplitude 5-Hz harmonic tests

	Peak Acceleration (g)			*Peak Relative Displacement (mm)*			*Slip (mm)*	*Uplift (mm)*	*Stress*[2] *(MPa)*
Test No.[1]	*Top*	*Midheight*	*Bottom*	*Top*	*Midheight*	*Bottom*			
25	5.9	NA[3]	6.0	22	20	5	0.2	2	7
37	5.4	NA	5.3	11	16	5	0.1	0.5	1
38	6.0	NA	5.9	33	31	4	0.9	2	17

1. Terminal attached to the bushing for Tests 31 to 37 only.
2. Stress is computed by multiplying measured strain by porcelain elastic modulus (assumed 97,000 MPa).
3. NA designates not available.

It is evident from Table 4-6 that when the terminal was not attached to the top of the bushing, the bushing experienced large accelerations at its top and bottom, and that the relative displacement (relative to the mounting frame) at the top and midheight of the bushing were significantly larger than the motion at the bottom of the bushing. At the gasket connection, large values of porcelain

stress, slip, and uplift were recorded. When the terminal was attached to the bushing, large accelerations were measured at the top and bottom of the bushing and the relative displacement at the bushing midheight was larger than the motion at the top. At the gasket connection, porcelain stress, slip, and uplift were all small.

To investigate the response of Bushing-2, data from Test Nos 37 and 38 were selected for further analysis.

4.3.4.4 Response of the simulator platform

Figure 4-18 presents the simulator response for a six-second segment of the harmonic tests from Test No 37. The simulator response from test No 38 was similar. The average simulator displacement history in the *x*- direction (Figure 4-18a) was calculated as one half of the sum of the channel 3 and channel 5 displacements. The average simulator translational acceleration history in the *x*- direction (Figure 4-18c) was calculated as one half of the sum of the channel 11 and channel 12 accelerations. The average frame translational acceleration history in the *x*- direction caused by the simulator rotational accelerations or pitch (about the *y*- axis) was computed by linearly combining the vertical accelerometer measurements (channels 15 through 18), dividing the computed value by the 192-in. (4.9-m) distance between these accelerometers, and multiplying the resulting value by the 73-in. (1.8-m) distance between the top of the platform and the top of the mounting frame (Figure 4-18e).

Although the desired target input motion for the harmonic tests was a constant-amplitude single-harmonic displacement history along the *x*-axis of the simulator (Figures 4-18a and b), the input histories were distorted because of the oil-column resonance in the vertical actuators. The simulator histories included harmonics of the target 5-Hz frequency and rotational accelerations. Examination of the simulator translational acceleration along the *x*-axis (Figure 4-18d) shows that the input acceleration history included harmonics of the 5-Hz input at 15 and 25 Hz. Examination of the simulator rotational acceleration about the *y*-axis (scaled and shown in Figure 4-18e as the *x*-acceleration at top of the mounting frame) shows rotational accelerations and harmonics of the 5-Hz target frequency (Figure 4-18f).

Figure 4-19 shows the 2-percent damped acceleration spectra for the recorded harmonic signal and the target harmonic signal. For reference, the 2-percent damped IEEE 693-1997 response spectrum for high-level qualification is also shown. *Rigidly* mounted Bushing-1 has a fundamental frequency of 20 Hz. At this frequency, the acceleration ordinate for the IEEE 693-1997 spectrum is 3g, and is labeled as point A in the figure. If the bushing had been subjected to target history, the bushing acceleration would have been 2.6g. However, the acceleration ordinate calculated using the measured response of the simulator platform was 9g (point C in the figure) — three times greater than the IEEE 693-1997 ordinate. This large spectral acceleration caused the oil leakage and slip of the UPPER-1 porcelain unit observed during Test Nos 25 and 38.

4.3.4.5 Response of the bushing

The zero-corrected acceleration histories for the bushing along the x-axis were studied by examining a six-second segment of the data from channels 19 and 25. The acceleration data for the test without the terminal is shown in Figure 4-20 and the acceleration data for the test with the terminal is shown in Figure 4-21. The peak acceleration at the top and bottom of the bushing for both tests exceeded 5g. For Test No 38 (test without the terminal), the acceleration histories were out-of-phase as shown by the large amplitude of the difference in the acceleration at the top and bottom of bushing; the power spectrum had a peak at 5 Hz and a larger peak at 15 Hz. For Test No 37 (test with the terminal), acceleration histories were nearly in-phase as shown by the much smaller amplitude of the difference between the acceleration at the top and bottom of bushing; the power spectrum had a peak at 5 Hz and a smaller peak at 15 Hz.

The zero-corrected displacement histories of the bushing relative to the mounting frame in the x-axis were studied by examining a six-second segment of the data from channels 31, 33, and 35. The displacements of the bushing relative to the support frame were computed by subtracting the history of the mounting frame displacement (channel 37) from the recorded bushing displacements (channels 31, 33, and 35). Slip of the UPPER-1 porcelain unit was computed by combining the data from the radial sensors, (channels 47 through 51) and applying geometric transformations to obtain the slip along the x-axis. The computed displacements for the test without the terminal and the test with the terminal are shown in Figure 4-22 and Figure 4-23, respectively. During Test No 38 (test without the terminal), the displacement at the bottom of bushing was small, there was significant slip of the UPPER-1 porcelain unit over the flange, and the displacement at the top of the bushing was larger than the displacement at the midheight. The residual displacement of the top and midheight of the bushing, at the conclusion of the test, were due to the slip of the porcelain. The slip history of the UPPER-1 porcelain unit shows slip initiating at approximately 4 seconds into the response. At the conclusion of the test, Bushing-2 had a permanent slip of 0.8 in. (20 mm). During Test No 37 (test with the terminal), displacement at the bottom of bushing was small, the displacement at the top of the bushing smaller than the displacement at the midheight (possibly due to the interaction between two modes of vibrations of the bushing when the terminal was attached). At the conclusion of the test, Bushing-2 had no significant residual slip.

The zero-corrected porcelain uplift histories along the x-axis for the UPPER-1 porcelain unit were studied by examining data from channels 51 and 53. The average vertical displacement in the z-direction was calculated as one-half of the sum of the channel 51 and channel 53 displacements. Rocking about the local y-axis was calculated as the difference between the channel 51 and 53 displacements divided by the 25-in. (635-mm) distance between these transducers. The data for the test without the terminal are shown in Figure 4-24 and the data for the test with the terminal are shown in Figure 4-25. During Test No 38 (test without the terminal), there was large uplift of the UPPER-1 porcelain unit. The uplift history of the UPPER-1 porcelain unit shows uplift initiating at approximately 4 seconds into the response. Slip and uplift of the UPPER-1 porcelain unit initiated at the same time, and resulted in oil leakage from the bushing. At the conclusion of

the test, the residual uplift of channel 51 was greater than that of channel 53, which indicates residual rotation at the gasket connection. The vertical displacements in the UPPER-1 porcelain unit were smaller, and there was no oil leakage and no residual uplift or rotation of the unit During Test No 37 (test with the terminal).

The zero-corrected stress histories for the UPPER-1 porcelain unit along the x-axis were studied by examining data from channels 39 and 41. The recorded strain data were converted to stress by multiplying the measured values by the porcelain modulus of elasticity (assumed to equal 97,000 MPa, see Chapter 2). The stress data for the test without the terminal are shown in Figure 4-26, and the stress data for the test with the terminal are shown in Figure 4-27. The stress histories shown in these figures are *relative* values and represent the change in porcelain stress during the earthquake simulator testing. In these figures, compressive stresses are designated as positive. To obtain the absolute stress in the UPPER-1 porcelain unit, the initial compressive post-tensioning stress of 0.9 ksi (6.2 MPa) has to be added to the values shown. As a result, data indicate no tensile stress in the UPPER-1 porcelain unit. During Test No 38 (test without the terminal), the relative stress values on the opposite sides of the UPPER-1 porcelain unit had opposite signs. On one side, there was additional compressive stress, whereas on the opposite side, some of the post-tensioning force was relieved. At the conclusion of the test, the residual stress in the UPPER-1 porcelain unit was positive on one side and negative on the other side. This observation is consistent with the differential residual vertical displacements discussed in the last paragraph. The strain gage data of Test No 37 (test with the terminal) show that the stress in the UPPER-1 porcelain unit was small — an observation consistent with the data presented in the last paragraph.

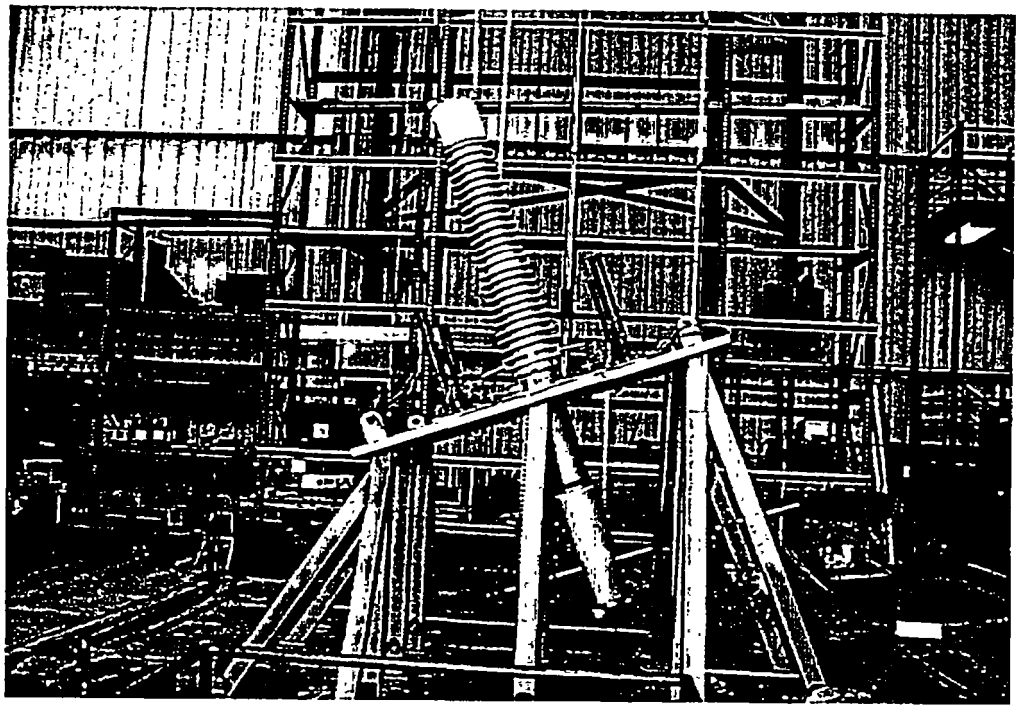

Figure 4-1 A rigidly mounted 230-kV bushing on the earthquake simulator

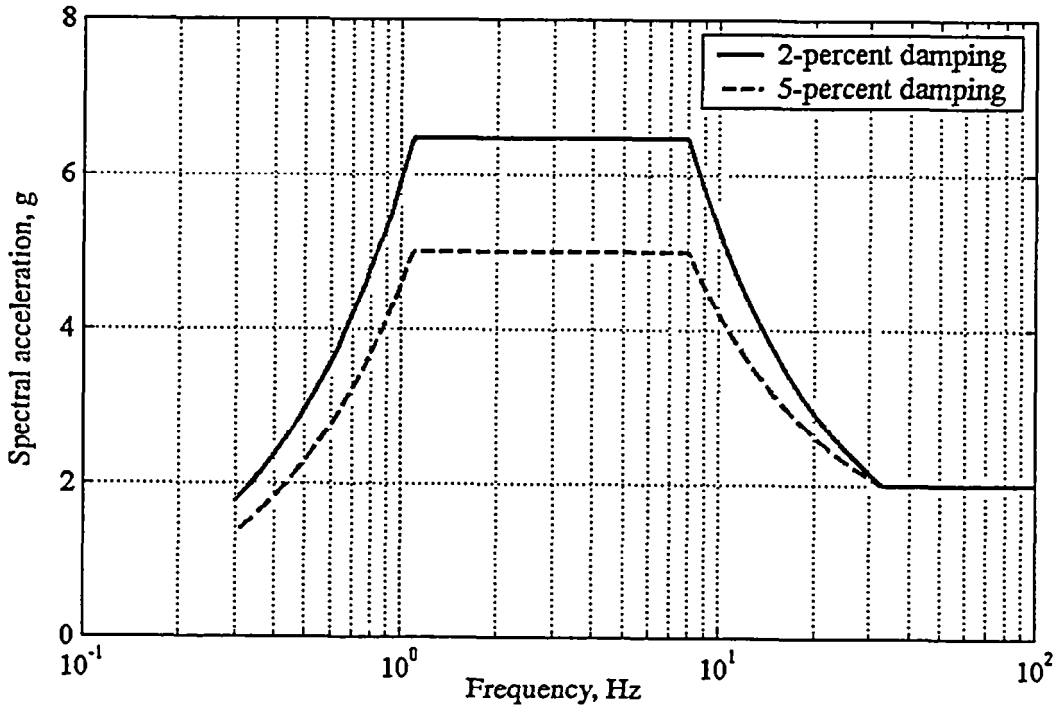

Figure 4-2 IEEE 693-1997 test response spectrum for High Level Qualification

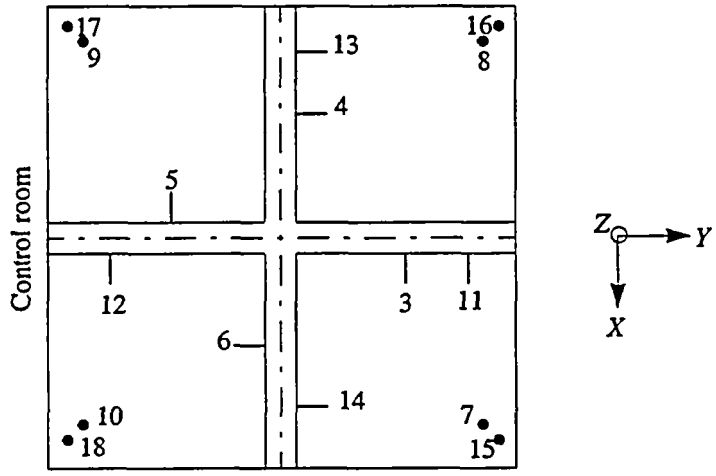

(a) Earthquake simulator (view from beneath)

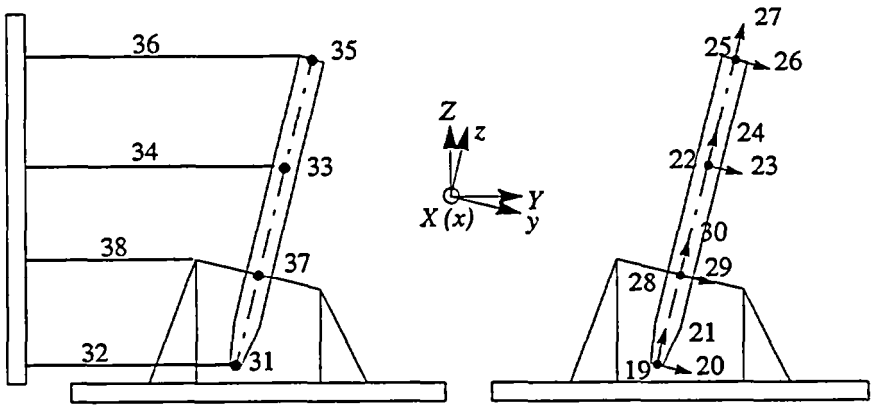

(b) Bushing and mounting frame

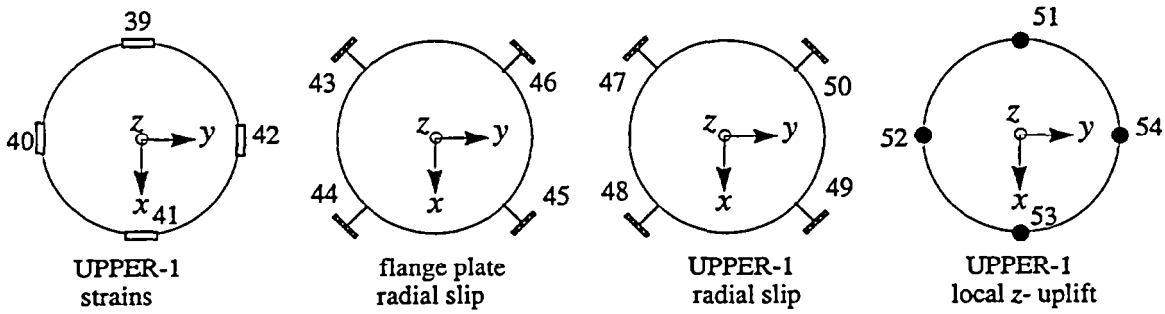

(c) UPPER-1 porcelain unit and flange plate

Figure 4-3 Instrumentation for 230-kV bushings

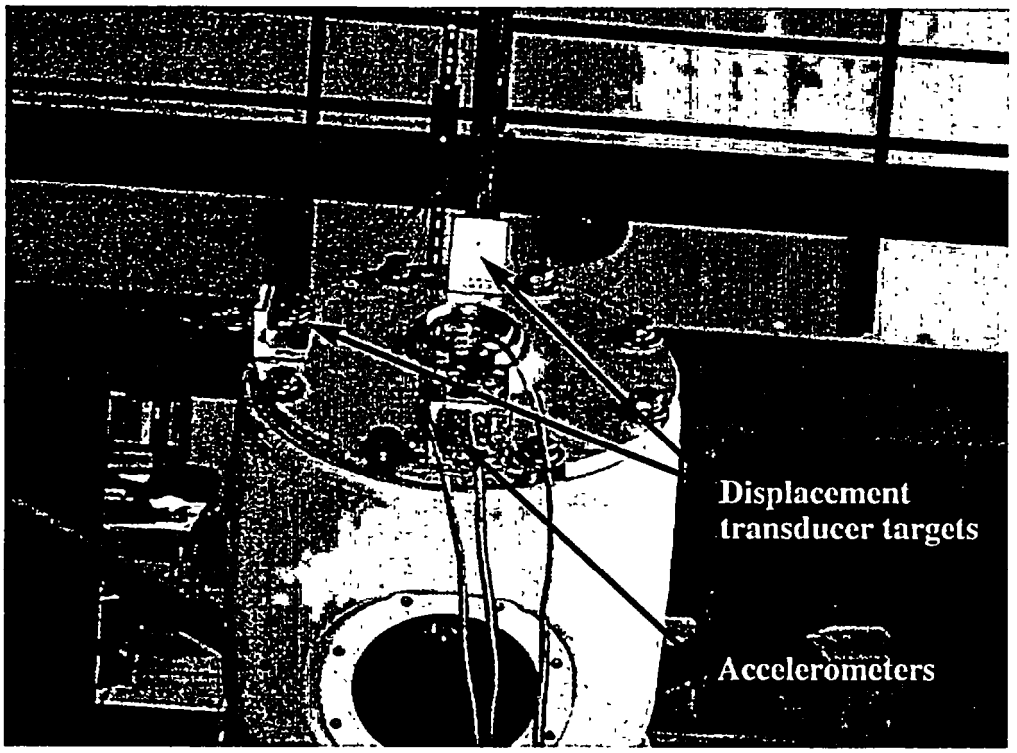

Figure 4-4 Instrumentation at top of Bushing-1

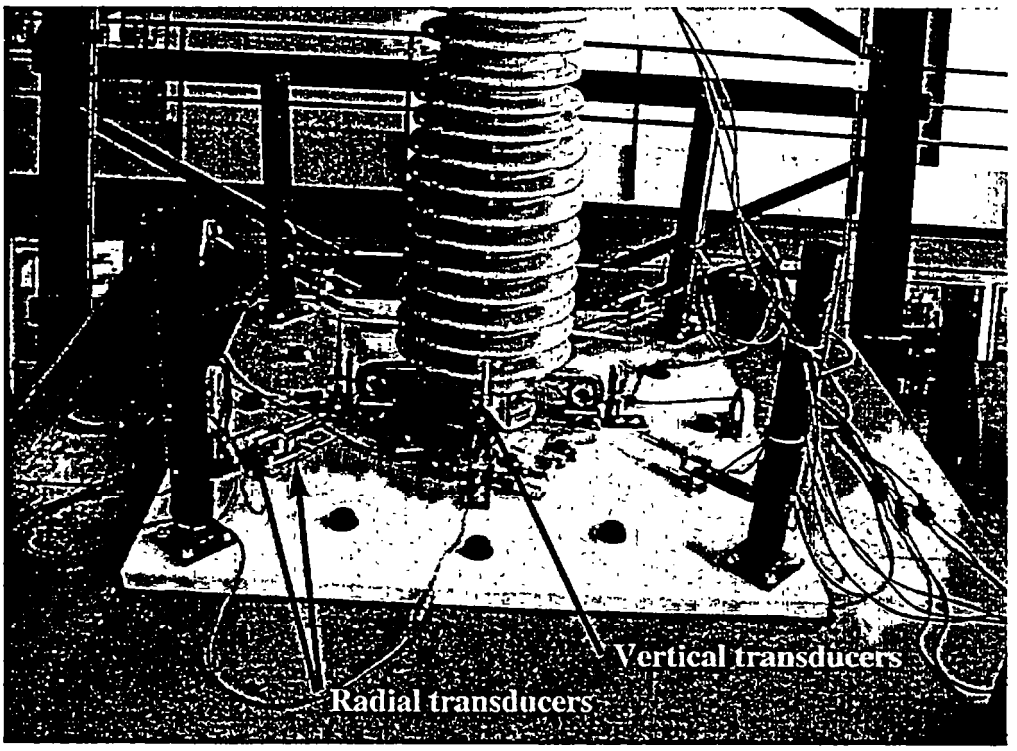

Figure 4-5 Instrumentation of the UPPER-1 porcelain unit

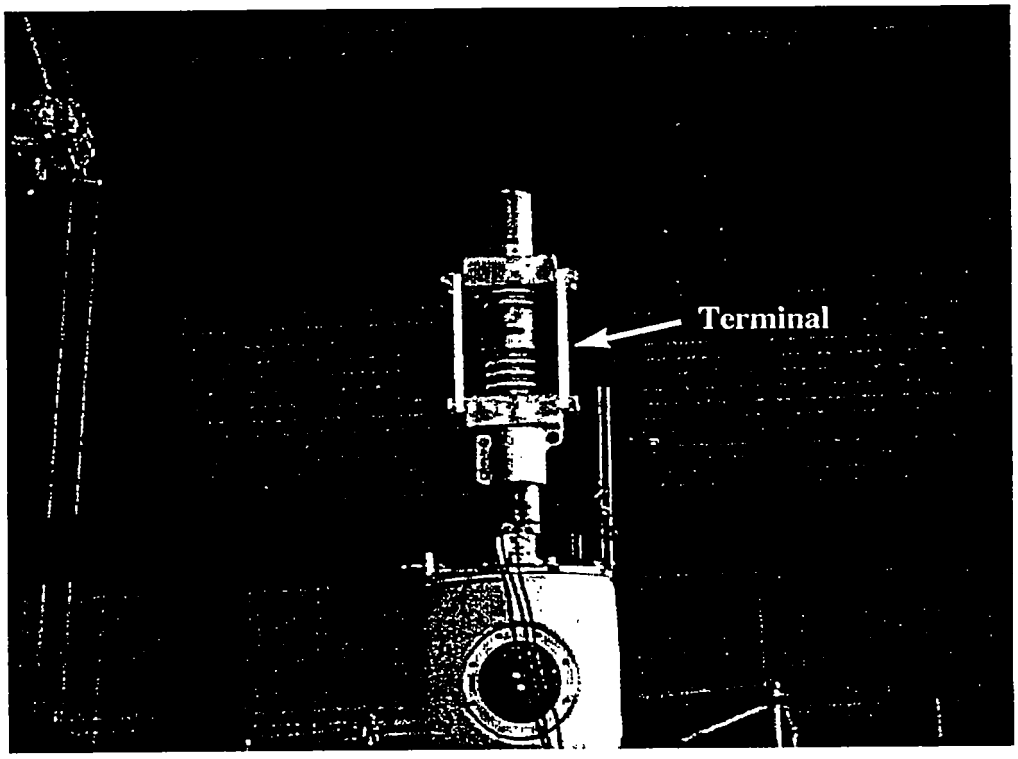

Figure 4-6 Terminal attached to the top of Bushing-2

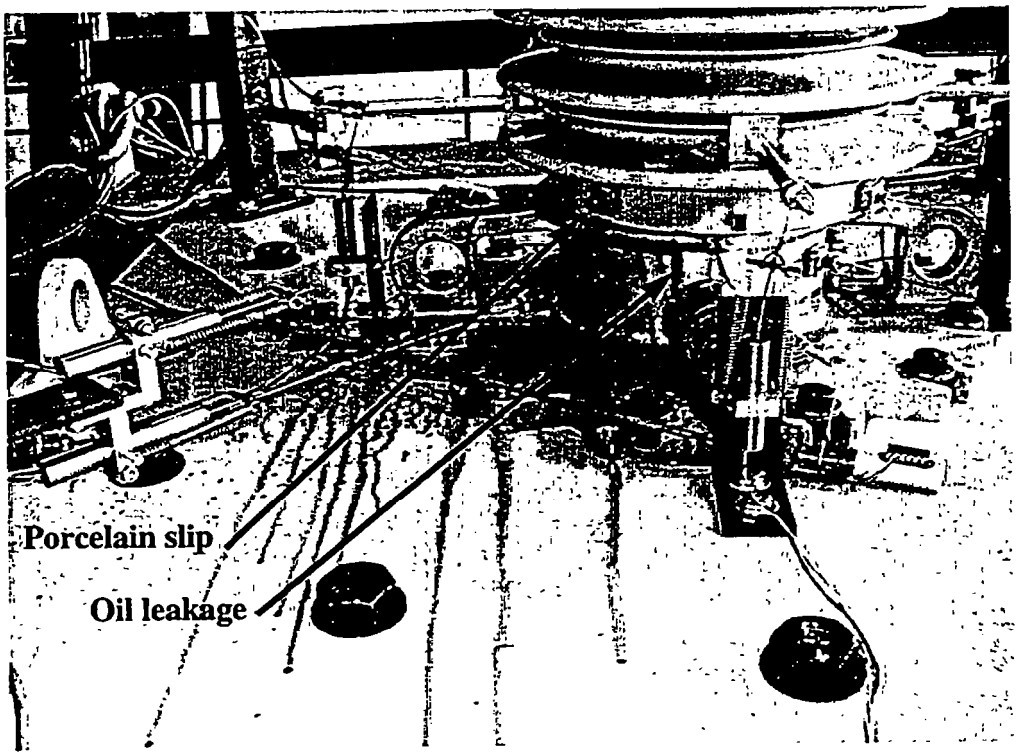

Figure 4-7 Bushing-2 after Test No 38 showing oil leakage and slip of porcelain

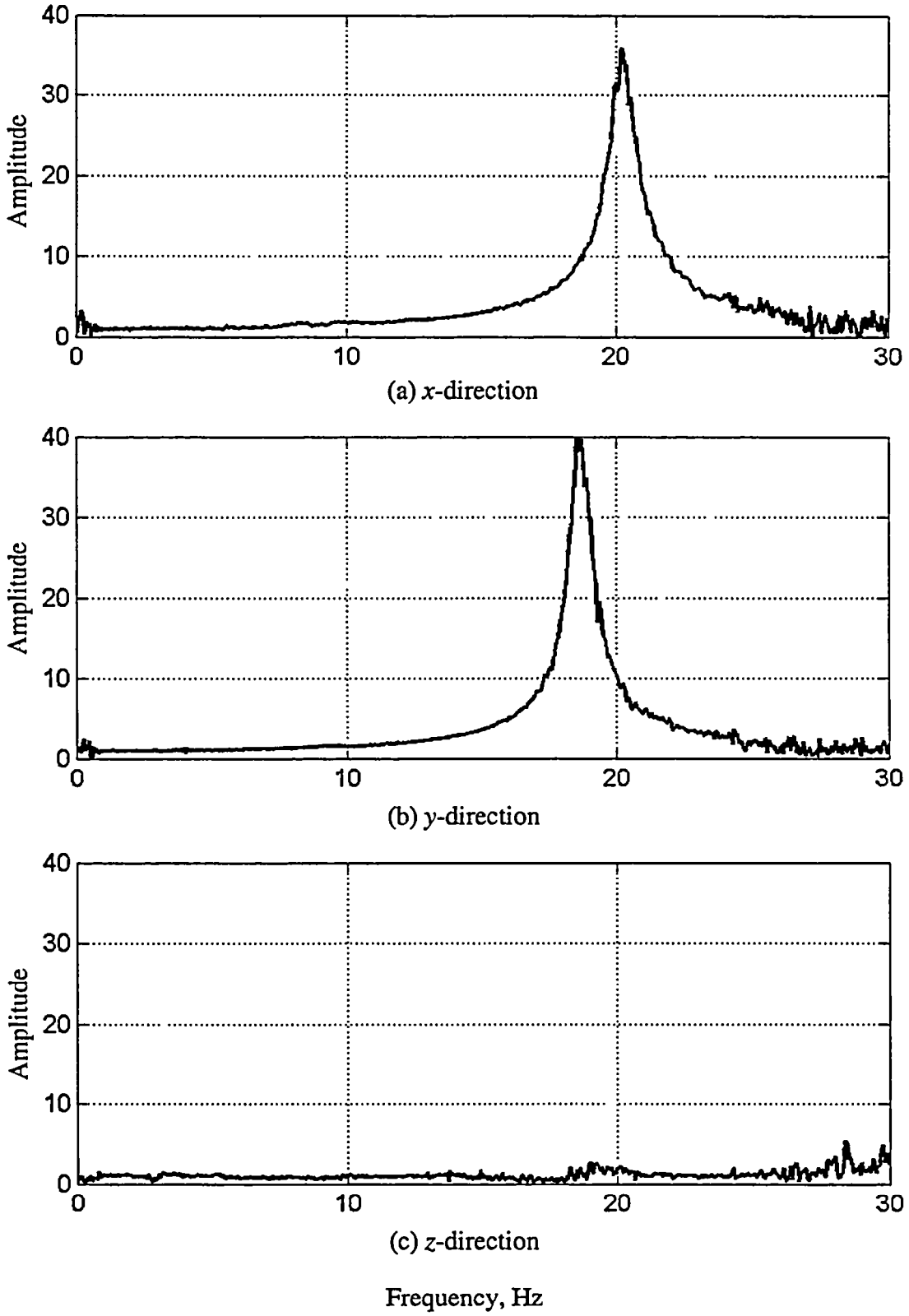

Figure 4-8 Transfer function amplitudes between the top of Bushing-1 and frame

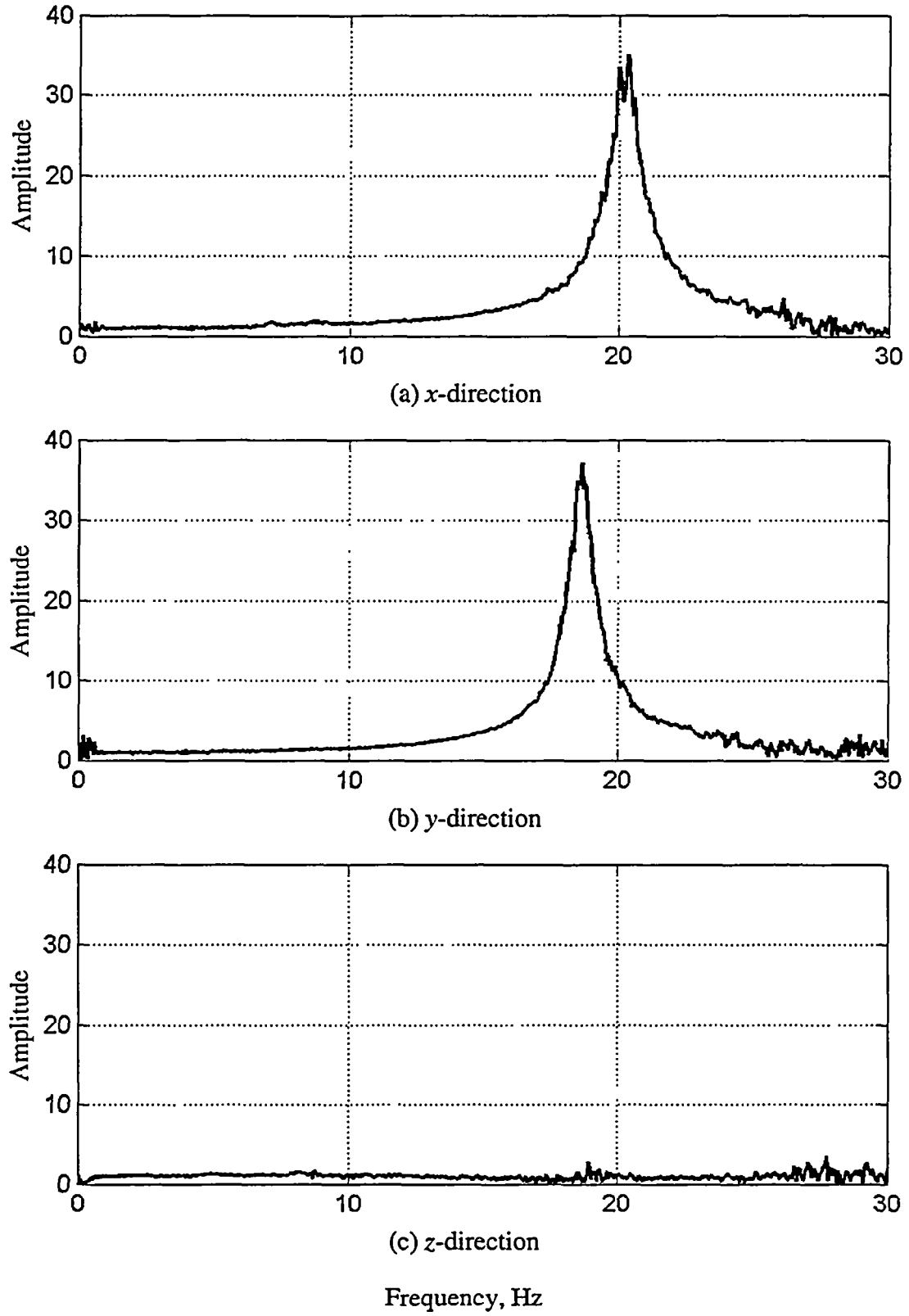

Figure 4-9 Transfer function amplitudes between the top of Bushing-2 and frame

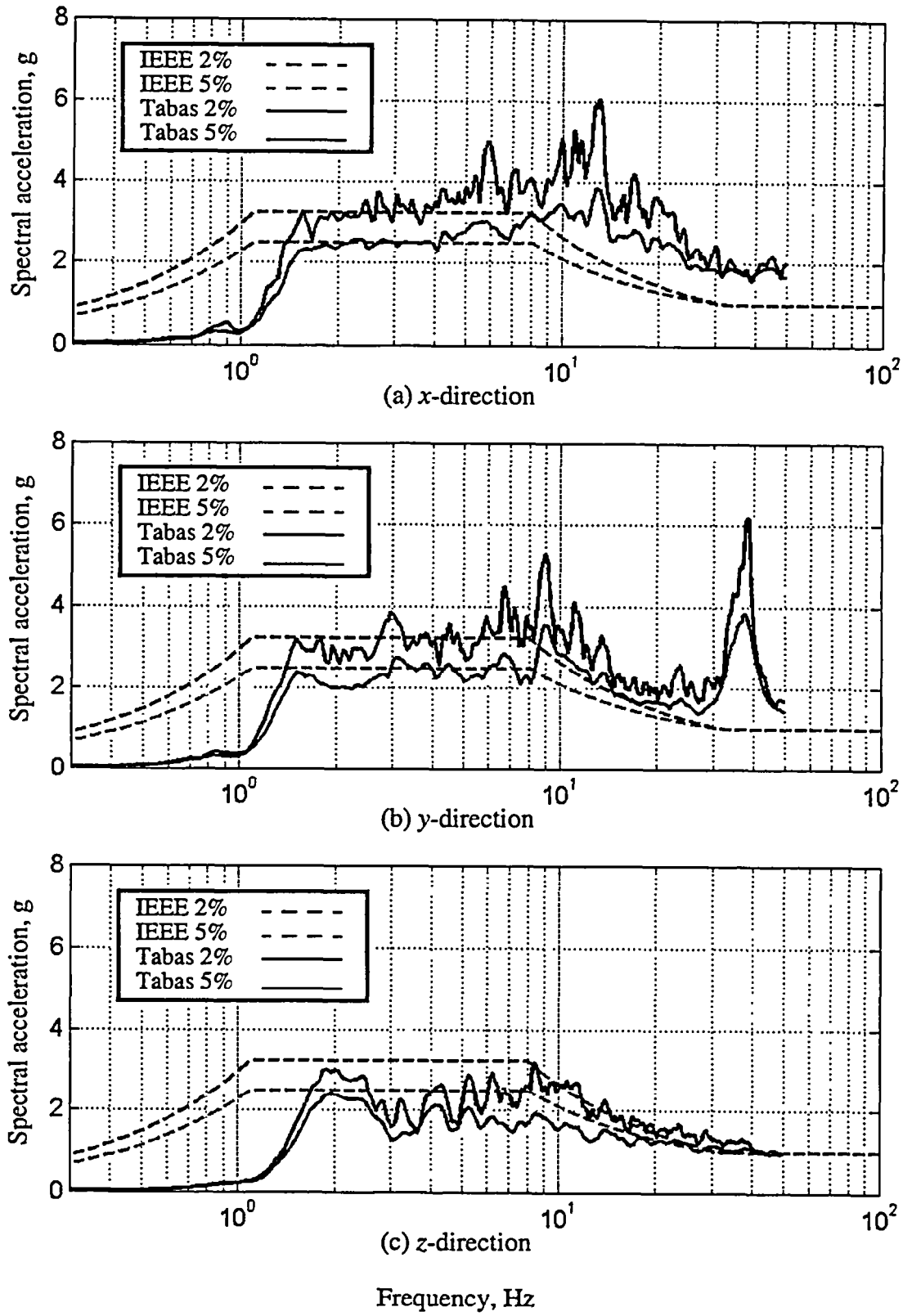

Figure 4-10 Response spectra for Bushing-1; Test No 12, target PGA=1.0g

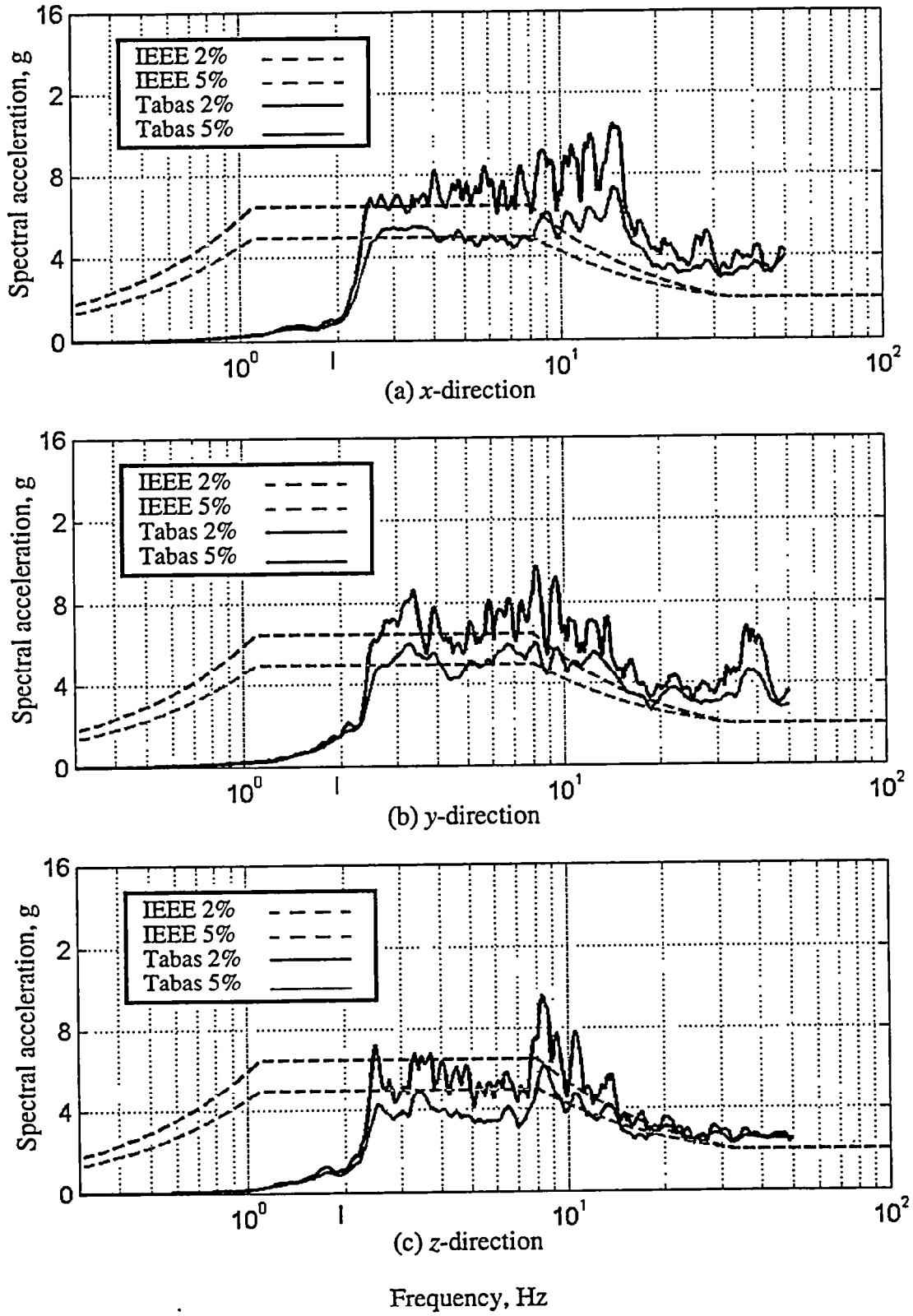

Figure 4-11 Response spectra for Bushing-1; Test No 17, target PGA=2.0g

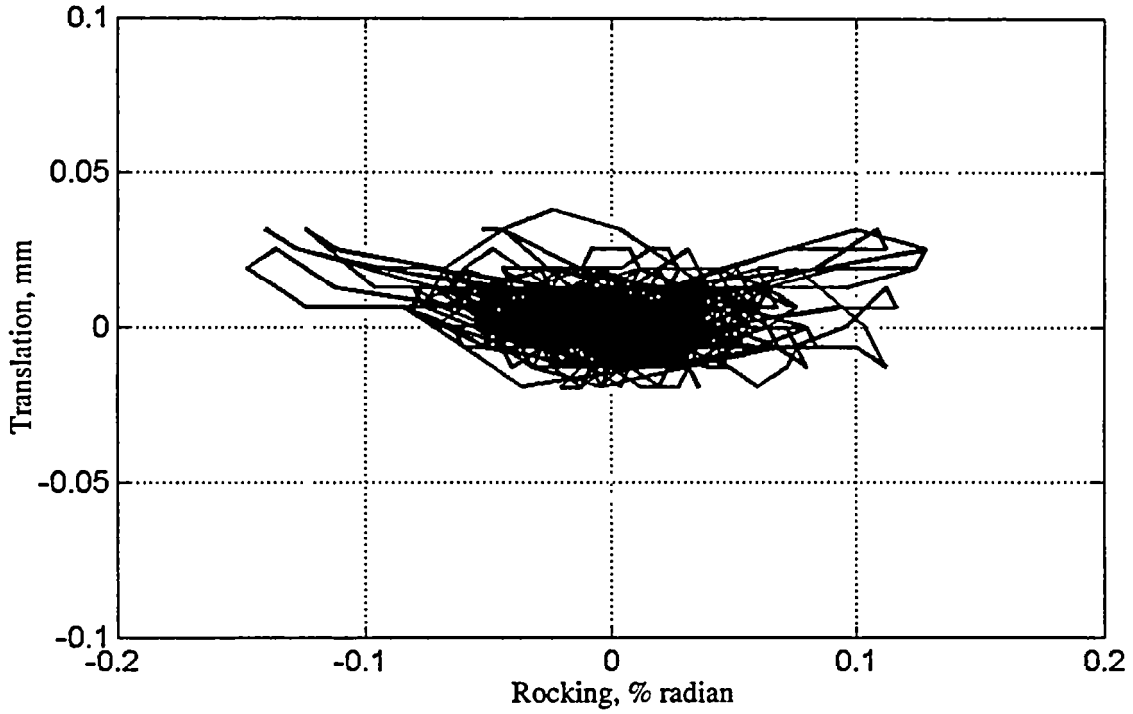

(a) About y- axis

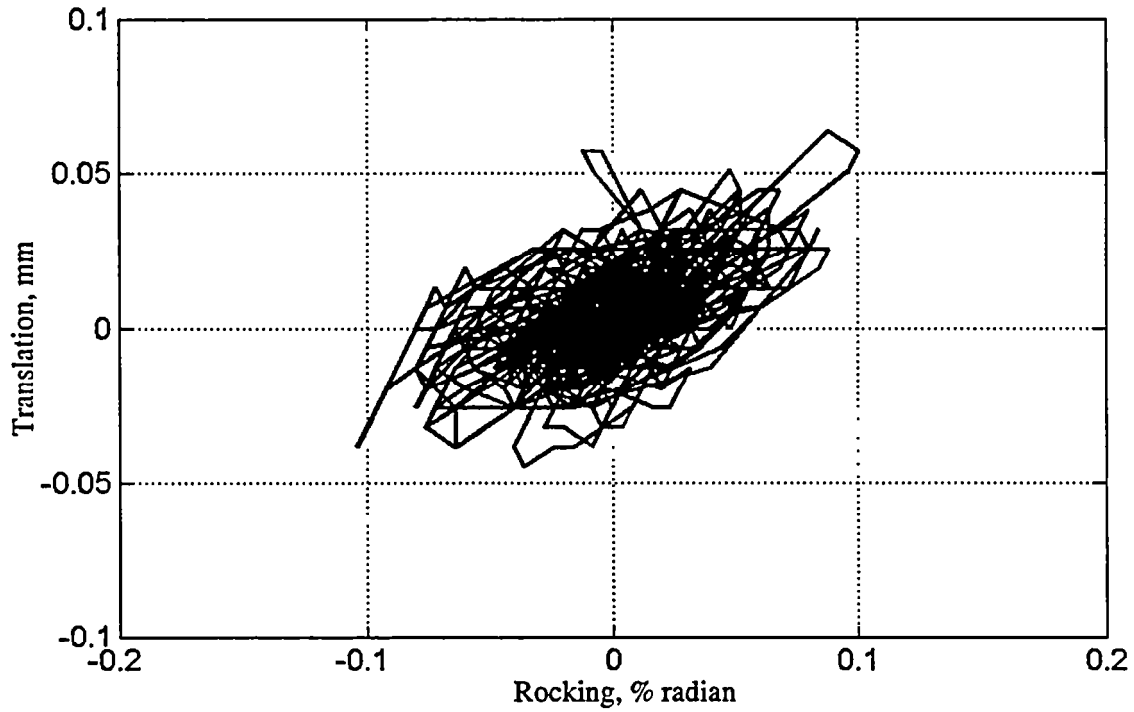

(b) About x- axis

Figure 4-12 Vertical displacement versus rocking for Bushing-1; Test No 17, target PGA=2.0g

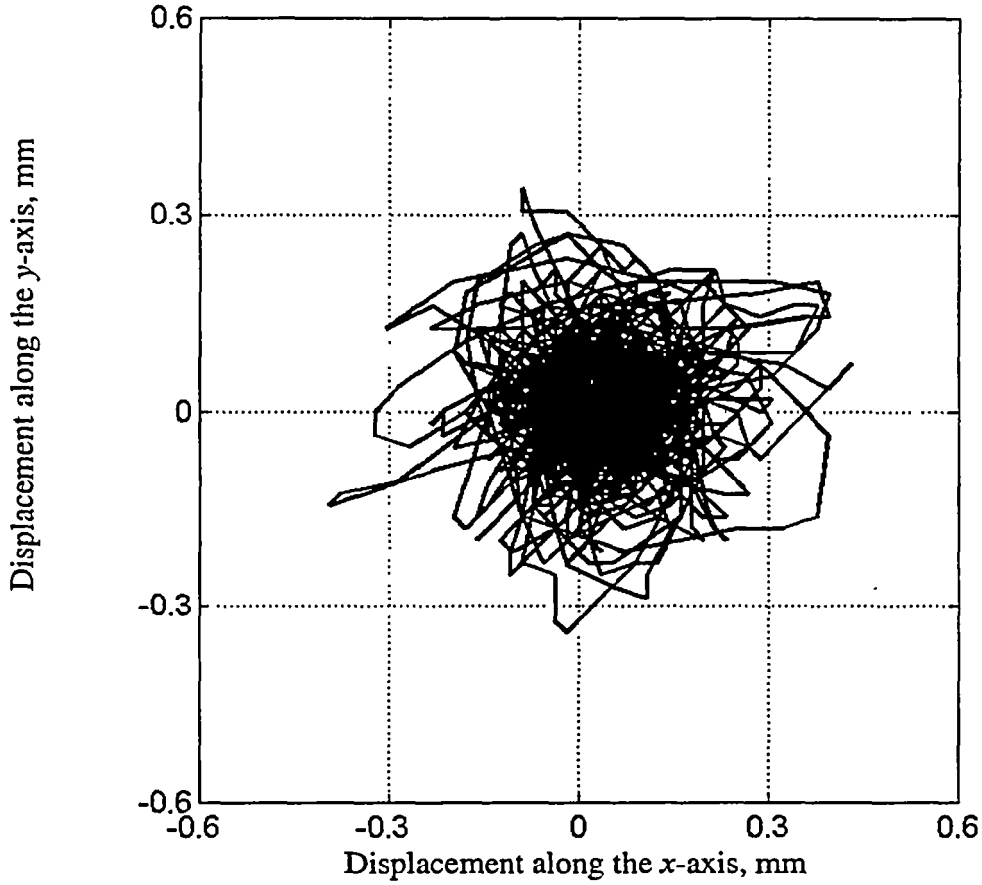

Figure 4-13 Orbit of motion for Bushing-1; Test No 17, target PGA=2.0g

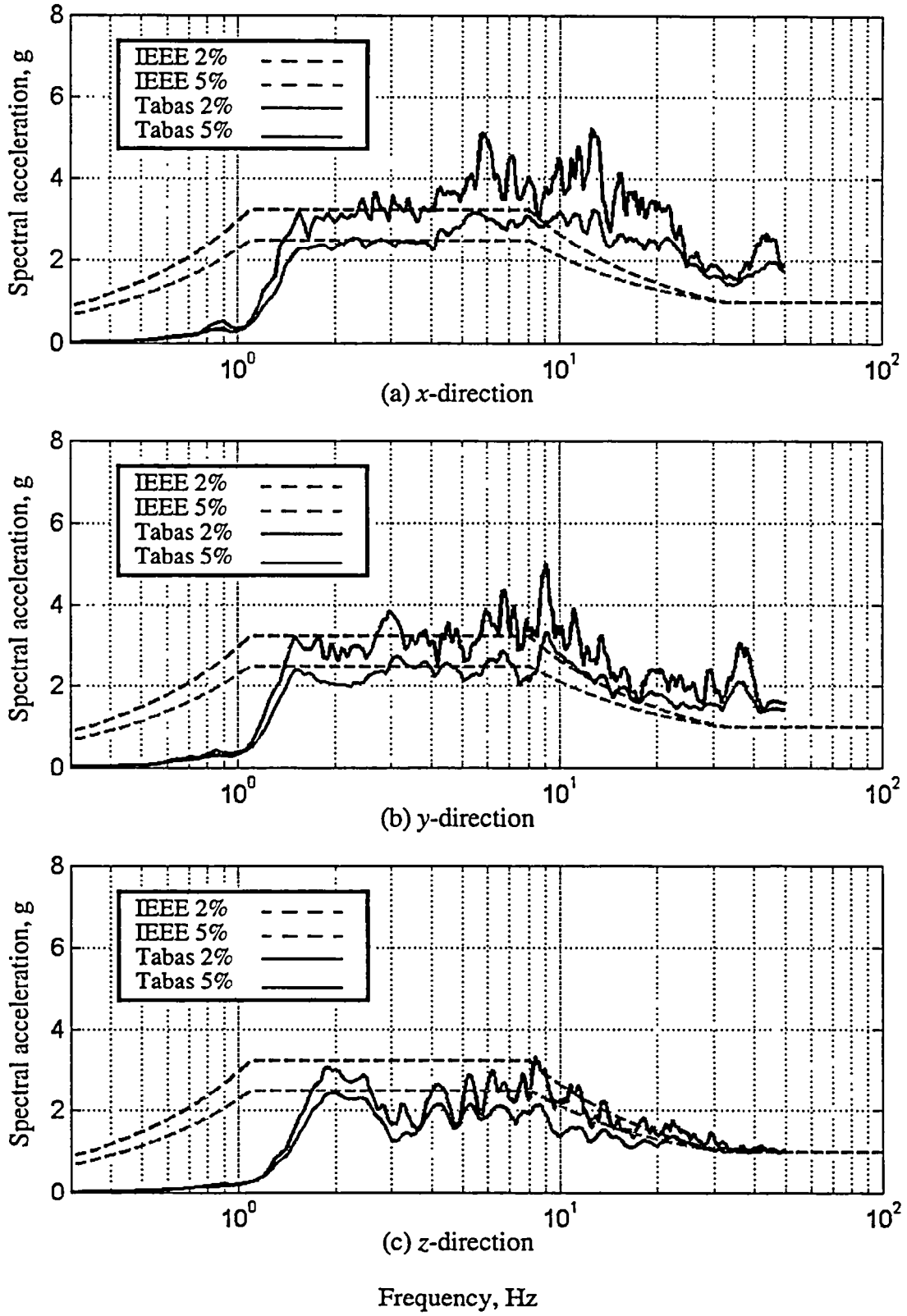

Figure 4-14 Response spectra for Bushing-2; Test No 19, target PGA=1.0g

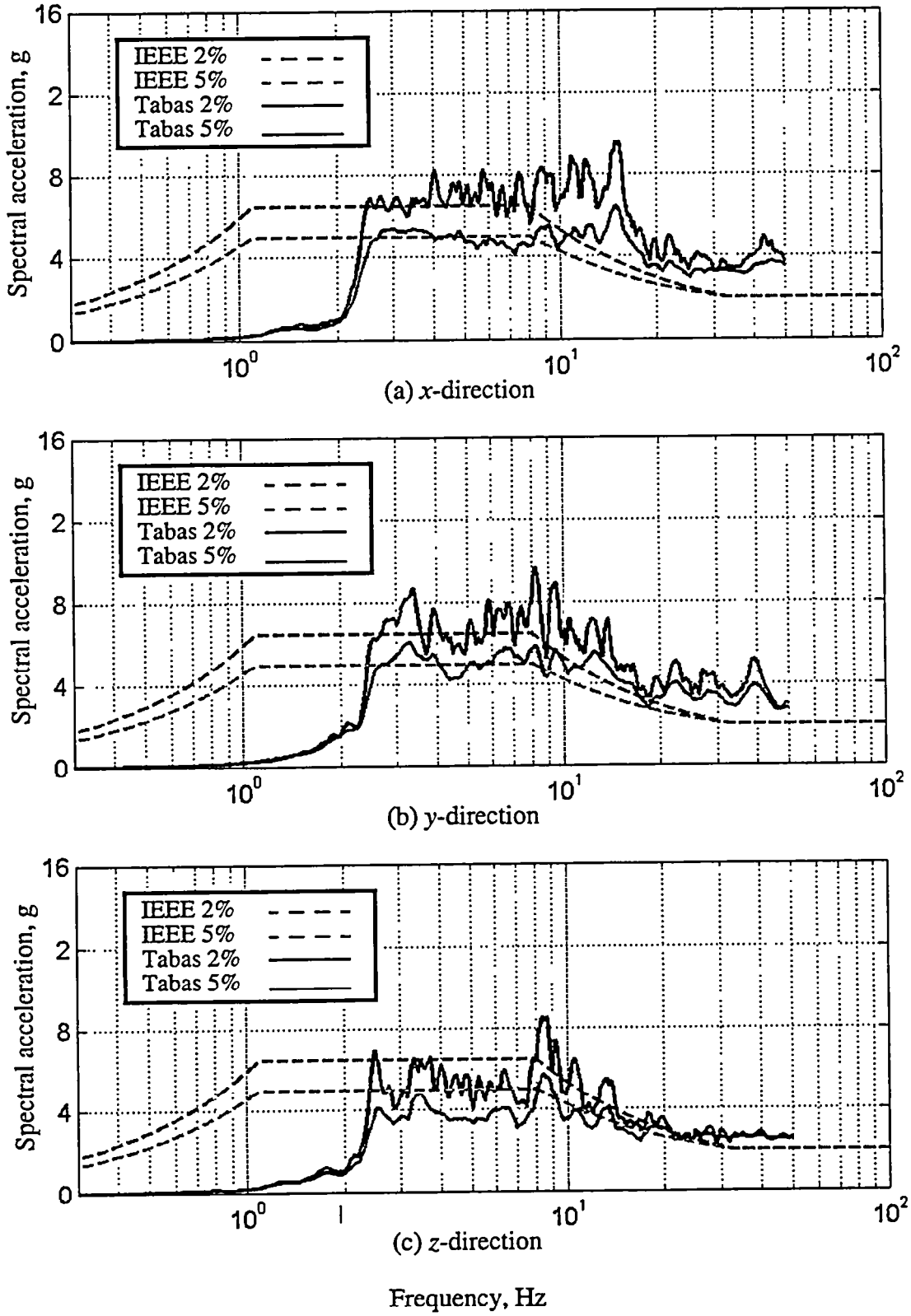

Figure 4-15 Response spectra for Bushing-2; Test No 24, target PGA=2.0g

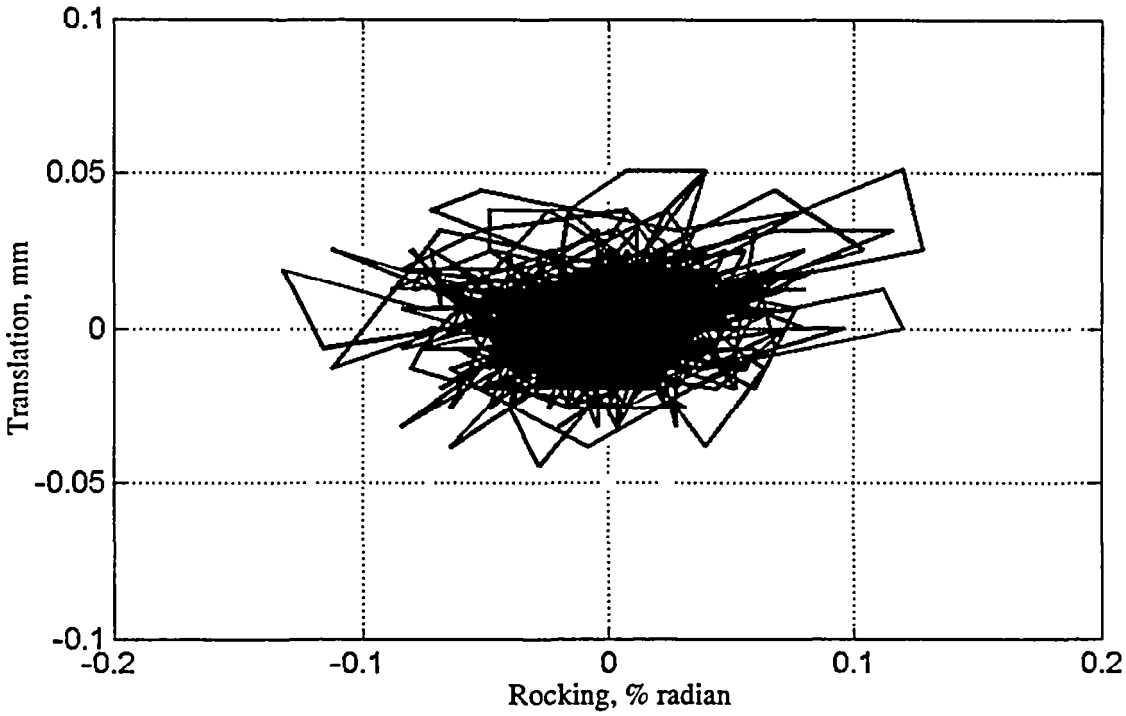

(a) About y- axis

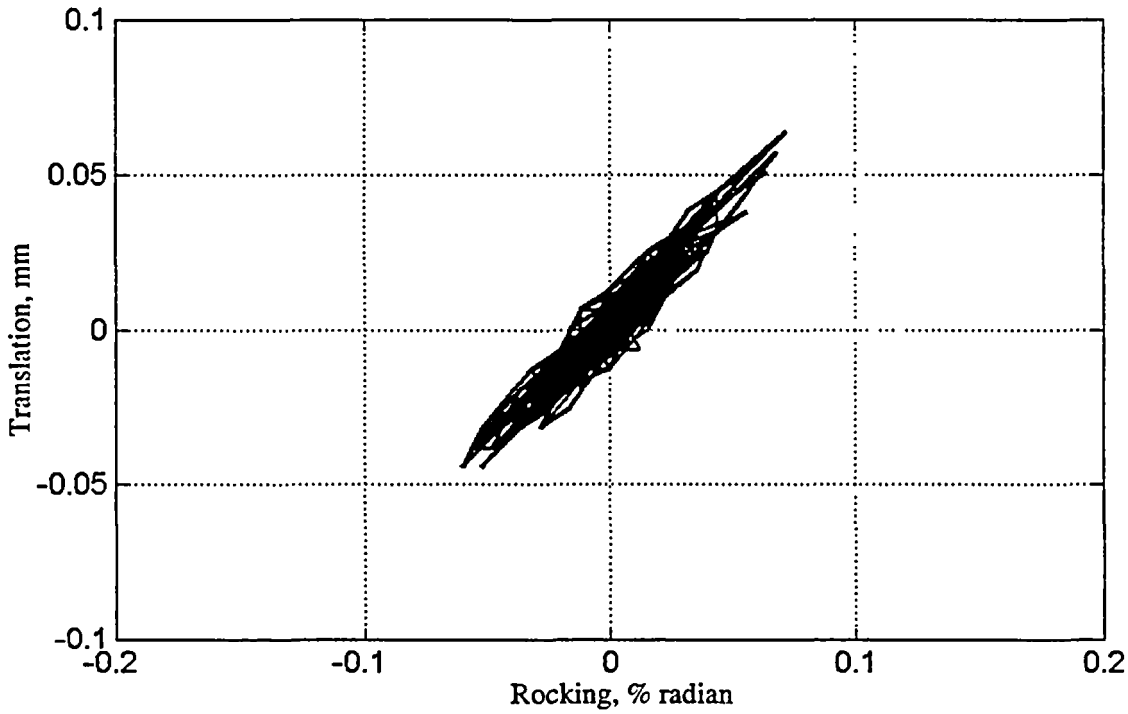

(b) About x- axis

Figure 4-16 Vertical displacement versus rocking for Bushing-2; Test No 24, target PGA=2.0g

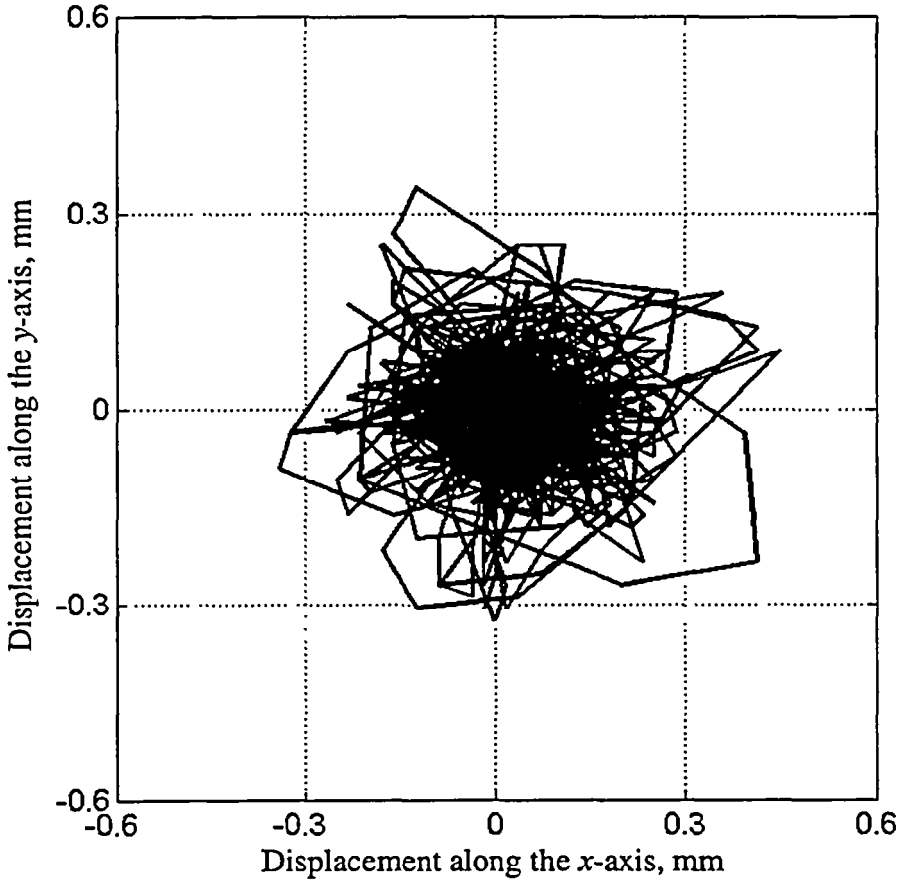

Figure 4-17 Orbit of motion for Bushing-1; Test No 24, target PGA=2.0g

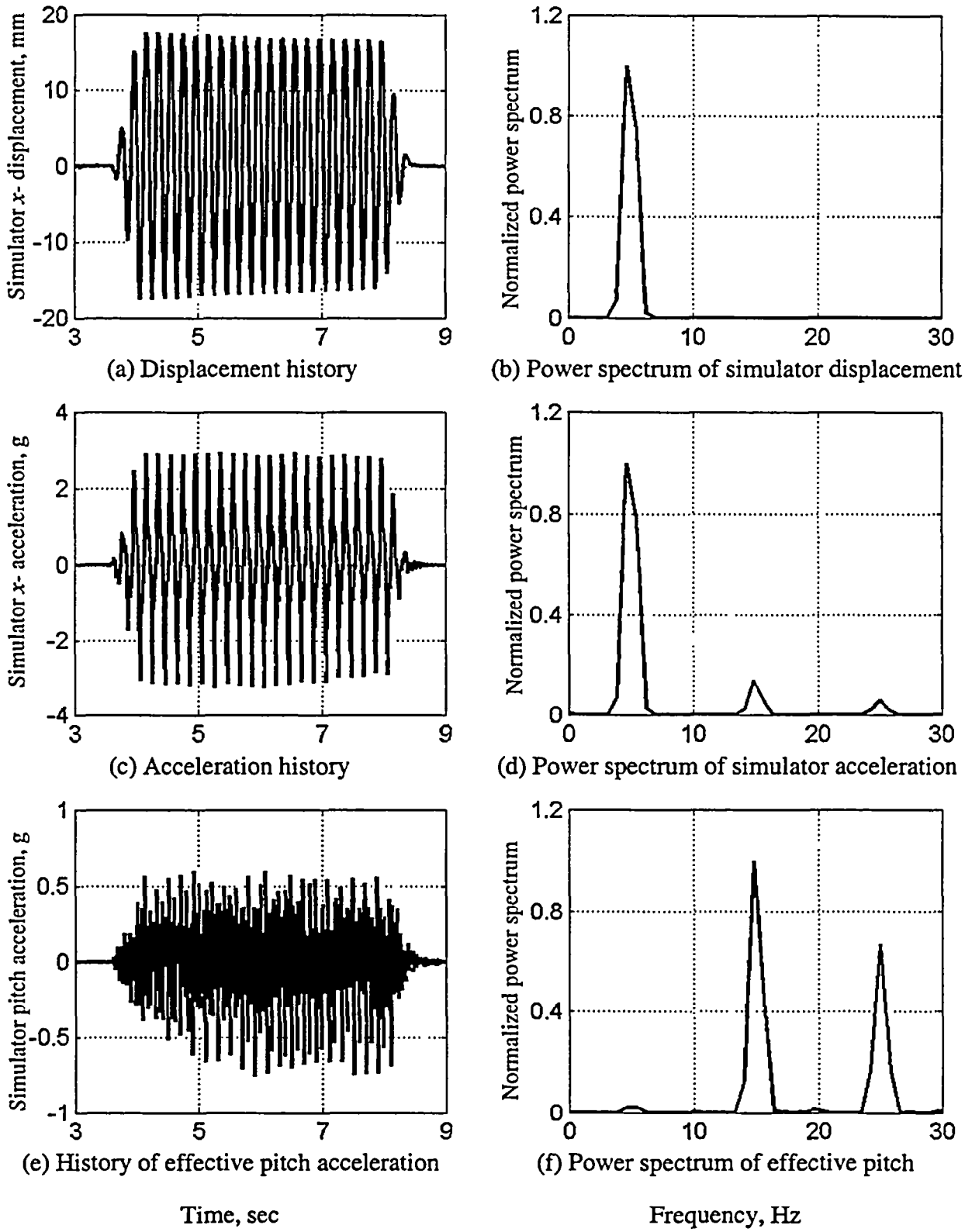

Figure 4-18 Simulator x- direction input for the high-amplitude 5-Hz harmonic tests, Test No 37

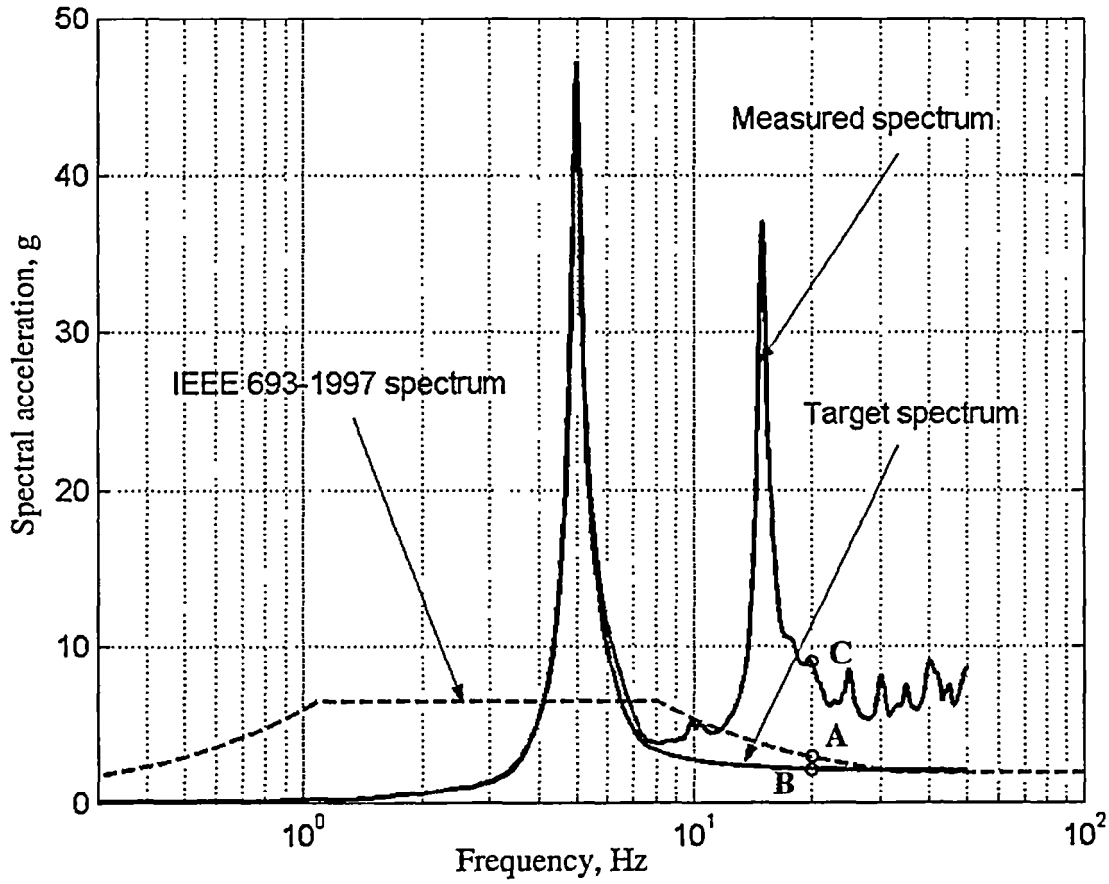

Figure 4-19 Response spectrum for high-amplitude harmonic tests

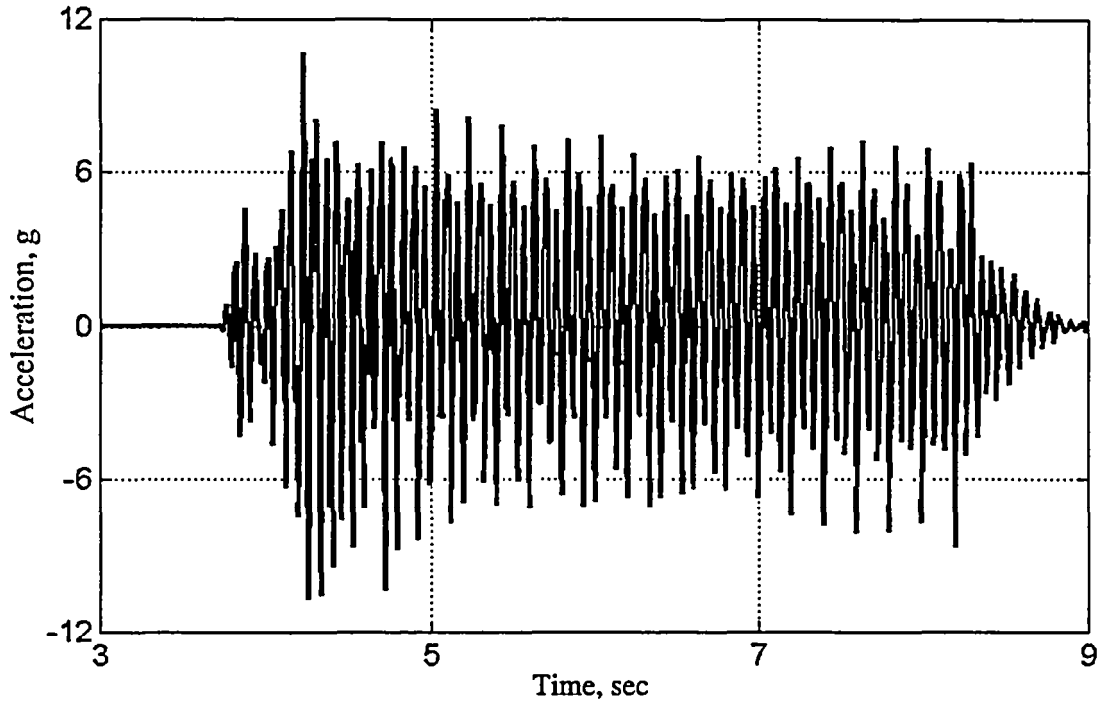

(a) History of the difference in acceleration between the top and bottom of bushing

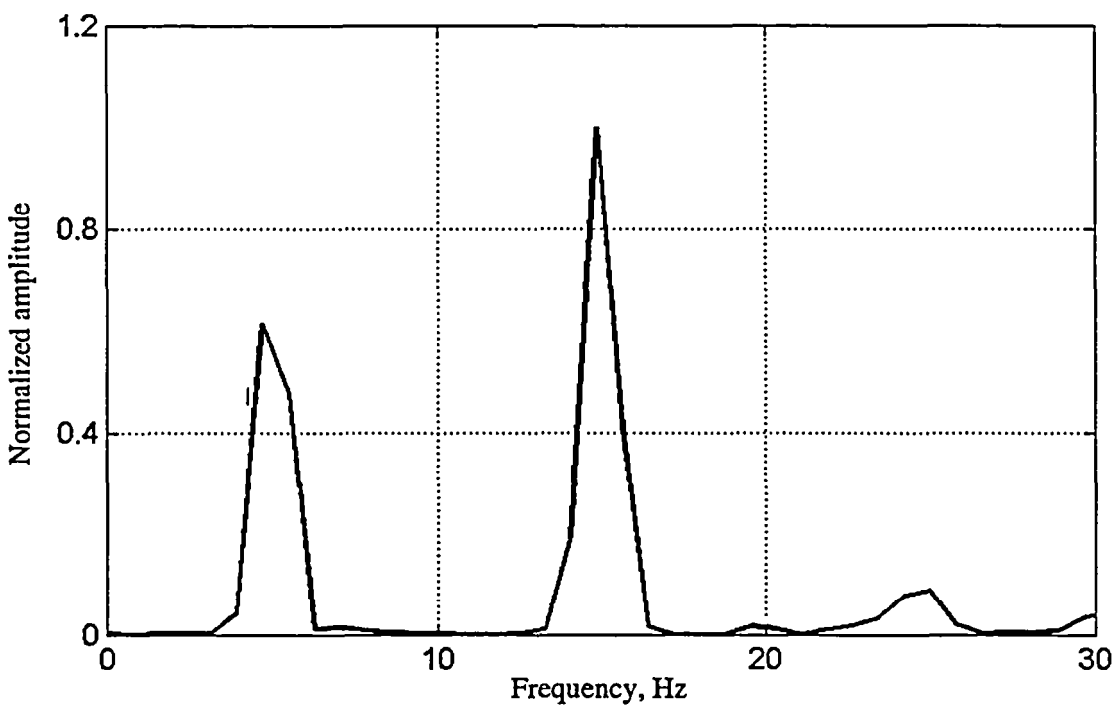

(b) Power spectrum for the acceleration at the top of the bushing

Figure 4-20 Acceleration response of Bushing-2 without terminal, Test No 38

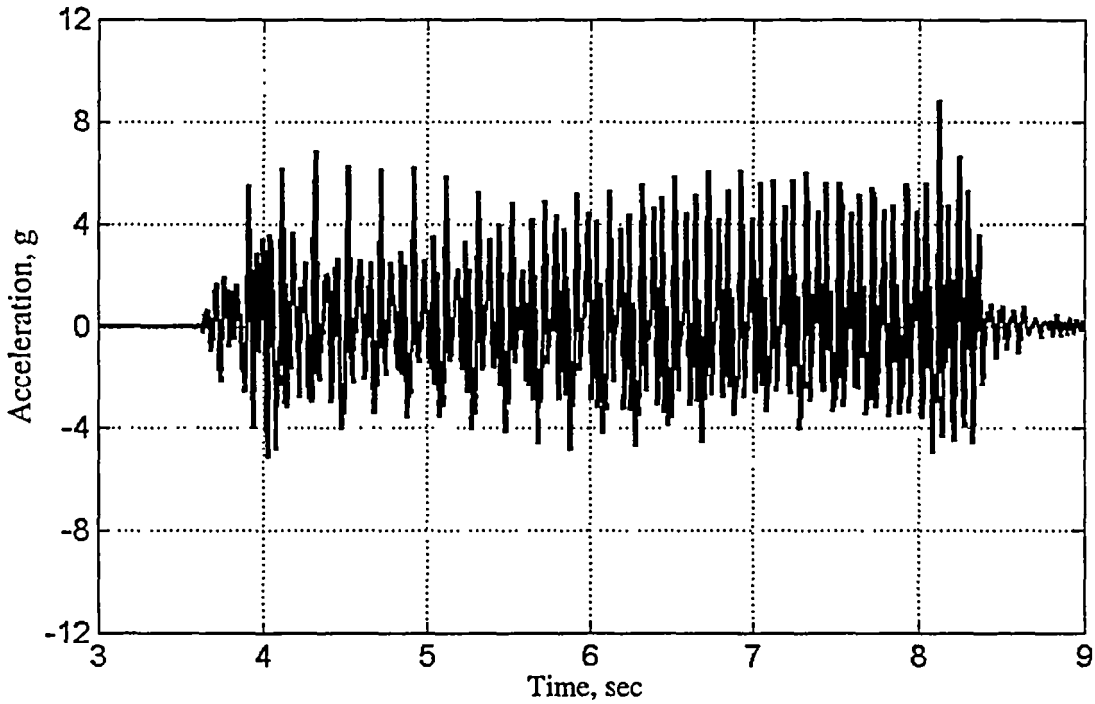

(a) History of the difference in acceleration between the top and bottom of bushing

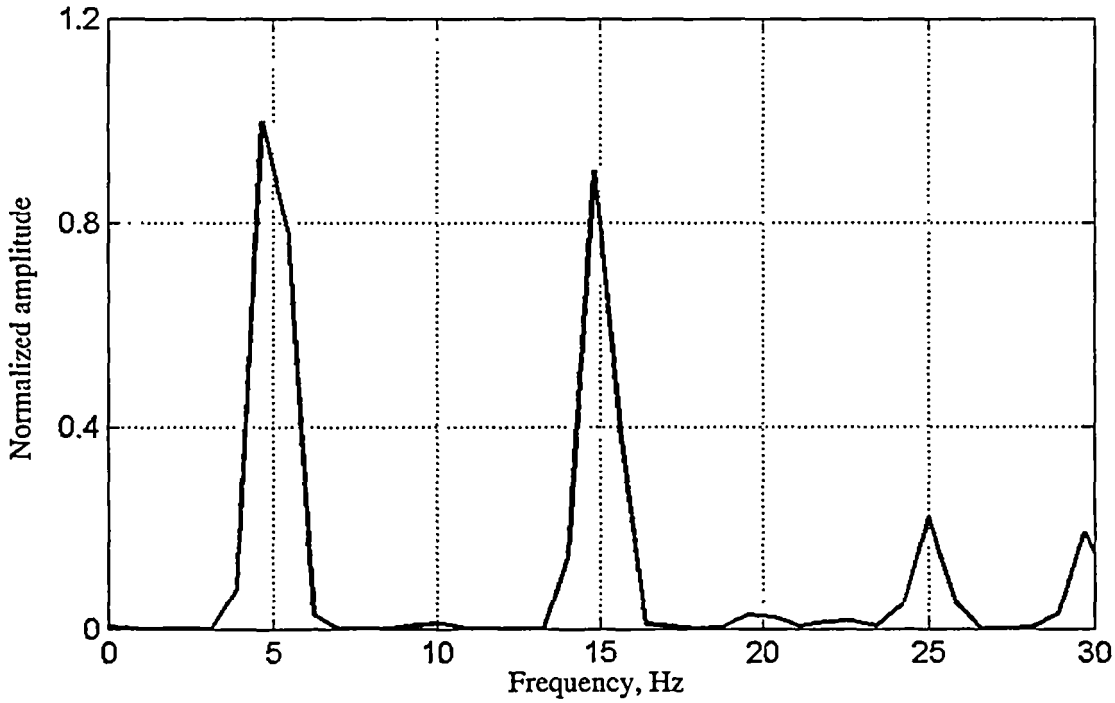

(b) Power spectrum for the acceleration at the top of the bushing

Figure 4-21 Acceleration response of Bushing-2 with terminal, Test No 37

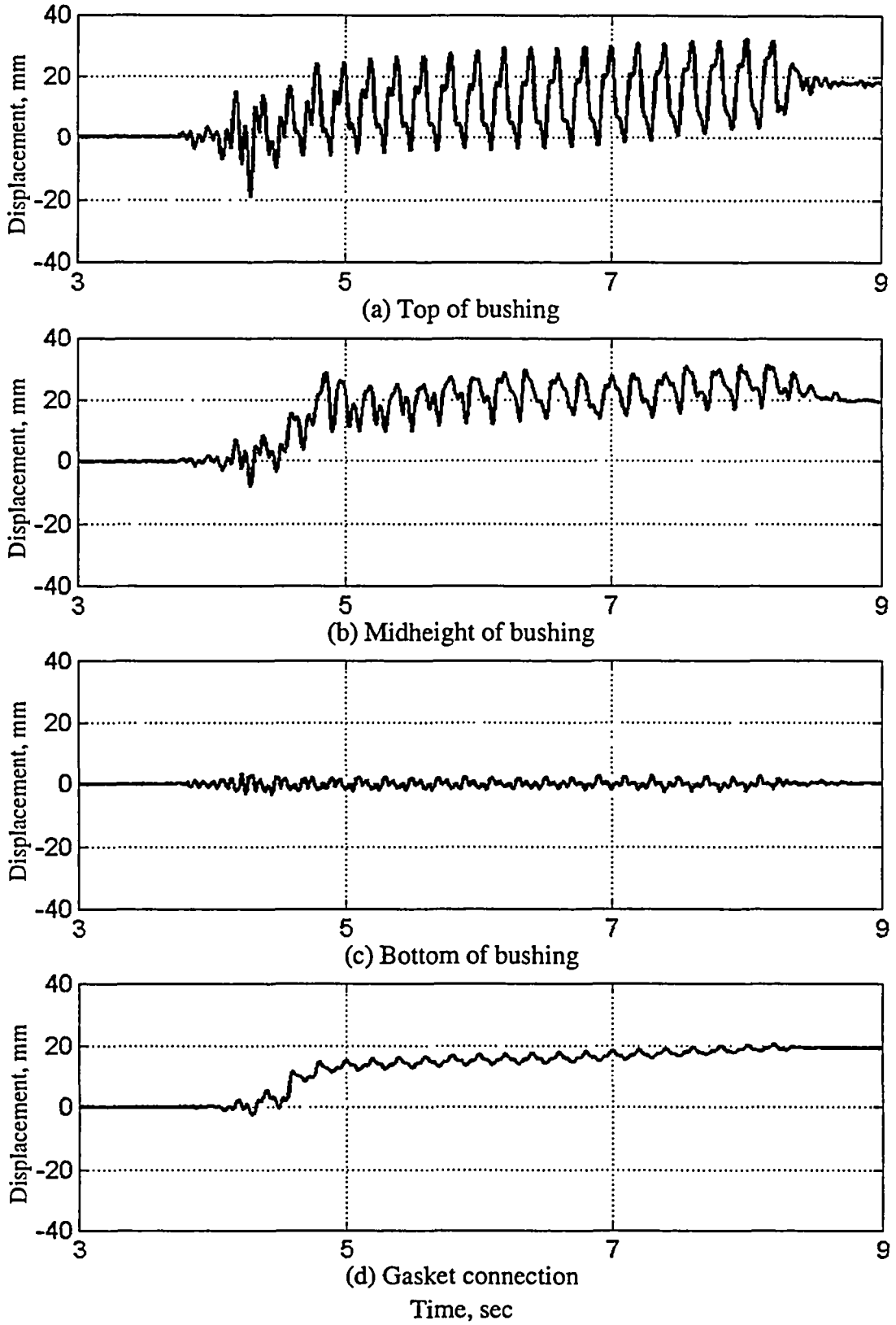

Figure 4-22 Displacement history of Bushing-2 relative to support frame, Test No 38

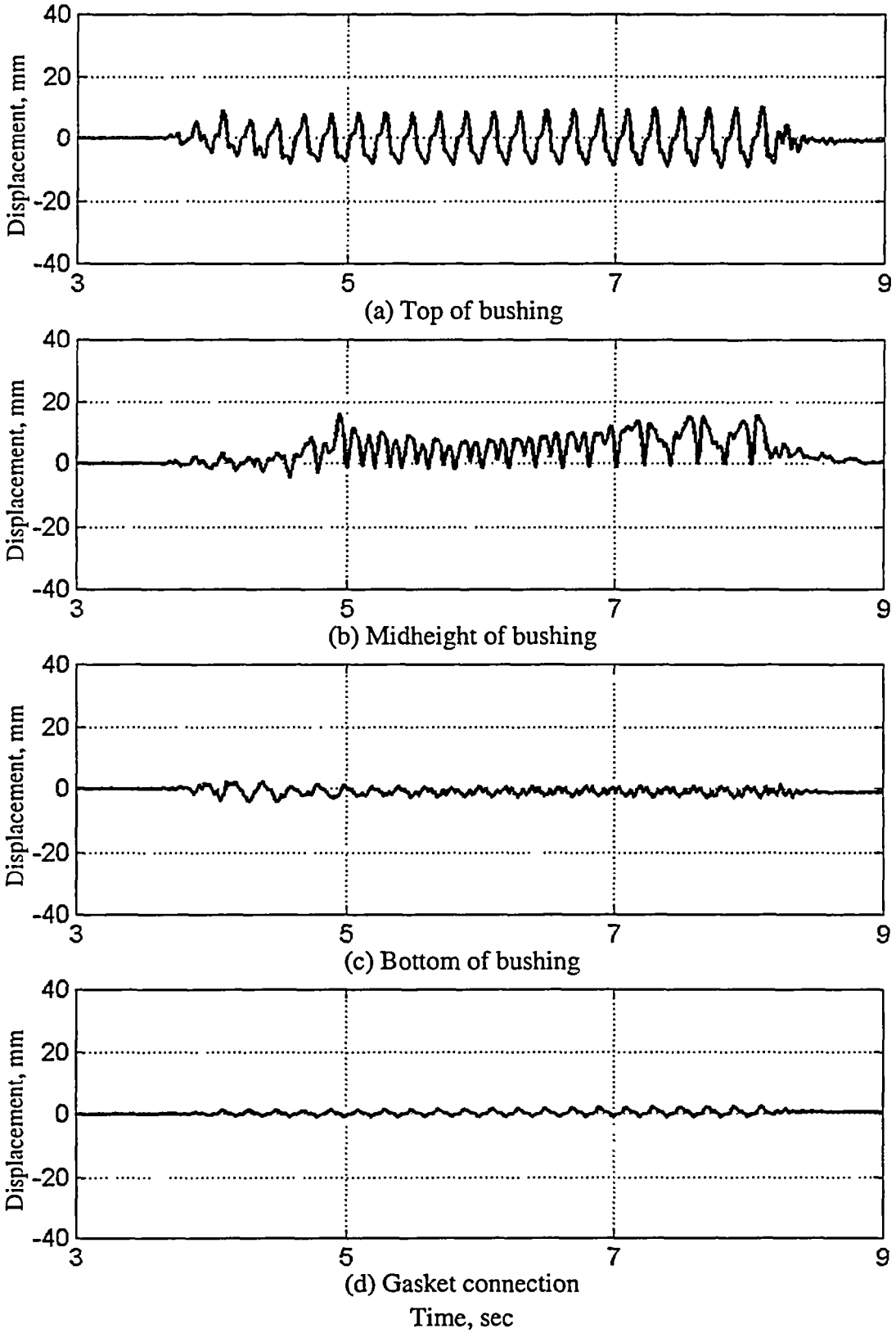

Figure 4-23 Displacement history of Bushing-2 relative to support frame, Test No 37

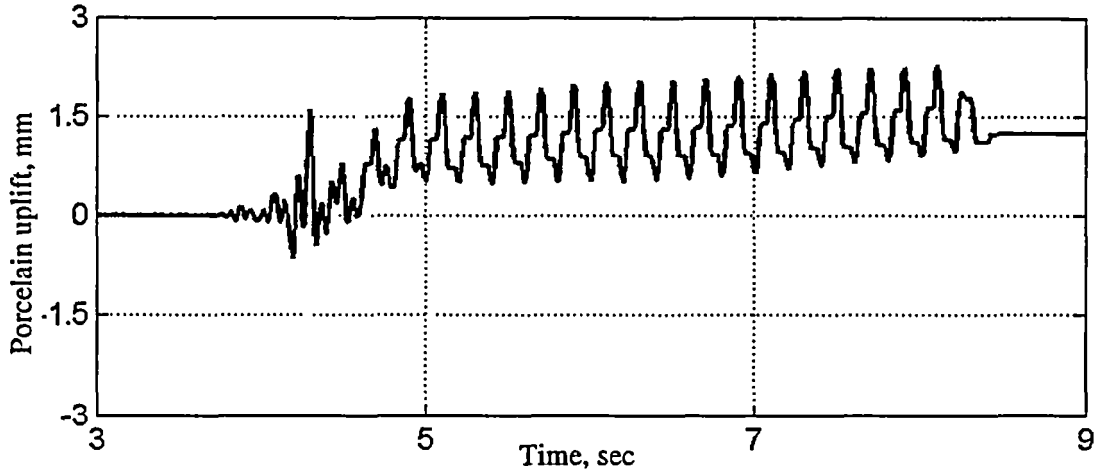

(a) Uplift history in x-direction (channel 51)

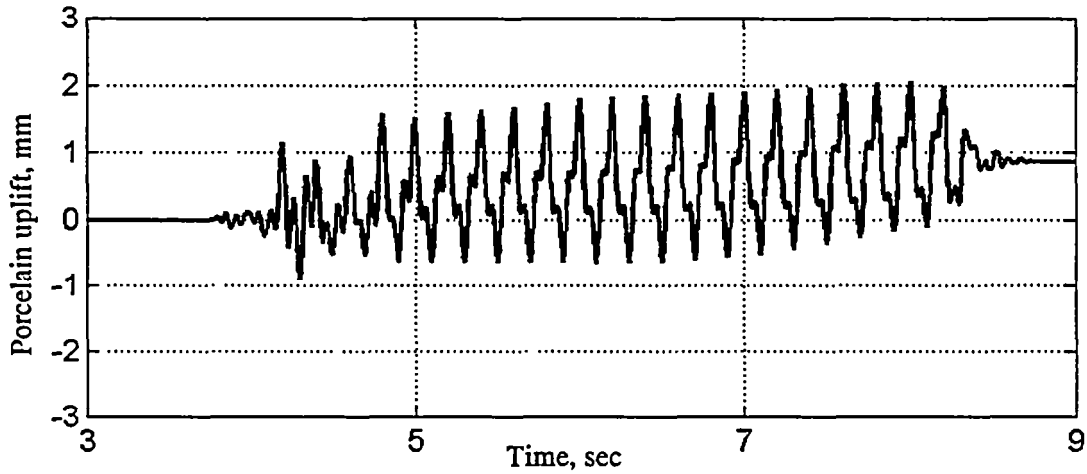

(b) Uplift history in x-direction (channel 53)

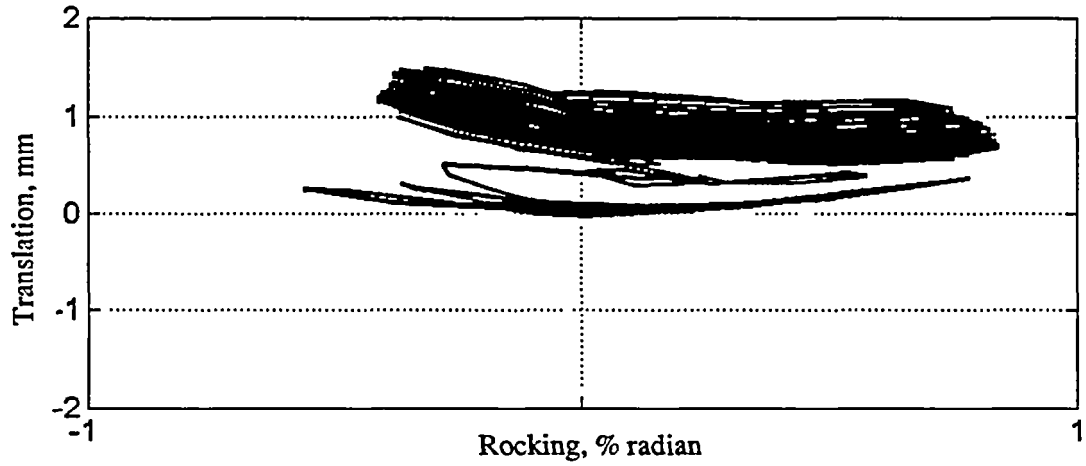

(c) Vertical displacement versus rocking about x-axis

Figure 4-24 Vertical displacement of the UPPER-1 porcelain unit, Test No 38

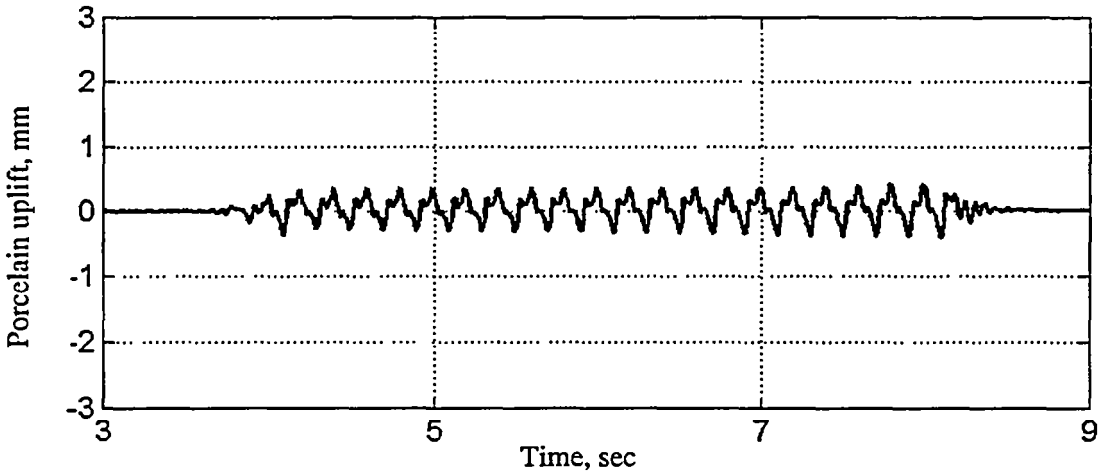

(a) Uplift history in x-direction (channel 51)

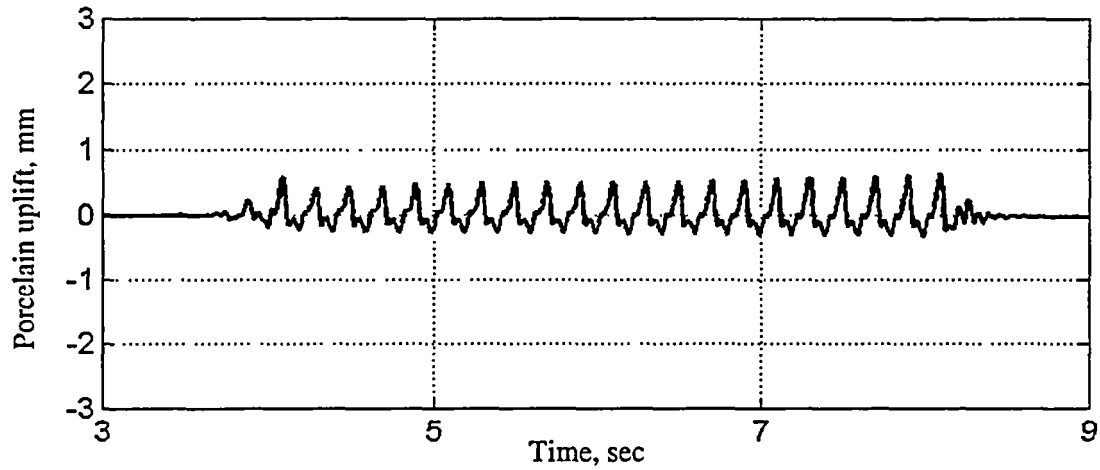

(b) Uplift history in x-direction (channel 53)

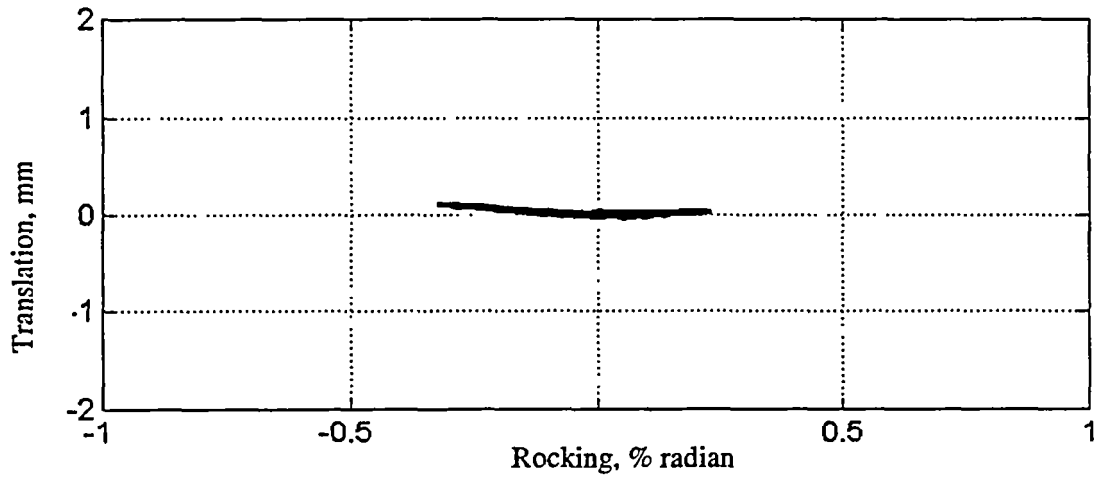

(c) Vertical displacement versus rocking about x-axis

Figure 4-25 Vertical displacement of the UPPER-1 porcelain unit, Test No 37

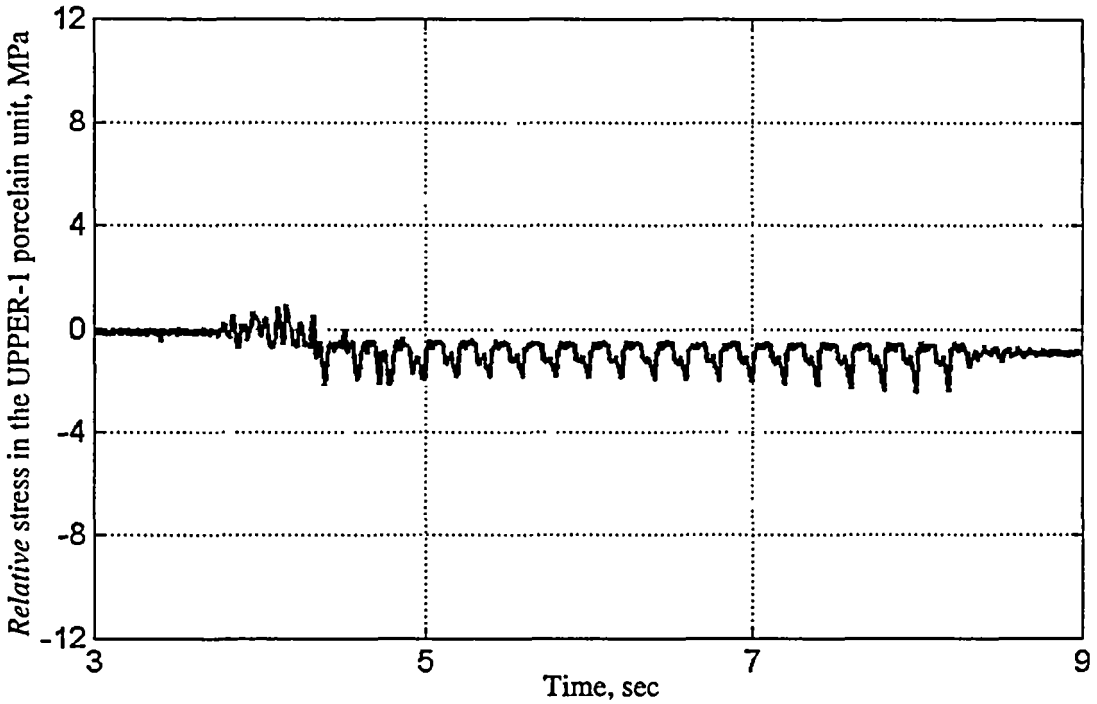

(a) Stress history of channel 39

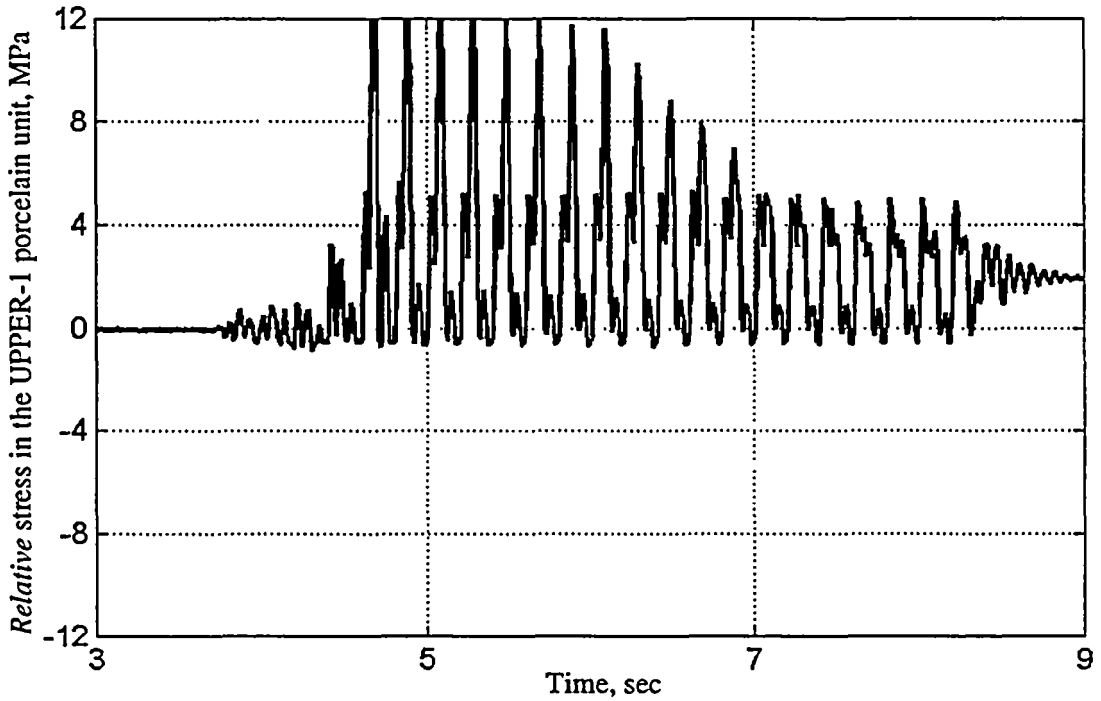

(b) Stress history of channel 41

Figure 4-26 Stress history of the UPPER-1 porcelain unit, Test No 38

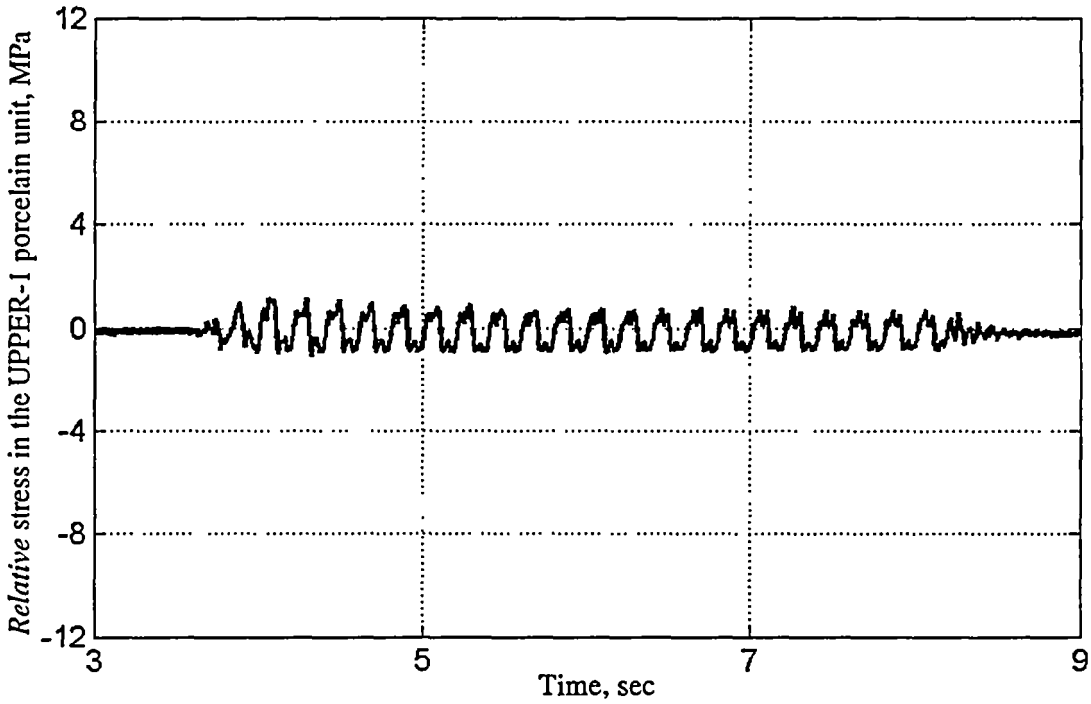

(a) Stress history of channel 39

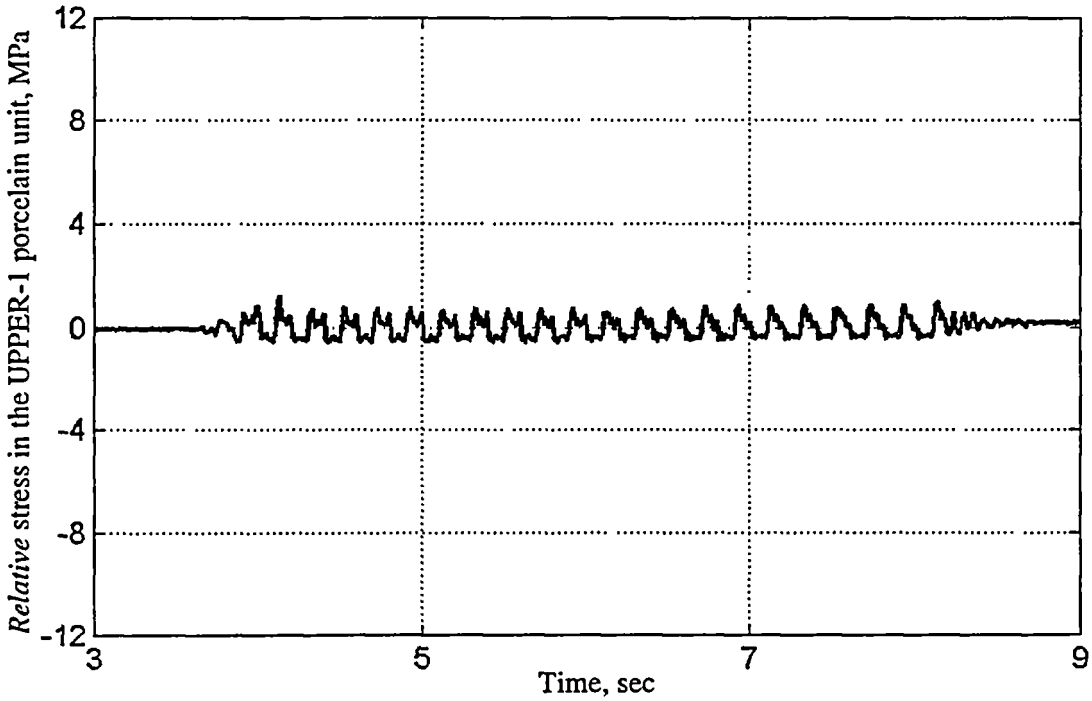

(b) Stress history of channel 41

Figure 4-27 Stress history of the UPPER-1 porcelain unit, Test No 37

5 Bushing Retrofit Details

5.1 Introduction

Oil leakage and excessive slip of the UPPER-1 porcelain unit over the flange have been observed in many porcelain bushings damaged in past earthquakes. Oil leakage is the most common failure mode and is caused by the uplift or rocking of the porcelain relative to the flange (see Chapter 2). Retrofitting in the field to eliminate oil leakage is difficult to achieve, since a more effective sealing or clamping mechanism would be required. Under emergency conditions such as those following a major earthquake, some utilities may choose to temporarily operate a transformer with a bushing that has leaked oil, provided that the gasket connection has re-sealed with only minor loss of oil, and there is high confidence that no internal damage has occurred. In contrast, most utilities will not operate a transformer bushing that has sustained large slip of porcelain relative to the flange. In a number of bushing failures, it has been hypothesized that excessive slip may have resulted in impact between the core tube condenser and the bushing flange. Damage to the condenser at the impact site, or contamination of the insulating oil in the bushing may have caused high electrical stresses that eventually lead to the bushing failures. Such bushing failures can be catastrophic and lead to costly transformer damage. In addition to preventing internal damage to the bushing components, reduction of slip displacement may limit the leakage of oil at the gasket connection by maintaining the porcelain in a central position, and possibly preventing gasket extrusion from the gasket connection, which has been observed in past failures. Reducing the slip displacement may therefore be an effective method of minimizing the damage sustained by porcelain bushings, and was the primary objective of the retrofit details developed by Dr. Schiff and the utilities.

The variation in bushing details poses a significant obstacle to developing a workable retrofit. Differing flange profiles, interferences caused by the lifting lugs and voltage tap fittings, and porcelain tolerances contribute to the need for a detail that can accommodate these variables. Because of difficulties, the detailing for the retrofit devices described in this chapter was not based on rigorous engineering analysis and design, and as such their details and effectiveness may not be readily extrapolated to other bushings.

5.2 Selection of a Candidate Retrofit Detail

Several criteria were used to develop the retrofit details for the bushings, namely, ease of application to different porcelain-to-flange interfaces (gasket connections), cost, and effect of the retrofit detail on the electrical functions of the bushing.

A retrofit detail using a ring, similar to shipping rings routinely used by manufacturers, was selected by the utilities and Dr. Schiff as the candidate detail. This detail is inexpensive and was intended to be placed around the gasket connection. A filler material was used to seal the gap between the inner face of the metal ring and the outer surface of the UPPER-1 porcelain unit. The primary intent of this detail was to restrain the porcelain from sliding over the flange.

For ease of installation, two semicircular rings were used. The two semicircular rings were bolted together as shown in Figure 5-1. To reduce the likelihood of slip of the UPPER-1 porcelain unit, the semicircular rings were extended approximately 1 in. (25 mm) above the gasket connection. Slots were cut in the lower part of the rings to accommodate the lifting lugs. The gap between the porcelain and the semicircular rings was grouted with a filler material. Three types of material were investigated: epoxy (silicone-brand), grout (cementitious), and rubber. The durability, elasticity, ease of placement, and electrical properties of the filler were evaluated.

5.3 Retrofit Rings

5.3.1 Introduction

Two retrofit rings were detailed for the testing program. Ring-1 was used for the static testing of Bushing-1. Ring-2 was used for the seismic testing of Bushing-2. Both rings used the same filler material. Ring-2 was a modified version of Ring-1 and was developed to both increase the bond between the filler and the ring and to prevent uplift and rotation of the ring.

5.3.2 Epoxy filler material

The filler material used for the retrofit rings was *CCS Bonder, Polyurea LWL* (Long Working Life) manufactured by ChemCo Systems Inc. of Redwood City of California. This material is a two-component (Part A or resin and Part B or hardener) elastomeric polyurea bonder designed for both interior and exterior use. The manufacturer recommends that the users remove any standing water from the surface prior to the application of the material. When mixing the two components, the proportions must be kept within 5 percent of the manufacturers recommended mix ratio of one-to-one. Proper mixing of the two components takes approximately two to three minutes and it is recommended that the material be allowed to cure overnight. The recommended minimum substrate temperature is 50° F (11° C). The material safety data sheet for the material indicates that it is of moderate hazard and does not require any special handling. The material can be cleaned with soap and water before it hardens. A safe solvent for the polyurea is DuPont DBE-6 Dimehyl Adipate (Dibasic Ester). A bond-breaker compound was applied to the ring and the bushing surface prior to placement of the ring to prevent the filler from bonding either to the ring or the bushing to facilitate removal and installation during the test program.

5.3.2.1 Geometry of Ring-1

Figure 5-1 shows the geometry of Ring-1. It was composed of two semicircular 1/4-in. (6-mm) thick 1.5-in. (38-mm) tall, plates bent to an inner radius of 14 in. (356 mm); 2 in. (51 mm) by 2.5 in. (64 mm) steel tabs were fillet welded to the semicircular rings. The two semicircular rings were connected by two 0.5 in. (13 mm) bolts at each end; 1-in. (25-mm) square washers were used to fill the gap between the semicircular rings.

Ring-1 was designed and installed to provide a uniform 5/8-in. (16-mm) gap (to be grouted with epoxy) between the inner surface of the ring and the outer surface of the porcelain. Holes were drilled and tapped in the ring around its circumference; 3/8 in. (10 mm) bolts were used to maintain the gap (the bolts were removed once the gap was grouted). To accommodate the lifting lugs, two notches were cut in the ring. The ring was placed such that the lower edge of the UPPER-1 porcelain unit was approximately 3/4 in. (19 mm) above the lower edge of the ring. Figure 5-3 shows Ring-1 placed around Bushing-1 during the static tests of the bushing.

5.3.3 Retrofit Ring-2

During the cyclic tests of Bushing-1, Ring-1 separated from the epoxy, rotated with respect to the bushing, and uplifted. Ring-1 improved the response of the 230-kV bushing only marginally. The detail was modified by Dr. Schiff and the utilities, and designated as Ring-2. The gap between the two semicircular rings was eliminated by reducing the gap between the porcelain and the ring from 5/8 in. (16 mm) to 3/8 in. (10 mm), and 1/2-in. (13-mm) thick steel angles were used to secure the ring to the bushing to prevent uplift of the ring.

Figure 5-2 shows the geometry of Ring-2. Ring-2 was designed and installed to provide a uniform 3/8 in. (10 mm) gap (to be grouted with epoxy) between the inner surface of the ring and the outer surface of the bushing. Ten steel tabs made from 3x3x1/2 in. (76x76x13 mm) steel angle sections were bolted to the ring at the location of the 3/8 in. (10 mm) threaded holes. The tabs were clipped under the bushing flange to prevent the uplift and rotation of the ring. The ring was placed such that its centerline coincided with the centerline of the gasket at the gasket connection. Figure 5-4 shows Ring-2 prior to placement around the gasket connection of Bushing-2.

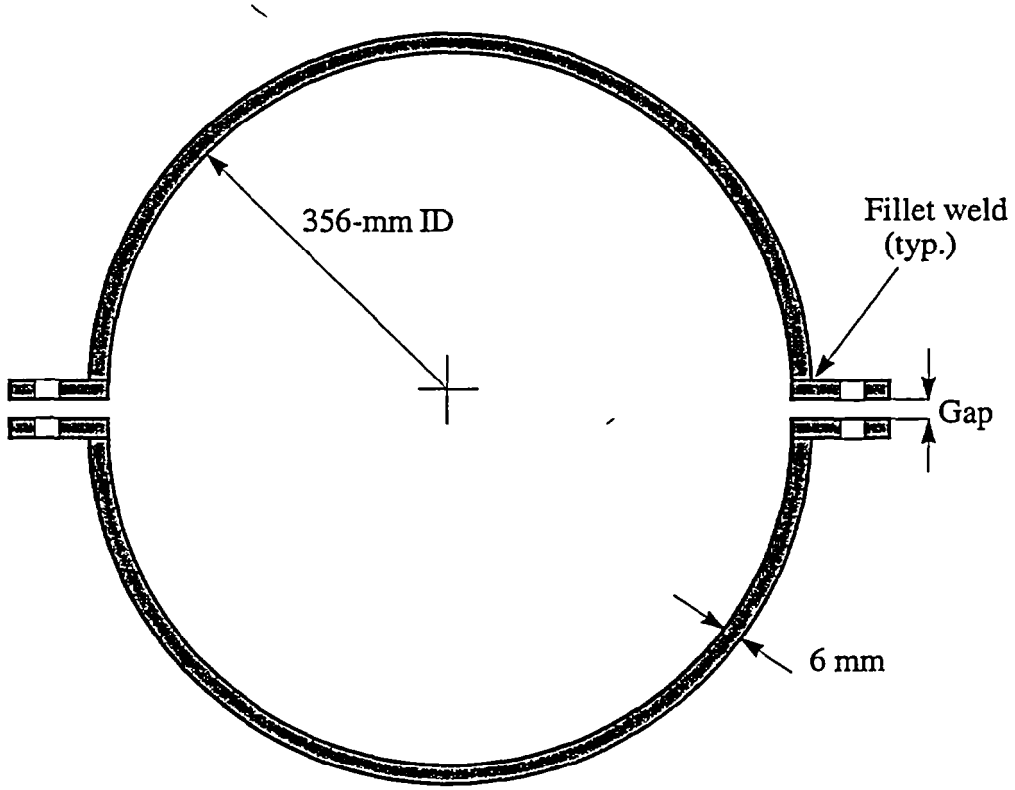

(a) Plan

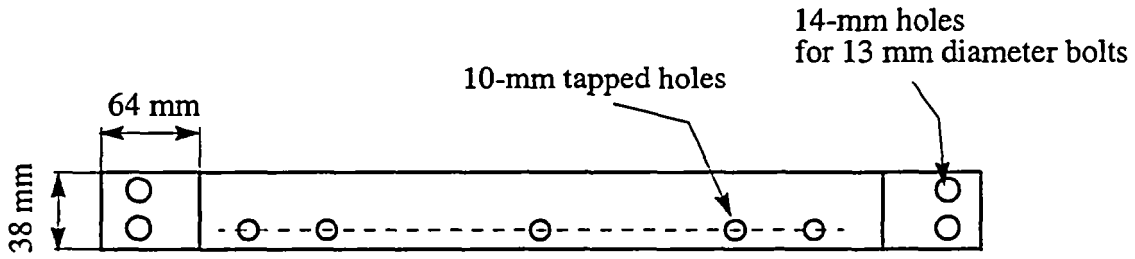

(b) Elevation

Figure 5-1 Geometry of Ring-1

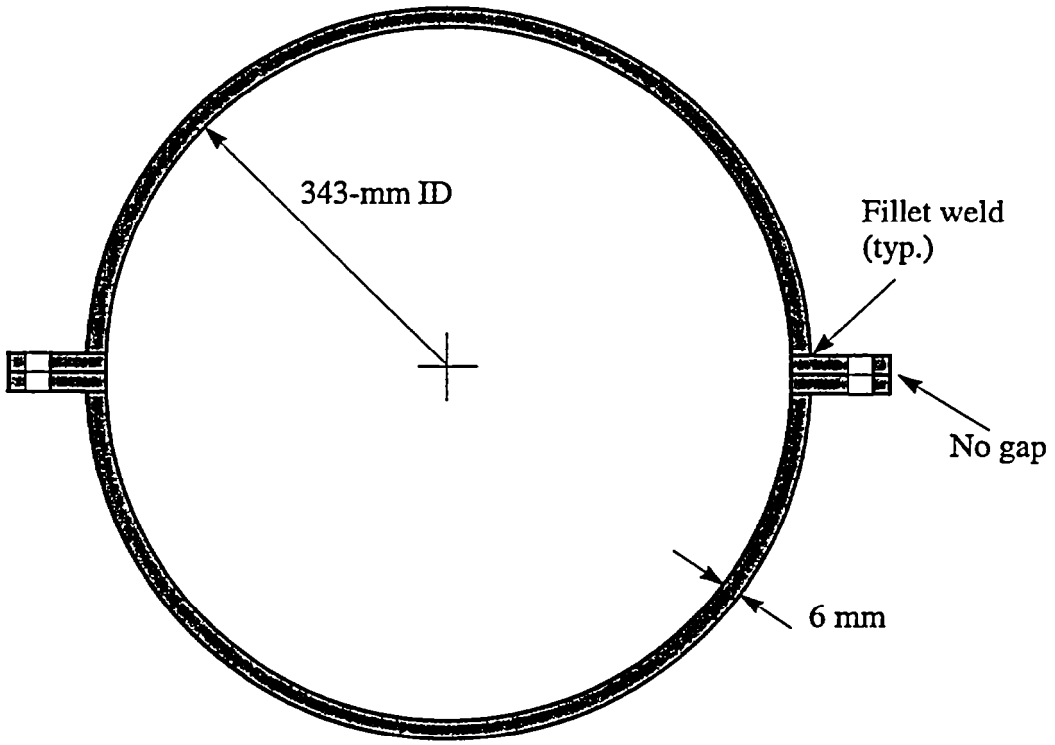

(a) Plan

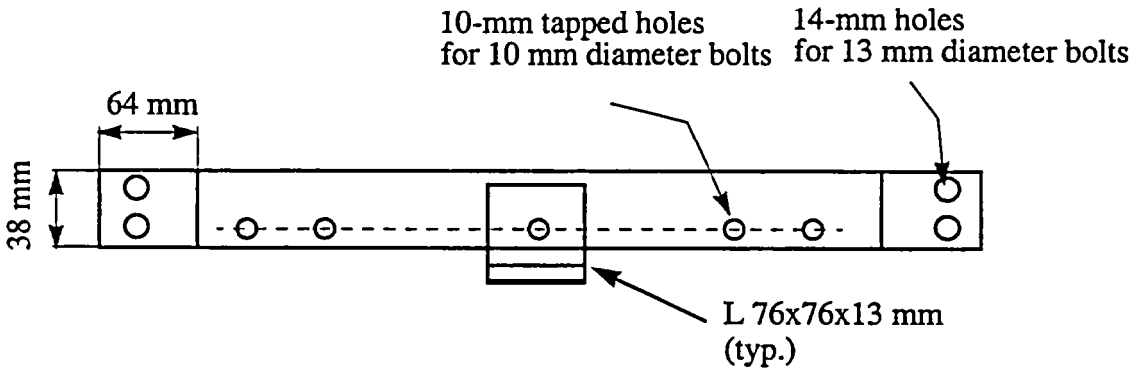

(b) Elevation

Figure 5-2 Geometry of Ring-2

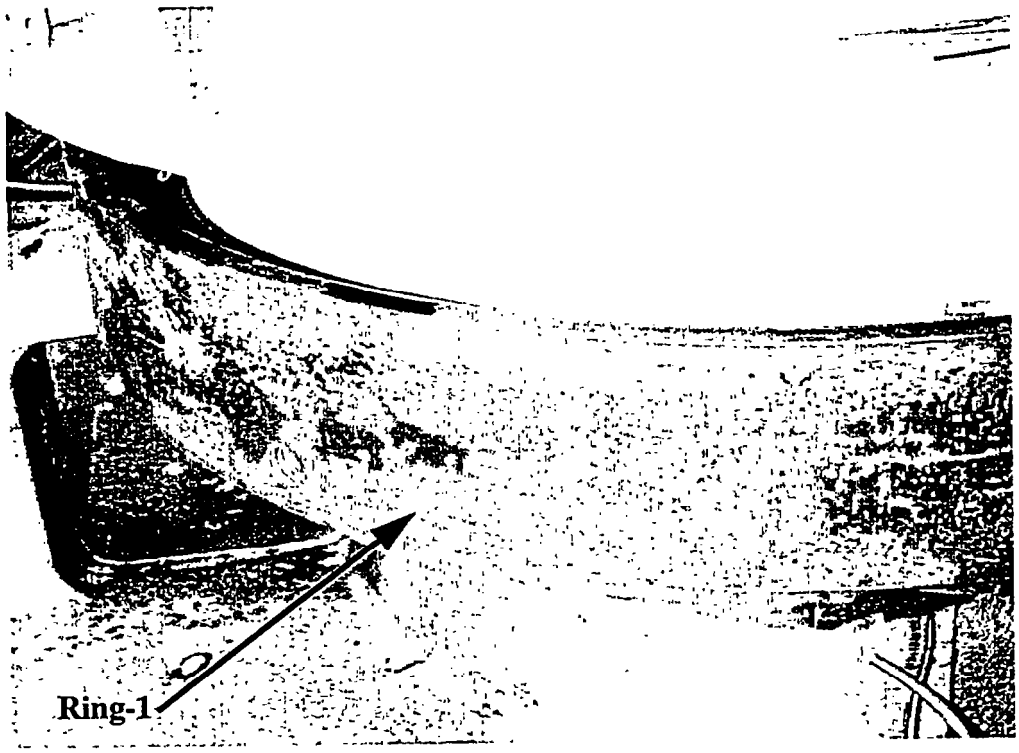

Figure 5-3 Ring-1 placed around the gasket connection of Bushing-1

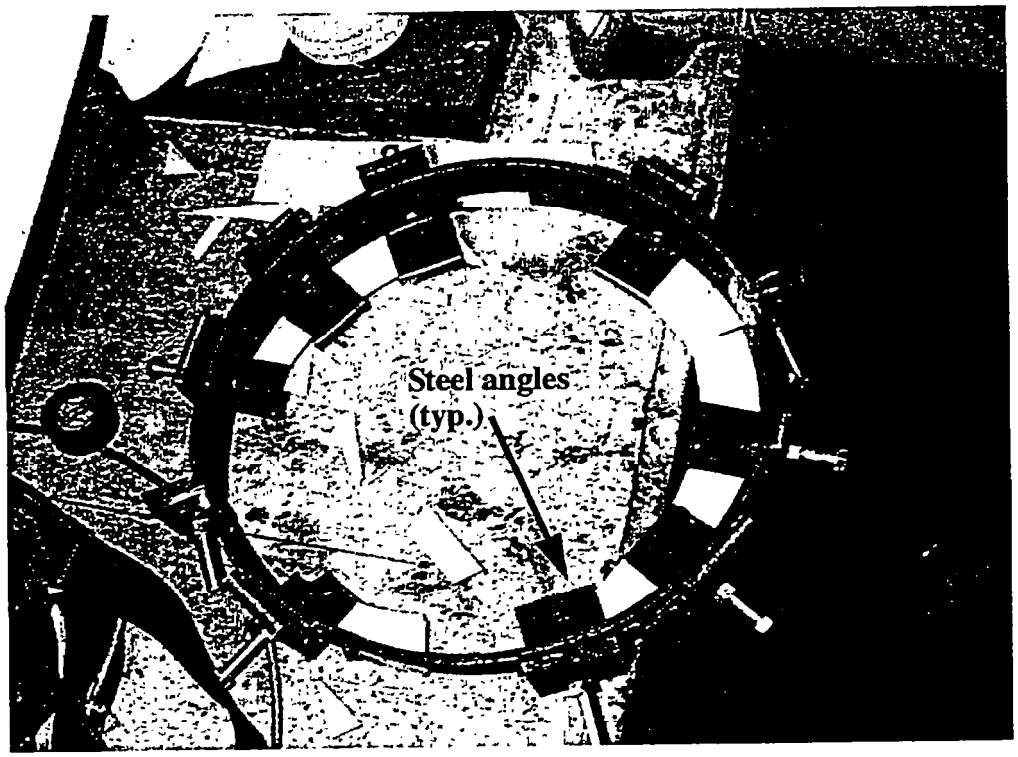

Figure 5-4 Ring-2 prior to installation around the gasket connection of Bushing-2

6 Static Cyclic Testing of Rigidly Mounted Bushing-1

6.1 Overview

Static tests were conducted to characterize the response of Bushing-1. The bushing was placed vertically in a stiff mounting frame and two actuators loaded the bushing horizontally. Bushing-1 was subjected to pull-back, quick-release tests, static cyclic (reversible) tests and static monotonic tests. The static tests were conducted at a low rate of loading and there was no dynamic effect. During the cyclic tests, three loading orbits (unidirectional, unidirectional with offset, and bidirectional) were used. Pull-back, quick-release tests were conducted to measure the dynamic properties of Bushing-1. Static tests were conducted to determine the limit states of response for the Bushing-1 as a function of the bushing post-tensioning force and actuator loading orbits, and to evaluate the efficacy of Ring-1 for retrofitting 230-kV bushings. The following sections present the experimental setup including the stiff mounting frame, instrumentation, and loading protocol and summary of experimental data.

6.2 Experimental Setup

6.2.1 Mounting frame

The *rigid* mounting frame used for static testing of Bushing-1 was a fully welded frame made of a 54 by 54 in. (1.4 x1.4 m) by 1.5-in. (38-mm)-thick top plate supported by four TS 5x5x3/8" (127x127x9.5 mm) columns. The frame was attached to the laboratory floor using four 1 in. (25 mm) high-strength post-tensioning rods, one per column. Four 3x3x3/8" (76x76x9.5 mm) angle braces were bolted to the top plate and attached to the existing reaction frame to provide lateral stiffness. Figure 6-1 shows Bushing-1 mounted on the test frame prior to the static tests. The four 3x3x3/8" (76x76x9.5 mm) angle braces can be seen on the left hand side of the photograph.

6.2.2 Post-tensioning mechanism

A 50-ton (450 kN) flat ram was used to post-tension the bushing. The post-tensioning (PT) setup consisted of: the flat ram located at the bottom of the bushing; a 48-in. (1.2-m) long TS 10x10x1/2" (250x250x13 mm) steel loading beam; a loading attachment bolted to the loading beam and resting on the loading plate in the dome of the bushing; a special bushing wrench that engaged the

loading plate in the dome of Bushing-1; and two 1.25 in. (32 mm) high-strength, fully threaded post-tensioning rods. The rods were anchored to the mounting frame at the bottom and to the loading beam at the top and were used to transfer the tensile force from the loading beam to the mounting frame. Figure 6-2 shows components of the post-tensioning assembly.

The post-tensioning procedure consisted of: loosening the 3/4 in. (19 mm) bolts attaching the bushing flange to the mounting frame, loading the bushing via the flat ram, monitoring the ram force via an in-line pressure sensor, and releasing the post-tensioning load in the bushing by loosening the nut at the top end of the bushing core (located in the dome). The post-tensioning force in the bushing was taken as the ram load at which the nut disengaged from the core.

6.2.3 Loading collar and joint collar

To distribute the horizontal actuator loads to Bushing-1, a loading collar was placed around the bushing. The collar consisted of a welded tubular section built up from four 10 x 3/8 in. (254 x 10 mm) steel plates. High-strength grout, placed between the porcelain and the collar, uniformly distributed the actuator load; 5/8-in. (16-mm)-thick plates were welded to two perpendicular faces of the collar to connect the actuators to the collar. One objective of the static tests was to characterize the response of the bushing at the gasket connection. To eliminate the movement at the joint between the UPPER-1 and UPPER-2 porcelain units (see Figure 6-3), a joint collar (similar to the loading collar) was installed. Figure 6-4 shows the loading and joint collars.

6.2.4 Loading mechanism and test control

The static cyclic tests were carried out using two actuators, each with a capacity of 10 kips (45 kN) and a stroke of 7.5 in. (190 mm). The actuators were attached to the loading collar with bolted clevises. Each actuator load was reacted via a trunnion mount that was attached to 4x4x3/8" (102x102x10 mm) angle steel supports that were welded to a TS 4x4x3/8" (102x102x10 mm) steel beam that was welded to the existing reaction frame. The applied force was measured using load cells in line with the actuators.

The center line of the horizontal actuators (point of application of the concentrated load) was located 47 in. (1.2 m) above the gasket connection. This dimension was selected to reproduce the ratio of the bending moment to the shear force at the gasket connection that would occur if the bushing mode shape was triangular in profile. Figure 6-4 shows the test setup prior to cyclic testing. The initial static cyclic test was conducted under displacement control with the actuator clevises oriented to allow rotation about the vertical axis.

6.2.5 Instrumentation

Sixteen channels of data were recorded for each static test. Table 6-1 lists the channel number, instrument type, response quantity, coordinate system, and location for each transducer. The bushing (x_{00} and y_{00}) and actuator (x_{45} and y_{45}) coordinate systems adopted for the testing program are shown in Figure 6-5. The numbers in this figure correspond to the channel number in Table 6-1.

Four channels (channels 1 through 4) recorded the force and displacement of the actuators. The displacements at top of the Bushing-1 and at the centerline of the actuators were monitored by four displacement transducers (channels 5 through 8). Four displacement transducers (channels 9 through 12), measured the radial displacement of the UPPER-1 porcelain unit relative to the flange plate. Four displacement transducers (channels 13 through 16) recorded the uplift of the UPPER-1 porcelain unit relative to the flange plate. Figure 6-6 shows the instrumentation at the top of Bushing-1. Figure 6-7 shows instrumentation of the UPPER-1 porcelain unit.

Table 6-1 Instrumentation for static tests of Bushing-1

Channel Number	*Transducer*[1]	*Response Quantity*	*Orientation*[2]	*Transducer Location*[3]
1	LC-1	actuator-1 force	x_{45}	actuator centerline
2	LC-2[4]	actuator-2 force	y_{45}	actuator centerline
3	LVDT-1	actuator-1 displacement	x_{45}	actuator centerline
4	LVDT-2	actuator-2 displacement	y_{45}	actuator centerline
5	DCDT-1	bushing displacement	x_{00}	top of bushing
6	DCDT-2	bushing displacement	y_{00}	top of bushing
7	DCDT-3	bushing displacement	x_{00}	actuator centerline
8	DCDT-4	bushing displacement	y_{00}	actuator centerline
9	DCDT-5	UPPER-1 slip	$-x_{45}$	gasket connection
10	DCDT-6	UPPER-1 slip	$-y_{45}$	gasket connection
11	DCDT-7	UPPER-1 slip	x_{45}	gasket connection
12	DCDT-8	UPPER-1 slip	y_{45}	gasket connection
13	DCDT-9	UPPER-1 uplift	z	gasket connection
14	DCDT-10	UPPER-1 uplift	z	gasket connection
15	DCDT-11	UPPER-1 uplift	z	gasket connection
16	DCDT-12	UPPER-1 uplift	z	gasket connection

1. LC = load cell; LVDT = displacement transducer; DCDT = displacement transducer.
2. For sensor orientation refer to Figure 6-5.
3. For location of instruments refer to Figure 6-5.
4. Channel used to measure the force during the pull-back tests.

6.3 Test Protocol

6.3.1 Pull-back, quick-release tests

Pull-back, quick-release tests were conducted to determine the lateral stiffness, vibration frequency, and modal damping of Bushing-1. The sequence of quick-release testing for Bushing-1 is presented in Table 6-2. The pull-back tests were carried out at selected intervals during the test program to evaluate the effects of bushing preload, the addition of Ring-1, and the lubrication of the gasket at the gasket connection on the dynamic properties of Bushing-1. These tests were conducted in both x_{00}- and y_{00}- directions (see Figure 6-5). Each test set was repeated to improve the accuracy of the results.

Table 6-2 Protocol for quick-release testing of Bushing-1

Test Set	*Test Date*	*Preload (kN)*	*Ring-1 Installed*	*Comments*
0	9/08/99	120	No	Initial quick-release test.
8	9/10/99	120	No	Gasket at the gasket connection was lubricated.
9	9/13/99	90	No	Bushing preload was reduced.
11	9/15/99	120	Yes	Bushing-1 was retrofitted with Ring-1.

The setup for the quick-release tests, shown in Figure 6-8, consisted of a nylon cable connecting the top of Bushing-1 to the reaction frame in-line with a turnbuckle, a load cell, and a machined bolt. During the pull-back stage of the tests, the bushing was gradually loaded to approximately 0.5 kips (2 kN). The applied force and the resulting displacement at top of the bushing were monitored and recorded using the in-line load cell and displacement transducers. The applied force was then released by cutting the machined bolt and the free vibration response was recorded.

6.3.2 Static tests

Static tests were conducted to determine the limit states of response for Bushing-1. One objective of the static testing of Bushing-1 was to characterize the bushing response as a function of the post-tensioning force. Another objective was to evaluate the efficacy of Ring-1.

The sequence for static testing of Bushing-1, including the test orbits, is presented in Table 6-3. Bushing-1 was tested using three cyclic (unidirectional, unidirectional with offset, and bidirectional) and one monotonic orbit. The orbits are shown in Figure 6-9. Unidirectional tests were conducted to characterize the response of Bushing-1. In the unidirectional with offset tests, an initial offset in the lateral direction was introduced to see if that offset increased rocking of the UPPER-1 porcelain unit at the gasket connection. In the bidirectional tests, Bushing-1 was displaced around a circular orbit to see if the circular orbit facilitated extrusion of the gasket from the gasket connection. The monotonic test was used to determine the limit state of response for Bushing-1.

The displacement history for each cyclic test, referred to as Test Set in the first column of Table 6-3 and shown in Figure 6-10, consisted of three complete cycles (referred to as Test Nos in the second column of Table 6-3) to a target displacement. The target displacement for Test No. 1 was 0.05 in. (1.25 mm) and the target displacements were increased by 0.05 in. (1.25 mm) for each subsequent test.

Previous analytical studies by the authors (Gilani et al., 1998) have shown that the stiffness of gasket in the gasket connection is the key determinant of the fundamental frequency and mode shape of porcelain transformer bushings. Gasket stiffness is a function of the contact pressure (equal to the preload divided by the plan area of the gasket) and the geometry of the groove into which the gasket is placed. Only the effect of contact pressure could be studied in this research program because the geometry of the groove could not be altered.

The manufacturer of Bushing-1 specifies a post-tensioning force of 27 kips (120 kN) for 230-kV type-U bushings. Test data from the manufacturer have shown that when the post-tensioning force is increased to 31 kips (138 kN), the springs in the bushing dome bottom out (reach the end of their travel). For a majority of the tests listed in Table 6-2, the post-tensioning force in the bushing was set at the manufacturer's specified value. To evaluate the effect of the post-tensioning force on the response of the bushing, static tests were conducted with the post-tensioning force set at 20 kips (90 kN): a 30-percent reduction in the preload. Static tests with a post-tensioning force set at 36 kips (160 kN): a 30-percent increase in the preload were not possible due to the travel limit of the springs in the bushing dome.

6.4 Experimental Results from Quick-Release Tests

Response histories of Bushing-1 for Test Set 0 are shown in Figure 6-11. The computed elastic (stiffness) and dynamic (frequency and damping ratio) properties at the top of Bushing-1 for quick-release tests are listed in Table 6-4. The stiffness of Bushing-1 was computed from the slope of the force-displacement relations (Figures 6-11a and 6-11b); the vibration frequencies of Bushing-1 were computed from peaks in the power spectra of the recorded displacement signals (Figures 6-11c and 6-11d); and the damping ratios of Bushing-1 were obtained using the log-decrement method (Clough and Penzien, 1993) for a segment of the free-vibration response history (Figures 6-11e and 6-11f). The effective weight of the bushing was computed from the stiffness and frequency data and assuming that the bushing is a single-degree-of-freedom system with a lumped mass at its top. The vibration properties of the bushing were approximately constant during the testing program.

Changes in the bushing post-tensioning force did not substantially alter the frequency of the bushing, although previous analytical studies have indicated that the fundamental frequency and mode shape of porcelain transformer bushings are directly dependent on the stiffness of the gasket in the gasket connection (Gilani, et al., 1998). This apparent discrepancy is due to the existing boundary condition of the gasket. For an unconfined gasket (the boundary condition on which the previous analysis was based), the relation between the gasket stiffness (tangent modulus) and the post-tensioning force can be derived using the stress-strain relation for the nitrile rubber (Elder, 1999). Figure 6-12 presents the gasket tangent modulus as a function of the post-tensioning force for the two unconfined gaskets. This figure shows that the gasket tangent stiffness is sensitive to

variations in the post-tensioning force in the range from 20 to 27 kips (90 to 120 kN). However, the gasket in Bushing-1 was confined in the flange groove (pocket). As a result, the tangent stiffness of the gasket was not sensitive to variations in the bushing preload in the 20 to 27 kip (90 to 120 kN) range, and the frequency of the Bushing-1 was not effected by modest changes in the preload.

Table 6-3 Protocol for static testing of Bushing-1

Test Set	*Test Nos*	*Test Date*	*Preload (kN)*	*Test orbit*[1]	*Ring-1 installed*	*Comments*[2]
1	1 to 8	9/08/99	120	a	No	Initial cyclic test.
2	1 to 4	9/09/99	120	b	No	Offset was 2.5 mm.
3	1 to 4	9/09/99	120	b	No	Offset was 5 mm.
4	1 to 6	9/09/99	120	c	No	Maximum orbit radius was 7.5 mm.
5	1 to 6	9/09/99	120	a	No	Gasket at the gasket connection was lubricated by oil.
6	1 to 6	9/09/99	120	a	No	Actuator 1 was disconnected and Bushing-1 was tested under load control.
7	1 to 6	9/10/99	120	a	No	Actuator 1 was disconnected and clevis for actuator 2 was rotated 90 degrees.
10	1 to 6	9/13/99	90	a	No	Bushing preload was reduced.
12	1 to 10	9/15/99	120	a	Yes	Ring-1 added to the gasket connection.
13	1 to 9	9/16/99	120	c	Yes	Maximum orbit radius was 11.25 mm.
14	-	9/16/99	120	d	Yes	Retrofitted Bushing-1 tested to failure.

1. a = unidirectional, b = unidirectional with offset, c = bidirectional, d = monotonic; see Figure 6-9.
2. For definition of offset and orbit radius see Figure 6-9.

The frequencies of Bushing-1 listed in Table 6-4 are approximately 20 percent lower than the values computed from the resonant-search tests listed in Table 4-4. These differences are due to the additional weight of the loading and joint collars, each weighing approximately 100 lbs (450 N).

6.5 Experimental Results from Static Tests of Bushing-1 without Ring-1

6.5.1 Unidirectional tests

The initial unidirectional test set, Test Set 1, was used to characterize Bushing-1 and to evaluate limit states of response for the bushing. There was no oil leakage or slip of the UPPER-1 porcelain unit for cycles with target displacements equal to or less than 0.3 in. (7.6 mm). During the 0.35-in. (8.75-mm) displacement cycles, the bushing leaked oil at the gasket connection and the UPPER-1 porcelain unit slipped a small amount. During the displacement cycles to 0.4 in. (10

mm), the bushing leaked a large amount of oil at the gasket connection and the UPPER-1 porcelain unit slipped significantly. The peak force in actuator 2 during these cycles was approximately 2 kips (9 kN). Figure 6-13 is a photograph of the gasket connection at the conclusion of Test Set 1 showing slip of the porcelain unit over the gasket connection.

Table 6-4 Modal properties obtained from frequency tests

	Lateral Stiffness (kN/mm)		*Frequency (Hz)*		*Damping Ratio (percent)*		*Effective Weight (N)*
Test Set	x^1_{00}	y_{00}	x_{00}	y_{00}	x_{00}	y_{00}	x_{00} or y_{00}
0	11	11	16	15	3	2	1030
8	11	10	16	15	3	3	1080
9	11	11	16	15	3	2	1030
11	11	10	16	15	3	2	1080

1. For definition of coordinate system, see Figure 6-5.

Figure 6-14 shows the relation between zero-corrected actuator-2 force and displacement at the top of the bushing during the 0.4-in. (10-mm) displacement cycles. The hysteretic behavior and lack of symmetry in force-displacement response were due to the slip of porcelain at the gasket connection and the test setup, respectively. Under displacement control testing, the displacements in actuators 1 and 2 (along the x_{45} and y_{45}) were specified as the target displacement and zero, respectively. As a result, the force in actuator 2 was not zero. Due to the force in the x_{45}- direction, the hysteretic response of Bushing-1 was not symmetric. The peak response values reported in this chapter were computed by averaging the maximum values in the forward and reverse half cycles.

At the conclusion of Test Set 1, the post-tensioning force in Bushing-1 was measured at 30.5 kips (137 kN), the bushing was de-stressed, oil was drained from the bushing, the bushing was partially disassembled, and the gasket at the gasket connection was examined. The gasket was neither distorted nor damaged, but was covered with a thin coat of oil (termed lubricated in this report).

Test Sets 5, 6, and 7 were conducted to investigate the effect of variations in the test setup on the response of the bushing. In Test Set 01, the gasket in the gasket connection was not lubricated, the actuator clevises were oriented to rotate in the horizontal plane, and the tests were conducted under displacement control. The maximum target displacement for Test Sets 5, 6, and 7 was set at 0.3 in. (7.5 mm) to avoid large slip of the UPPER-1 porcelain unit. Test Set 05 was conducted to study the effect of gasket lubrication on the response of the bushing. Prior to Test Sets 6 and 7, actuator 1 (along the x_{45} axis) was disengaged. Both Test Sets were conducted under load control. For Test Set 7, the clevis on actuator 2 was rotated 90 degrees to rotate in the vertical plane.

Figure 6-15 shows the zero-corrected displacement response of Bushing-1 at a target actuator displacement of 0.3 in. (7.6 mm) for Test Sets 1, 5, 6, and 7. The displacement histories are shown at three heights: top of bushing, actuator centerline, and gasket connection.

For Test Set 1, the initial cyclic test, the displacement history at the gasket connection is linear (Figure 6-15a) and corresponds primarily to the recoverable shear deformation in the gasket. For Test Set 5, cyclic tests with the lubricated gasket, the displacement history at the gasket connection is nonlinear (Figure 6-15b) due to the non-recoverable slip of the UPPER-1 porcelain unit.

The response of Bushing-1 from Test Set 1 using displacement control testing (Figure 6-15a) and Test Set 6 using load control testing (Figure 6-15c) are similar. A comparison of displacement histories from Test Set 6 (Figure 6-15c) and Test Set 7 (Figure 6-15d) shows that the clevis orientation and the test control had little or no effect on the response.

Test Set 10 was conducted to characterize the bushing response for a smaller post-tensioning force of 20 kips (90 kN). Oil leaked from the gasket connection during the tests to target actuator displacements of 0.2 in. (5 mm) and 0.25 in. (6.25 mm). During the tests to a maximum displacement of 0.3 in. (7.5 mm), oil leaked from the gasket connection and the UPPER-1 porcelain unit slipped over the flange. The post-tensioning force was checked following Test Set 10 and was found to be unchanged. A reduction in the post-tensioning force or preload reduced the uplift displacement at which the bushing will leak oil.

6.5.2 Unidirectional tests with offset

Two unidirectional tests along the y_{45} axis with an initial offset along the x_{45} axis, (see Figure 6-10b) were conducted. During Test Set 2, the bushing was initially displaced 0.1 in. (2.5 mm) in the x_{45} direction and then was cyclically loaded in the y_{45} direction. During Test Set 3, the bushing was initially displaced 0.2 in. (5.0 mm) in the x_{45} direction prior to cyclic loading in the y_{45} direction. For both Test Sets, the maximum target displacement along the y_{45} axis was 0.2 in. (5 mm). No oil leakage or slip of UPPER-1 porcelain unit over the flange was observed for either test. Figure 6-16 shows the actuator force-displacement response at the top of the bushing for the cycles to 0.2 in. (5 mm) of Test Set 3. The hysteresis loops along the y_{45} axis (Figure 6-16b) are not symmetric for the reasons cited in Section 6.5.1.

6.5.3 Bidirectional tests

Cyclic tests using the bidirectional (circular) orbit of Figure 6-10c were conducted to investigate whether circular motion of the bushing could dislodge the gasket from the groove in the flange plate. The cyclic tests were conducted to a maximum actuator displacement of 0.3 in. (7.5 mm). During the tests to a maximum displacement of 0.25 in. (6.25mm) and 0.3 in. (7.5 mm), there was minuscule oil leakage, and small slip of the UPPER-1 porcelain unit. No extrusion of the gasket was observed during the tests. Figure 6-17a shows the actuator 1-actuator 2 displacement orbit, and Figure 6-17b shows the actuator 1-actuator 2 force orbit during the cycles to a peak displacement of 0.3 in. (7.5 mm).

6.6 Experimental Results from Static Tests of Bushing-1 with Ring-1

6.6.1 Background

At the conclusion of Test Set 10, Bushing-1 was de-stressed, drained of oil, and partially disassembled. The gasket at the gasket connection inspected and air dried, the porcelain units were re-centered, and the bushing was post-tensioned to 27 kips (120 kN) and was refilled with oil. After post-tensioning, the retrofit ring (Ring-1) was attached around the gasket connection of the bushing. Pull-back, quick-release, unidirectional and bidirectional cyclic and monotonic tests were carried out to compute the dynamic properties of the retrofitted bushing, to evaluate the effect of the retrofit ring on response of the bushing, and to test the bushing to failure. Test results from quick-release tests are listed in Table 6-4. A summary of test results from the cyclic and monotonic tests is presented below.

6.6.2 Unidirectional tests

The unidirectional tests were conducted to a maximum actuator displacement of 0.5 in. (11.25 mm). During the tests to target displacements of 0.4 in. (10 mm) and 0.45 in. (12.5 mm), oil leaked from the gasket connection. During the 0.5-in. (12.5-mm) displacement cycles, Bushing-1 leaked oil and Ring-1 rotated about a horizontal (x-y plane) axis. Figure 6-18 shows Bushing-1 at the conclusion of the unidirectional tests. The original and final positions of Ring-1 are identified in the figure. Figure 6-19 shows oil leakage following Test Set 13.

6.6.3 Bidirectional tests

The bidirectional tests were conducted to a maximum actuator displacement of 0.45 in. (12.5 mm). During the tests to a maximum displacement of 0.35 in (8.75 mm) and 0.4 in (10 mm), the bushing leaked oil from the gasket connection. During the 0.45-in. (11.25-mm) displacement cycles, oil leaked from the gasket connection, Ring-1 rotated about a horizontal (x-y plane) axis and separated from the epoxy filler material (which was used to grout the gap between Bushing-1 and Ring-1), and the UPPER-1 porcelain unit twisted about the vertical (z-) axis. Figure 6-20 shows the separation of Ring-1 from the epoxy filler material at the conclusion of the bidirectional tests. Figure 6-21 shows the twist of UPPER-1 porcelain unit at the conclusion of the bidirectional tests.

6.6.4 Monotonic test

Actuator 2 (along the y_{45} axis) was disconnected from Bushing-1 and the bushing was monotonically loaded by actuator 1 (along the x_{45} axis). When the displacement in actuator 1 exceeded 0.4 in. (10 mm), Bushing-1 began to leak oil. At actuator displacements larger than approximately 1.5 in. (38 mm), the oil leakage was continuous. As the actuator displacement was increased further, Ring-1 rotated and separated from the epoxy filler material. The side of Ring-1 closest to actuator 1 (see Figure 6-4) lifted with respect to the UPPER-1 porcelain unit. At an actuator displacement of approximately 5.5 in. (140 mm), a loud noise was heard. Testing continued to the actuator stroke limit of approximately 6 in. (152 mm). At this displacement, the

maximum force in actuator 1 exceeded 5 kips (22 kN). To complete the test, actuator 1 was slowly retracted to its original position. During retraction, the uplifted side of Ring-1 pressed against the surface of the bottom shed in the UPPER-1 porcelain unit (see Figure 2-4) and fractured the porcelain in two locations. Testing was stopped at an actuator force equal to zero.

At the conclusion of Test Set 14, Ring-1 was removed. Examination of Bushing-1 revealed that the UPPER-1 porcelain unit had slid as shown in Figure 6-22, and Ring-1 had rotated and separated from the epoxy filler material and had made contact with and fractured the bottom shed of the UPPER-1 porcelain unit (see Figure 6-23). Although the gasket in the gasket connection had severed at one location as shown in Figure 6-24, it had not extruded from the groove in the flange. The cast aluminum flange of Bushing-1 had fractured as shown in Figure 6-25. This fracture was the likely cause of the loud noise heard during the test. Bushing-1 was then de-stressed. The post-tensioning force in the bushing was measured to be 29.3 kips (130 kN).

Figure 6-26a shows the relation between displacement at the top of the bushing and the force in actuator 1, and Figure 6-26b shows the relation between displacement at the gasket connection and force in the actuator 1. Up to an actuator load of approximately 1.4 kips (6 kN), the force-displacement relations are linear. At larger values of actuator force, the stiffness of the bushing is significantly reduced due to the large slip of the UPPER-1 porcelain unit over the bushing flange.

6.7 Evaluation of Response of Bushing-1

6.7.1 Introduction

The data from static tests of Bushing-1 were used to characterize the response of the bushing and to evaluate the efficacy of Ring-1.

6.7.2 Modification of recorded data

Prior to examining the response of Bushing-1, the recorded data were corrected by first transforming the data to the appropriate coordinate system and then by applying the second order geometric corrections. For the pull-back, quick-release tests, the recorded data were transformed to the x_{00}-y_{00} coordinate system (coinciding with the bushing x-y axes) and for the static tests, the recorded data were transferred to the x_{45}-y_{45} coordinate system (coinciding with the axes of the two actuators). The transformation between these two coordinate systems is given by:

$$\begin{bmatrix} x_{45} \\ y_{45} \end{bmatrix} = \frac{1}{\sqrt{2}} \begin{bmatrix} 1 & -1 \\ -1 & 1 \end{bmatrix} \begin{bmatrix} x_{00} \\ y_{00} \end{bmatrix} \tag{6-1}$$

The recorded data from the radial sensors at the gasket connection (channels 9-12 of Table 6-1) were used to compute the horizontal motion of the UPPER-1 porcelain unit at the gasket connection (u_{45} and v_{45}, denote the translation of the UPPER-1 porcelain unit along the x_{45} and y_{45} directions; the twist about the z-axis was small and was ignored).

The data collected from the sensors recording the vertical motion of the UPPER-1 porcelain unit at the gasket connection (channels 13-16, see Table 6-1) were corrected to eliminate the second-order geometric effects due to the horizontal motion of the UPPER-1 porcelain unit at the gasket connection. The corrected data were used to compute the concentrated rotation at the gasket connection (due to the flexibility of the gasket). Rotation about the y_{00}-axis was calculated as the difference between the channel 15 and 13 displacements divided by the 25-in. (635-mm) distance between these transducers. Rotation about the x_{00}-axis was calculated as the difference between the channel 16 and 14 displacements divided by the 25-in. (635-mm) distance between these transducers. Rotation about the x_{45}-axis was computed by computing the vector sum of the rotations about the x_{00} and y_{00} axes.

6.7.3 Displacement response of Bushing-1

Test Set 1 was used to further characterize the response of Bushing-1. During Test No 3 to a target displacement of 0.1 in. (2.5 mm), the slip of the UPPER-1 porcelain unit was negligible and the maximum force in actuator 2 (along y_{45}-axis) was 1.16 kips (5.1 kN). Maximum displacements of 0.11 in. (2.8 mm), 0.07 in. (1.8 mm), and 0.017 in. (0.4 mm), were measured along the y_{45}-axis at the top of the bushing, at the actuator, and at the gasket connection, respectively. At the gasket connection, concentrated rotations were 0.06 percent radian about the y_{00}-axis and 0.04 percent radian about the x_{00}-axis, respectively; the rotation about the x_{45}-axis was estimated by averaging these value. The displacement of 0.05 in. (1.4 mm) at the top of the bushing along the y_{45}-axis due to this rotation at the gasket connection was calculated by multiplying the 74-in. (1.9-m) height of the segment of the bushing between the gasket connection and the top of the bushing by the rotation about the x_{45} axis.

As noted in Chapter 2, the bushing displacement (in the segment between the gasket connection and the top of bushing) comprises contributions from the cantilever deformation of the porcelain stacks, the concentrated rotation at the gasket connection, the shear deformation in the gasket, and the slip of UPPER-1 porcelain unit over the flange. The total displacement at the top of Bushing-1 for Test No 3 of Test Set 1 consisted of 15 percent contribution from the shear deformation of the gasket in the gasket connection and 50 percent from the concentrated rotation at the gasket connection.

6.7.4 Slip properties of the gasket at the gasket connection

As noted in Chapter 2, two factors resist the slip of the porcelain unit over the gasket: (1) the friction between the nitrile gasket and porcelain and (2) the restraint provided by the core kraft paper assembly. Data recorded during Test Sets 1 and 5 were used to estimate the slip coefficient between at the gasket connection. During Test Set 1, the gasket was not covered with oil (herein termed dry), whereas during Test Set 5, the gasket was partially covered with oil (herein termed lubricated). Figure 6-27 shows the relation between the force in actuator 2 and the displacement of the UPPER-1 porcelain unit at the gasket connection along the y_{45}- axis.

Figure 6-27a shows the force-displacement relation for Test No 8 (target actuator displacement of 0.40 in. or 10 mm) for Test Set 1. During this test, the UPPER-1 porcelain unit slipped when the force in actuator 2 was approximately 2.4 kips (11 kN). The slip coefficient at the gasket connection was obtained as the ratio of this force and the post-tensioning of 27 kips (120 kN). Figure 6-27b shows the force-displacement relation for Test No 6 (target actuator displacement of 0.30 in. or 7.5 mm) for Test Set 5. During this test, the UPPER-1 porcelain unit slipped when the force in actuator 2 was approximately 1.9 kips (9 kN). The slip coefficient at the gasket connection was obtained as the ratio of this force and the post-tensioning force of 27 kips (120 kN). A comparison of the actuator force required to initiate slip of the porcelain over the gasket for the dry and lubricated gaskets suggests that the core kraft paper assembly provides a significant portion of the resistance to the slip of the UPPER-1 porcelain unit.

6.7.5 Efficacy of Ring-1

Test data from Test No 8 of Test Set 1 (Bushing-1 without Ring-1) and Test No 8 of Test Set 12 (Bushing-1 with Ring-1) were used to evaluate the efficacy of Ring-1 in improving the response of Bushing-1. Figure 6-28a shows the relation between the force in actuator 2 and the displacement of the UPPER-1 porcelain unit at the gasket connection along the y_{45}- axis for these two tests. The addition of Ring-1 neither prevented nor significantly reduced the slip of the UPPER-1 porcelain unit over the flange. Figure 6-28b shows the relation between the force in actuator 2 and vertical (z-axis) motion at the face of the UPPER-1 porcelain unit at the gasket connection for the two tests. The addition of Ring-1 did not prevent the uplift of the UPPER-1 porcelain unit at the gasket connection.

During the bidirectional tests of Test Set 13, Ring-1 did not prevent slip or rotation of UPPER-1 porcelain unit at the gasket connection. During the monotonic test to failure of Test Set 14, Ring-1 rotated, separated from the epoxy filler material and fractured the bottom shed of the UPPER-1 porcelain unit.

6.8 Summary

Test data from the quick-release and static tests of Bushing-1 were used to evaluate the dynamic properties of the bushing and characterize its response.

Data from the pull-back, quick-release tests were used to measure the frequency and damping ratio of the bushing. The frequency of the bushing in the x- and y-directions were approximately 16 and 15 Hz. The additional mass of the loading and the joint collars reduced the fundamental frequency of the bushing and increased its effective weight. Due to the confinement of the gasket in the groove, the bushing frequency was not effected by the reduction in the preload from 27 kips (120 kN) to 20 kips (90 kN).

Data from the static tests were used to characterize the response of the bushing response and to evaluate limit states of response. During the first unidirectional test, oil leaked from the gasket connection at an actuator displacement of 0.4 in. (10 mm). Reduction in the post-tensioning force from 27 kips (120 kN) to 20 kips (90 kN), reduced the uplift displacement at which the bushing

leaked oil. When the gasket was lubricated with oil, the actuator force required to initiate slip of the UPPER-1 porcelain unit over the flange was reduced. During the tests in which Ring-1 was added to the bushing, oil leaked from the gasket connection, the UPPER-1 porcelain unit twisted above the flange, and Ring-1 rotated and separated from the filler material.

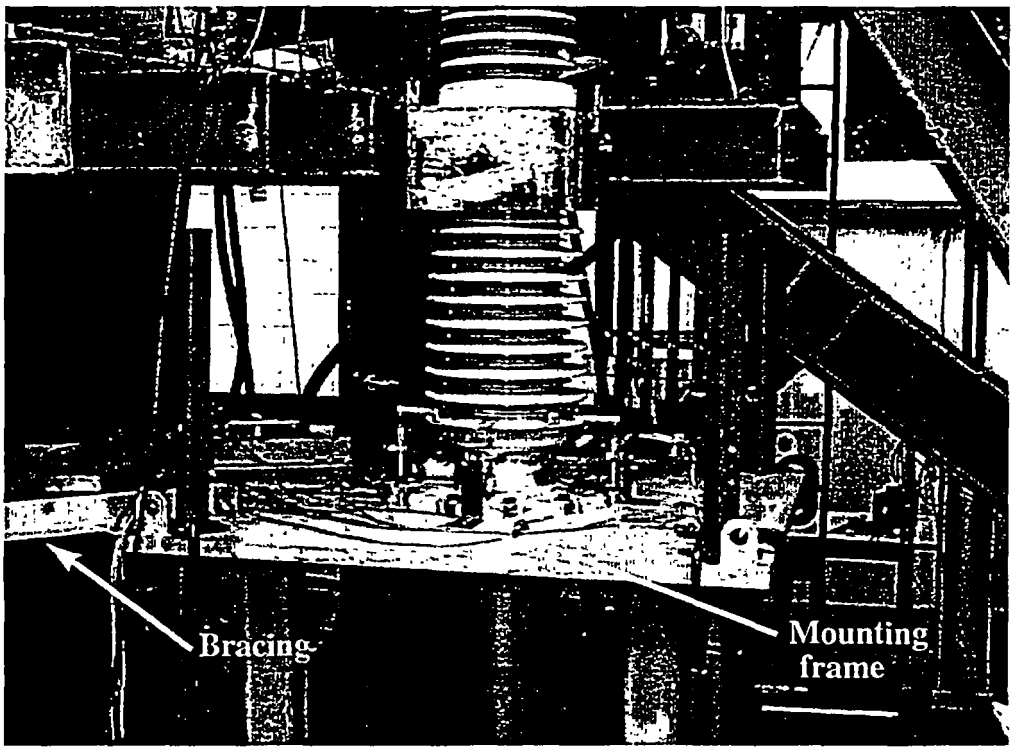

Figure 6-1 Bushing-1 and the mounting frame

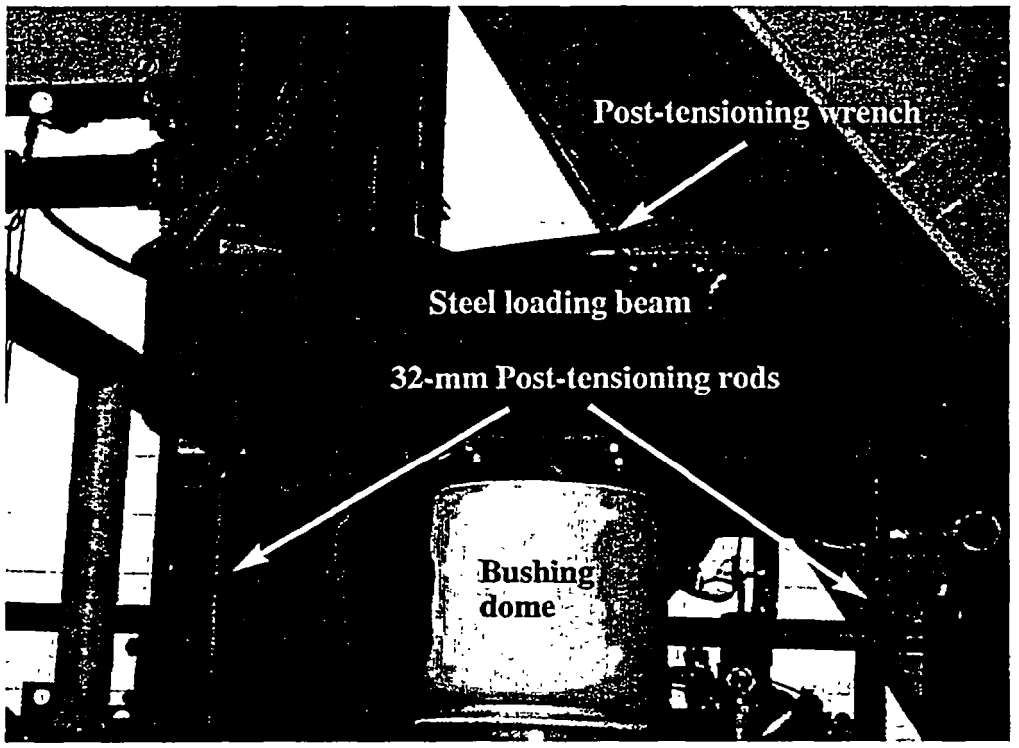

Figure 6-2 Post-tensioning setup for Bushing-1

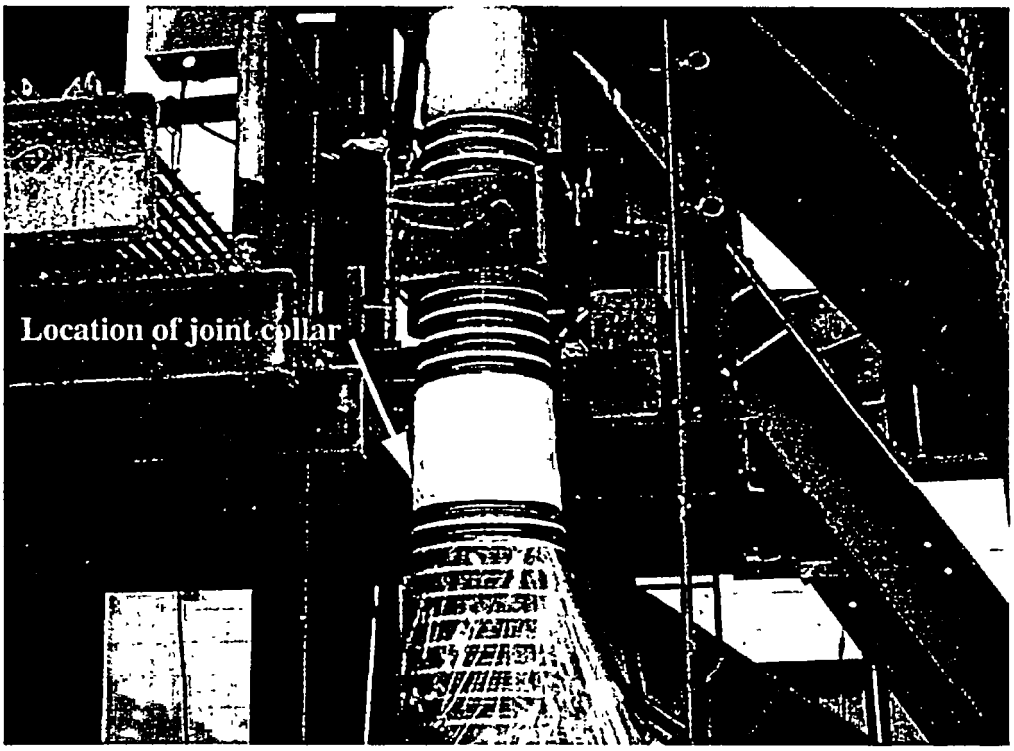

Figure 6-3 Joint collar for Bushing-1

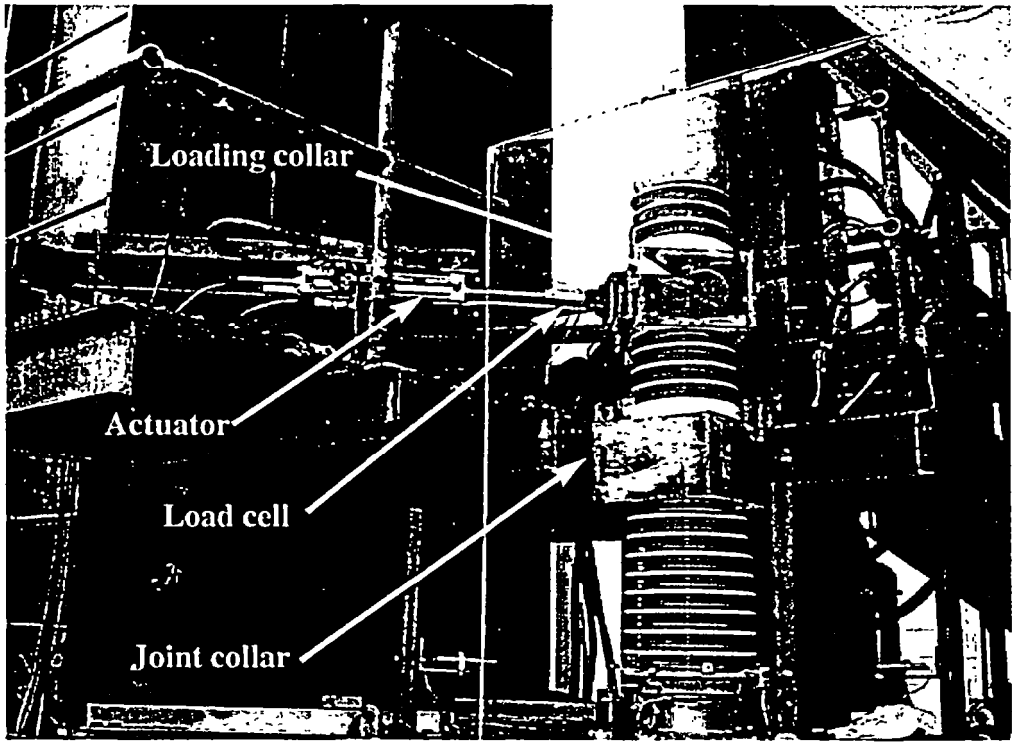

Figure 6-4 Bushing-1 prior to cyclic testing

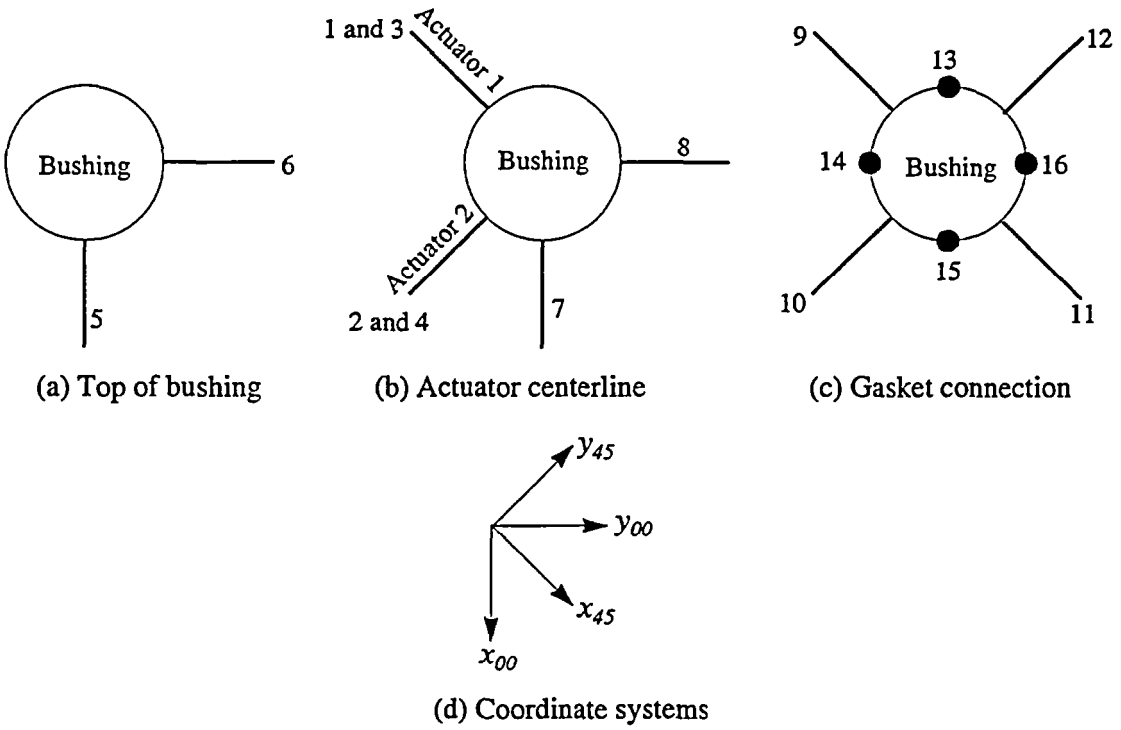

(a) Top of bushing (b) Actuator centerline (c) Gasket connection

(d) Coordinate systems

Figure 6-5 Instrumentation for static tests of Bushing-1

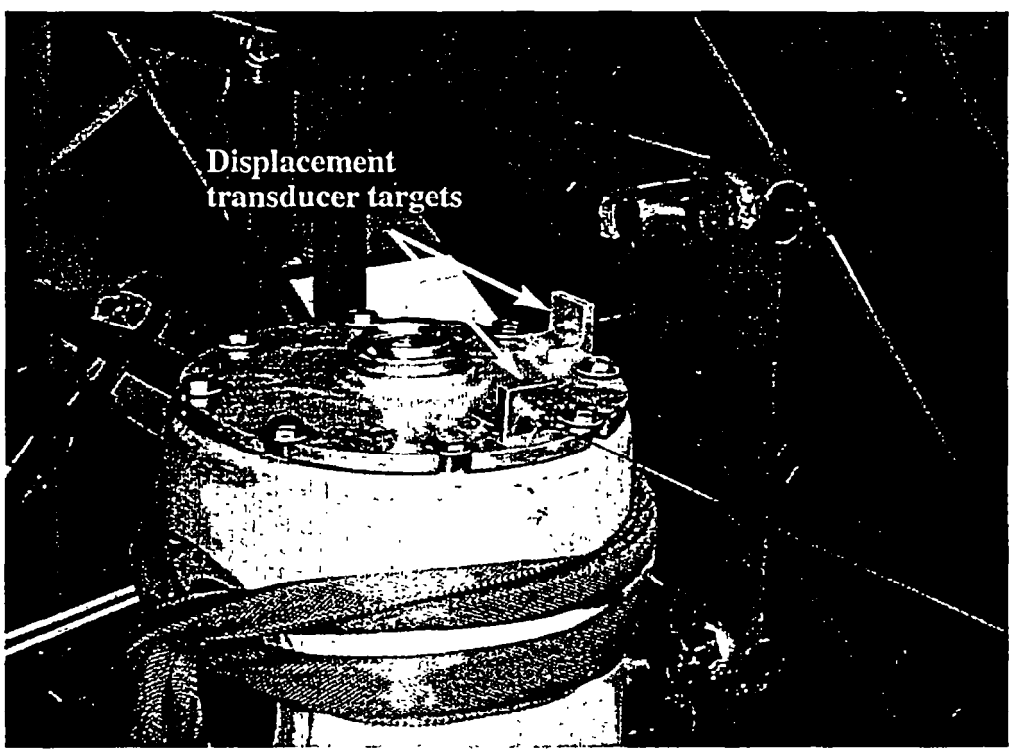

Figure 6-6 Instrumentation at the top of Bushing-1

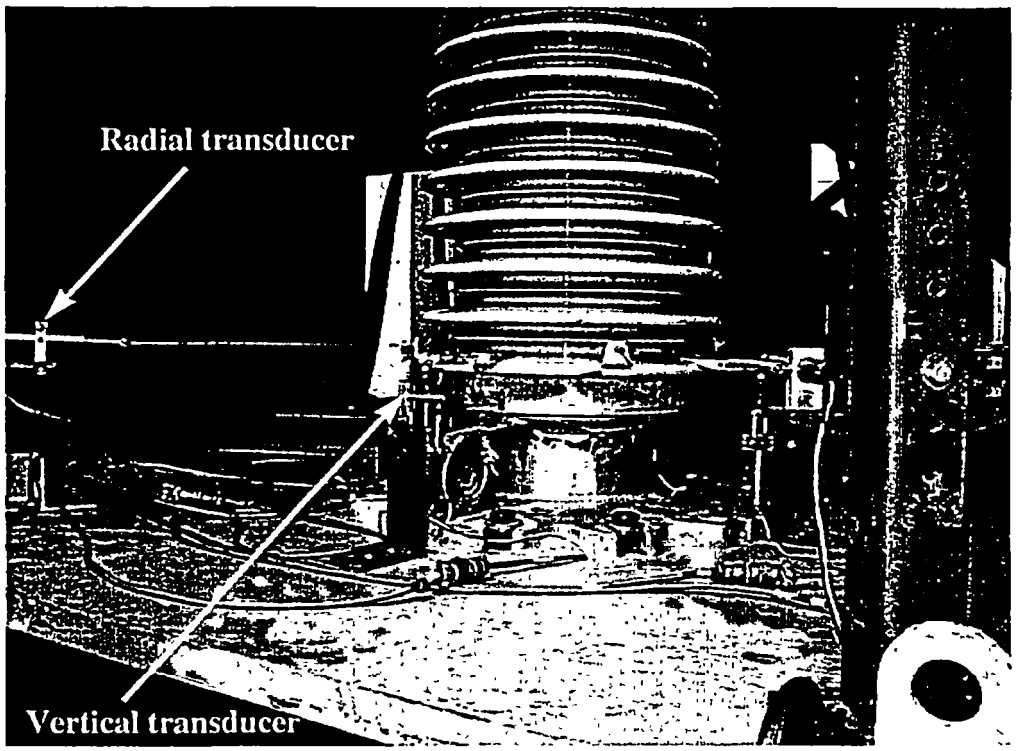

Figure 6-7 Instrumentation of the UPPER-1 porcelain unit

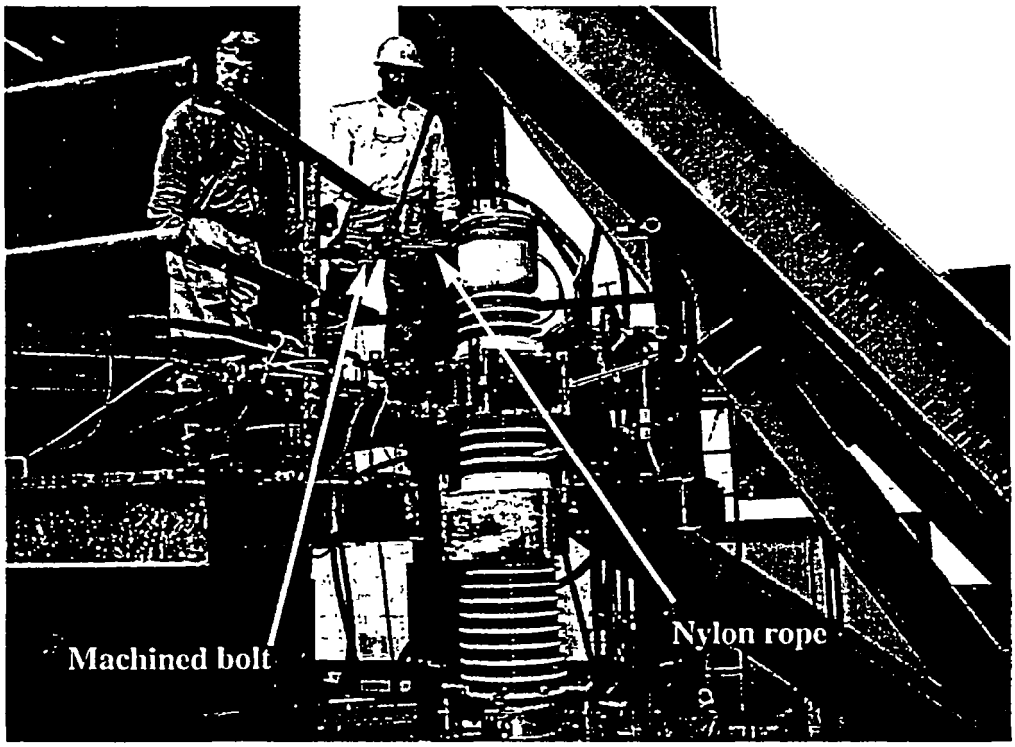

Figure 6-8 Test setup for pull-back, quick-release test

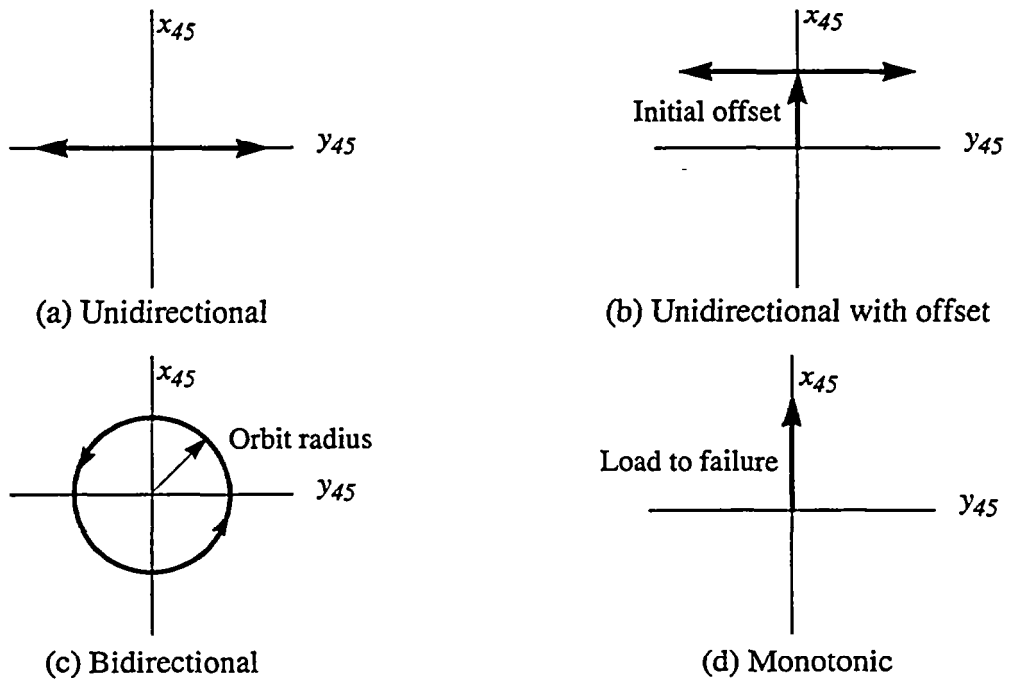

Figure 6-9 Displacement orbits for static tests

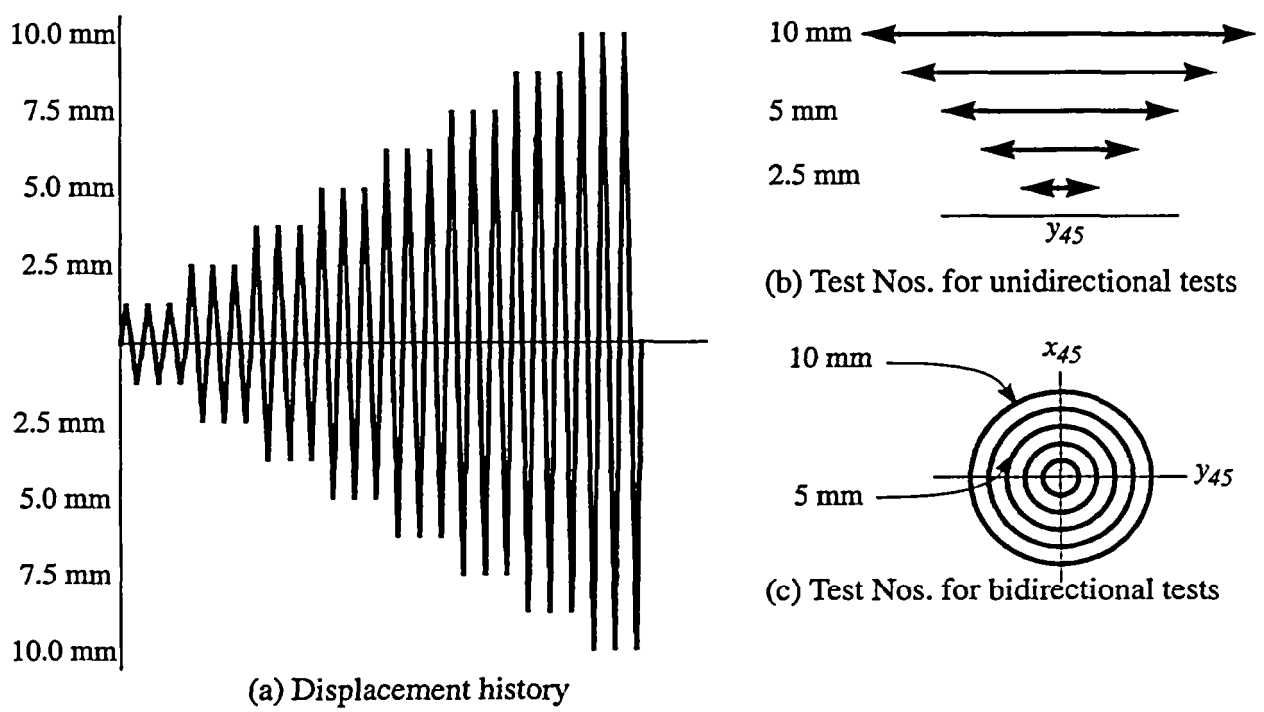

Figure 6-10 Displacement history for static cyclic tests

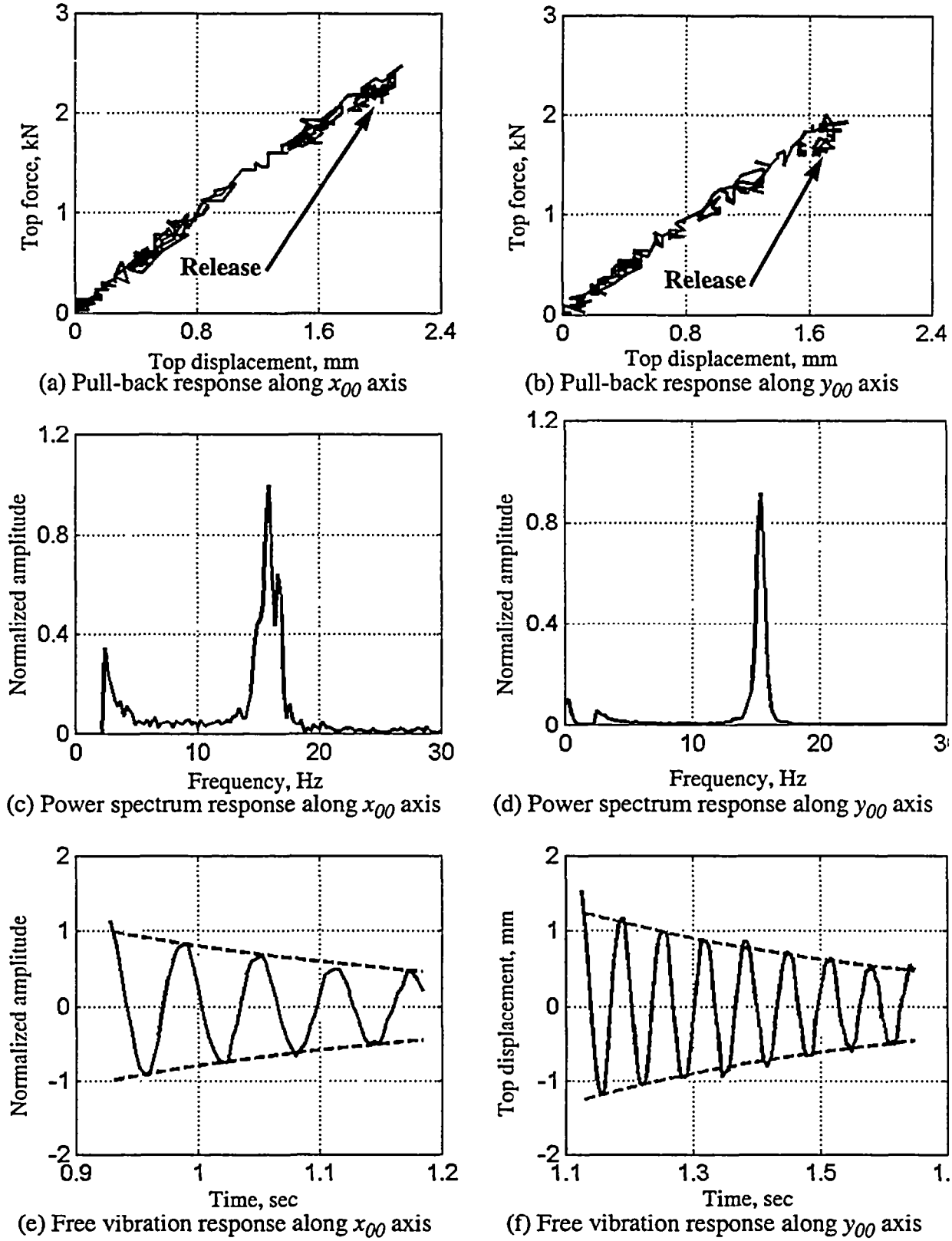

(a) Pull-back response along x_{00} axis

(b) Pull-back response along y_{00} axis

(c) Power spectrum response along x_{00} axis

(d) Power spectrum response along y_{00} axis

(e) Free vibration response along x_{00} axis

(f) Free vibration response along y_{00} axis

Figure 6-11 Time and frequency response of displacement sensors

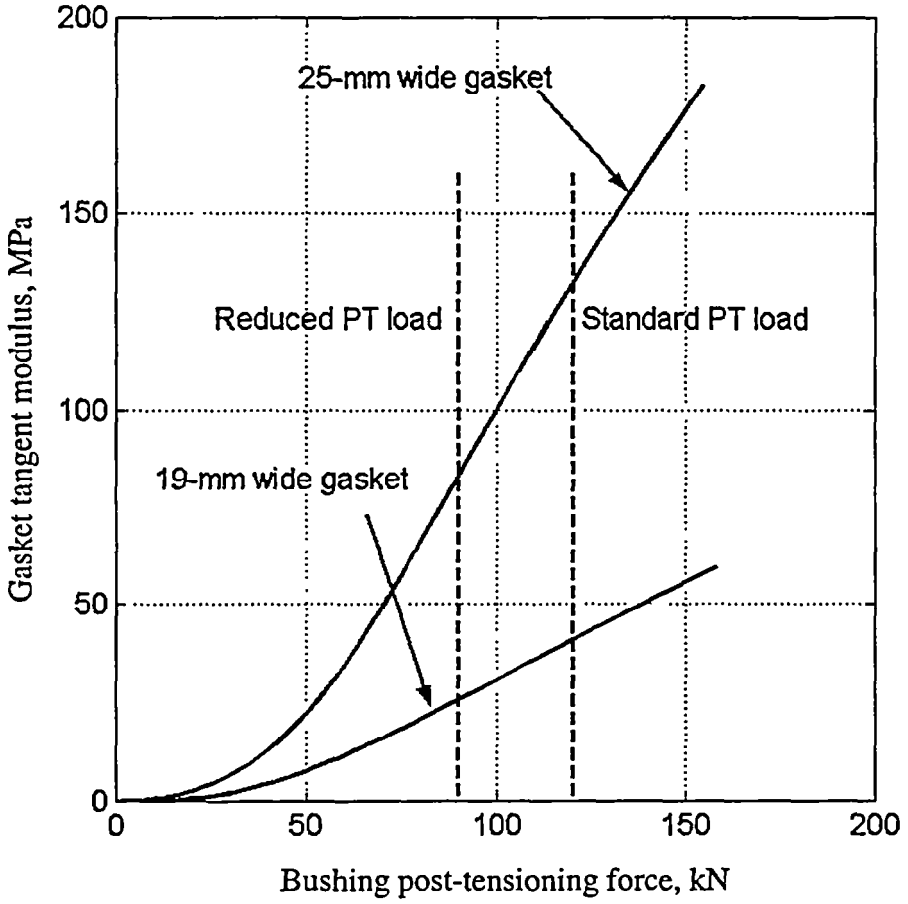

Figure 6-12 Effect of preload on the gasket stiffness

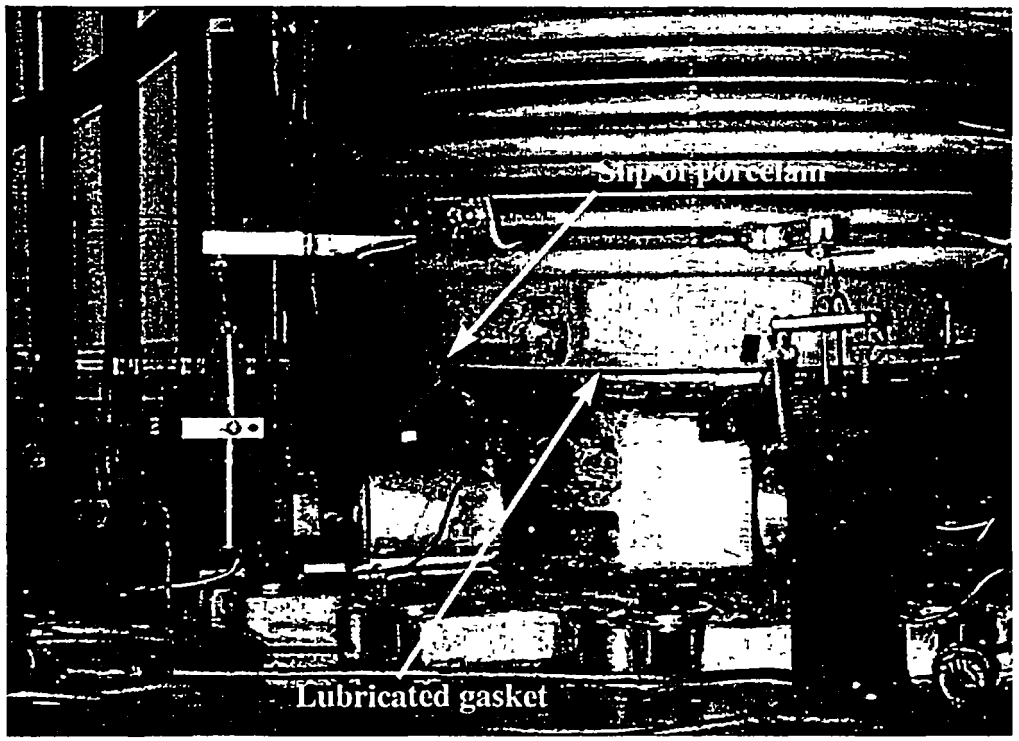

Figure 6-13 Bushing-1 at conclusion of Test Set 1

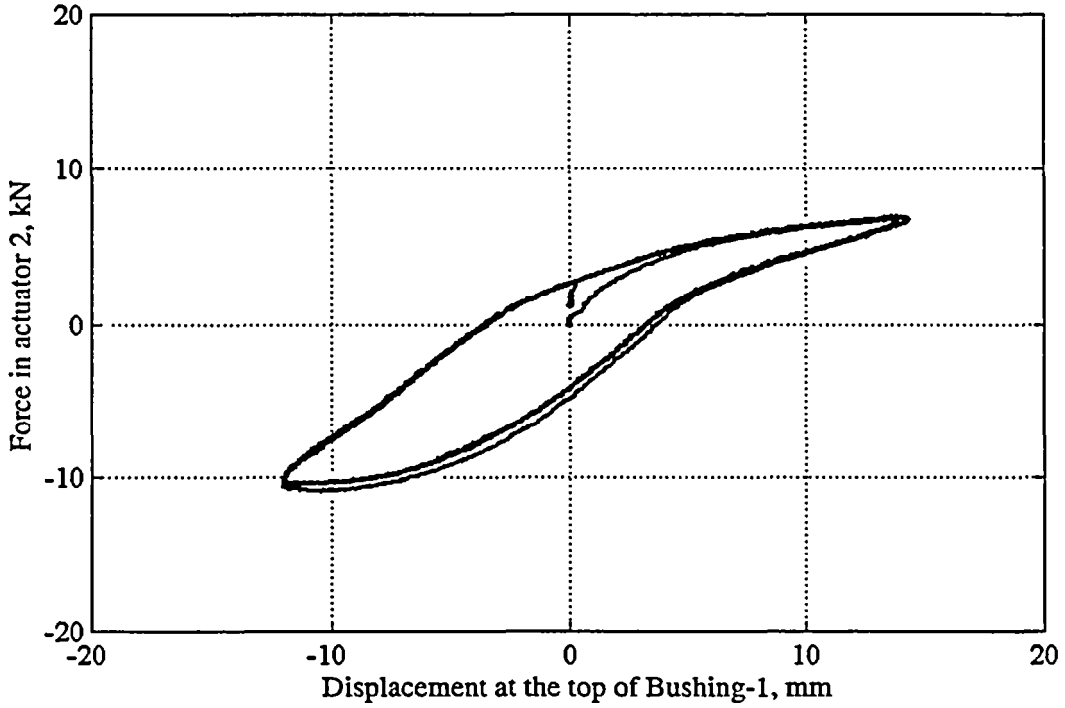

Figure 6-14 Force-displacement response of Bushing-1 (Test No 8, Test Set 1)

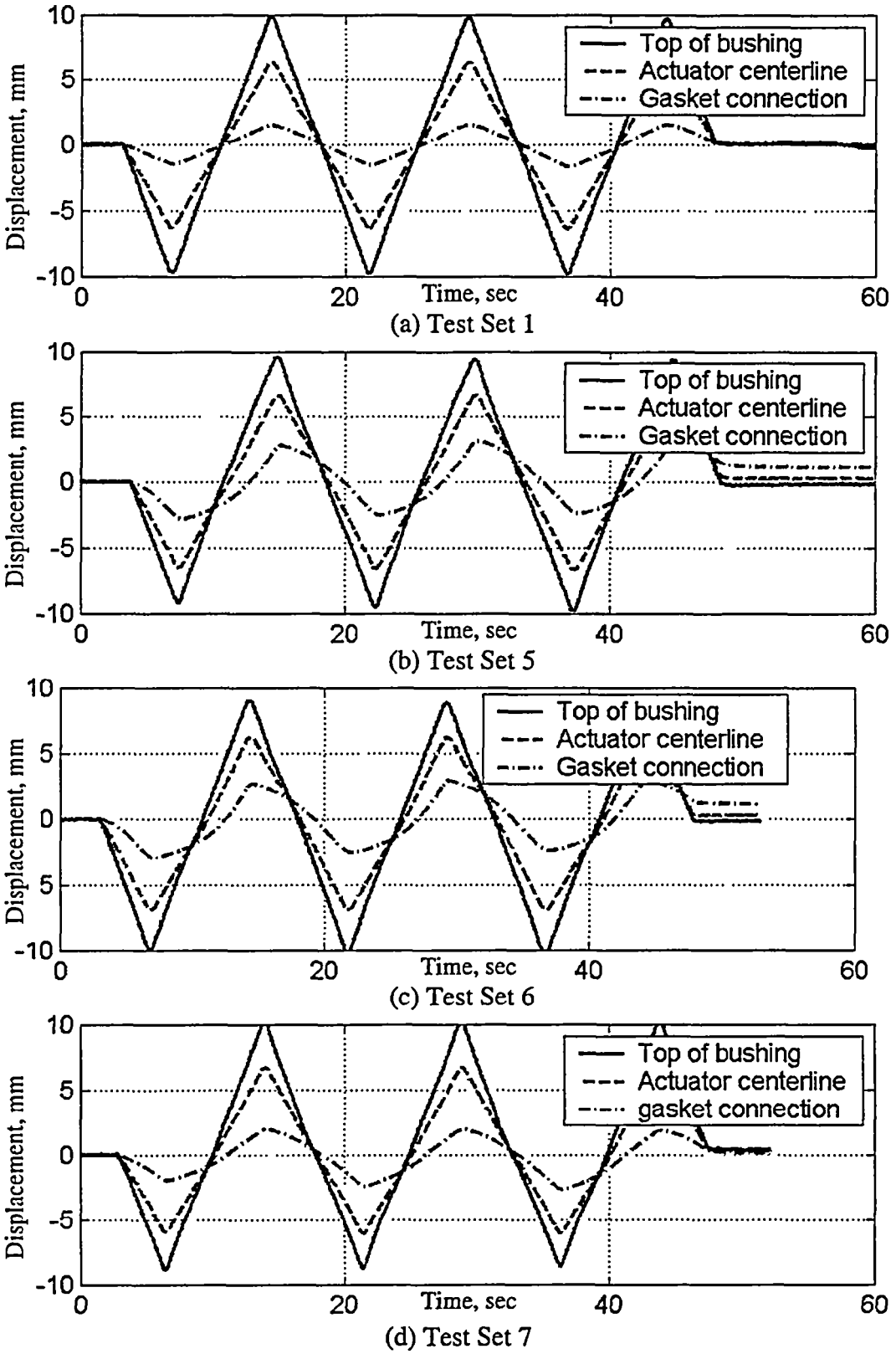

Figure 6-15 Displacement histories of Bushing-1 for Test Sets 1, 5, 6, and 7

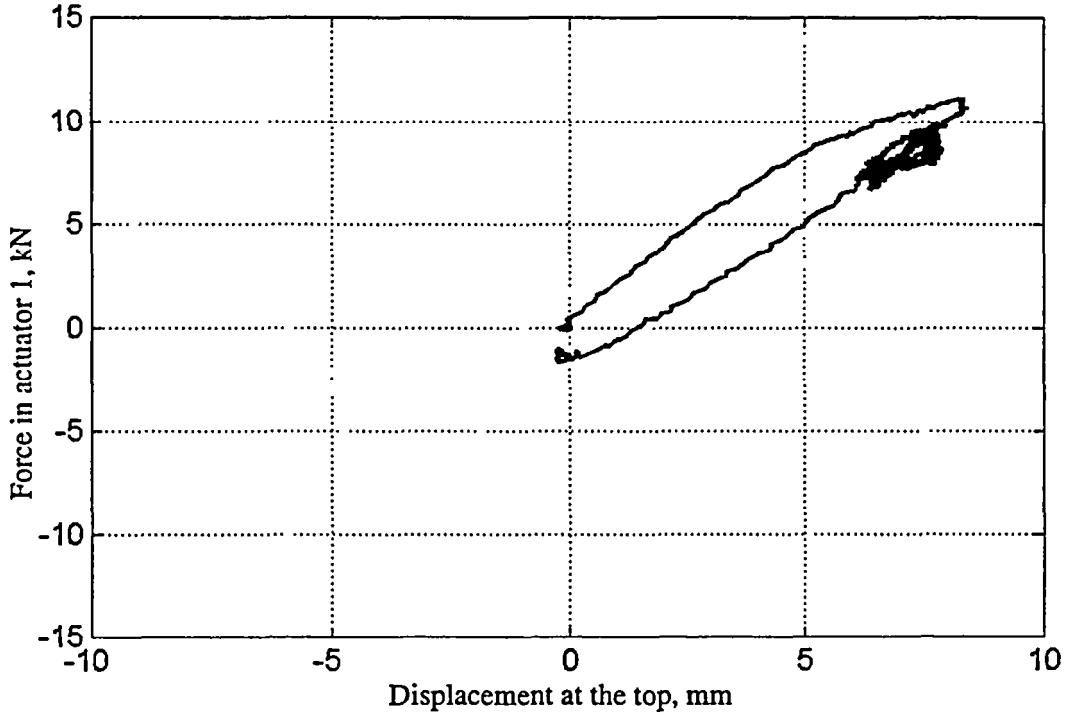

(a) Response along the x_{45} axis

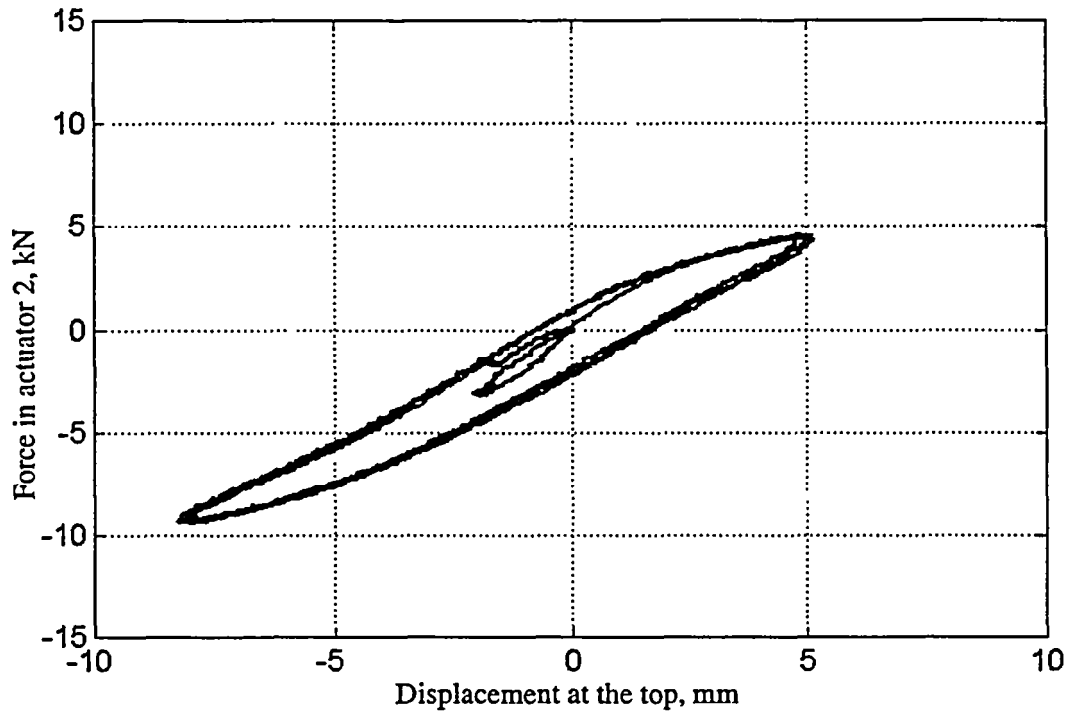

(b) Response along the y_{45} axis

Figure 6-16 Force-displacement history for Bushing-1, Test No 4, Test Set 3

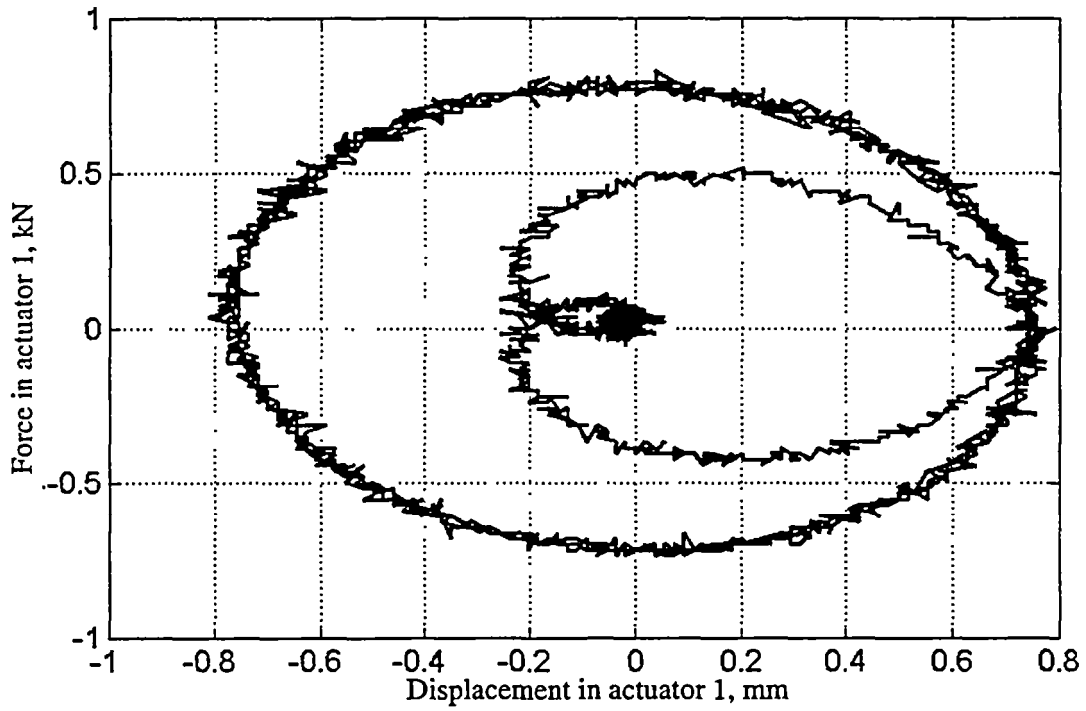

(a) Displacement orbits

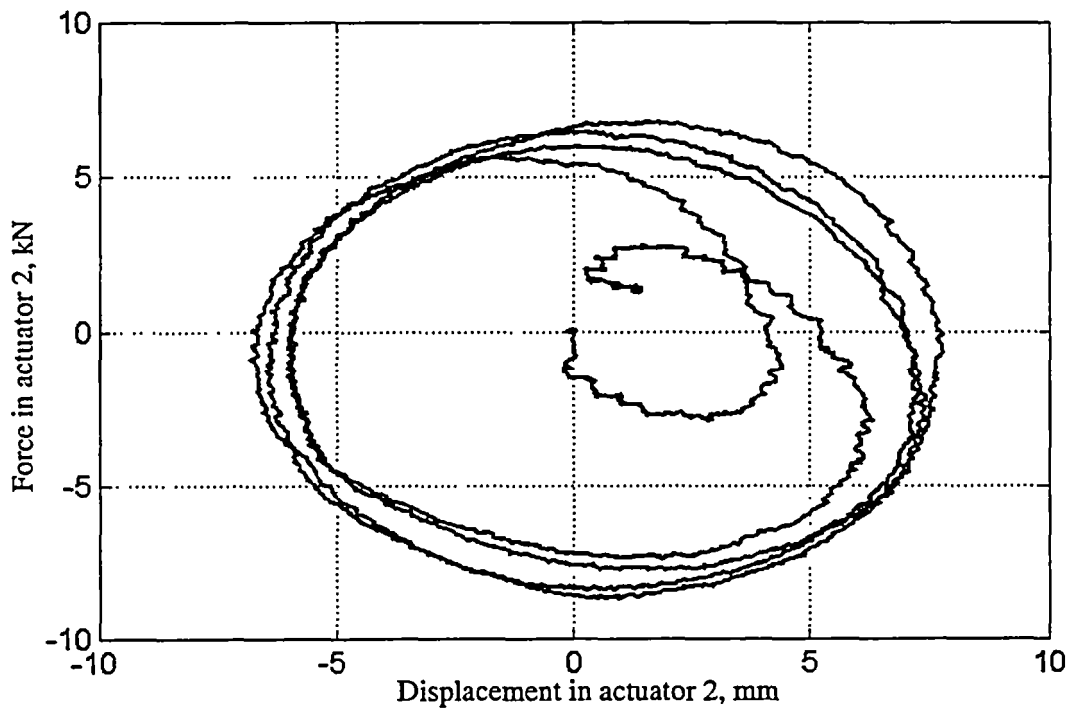

(b) Force orbits

Figure 6-17 Actuator orbits during bidirectional tests (Test No 6, Test Set 4)

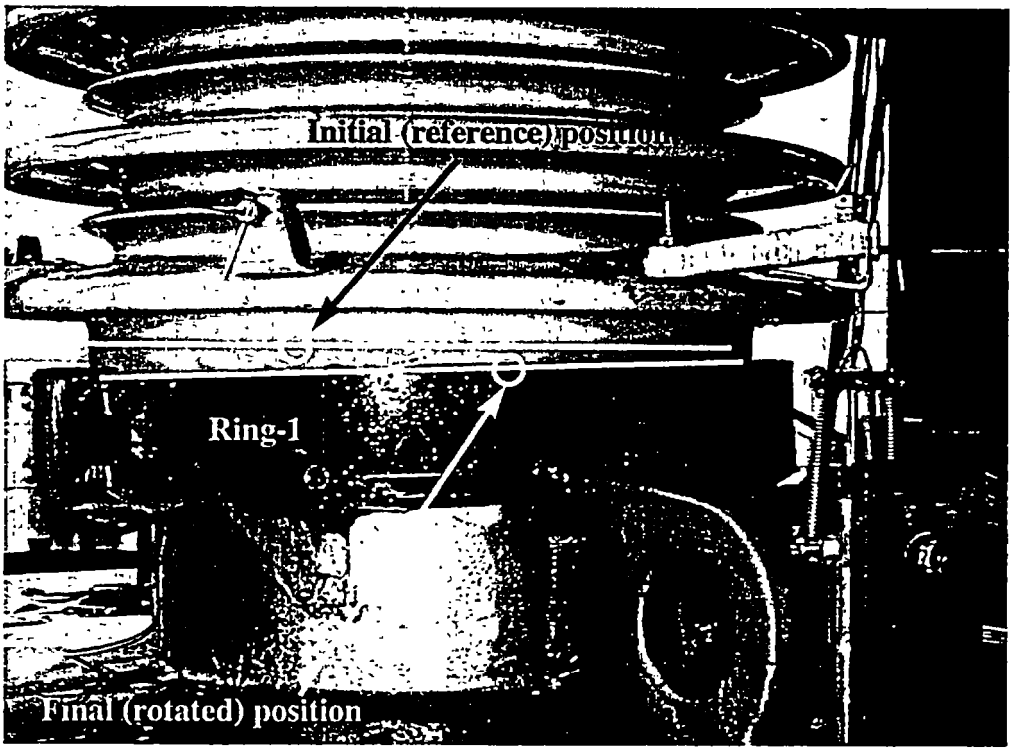

Figure 6-18 Rotation of Ring-1 following Test Set 12

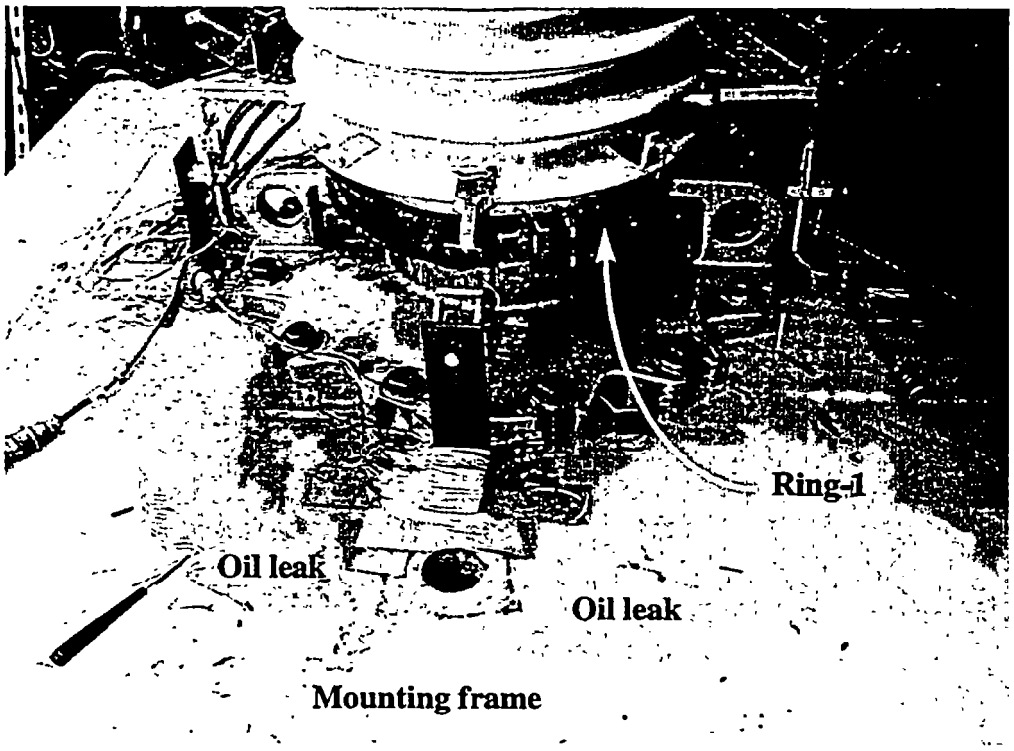

Figure 6-19 Oil leakage from the gasket connection following Test Set 12

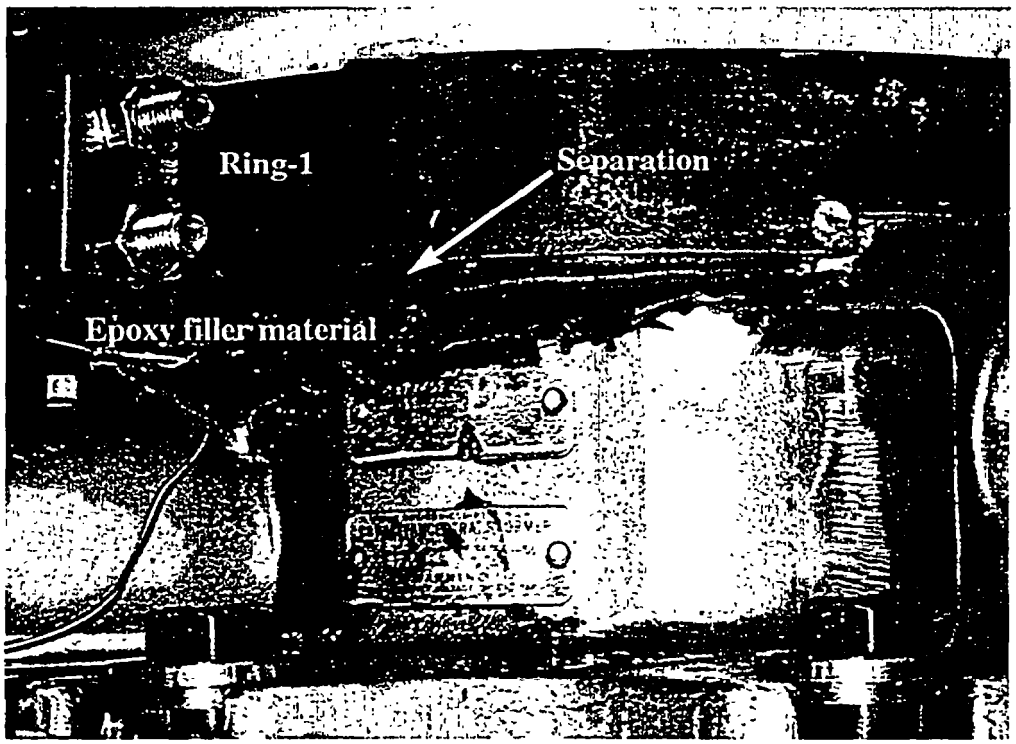

Figure 6-20 Separation of Ring-1 from the epoxy filler material, Test Set 13

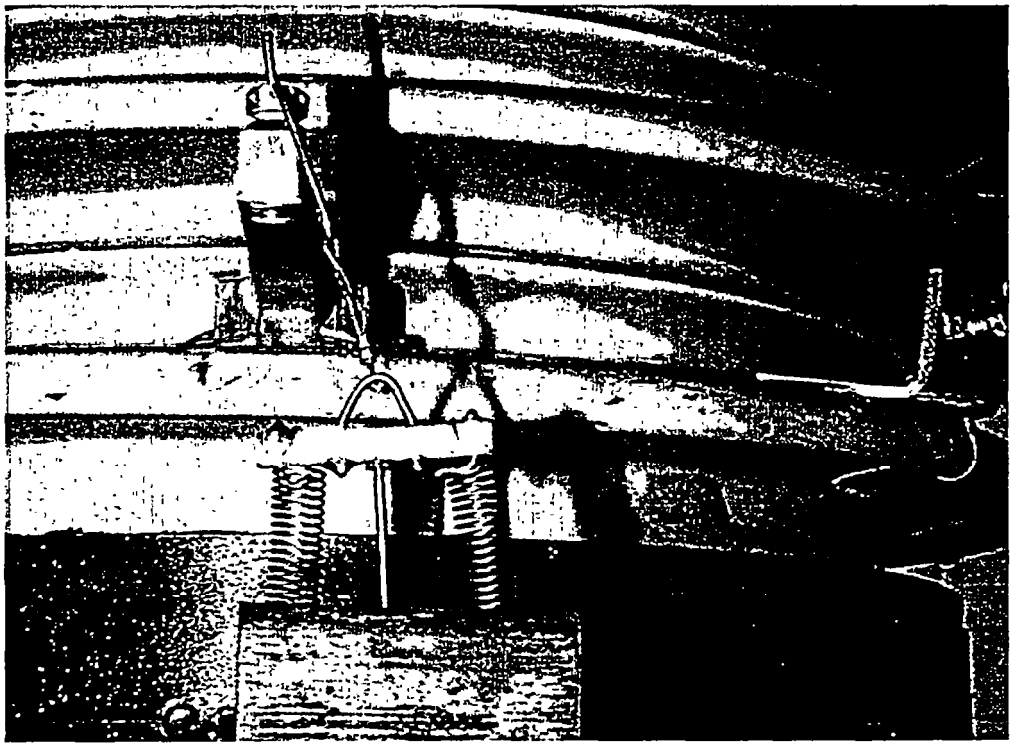

Figure 6-21 Twist of the UPPER-1 porcelain unit over the flange, Test Set 13

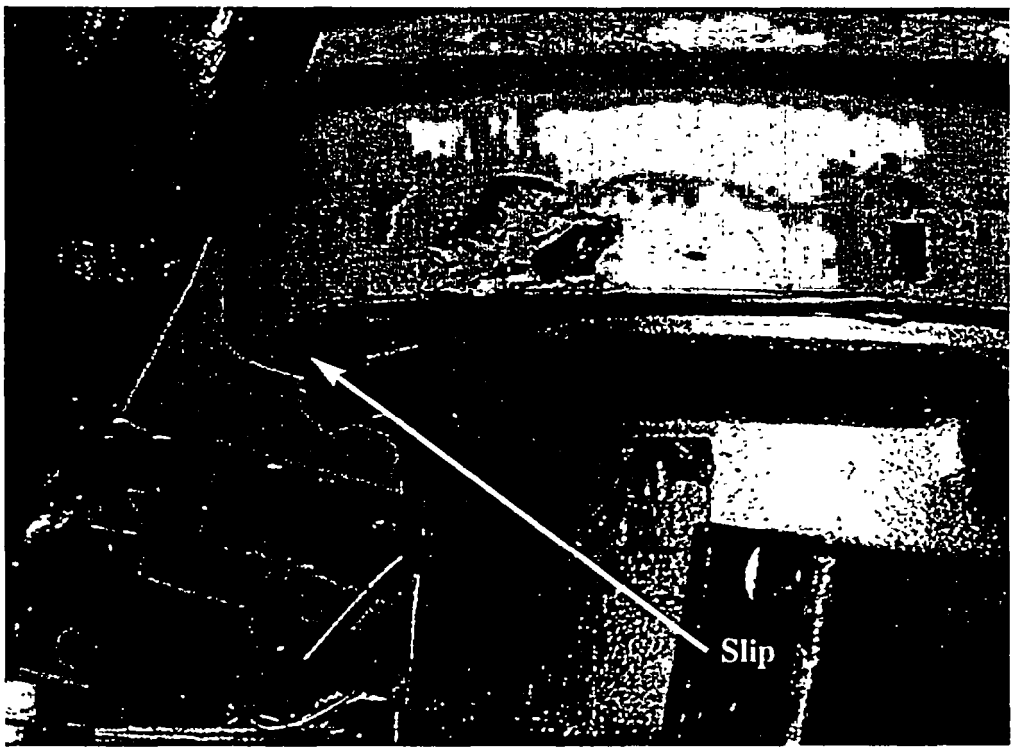

Figure 6-22 Slip of the UPPER-1 porcelain unit following Test Set 14

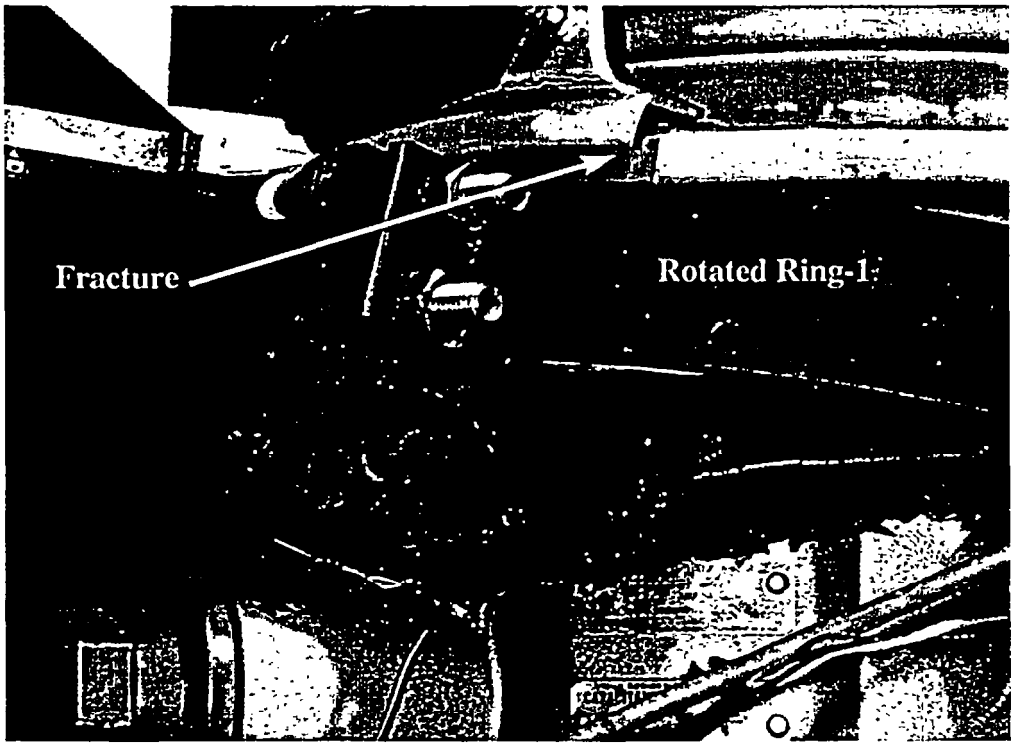

Figure 6-23 Fracture of the bottom shed of the UPPER-1 porcelain unit, Test Set 14

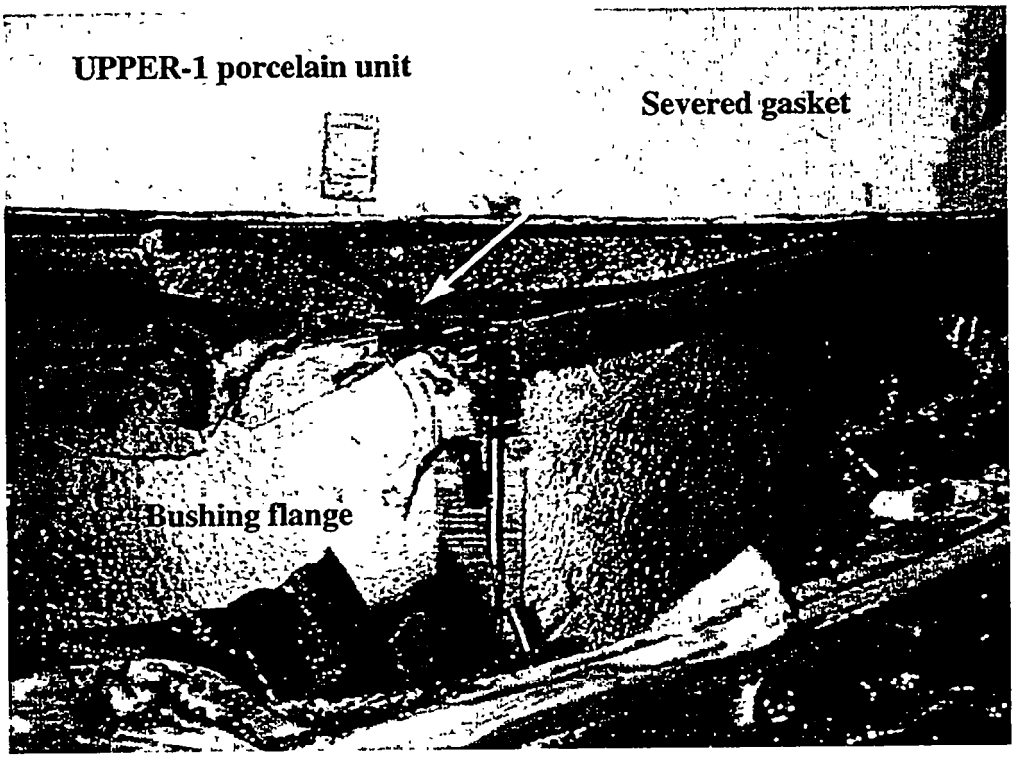

Figure 6-24 Torn portion of gasket at the gasket connection, Test Set 14

Figure 6-25 Fracture of cast aluminum flange following Test Set 14

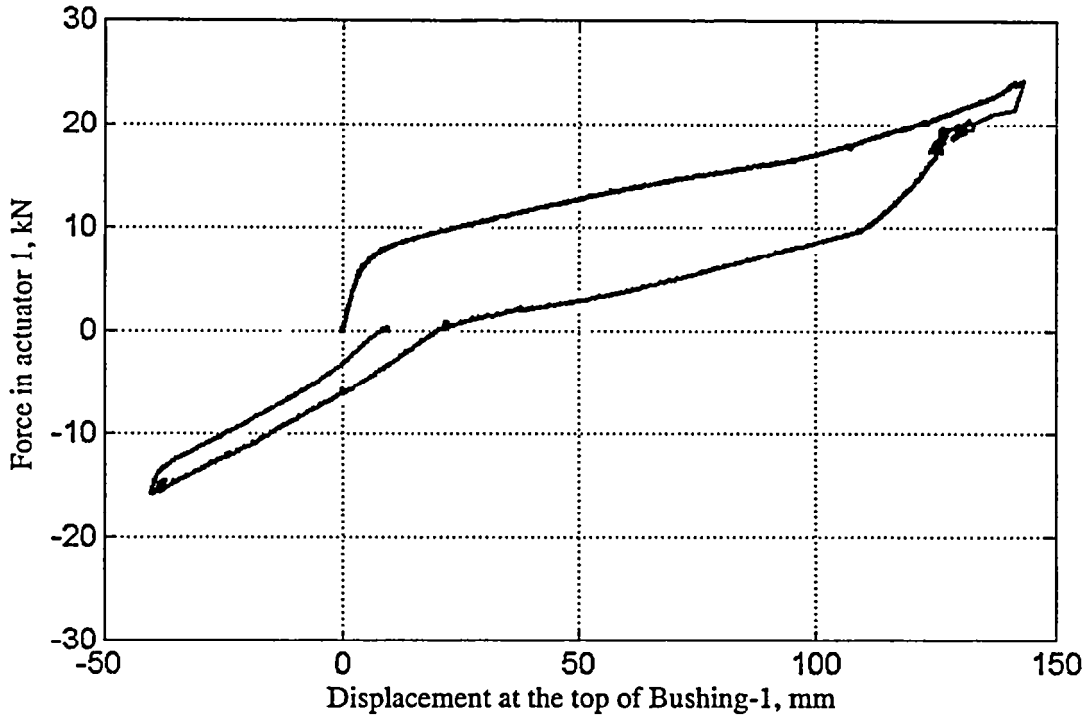

(a) Hysteretic response at the top of Bushing-1

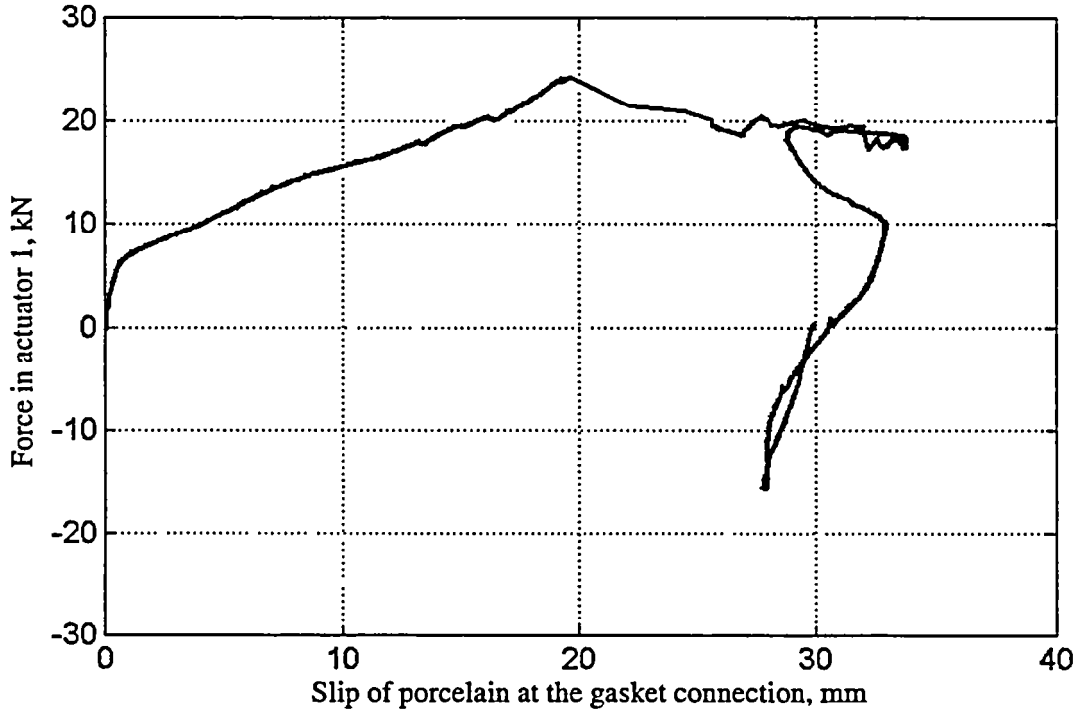

(b) Hysteretic response at the gasket connection of Bushing-1

Figure 6-26 Response of Bushing-1 during the monotonic test (Test Set 14)

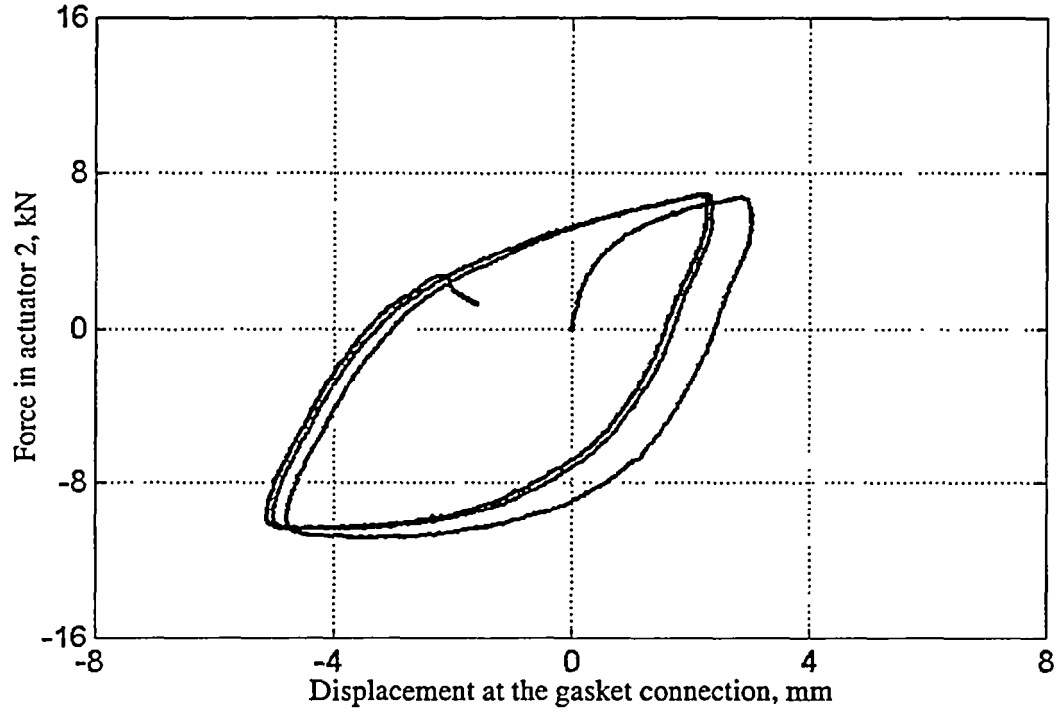

(a) Hysteretic response at the gasket connection, Test No 8, Test Set 01 (dry gasket)

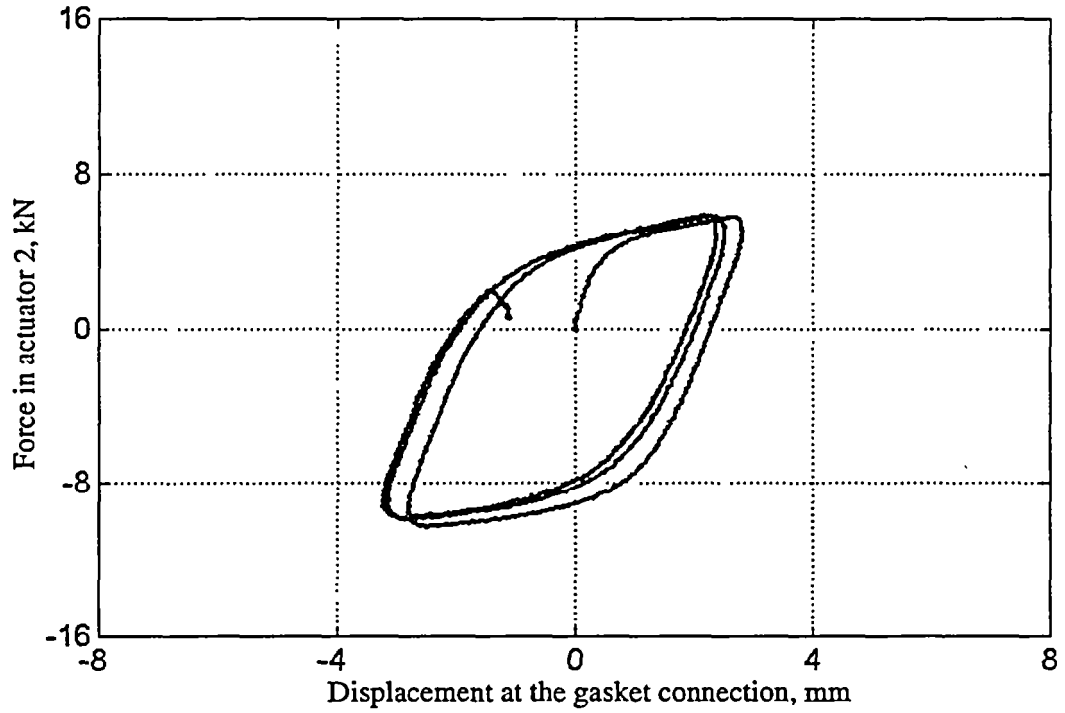

(b) Hysteretic response at the gasket connection, Test No 6, Test Set 05 (lubricated gasket)

Figure 6-27 Force-displacement response of Bushing-1 at the gasket connection

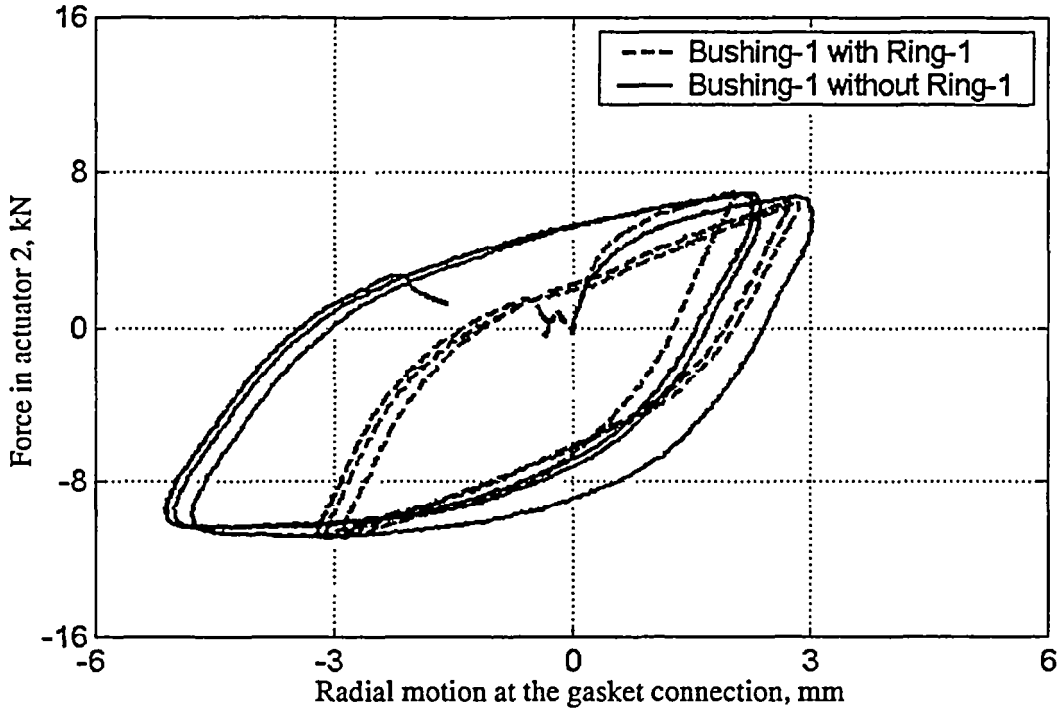

(a) Actuator 2 force-porcelain slip relation at the gasket connection

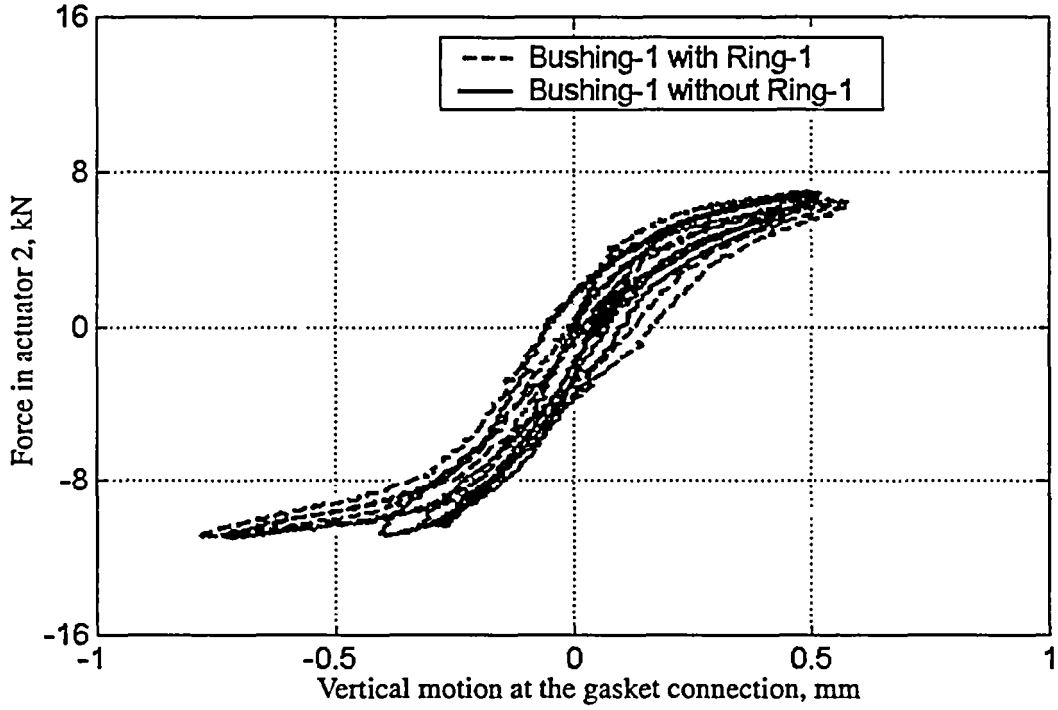

(b) Actuator 2 force-porcelain uplift relation at the gasket connection

Figure 6-28 Response of Bushing 1 at the gasket connection (Test Sets 1 and 12)

7 Fragility Testing of Flexibly Mounted Bushing-2

7.1 Overview

Triaxial earthquake simulator testing was used to evaluate the seismic response of Bushing-2 mounted on a *flexible* support and to evaluate the efficacy of the Ring-2 retrofit detail. The following sections describe the test setup including the *flexible* mounting attachment, the earthquake motions developed for the fragility tests, the instrumentation of the bushing, and selected test results.

7.2 Attachment of 230-kV Bushings to Transformers

Porcelain transformer bushings are typically mounted either to the transformer top plate or to a turret that is attached to the transformer top plate or cantilevered from the side of the transformer. The top plate of the transformers for 230-kV bushings are typically 3/8 in. (10 mm) to 1/2 in. (13 mm) thick; longitudinal and transverse stiffeners are usually welded to the underside of the top plate to provide additional vertical stiffness. In a typical installation, a 1/4-in. (6-mm) thick annular gasket (herein referred to as the mounting gasket) with a Durometer hardness of between 55 to 65 is inserted between the bushing flange and the transformer or turret top plate. The flexibility in both the transformer top plate and the mounting gasket lowers the fundamental frequency of the transformer-bushing system. Field data and analytical studies (Villaverde, et al., 1999) have shown that for the 230-kV bushings mounted on transformers, the frequency of the bushing-transformer system was between 6 and 8 Hz and that the ground accelerations were amplified at the bushing flange.

The *flexible* support described in this chapter was designed to lower the frequency of the bushing-support system (the fundamental frequency of the bushing mounted on the support frame is referred to as the frequency of the bushing-support system hereafter) but did not amplify the horizontal input motions at the bushing flange.

7.3 Test Setup

7.3.1 Mounting setup

In lieu of detailed information regarding transformer design, modeling, and connection details, a flexible mounting plate that reduced the frequency of the installed Bushing-2 from 20 Hz to 7 Hz was designed. Finite element analysis program SAP 2000 (CSI, 1997) was used to select the plan dimensions and the thickness of the mounting plate.

The *flexible* support, shown in Figure 7-1, consisted of a 1/2-in. (13-mm) thick plate supported by 1 in. (25 mm) plates along each edge. Small 1 in. (25 mm) stiffener plates were welded to each support plate to provide additional lateral stiffness. The *flexible* support was fillet welded to the top of the existing rigid mounting frame to facilitate testing of the bushing at 20 degrees to the vertical. A 1/4-in. (6.3-mm) thick Shore-A annular neoprene rubber gasket with a Durometer hardness of between 55 and 65 was inserted between the bushing flange and the *flexible* mounting plate. Figure 7-2 shows Bushing-2 installed in the mounting frame atop the earthquake simulator. Figure 7-3 is a photograph of the flange connection and shows the mounting gasket. Figure 7-4 shows Ring-2 installed on Bushing-2.

The twelve 3/4-in. (19-mm) bolts connecting the bushing flange to the *flexible* plate were tightened, one at a time, to the manufacturer-specified torque of 100 ft-lbs (136 N-m). However, due to the compressibility of the mounting gasket, the specified torque was not sustained completely. After retightening the bolts a second time, all bolts retained a minimum torque of 60 ft-lbs (82 N-m). During the course of testing program, the torque in the bolts was periodically checked to detect slip (if any) of the bushing flange relative to the *flexible* plate.

7.3.2 Simulator input motions

The test protocol for Bushing-2 installed on a *flexible* mounting frame included resonant-search tests: triaxial earthquake ground motion tests: and pull-back, quick-release tests. The quick-release tests were conducted to investigate the effect of support flexibility, terminal mass, and the mounting gasket on the dynamic properties of bushing-frame system. Information on these tests follow.

7.3.2.1 Resonant-search tests

Sine-sweep and broad band white-noise tests were used to establish the dynamic characteristics (natural frequencies and damping ratios) of a bushing. These so-called *resonant-search* tests were undertaken using unidirectional excitation along each global axis of the earthquake simulator platform. For both sine-sweep and white-noise tests, a simulator input acceleration amplitude of 0.1g was used.

Pull-back, quick-release tests were conducted to measure the lateral stiffness and dynamic properties of the bushing. The pull-back tests were conducted using a maximum concentrated force of approximately 0.5 kips (2 kN) applied at the top of the bushing.

7.3.2.2 Earthquake test response spectrum

IEEE 693-1997 identifies several response spectra of identical shapes but different amplitudes for the qualification of transformer bushings. For a detailed description of these spectra, the reader is referred to Appendix A. Figure 7-5 shows an IEEE 693-1997 High Level qualification response spectrum used for checking porcelain stresses and oil leakage. The spectrum is anchored to a peak ground acceleration (PGA) equal to 2.0g. Spectrum-compatible earthquake histories were generated using the procedures set forth in Section 3.2.3.

Two separate and independent three-component records were utilized for fragility testing. Chapter 3 provides details for these records. The Tabas-A motion was used for all the tests up to and including motions with target PGAs of 1.0g. The Tabas-B motion was used for tests with target PGAs exceeding 1.0g but less than 2.0g.

At the request of the utility participants, one additional three-component spectrum-compatible input motion was used for testing Bushing-2. This motion (hereafter referred to as CERL) was the motion used by the Construction Engineering Research Laboratories of the US Army Corps of Engineers to test a 500-kV bushing and was generated using random input motion (Wilcoski, et al., 1997). Figure 7-6 through Figure 7-8 present the acceleration history, power spectrum, and response spectra for the three components of the spectrum-compatible CERL record. The power spectra for these three histories are narrow banded and are not representative of strong motion shaking.

7.3.3 Instrumentation

For seismic testing, IEEE 693-1997 (see Appendix A) states that porcelain bushings must be instrumented to record (a) maximum vertical and horizontal accelerations at the top of the bushing, at the bushing flange, and at the top of the earthquake simulator platform, (b) maximum displacement of the top of the bushing relative to the flange, and (c) maximum porcelain stresses at the base of the bushing near the flange. The instrumentation scheme developed for the tests described in this chapter differed from the IEEE 693-1997 requirements. Specifically, since previous tests of 230-kV bushings at PEER had shown that the porcelain stresses were significantly smaller than the ultimate value, no strain gages were attached to the UPPER-1 porcelain unit.

The instrumentation scheme developed for the tests described in this chapter consisted of 59 transducers and 61 channels of data. Table 7-1 lists the channel number, instrument type, response quantity, coordinate system, and location for each transducer. Figure 7-9 presents information on the instrumentation of the earthquake simulator platform (Figure 7-9a), the flexible mounting plate (Figure 7-9b), the bushing and the mounting frames (Figure 7-9c), and the UPPER-1 porcelain unit (Figure 7-9d). The global (X, Y, Z) and local (x, y, z) coordinate systems adopted for the testing program are shown in the figure. Figure 7-10 is a photograph of the instrumentation at the top of Bushing-2. Figure 7-11 is a photograph of the instrumentation immediately above the flange plate.

Sixteen channels (channels 3 through 18) recorded the acceleration and displacement of the earthquake simulator platform in the global coordinate system. The accelerations of the *rigid* mounting frame in the local coordinate system (channels 28 through 30) and the absolute displacements of the *rigid* mounting frame in the global coordinate system (channels 40 and 41) were recorded. The accelerations of the *flexible* mounting plate in the local coordinate system (channels 31 through 33) and the absolute displacements of the *flexible* mounting plate in the global coordinate system (channels 42 and 43) were recorded. The accelerations of the bushing in the local coordinate system (channels 19 through 27) and the absolute displacements of the bushing in the global coordinate system (channels 34 through 39) were measured at the top, midheight, and bottom of the bushing. Four displacement transducers (channels 44 through 47), located immediately above the gasket, measured radial slip of the UPPER-1 porcelain unit relative to the *rigid* support frame. Four displacement transducers (channels 48 through 51) recorded the UPPER-1 porcelain unit displacements (relative to the *flexible* plate) across the gasket, parallel to the local-z axis of the bushing. Another two displacement transducers (channels 52 and 53), located immediately above the gasket, measured the twist of the UPPER-1 porcelain unit relative to the *rigid* support frame. Eight displacement transducers (channels 54 through 61) measured the out-of-plane deformation of the *flexible* mounting plate along the local z- axis, relative to the *rigid* frame. Channels 55, 57, 59, and 61 were located approximately 11 in. (280 mm) from the centerline of the bushing. Channels 54, 56, 58, and 60 were located approximately 21 in. (533 mm) from the centerline of the bushing.

7.3.4 Preparation of Bushing-2

Previous tests of Bushing-2 mounted on a *rigid* support was described in Chapter 4. Prior to retesting this bushing on the *flexible* support, the bushing was de-stressed, drained of its oil, and partially disassembled. The gasket at the gasket connection was inspected and air dried, the porcelain units were re-centered, the bushing was post-tensioned to 27 kips (120 kN), and then refilled with oil.

7.4 Summary of Experimental Data from Pull-Back, Quick-Release Tests

7.4.1 Introduction

Pull-back, quick-release tests were conducted to evaluate the effect of the plate flexibility, the mounting gasket, and the top terminal on the dynamic properties of Bushing-2. Three sets of tests were conducted. A complete set of data was collected from the pull-back, quick-release tests at the top of the bushing along the x-axis. Additional data was gathered from the pull-back, quick-release tests at the top of the bushing in the y- direction and from the tests at the bottom of the bushing in the x- direction.

Table 7-1 Instrumentation of Bushing-2 mounted on the flexible plate

Channel Number	*Transducer*[1]	*Response Quantity*	*Coordinate System and Orientation*[2]	*Transducer Location*[3]
3	LVDT	platform displacement	global *X*	simulator platform
4	LVDT	platform displacement	global *Y*	simulator platform
5	LVDT	platform displacement	global *X*	simulator platform
6	LVDT	platform displacement	global *Y*	simulator platform
7	LVDT	platform displacement	global *Z*	simulator platform
8	LVDT	platform displacement	global *Z*	simulator platform
9	LVDT	platform displacement	global *Z*	simulator platform
10	LVDT	platform displacement	global Z	simulator platform
11	A	platform acceleration	global *X*	simulator platform
12	A	platform acceleration	global *X*	simulator platform
13	A	platform acceleration	global *Y*	simulator platform
14	A	platform acceleration	global *Y*	simulator platform
15	A	platform acceleration	global *Z*	simulator platform
16	A	platform acceleration	global *Z*	simulator platform
17	A	platform acceleration	global *Z*	simulator platform
18	A	platform acceleration	global Z	simulator platform
19	A	bushing acceleration	local *x*	bottom of bushing
20	A	bushing acceleration	local *y*	bottom of bushing
21	A	bushing acceleration	local *z*	bottom of bushing
22	A	bushing acceleration	local *x*	midheight of bushing
23	A	bushing acceleration	local *y*	midheight of bushing
24	A	bushing acceleration	local *z*	midheight of bushing
25	A	bushing acceleration	local *x*	top of bushing
26	A	bushing acceleration	local *y*	top of bushing
27	A	bushing acceleration	local *z*	top of bushing
28	A	frame acceleration	local *x*	rigid mounting frame
29	A	frame acceleration	local *y*	rigid mounting frame
30	A	frame acceleration	local *z*	rigid mounting frame
31	A	frame acceleration	local *x*	flexible mounting plate
32	A	frame acceleration	local *y*	flexible mounting plate
33	A	frame acceleration	local *z*	flexible mounting plate

Table 7-1 Instrumentation of Bushing-2 mounted on the flexible plate

Channel Number	*Transducer*[1]	*Response Quantity*	*Coordinate System and Orientation*[2]	*Transducer Location*[3]
34	LP	bushing displacement	global *X*	bottom of bushing
35	LP	bushing displacement	global *Y*	bottom of bushing
36	LP	bushing displacement	global *X*	midheight of bushing
37	LP	bushing displacement	global *Y*	midheight of bushing
38	LP	bushing displacement	global *X*	top of bushing
39	LP	bushing displacement	global *Y*	top of bushing
40	LP	frame displacement	global *X*	rigid mounting frame
41	LP	frame displacement	global *Y*	rigid mounting frame
42	LP	frame displacement	global *X*	flexible mounting plate
43	LP	frame displacement	global *Y*	flexible mounting plate
44	DCDT	UPPER-1 slip	local *x*	gasket connection
45	DCDT	UPPER-1 slip	local *y*	gasket connection
46	DCDT	UPPER-1 slip	local *x*	gasket connection
47	DCDT	UPPER-1 slip	local *y*	gasket connection
48	DCDT	UPPER-1 uplift	local *z*	gasket connection
49	DCDT	UPPER-1 uplift	local *z*	gasket connection
50	DCDT	UPPER-1 uplift	local *z*	gasket connection
51	DCDT	UPPER-1 uplift	local *z*	gasket connection
52	DCDT	UPPER-1 twist	local *x*	gasket connection
53	DCDT	UPPER-1 twist	local *x*	gasket connection
54	DCDT	flexible plate uplift	local *z*	flexible mounting plate
55	DCDT	flexible plate uplift	local *z*	flexible mounting plate
56	DCDT	flexible plate uplift	local *z*	flexible mounting plate
57	DCDT	flexible plate uplift	local *z*	flexible mounting plate
58	DCDT	flexible plate uplift	local *z*	flexible mounting plate
59	DCDT	flexible plate uplift	local *z*	flexible mounting plate
60	DCDT	flexible plate uplift	local *z*	flexible mounting plate
61	DCDT	flexible plate uplift	local *z*	flexible mounting plate

1. A = accelerometer; LVDT = displacement transducer; LP = linear potentiometer; SG = strain gage; DCDT = displacement transducer.
2. For the local (*x*-, *y*-, *z*-) and global (*X*- *Y*- *Z*-) coordinate systems see Figure 7-9.
3. For transducer locations on the bushing see Figure 7-9.

7.4.2 Test setup

The test setup for the pull-back, quick-release tests, consisted of a nylon cable connecting the top (or the bottom) of bushing to the reaction frame in-line with a turnbuckle, a load cell, and a machined bolt. During the pull-back stage, the bushing was gradually pulled to approximately 0.5 kips (2 kN). The applied force and the resulting bushing displacement were monitored and recorded using the in-line load cell and displacement transducers. Next, the applied force was suddenly released by cutting the machined bolt. The resulting free vibration response was recorded using accelerometers mounted on the top and bottom of the bushing.

7.4.3 Evaluation of the dynamic properties

The vibration frequencies of Bushing-2 were computed from peaks in the power spectra of the recorded accelerations. The damping ratios were computed from the log-decrement method (Clough and Penzien, 1993). The effective weight of the bushing was computed using the bushing lateral stiffness and frequency and assuming that the bushing is a single-degree-of-freedom system with a lumped mass at the top (or bottom).

7.4.4 Summary of experimental results

The computed dynamic properties of Bushing-2 from the pull-back, quick-release tests along the *x*- direction at the top of the bushing are listed in Table 7-2. The fundamental frequencies of the bushing-support system were 19 and 7.5 Hz for the *rigidly* mounted and *flexibly* mounted bushing, respectively. The computed system frequency for the *rigidly* mounted bushing was consistent with the values previously computed in Chapter 4, and the computed system frequency for *flexibly* mounted bushing was consistent with both the values measured in the field and the value computed from the finite element analysis. The addition of the 1/4-in. (6-mm) thick mounting gasket at the bushing flange-to-support connection reduced the lateral stiffness of the bushing-support system by approximately 25 percent. When the top terminal was not attached to the top of Bushing-2, the effective weight of the bushing was 140 lbs (630 N) for the *rigidly* mounted bushing and 190 lbs (860 N) for the *flexibly* mounted bushing. The tabulated effective weight of 140 lbs (630 N) is approximately 25 percent of the estimated weight of the portion of bushing extending from the bushing flange to the top of bushing (see Chapter 2). When the terminal was attached to the top of the bushing, the fundamental frequency of the bushing-support system was reduced from 19 to 14 Hz for the *rigidly* mounted bushing and from 7.5 to 6.5 Hz for the *flexibly* mounted bushing.

Table 7-2 Modal properties of Bushing-2 along the x-axis[1]

Test ID	*Mounting Frame*[2]	*Top Terminal Installed*[3]	*Mounting Gasket Installed*[4]	*Stiffness (kN/mm)*	*Frequency (Hz)*	*Damping Ratio (% critical)*	*Effective Weight (N)*
1	Rigid	No	No	0.9	19	2	630
2	Rigid	Yes	No	0.9	14	3	1080
3	Rigid	No	Yes	0.8	18	3	630
4	Rigid	Yes	Yes	0.8	13	4	1220
5	Flexible	No	No	0.2	7.5	2	860
6	Flexible	Yes	No	0.2	6.5	3	1170
7	Flexible	No	Yes	0.1	6.5	4	860
8	Flexible	Yes	Yes	0.1	5.5	5	1220

1. Loads imposed at top of bushing.
2. Rigid mounting frame is shown in Figure 4.1; flexible mounting plate is shown in Figure 7-1.
3. Top terminal, shown in Figure 4-6, weighs 280 N; the threaded rod attachment weighs 50 N.
4. Mounting gasket: 6-mm thick annular rubber.

The computed dynamic properties of Bushing-2 from the pull-back, quick-release tests in the y-direction at the top of the bushing are listed in Table 7-3.

Table 7-3 Modal properties of Bushing-2 along the y-axis[1]

Test ID	*Mounting Frame*[2]	*Mounting Gasket Installed*[3]	*Stiffness (kN/mm)*	*Frequency (Hz)*	*Damping Ratio (% critical)*	*Effective Weight (N)*
1	Flexible	No	0.2	7.4	2	880
2	Flexible	Yes	0.1	6.4	4	860

1. Loads imposed at top of bushing.
2. Flexible mounting plate is shown in Figure 7-1.
3. Mounting gasket: 6-mm thick annular rubber.

The computed dynamic properties of Bushing-2 from the pull-back, quick-release tests in the x-direction at the bottom of the bushing are listed in Table 7-4.

Table 7-4 Modal properties of Bushing-2 along the x- axis[1]

Test ID	*Mounting Frame*[2]	*Mounting Gasket Installed*[3]	*Stiffness (kN/mm)*	*Frequency (Hz)*	*Damping Ratio (% critical)*	*Effective Weight (N)*
1	Rigid	No	2.1	52	2	200

1. Loads imposed at bottom of bushing.
2. Rigid mounting frame is shown in Figure 4.1.
3. Mounting gasket: 6-mm thick annular rubber.

7.5 Experimental Results from Seismic Tests

7.5.1 Introduction

The objective of the testing program was to determine the dynamic properties and seismic response of the *flexibly* mounted Bushing-2 and to evaluate the efficacy of retrofit Ring-2 detail in improving the seismic response of the bushing.

7.5.2 Summary of experimental data

The list of earthquake tests and key observations for Bushing-2 with and without retrofit Ring-2 are presented in Table 7-5 and Table 7-6, respectively.

After each earthquake test, the response data were analyzed, the bushing was inspected for damage and oil seepage, and the bolts joining the bushing flange plate to the *flexible* mounting frame were checked for tightness. All bolts were found to be tight after all tests.

For all tests, the transducer response histories were processed using the computer program Matlab (Mathworks, 1999). Experimental histories were low-passed filtered using a rectangular filter with a cut-off frequency of 50 Hz and then zero-corrected.

7.5.3 Dynamic properties of Bushing-2 mounted on the flexible plate

Sine-sweep and white-noise tests were used to calculate the modal frequencies and damping ratios for Bushing-2. Figure 7-16 shows the transfer functions between the top of the bushing and the *flexible* plate in the three local directions (x, y, z) for Bushing-2, as calculated from Test Nos 1 through 3 of Table 7-5. The resonant frequencies in the local x- and y-directions are approximately 6.8 Hz and 6.5 Hz, respectively. Damping ratios of between 3 to 4 percent of critical were obtained using the half-power bandwidth method. The addition of Ring-2 did not significantly alter the dynamic properties of Bushing-2 — similar fundamental frequencies and damping ratios were obtained for the retrofitted bushing.

Table 7-7 summarizes the measured dynamic properties of Bushing-2 in the x- and y-directions; modal data could not be determined for the local z-direction. The modal frequencies differ slightly in x- and y- directions due to the unsymmetrical distribution of lifting lugs immediately above the flange plate of the bushing.

Table 7-5 Summary of earthquake testing of flexibly mounted Bushing-2 without Ring-2

Test No.	*Test Date*	*Identification*[1]	*PGA*[2]	*Comments*
1	12/14/99	WN-X	0.1g	
2	12/14/99	WN-Y	0.1g	
3	12/14/99	WN-Z	0.1g	
4	12/14/99	SS-X	0.1g	
5	12/14/99	SS-Y	0.1g	
6	12/14/99	SS-Z	0.1g	
7	12/14/99	Tabas-A	0.1g	
8	12/14/99	CERL	0.1g	
9	12/14/99	Tabas-A	0.2g	
10	12/14/99	Tabas-A	0.3g	
11	12/14/99	Tabas-A	0.5g	
12	12/14/99	Tabas-A	0.7g	
13	12/14/99	Tabas-A	1.0g	Spectrum equivalent to moderate level qualification.
14	12/14/99	Tabas-B	1.2g	
15	12/14/99	Tabas-B	1.4g	Small oil leakage at the gasket connection[3]; see Figure 7-12.
16	12/14/99	Tabas-B	1.6g	Oil leakage; minor slip of the UPPER-1 porcelain unit.
17	12/14/99	Tabas-B	1.8g	Large slip of the UPPER-1 porcelain unit; gasket visible; see Figure 7-13.
18	12/14/99	Tabas-B	2.0g	Large slip of the UPPER-1 porcelain unit; gasket visible and extruding from the gasket connection; see Figure 7-14.

1. WN = white-noise, SS = sine-sweep; -*X*, -*Y*, and -*Z* denote direction of testing in global coordinate system; Tabas-A = spectrum-compatible Tabas-A earthquake histories; Tabas-B = spectrum-compatible Tabas-B earthquake histories; CERL = spectrum-compatible CERL histories.
2. PGA = target peak acceleration of the simulator platform.
3. Connection of the UPPER-1 porcelain unit to the flange plate.

Table 7-6 Summary of earthquake testing of flexibly mounted Bushing-2 with Ring-2

Test No.	*Test Date*	*Identification*[1]	*PGA*[2]	*Comments*
1	12/17/99	WN-X	0.1g	
2	12/17/99	WN-Y	0.1g	
3	12/17/99	WN-Z	0.1g	
4	12/17/99	SS-X	0.1g	
5	12/17/99	SS-Y	0.1g	
6	12/17/99	SS-Z	0.1g	
7	12/17/99	Tabas-A	0.1g	
8	12/17/99	CERL	0.1g	
9	12/17/99	Tabas-A	0.2g	
10	12/17/99	Tabas-A	0.3g	
11	12/17/99	Tabas-A	0.5g	
12	12/17/99	Tabas-A	0.7g	
13	12/17/99	Tabas-A	1.0g	Spectrum equivalent to moderate level qualification.
14	12/17/99	Tabas-B	1.2g	
15	12/17/99	Tabas-B	1.4g	
16	12/17/99	Tabas-B	1.6g	
17	12/17/99	Tabas-B	1.8g	
18	12/17/99	Tabas-B	2.0g	Spectrum equivalent to high level qualification.
19	12/17/99	CERL	1.0g	
20	12/17/99	Tabas-B	2.2g	
21	12/17/99	Tabas-B	2.4g	
22	12/17/99	Tabas-B	2.6g	Oil leakage at the gasket connection[3].
23	12/17/99	Tabas-B	2.8g	Oil leakage at the gasket connection and twist of the UPPER-1 porcelain unit; see Figure 7-15.
24	12/17/99	Tabas-B	3.0g	Excessive oil leakage and uplift of the UPPER-1 porcelain unit during the test.
25	12/17/99	WN-X	0.1g	
26	12/17/99	WN-Y	0.1g	
27	12/17/99	WN-Z	0.1g	

1. WN = white-noise, SS = sine-sweep; -X, -Y, and -Z denote direction of testing in global coordinate system; Tabas-A = spectrum-compatible Tabas-A earthquake histories; Tabas-B = spectrum-compatible Tabas-B earthquake histories; CERL = spectrum-compatible CERL histories.
2. PGA = target peak acceleration of the simulator platform.
3. Connection of the UPPER-1 porcelain unit to the flange plate.

Table 7-7 Modal properties of Bushing-2 from resonance-search tests

		Frequency (Hz)		*Damping Ratio (% critical)*	
Test No.	*Ring-2 Installed*	*x-direction*	*y-direction*	*x-direction*	*y-direction*
1-6	No	6.8	6.5	4	4
1-6	Yes	6.8	6.5	3	3
25-27	Yes	6.5	6.3	4	4

7.5.4 Response of the rigid mounting frame and the flexible plate

The measured peak accelerations of the simulator platform, the *rigid* frame, and the *flexible* mounting plate for the seismic tests of Bushing-2 are presented in Table 7-8. The data are tabulated for the tests of Bushing-2 without Ring-2; data for the tests of Bushing-2 with Ring-2 were similar. The transfer functions of Figure 7-17, as calculated from Test Nos 1 through 3 of Table 7-5, show that there is almost no amplification of the longitudinal (x-) acceleration, some reduction in the lateral (y-) acceleration, but large amplification of vertical (z-) acceleration due to the flexibility of the 1/2-in. (13-mm) thick plate. The out-of-plane (z- direction) frequency of the flexible plate, with the bushing installed, is approximately 17 Hz.

7.5.5 Response of Bushing-2 without Ring-2

7.5.5.1 Peak response

The peak acceleration and displacement responses of the Bushing-2 (at the top, midheight, and bottom) without the retrofit ring are presented in Table 7-9. The maximum responses at the midheight of the bushing were less than those at the top or bottom. The values of peak absolute accelerations are defined as the maximum of the vector sum of acceleration components in the local x- and local y-directions, evaluated from acceleration histories. Similarly, the values of peak displacements relative to the mounting frame are defined as the maximum of the vector sum of relative displacement components in the global X- and local Y- directions, evaluated from displacement histories.

Although the target PGAs are listed in increasing order in Table 7-9, the tabulated response values do not necessarily increase in a corresponding manner. Among the factors contributing to this variation are the temperature-dependent dynamics of the simulator's hydraulic system, interaction between the simulator platform and bushing-support system, simulator rotational accelerations, and the phase difference between the x- (or X-) and y- (or Y-) components of response used to compute the vector sum of response.

Table 7-8 Peak acceleration response of the simulator platform and the mounting frames

			Simulator Platform (g)			*Rigid Frame (g)*			*Flexible Plate (g)*		
Test No.[1]	*Identification*[2]	*PGA*[3]	*X*[4]	*Y*	*Z*	*x*	*y*	*z*	*x*	*y*	*z*
7	Tabas-A	0.1g	0.1	0.2	0.1	0.2	0.3	0.1	0.2	0.2	0.2
8	CERL	0.1g	0.2	0.2	0.1	0.3	0.3	0.1	0.3	0.2	0.2
9	Tabas-A	0.2g	0.3	0.4	0.1	0.5	0.5	0.2	0.4	0.3	0.3
10	Tabas-A	0.3g	0.5	0.4	0.2	0.6	0.6	0.3	0.6	0.4	0.4
11	Tabas-A	0.5g	0.6	0.5	0.4	0.9	0.8	0.5	0.9	0.5	0.5
12	Tabas-A	0.7g	0.9	0.7	0.5	1.0	0.9	0.7	1.0	0.6	0.9
13	Tabas-A	1.0g	1.2	1.0	0.5	1.7	1.1	0.7	1.6	0.8	0.8
14	Tabas-B	1.2g	1.2	1.1	0.7	1.4	1.1	1.0	1.4	0.9	0.9
15	Tabas-B	1.4g	1.4	1.2	1.0	1.6	1.4	1.3	1.6	1.1	1.1
16	Tabas-B	1.6g	1.6	1.5	0.9	2.0	1.6	1.2	2.0	1.3	1.4
17	Tabas-B	1.8g	1.9	1.6	1.0	2.3	1.8	1.1	2.2	1.0	1.2
18	Tabas-B	2.0g	2.4	1.9	0.9	2.6	2.1	1.2	2.4	1.6	1.2
19	CERL	1.0g	1.4	1.6	0.4	1.5	1.5	0.7	1.4	1.2	0.8
20	Tabas-B	2.2g	2.7	2.2	0.8	3.0	2.3	1.0	2.8	1.7	1.4
21	Tabas-B	2.4g	2.9	2.5	0.9	3.3	2.5	1.3	3.0	1.9	1.6
22	Tabas-B	2.6g	3.2	2.6	0.8	3.6	3.2	1.3	3.4	2.1	1.7
23	Tabas-B	2.8g	3.4	2.8	0.8	4.1	3.4	1.4	3.6	2.2	1.6
24	Tabas-B	3.0g	3.8	3.0	0.8	4.7	3.6	1.4	4.1	2.3	1.8

1. Data are from the retrofitted bushing seismic tests.
2. Tabas-A = spectrum-compatible Tabas-A earthquake histories; Tabas-B = spectrum-compatible Tabas-B earthquake histories; CERL = spectrum-compatible CERL histories.
3. PGA = target peak acceleration of the simulator platform.
4. For orientation of global (*X*- *Y*- *Z*-) and local (*x*- *y*- *z*-) coordinate systems, refer to Figure 7-9.

7.5.5.2 Bushing response

The global response of Bushing-2 was assessed by analysis of data from Test No 13 (Tabas-A, target PGA equal to 1.0g) and Test No 18 (Tabas-B, target PGA equal to 2.0g).

Table 7-9 Peak responses of the Bushing-2 without Ring-2

			Peak Acceleration (g)			*Peak Relative Displacement (mm)*		
Test No.	*Identification*[1]	*PGA*[2]	*Top*	*Midheight*	*Bottom*	*Top*	*Midheight*	*Bottom*
7	Tabas-A	0.1g	0.6	0.4	0.7	4	2	3
8	CERL	0.1g	0.5	0.3	0.7	3	2	3
9	Tabas-A	0.2g	0.9	0.5	1.1	5	2	3
10	Tabas-A	0.3g	1.1	0.6	1.5	6	3	4
11	Tabas-A	0.5g	1.6	1.0	2.1	9	4	6
12	Tabas-A	0.7g	2.2	1.3	3.2	13	6	8
13	Tabas-A	1.0g	2.9	1.9	3.0	17	9	10
14	Tabas-B	1.2g	3.3	1.8	3.5	21	10	13
15	Tabas-B	1.4g	3.8	2.0	4.2	28	13	16
16	Tabas-B	1.6g	3.9	2.4	4.2	33	17	17
17	Tabas-B	1.8g	5.0	2.6	4.2	41	23	18
18	Tabas-B	2.0g	4.8	3.0	4.5	40	19	21

1. Tabas-A = spectrum-compatible Tabas-A earthquake histories; Tabas-B = spectrum-compatible Tabas-B earthquake histories; CERL = spectrum-compatible CERL histories.
2. PGA = target peak acceleration of the simulator platform.

During Test No 13, (Tabas-A, target PGA equal to 1.0g) a maximum acceleration and displacement relative to the mounting frame of 2.9g and 0.7 in. (17 mm) respectively, were recorded at the top of the bushing. Acceleration response spectra for Bushing-2 in the local coordinate system, generated using measured acceleration histories of the *flexible* plate are shown in Figure 7-18. For information, the 2-percent and 5-percent damped IEEE 693-1997 response spectra for Moderate Level qualification are also shown in this figure. The spectrum acceleration ordinates in the *y*- and *z*- directions are smaller than those of the IEEE spectra.

During Test No 18, (Tabas-B, target PGA equal to 2.0g) a maximum acceleration and displacement relative to the mounting frame of 4.8g and 1.6 in. (40 mm) respectively, were recorded at the top of the bushing. Acceleration response spectra for Bushing-2 in the local coordinate system, generated using measured acceleration histories of the *flexible* plate are shown in Figure 7-19. For information, the 2-percent and 5-percent damped IEEE 693-1997 response spectra for High Level qualification are also shown in this figure. The spectrum acceleration ordinates in the *y*- and *z*- directions are smaller than those of the IEEE spectra.

Figure 7-20 presents the zero-corrected vertical displacement history of the UPPER-1 porcelain unit, measured at the height of the radial displacement transducers, relative to the *rigid* mounting frame. The vertical displacement histories were obtained by subtracting the vertical deformation of the *flexible* plate with respect to the *rigid* frame (e.g., channel 55) from the recorded vertical

history of the UPPER-1 porcelain unit relative to the *flexible* plate (e.g., channel 48). To obtain the vertical displacements at the side of the bushing, geometric corrections were applied to the measurements. The uplift of the UPPER-1 porcelain unit over the flange is given by residual positive vertical displacements. The settlement of the UPPER-1 porcelain unit is given by the residual negative vertical displacement. The maximum vertical displacement at the side of the porcelain unit was approximately 0.09 in. (2 mm). At the conclusion of the test, the residual vertical displacement on one side of the bushing was +0.03 in. (+0.8 mm) and -0.04 in. (-1 mm) on the opposite side. The gasket had extruded from the groove (Figure 7-14), resulting in a permanent uplift at one side of the bushing. The UPPER-1 porcelain unit had slipped (Figure 7-13) and rotated downward resulting in a permanent settlement on the opposite side.

Figure 7-21 presents the zero-corrected horizontal displacement and twist histories of the UPPER-1 porcelain unit, measured at the height of the radial displacement transducers, relative to the rigid mounting frame. These displacements and twists can be considered equal to those relative to the flange plate because the lateral stiffness of the flexible mounting plate was large. The shear deformation in the gasket and the slip of the UPPER-1 porcelain over the flange contribute to the measured displacements, although the slip contribution is the larger of the two. The slip in the x- direction was computed as one half of the sum of channels 44 and 46; the slip in the y- direction was computed as one half of the sum of channels 45 and 47. The twist around the z- axis was computed as the difference between channels 52 and 53 divided by 21-in. (533-mm) distance between these transducers. The maximum and residual twist (rotation) about the z-axis were approximately 1.4 and 0.3 percent radian, respectively. The computed maximum and residual slips were approximately 0.35 in. (9 mm) and 0.26 in. (7 mm) along the x- axis, and 0.3 in. (8 mm) and 0.2 in. (5 mm) along the y- axis.

7.5.5.3 Post-test tear-down of Bushing-2

At the conclusion of the seismic tests, the bushing was removed from the test fixture and disassembled. At that time, the gasket in the gasket connection had been extruded from the groove in the flange (see Figure 7-14) and the post-tensioning force in the bushing was measured at 9.5 kips (42 kN), that is approximately one-third the original value of 27 kips (120 kN). The bushing was de-stressed, its oil drained, and the porcelain stack above the flange was separated from the bushing flange, thus exposing the gasket in the gasket connection. There was no structural damage to either the UPPER-1 porcelain unit or the bushing flange. Examination of the gasket revealed a number of small surface cracks. Figure 7-22 indicates the location of the largest tear. Figure 7-23 is a plan view of the gasket indicating all observed cracks. The gasket also developed a small lip on its top surface (likely as a result of contact between the gasket and the edge of the groove into which it was placed) and was coated with oil due to leakage of oil at the gasket connection.

Although there were several small cracks in the gasket, none extended far below the surface. As such, the gasket was used for the remainder of the test program. The gasket was air-dried, the porcelain stacks were re-centered, and the bushing was refilled with oil and post-tensioned to 27 kips (120 kN) prior to the installation of Ring-2.

7.5.6 Response of Bushing-2 retrofitted with Ring-2

7.5.6.1 Peak response

The peak acceleration and displacement responses of the Bushing-2 (at the top, midheight, and bottom) retrofitted with Ring-2 are presented in Table 7-10. The maximum responses at the midheight of the bushing were always less than those at the top or bottom. The values of peak absolute accelerations are defined as the maximum of the vector sum of acceleration components in the local x- and local y-directions, evaluated from acceleration histories. The values of peak displacements relative to the mounting frame are defined as the maximum of the vector sum of relative displacement components in the global *X*- and local *Y*-directions, evaluated from displacement histories. The tabulated peak accelerations in Table 7-8 indicate that the CERL histories (Test No 19) had larger input peak accelerations than the Tabas histories (Test No 13), but the peak bushing accelerations are larger for the Tabas histories as indicated in Table 7-10. The power spectra for the CERL histories presented in Figure 7-6 through Figure 7-8 show that the CERL record has significant energy concentrated between 1 to 2 Hz. However, such energy did not significantly excite the *flexibly* mounted Bushing-2 because its fundamental frequency ranged between 5 and 6 Hz (see Table 7-2). As such, the Tabas histories provided a more severe test for this bushing than the CERL histories and tests using the CERL histories with target PGAs greater that 1.0g were not conducted.

7.5.6.2 Bushing response

The global response of Bushing-2 retrofitted with Ring-2 was assessed by analysis of data from Test No 13 (Tabas-A, target PGA equal to 1.0g), Test No 18 (Tabas-B, target PGA equal to 2.0g), Test No 19 (CERL, target PGA equal to 1.0g), and Test No 24 (Tabas-B, target PGA equal to 3.0g).

During Test No 13, (Tabas-A, target PGA equal to 1.0g) a maximum acceleration and displacement relative to the mounting frame of 3.4g and 0.8 in. (21 mm) respectively, were recorded at the top of the bushing. Acceleration response spectra for Bushing-2 in the local coordinate system, generated using measured acceleration histories of the *flexible* plate are shown in Figure 7-24. For information, the 2-percent and 5-percent damped IEEE 693-1997 response spectra for Moderate Level qualification are also shown in this figure. The spectrum acceleration ordinates in the *y*- and *z*- directions are smaller than those of the IEEE spectra.

During Test No 18, (Tabas-B, target PGA equal to 2.0g) a maximum acceleration and displacement relative to the mounting frame of 6.4g and 1.8 in. (45 mm) respectively, were recorded at the top of the bushing. Acceleration response spectra for Bushing-2 in the local coordinate system, generated using measured acceleration histories of the *flexible* plate are shown in Figure 7-25. For information, the 2-percent and 5-percent damped IEEE 693-1997 response spectra for High Level qualification are also shown in this figure. The spectrum acceleration ordinates in the *y*- and *z*- directions are smaller than those of the IEEE spectra.

Table 7-10 Peak responses of the Bushing-2 retrofitted with Ring-2

			Peak Acceleration (g)			*Peak Relative Displacement (mm)*		
Test No.	*Identification*[1]	*PGA*[2]	*Top*	*Midheight*	*Bottom*	*Top*	*Midheight*	*Bottom*
7	Tabas-A	0.1g	0.6	0.3	0.8	4	2	3
8	CERL	0.1g	0.5	0.4	0.8	4	2	3
9	Tabas-A	0.2g	1.1	0.6	1.2	8	4	6
10	Tabas-A	0.3g	1.6	0.8	1.5	12	4	8
11	Tabas-A	0.5g	3.3	1.8	2.5	22	9	14
12	Tabas-A	0.7g	2.9	1.7	3.1	19	8	13
13	Tabas-A	1.0g	3.4	2.2	3.8	21	9	16
14	Tabas-B	1.2g	3.4	1.8	3.5	20	9	15
15	Tabas-B	1.4g	4.5	2.3	4.2	27	12	20
16	Tabas-B	1.6g	5.5	2.6	4.6	33	15	24
17	Tabas-B	1.8g	6.3	2.8	4.5	40	18	29
18	Tabas-B	2.0g	6.4	3.0	5.5	45	20	31
19	CERL	1.0g	3.1	1.7	3.3	20	8	14
20	Tabas-B	2.2g	6.8	3.3	5.8	52	22	33
21	Tabas-B	2.4g	7.7	4.2	6.6	60	25	36
22	Tabas-B	2.6g	7.3	4.3	7.0	64	27	34
23	Tabas-B	2.8g	7.3	4.0	5.8	58	25	32
24	Tabas-B	3.0g	7.7	4.0	6.6	61	26	33

1. Tabas-A = spectrum-compatible Tabas-A earthquake histories; Tabas-B = spectrum-compatible Tabas-B earthquake histories; CERL = spectrum-compatible CERL histories.
2. PGA = target peak acceleration of the simulator platform.

During Test No 19, (CERL, target PGA equal to 1.0g) a maximum acceleration and displacement relative to the mounting frame of 3.1g and 0.8 in. (20 mm) respectively, were recorded at the top of the bushing. Acceleration response spectra for Bushing-2 in the local coordinate system, generated using measured acceleration histories of the *flexible* plate are shown in Figure 7-26. For information, the 2-percent and 5-percent damped IEEE 693-1997 response spectra for Moderate Level qualification are also shown in this figure. The spectrum acceleration ordinates in the *y*- and *z*- directions are smaller than those of the IEEE spectra.

During Test No 24, (Tabas-B, target PGA equal to 3.0g) a maximum acceleration and displacement relative to the mounting frame of 7.6g and 2.4 in. (61 mm) respectively, were recorded at the top of the bushing. Acceleration response spectra for Bushing-2 in the local coordinate system, generated using measured acceleration histories of the *flexible* plate are shown in Figure 7-27. For information, the 2-percent and 5-percent damped IEEE 693-1997 response spectra anchored at a PGA of 3.0g are also shown in this figure. The spectrum acceleration ordinates in the *y*- and *z*- directions are smaller than those of the IEEE spectra.

Figure 7-28 presents the zero-corrected vertical displacement history of the UPPER-1 porcelain unit, measured at the height of the radial displacement transducers, relative to the *rigid* mounting frame. The vertical displacement histories were calculated per Section 7.5.6.2. The maximum uplift at the edge of the porcelain unit was approximately 0.13 in. (3 mm). At the test conclusion, the residual uplift of the UPPER-1 porcelain unit was approximately 0.004 in. (0.1 mm), and for approximately 2 seconds in the history (14 to 16 seconds), there was a gap between the UPPER-1 porcelain unit and the flange in the *y*- direction.

Figure 7-29 presents the zero-corrected horizontal displacement and twist histories of the UPPER-1 porcelain unit, measured at the height of the radial displacement transducers, relative to the rigid mounting frame. These displacements and twists can be considered equal to those relative to the flange plate because the lateral stiffness of the flexible mounting plate was large. The shear deformation in the gasket and the slip of the UPPER-1 porcelain over the flange contribute to the measured displacements, although the slip contribution is the larger of the two. The slip in the *x*- direction was computed as one half of the sum of channels 44 and 46; the slip in the *y*- direction was computed as one half of the sum of channels 45 and 47. The twist around the *z*- axis was computed as the difference between channels 52 and 53 divided by the 21-in. (533-mm) distance between these transducers. The maximum twist (rotation) about the *z*-axis were approximately 0.22 percent radian. The computed maximum slips were approximately 0.16 in. (4 mm) and 0.21 in. (5 mm) along the *x*- and *y*- axes, respectively. There was negligible permanent slip in the bushing.

7.5.6.3 Post-test tear-down of Bushing-2

At the conclusion of the seismic tests, Ring-2 was removed, the bushing was removed from the test fixture and disassembled. A small portion of the gasket had extruded from the groove. The PT force in the bushing was measured at 22 kips (98 kN): approximately 80 percent the original value of 27 kips (120 kN). The bushing was de-stressed, its oil drained, and the porcelain stack above the flange was separated from the bushing flange, exposing the gasket in the gasket connection. There was no structural damage to either the UPPER-1 porcelain unit or the bushing flange. Examination of the gasket revealed a number of cracks in addition to those reported in Section 7.5.5.3. Figure 7-30 is a plan view of the gasket showing all cracks. A small portion of the gasket was torn and the gasket was coated with oil due to leakage at the gasket connection.

7.6 Effect of Support Flexibility and Ring-2 on the Response of Bushing-2

The main objectives of the testing program described in this chapter were to evaluate the seismic response of the bushing mounted on a *flexible* support and to evaluate the efficacy of Ring-2 in improving the seismic response of the bushing. The following sections describe the effect of the *flexible* plate and Ring-2 on the seismic response of Bushing-2.

7.6.1 Influence of support flexibility

For bushings mounted on transformers, the rotational flexibilities of the turret and top plate of the transformer amplify the *vertical* component of the ground acceleration. The flexibilities of the turret and top plate of the transformer have two effects on the *horizontal* response of the bushing-transformer system. A typical IEEE 693-1997 acceleration spectrum is reproduced in Figure 7-31 and is used to illustrate these two effects. The spectral acceleration for a *rigidly* mounted bushing is identified by point A in the figure. Installation of the bushing on a turret or transformer tank top plate with rotational flexibility reduces the frequency of the bushing-transformer system and results in larger spectral accelerations (point B in the figure). Installation of the bushing on a turret or transformer tank top plate with horizontal flexibility will amplify the motions at the flange of the bushing and result in larger spectral accelerations (point C in the figure). For bushings mounted directly on transformer top plates, the amplification factor will nearly equal unity (Bellorini, 1997) due to the large lateral stiffness of the transformer. For bushings attached to turrets, this amplification factor could be greater than unity.

The second factor is explicitly accounted for in IEEE 693-1997 through the use of an amplification factor equal to 2.0. The *flexible* support used in the studies reported herein replicated the first but not the second effect. As such, the histories used for the tests reported in this chapter incorporated the IEEE amplification factor of 2. For example the spectrum for High Level qualification was anchored at 2g as shown in Figure 7-5.

The reduction in the frequency of the bushing-support system from 20 Hz to 7 Hz substantially increased the response of the 230-kV bushing. Figure 7-5 provides insight into the likely increase in the response for IEEE 693-1997 spectrum compatible ground motions. For a *rigidly* mounted 230-kV bushing with a frequency of 20 Hz, the 2-percent damped spectral acceleration is approximately 3g. A change in the frequency of this bushing to 7 Hz increases the spectral accelerations by a factor of 2.1 to 6.4g.

The vertical displacement data from channels 54 through 61 from Test No 24 was used to examine the response of the *flexible* plate. Displacement histories of two typical records (channels 60 and 61) are shown in Figure 7-32. The displacements near the bushing flange had a maximum value of 0.17 in. (4 mm) and were two to three times larger than the displacements at the plate mid-circle (see Figure 7-9). The displacement histories for the sensors on a side of the bushing (e.g., channels 56 and 57) were in-phase. These displacements were out-of-phase with the displacement histories on the opposite side of the bushing (e.g. channels 57 and 61). This is caused by the rocking motion of the bushing on the *flexible* plate.

7.6.2 *Efficacy of Ring-2*

To evaluate the efficacy of Ring-2, data collected from identical tests for Bushing-2 both without and with Ring-2 were examined. For the retrofitted bushing, visual inspection of the gasket connection was not possible prior to the end of the test program and the subsequent removal of the ring. As such, it was not possible to determine the first test during which oil leaked from the bushing. However, a comparison of zero-corrected data collected from Test Nos 14 (Tabas-B, target PGA equal to 1.2g), 15 (Tabas-B, target PGA equal to 1.4g), and 18 (Tabas-B, target PGA equal to 2.0g) for Bushing-2 with and without Ring-2 provides information regarding the response of Bushing-2 at the gasket connection. Table 7-11 presents selected slip, uplift, and twist data for the UPPER-1 porcelain unit.

Table 7-11 Response of the UPPER-1 porcelain unit

Ring-2 Installed	*Test No*[1]	*Radial Slip (mm)*		*Vertical Uplift (mm)*		*Twist (% radian)*	
		Peak	*Residual*	*Peak*	*Residual*	*Peak*	*Residual*
No	14	2	-	0.8	-	0.08	-
	15	4	-	1	-	0.6	0.4
	18	9	7	2	0.8	1.4	0.3
Yes	14	2	-	0.8	-	0.02	-
	15	3	-	1	-	0.03	-
	18	4	-	2	-	0.05	0.02

1. Test No 14: last test without oil leakage for Bushing-2 without Ring-2; Test No 15: first test with oil leakage for Bushing-2 without Ring-2; Test No 18: test with acceleration spectrum equivalent to the IEEE 693-1997 spectrum for high-level qualification.

From Table 7-11, it is clear that the addition of Ring-2 reduced the maximum and residual slip and maximum and residual twist of the UPPER-1 porcelain unit. Ring-2 reduced the residual uplift of the porcelain but had negligible influence on the maximum porcelain uplift.

For earthquake tests with target PGAs exceeding 2.4g, oil leaked from the ring-to-bushing connection. Although the ring retrofit detail delayed oil leakage, it was unable to prevent oil leakage for extreme shaking.

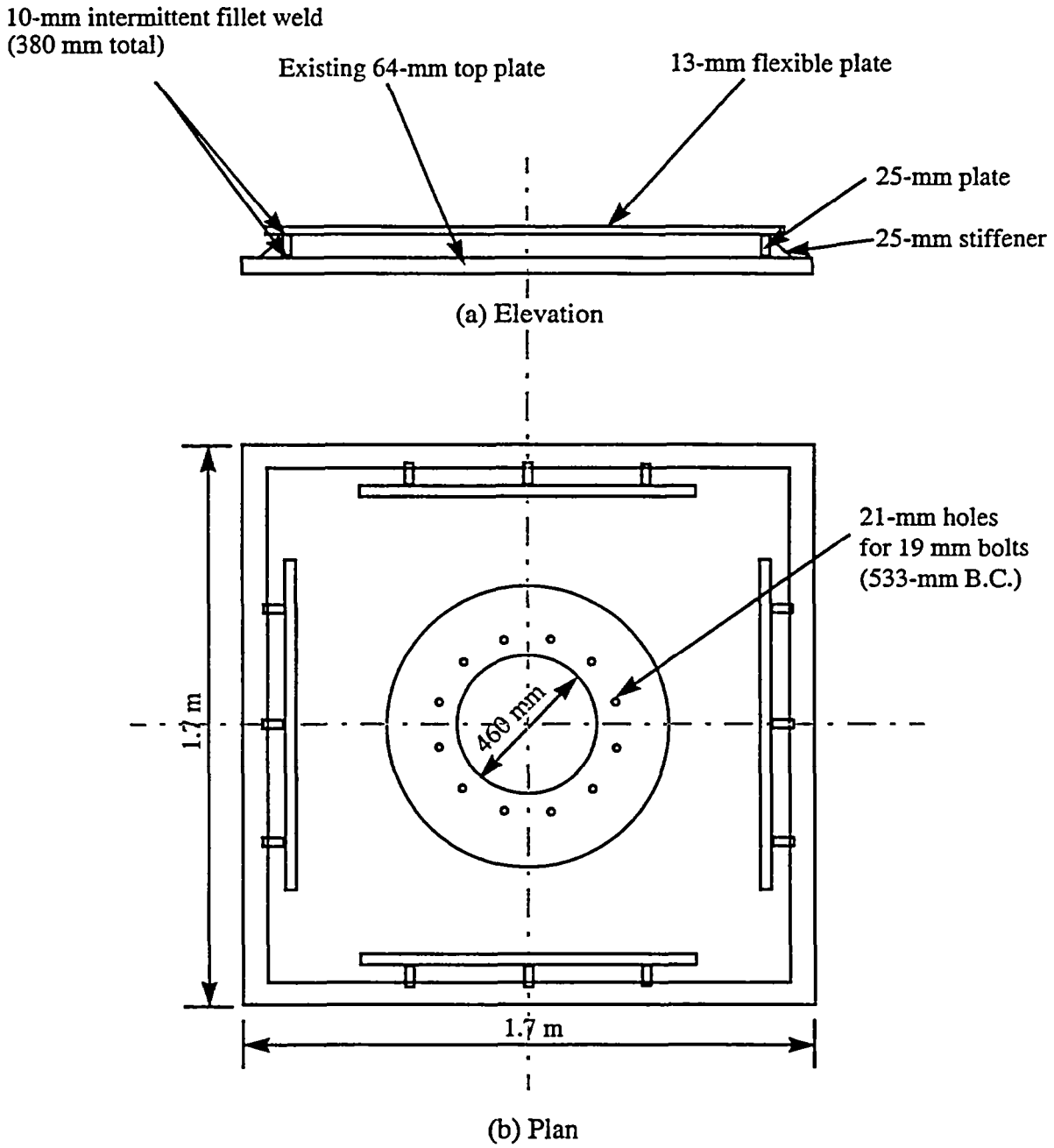

Figure 7-1 Details for flexible plate

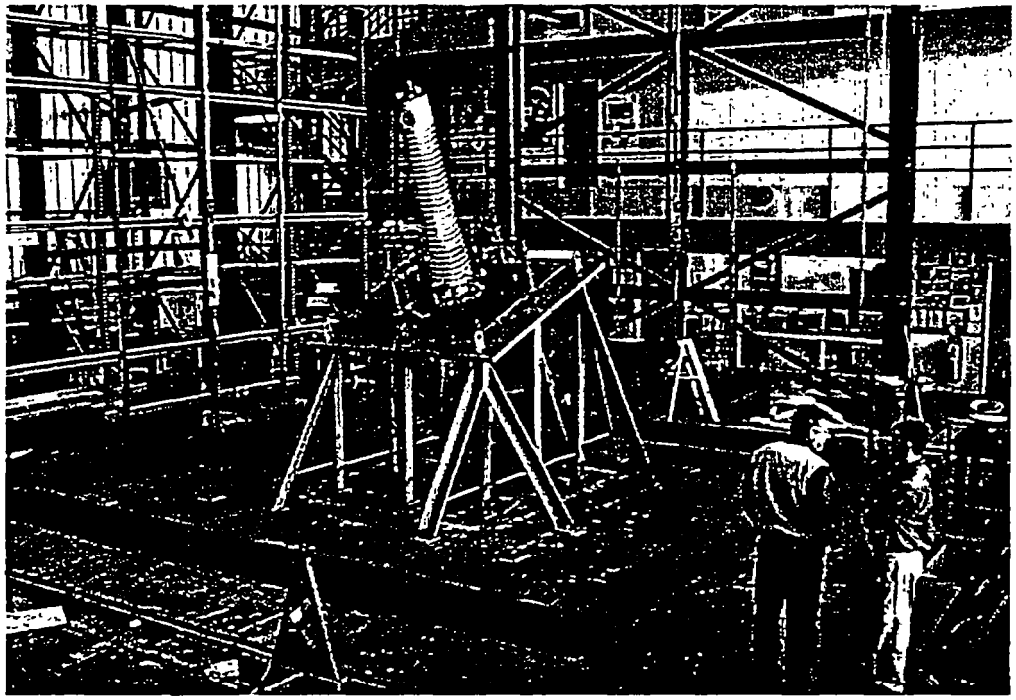

Figure 7-2 230 kV-bushing installed atop the flexible plate

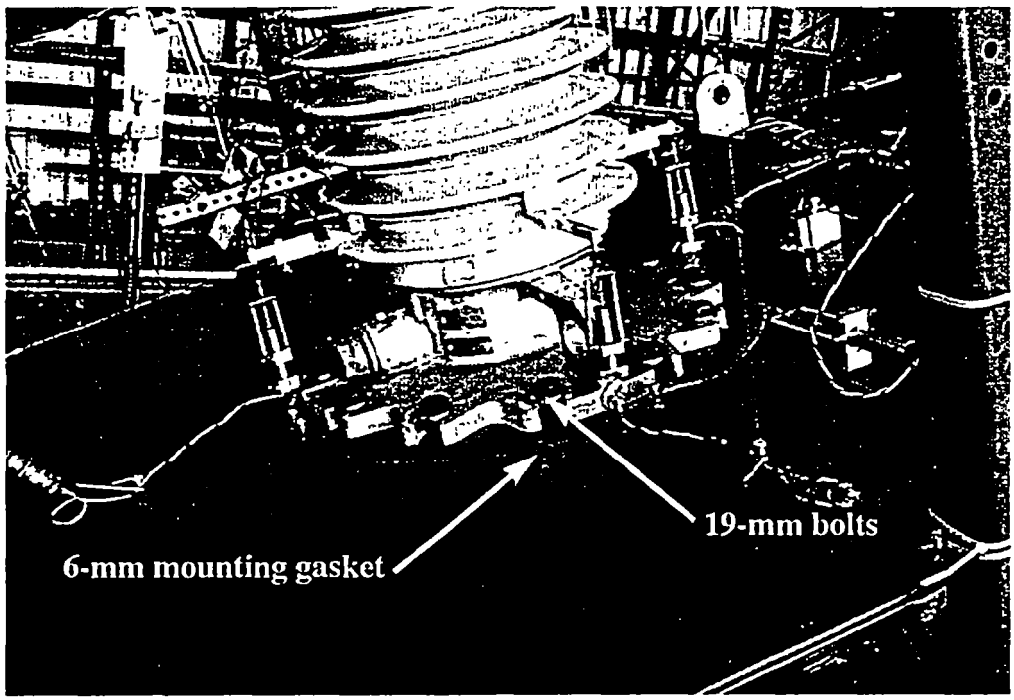

Figure 7-3 View of the flange connection showing the mounting gasket and bolts

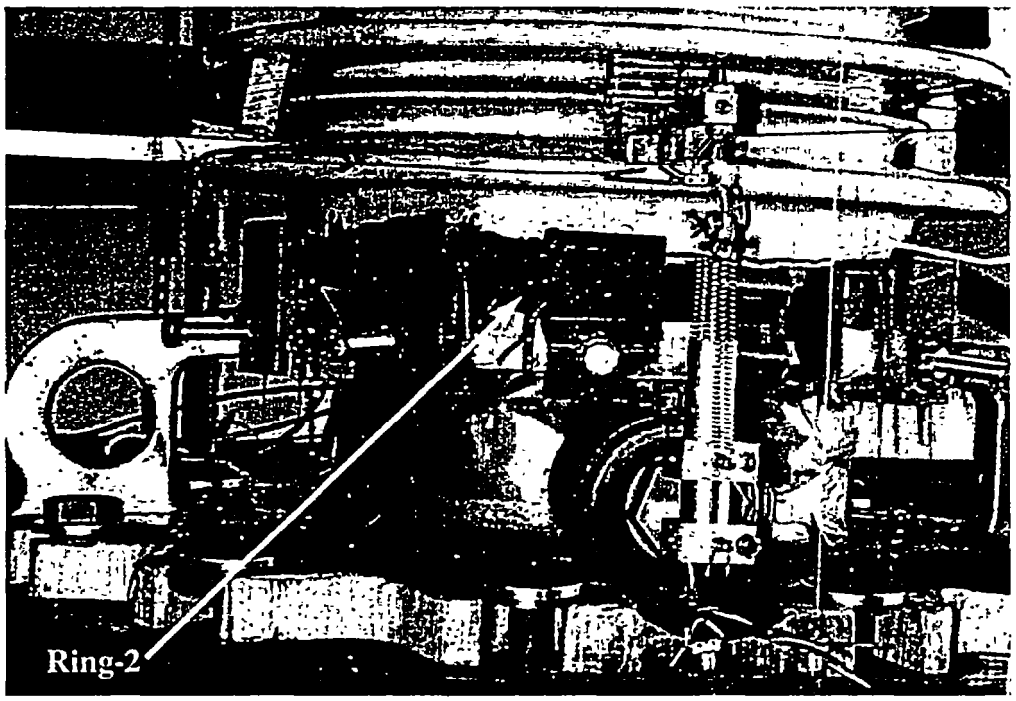

Figure 7-4 Gasket connection showing Ring-2 retrofit detail

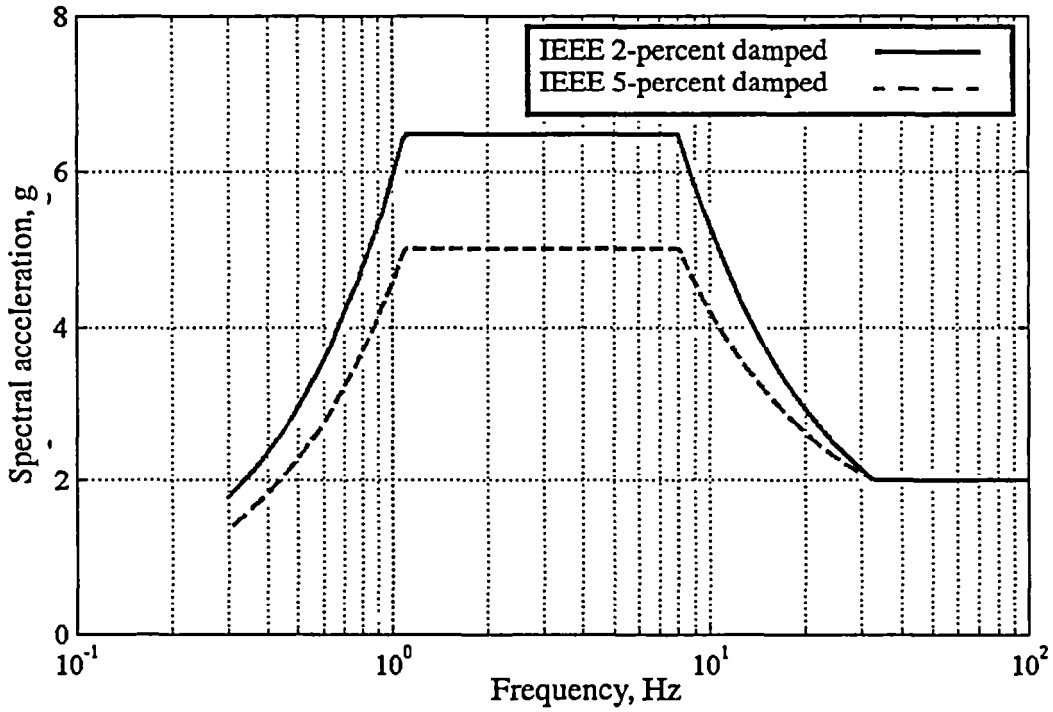

Figure 7-5 IEEE 693-1997 test response spectrum for High Level Qualification

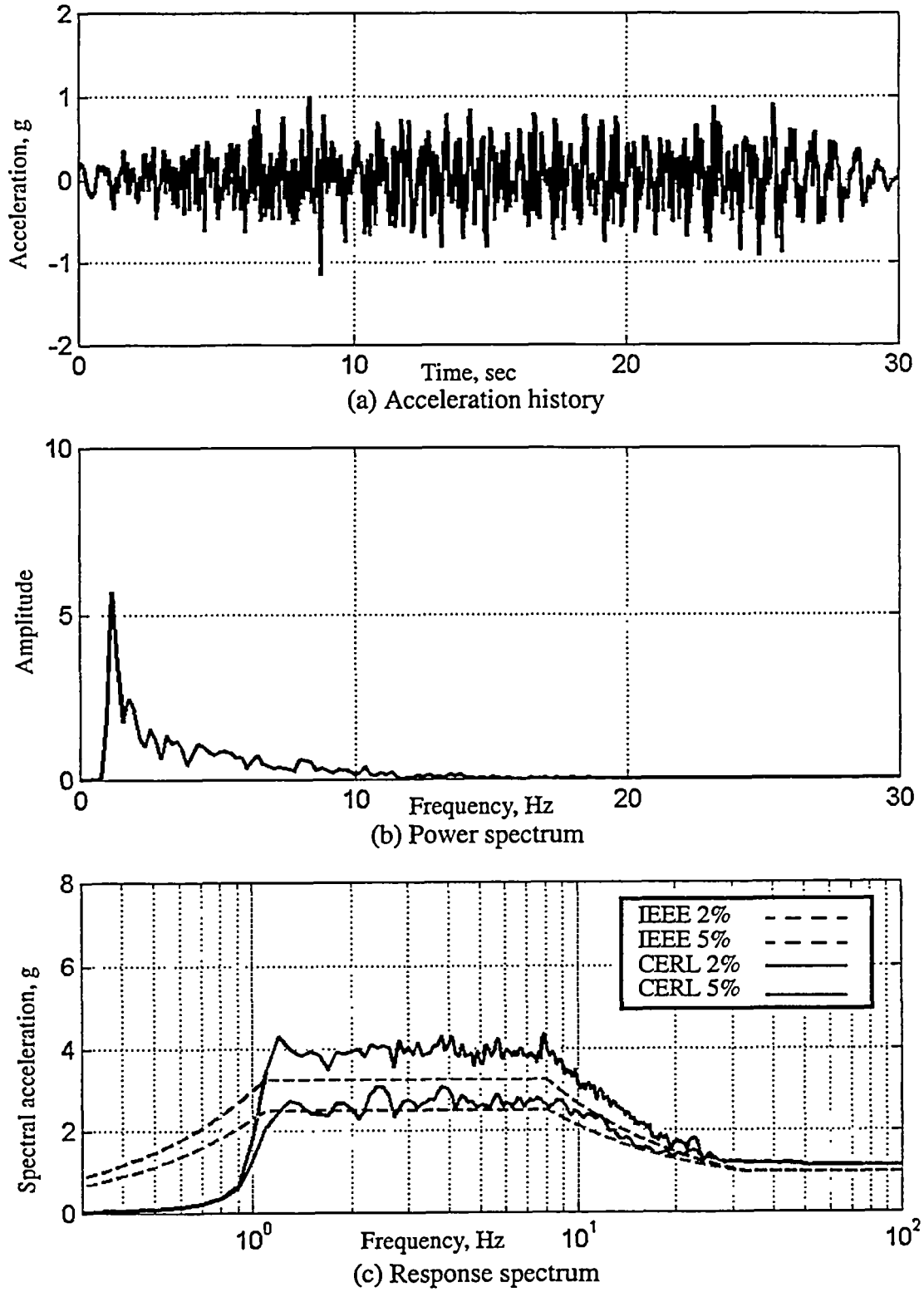

Figure 7-6 Acceleration history, power spectrum, and response spectrum for the longitudinal (*X*-component of the CERL record

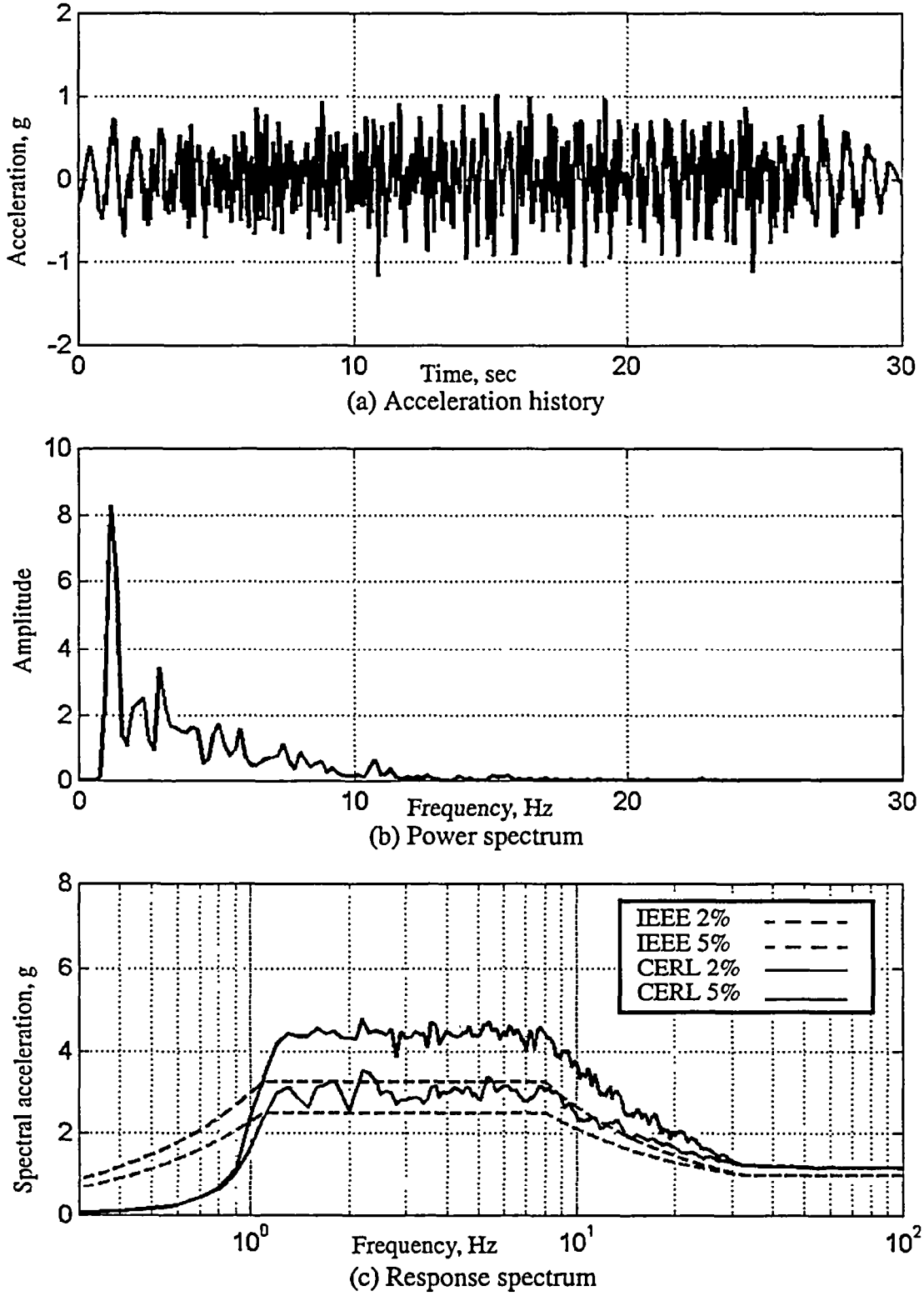

Figure 7-7 Acceleration history, power spectrum, and response spectrum for the transverse (*Y*-component of the CERL record

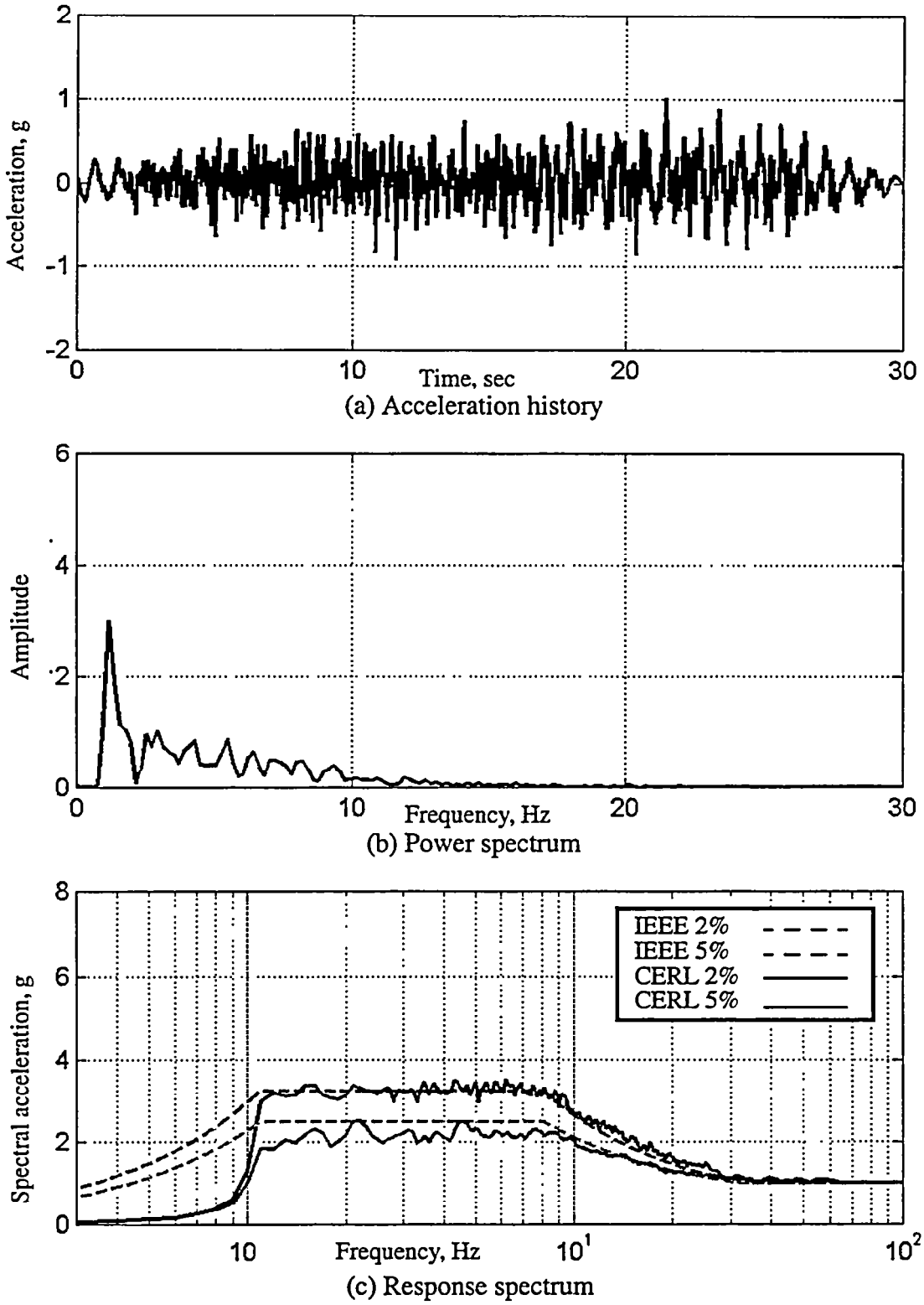

Figure 7-8 Acceleration history, power spectrum, and response spectrum for the vertical (Z-component of the CERL record

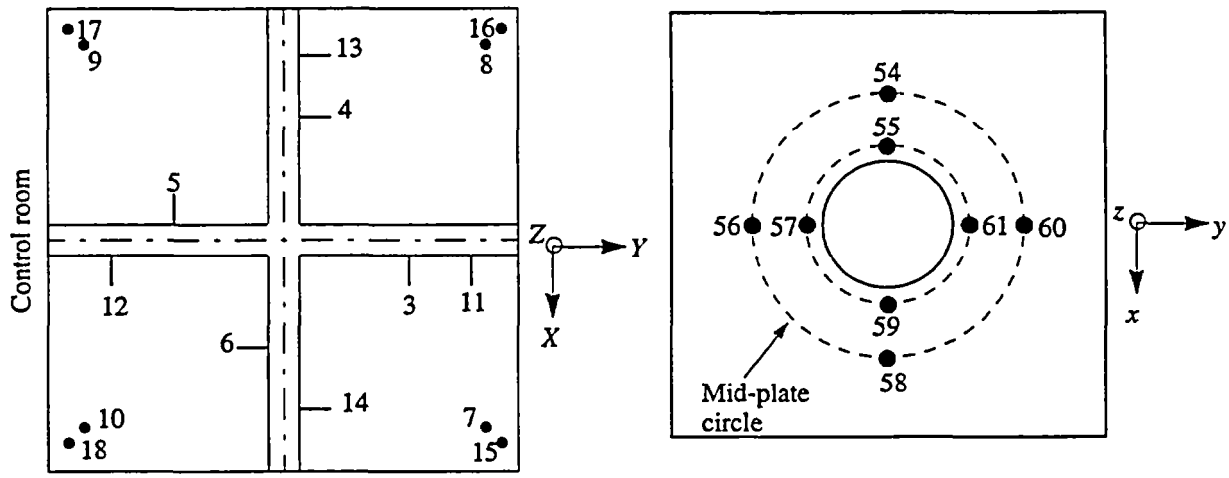

(a) Earthquake simulator

(b) *Flexible* mounting plate

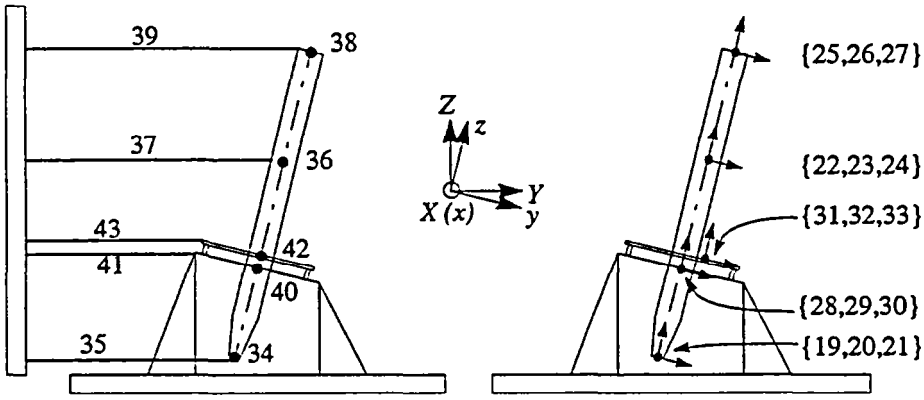

(c) Bushing and mounting frames

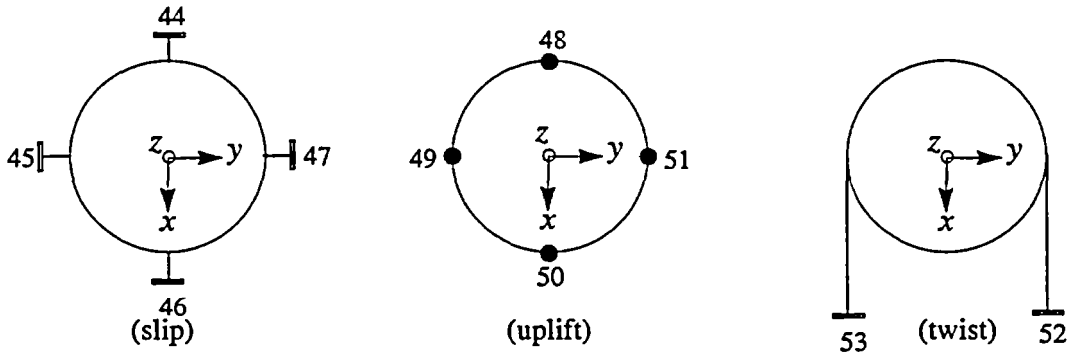

(d) UPPER-1 porcelain unit

Figure 7-9 Instrumentation for seismic testing of Bushing-2 mounted on a flexible plate

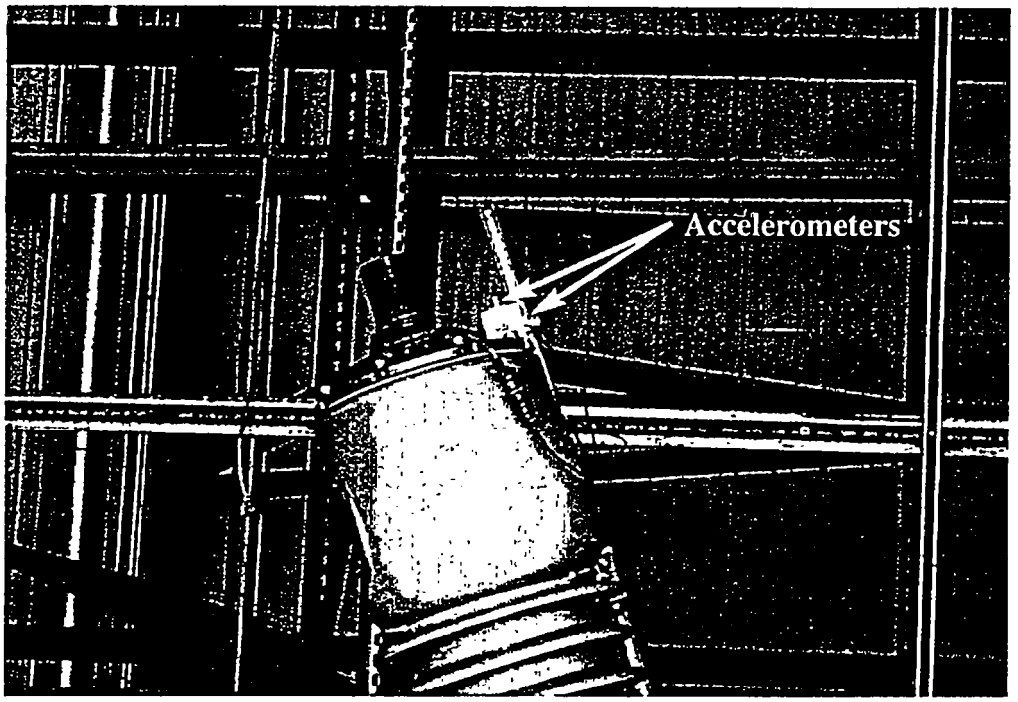

Figure 7-10 Instrumentation at the top of Bushing-2

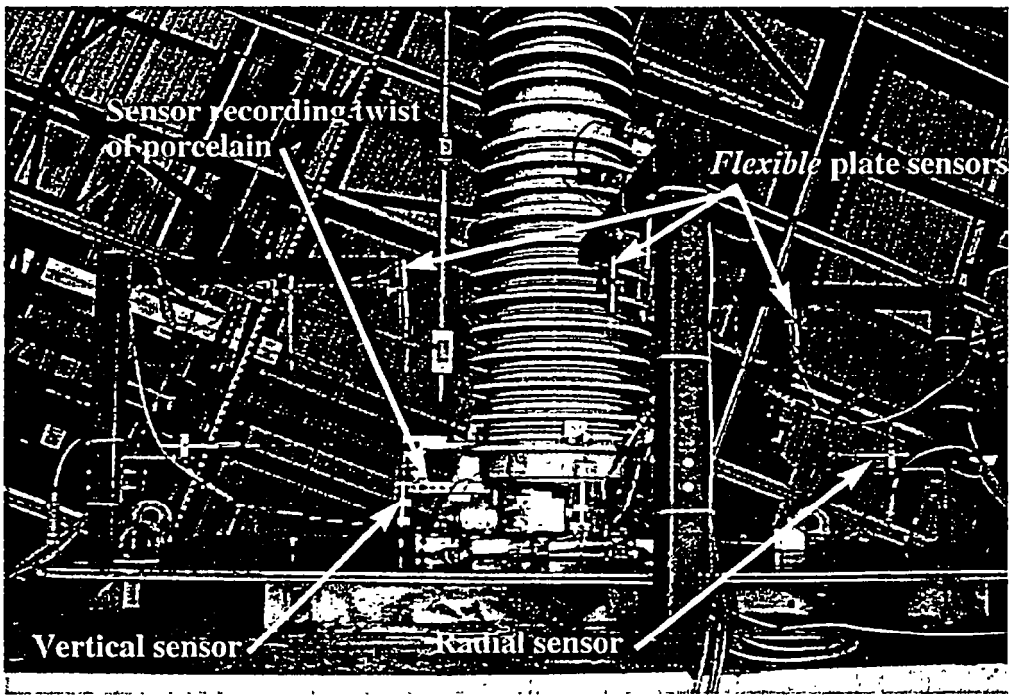

Figure 7-11 Instrumentation of the UPPER-1 porcelain unit and the flexible mounting plate

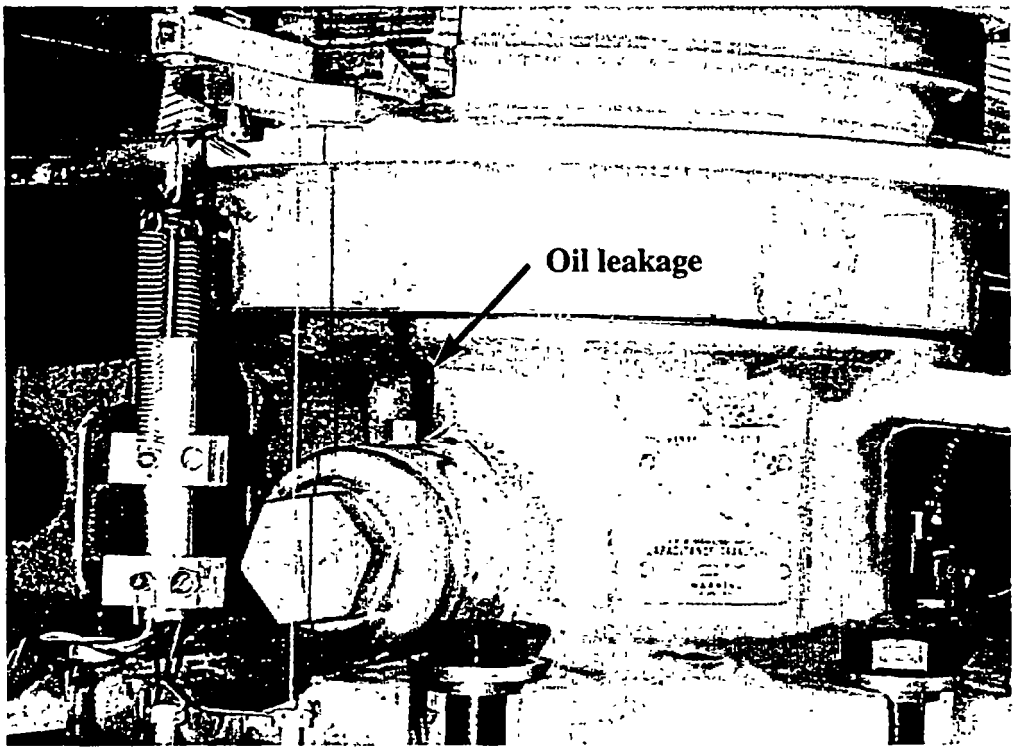

Figure 7-12 Bushing-2 after Test No 15 (target PGA=1.4g) showing oil leakage

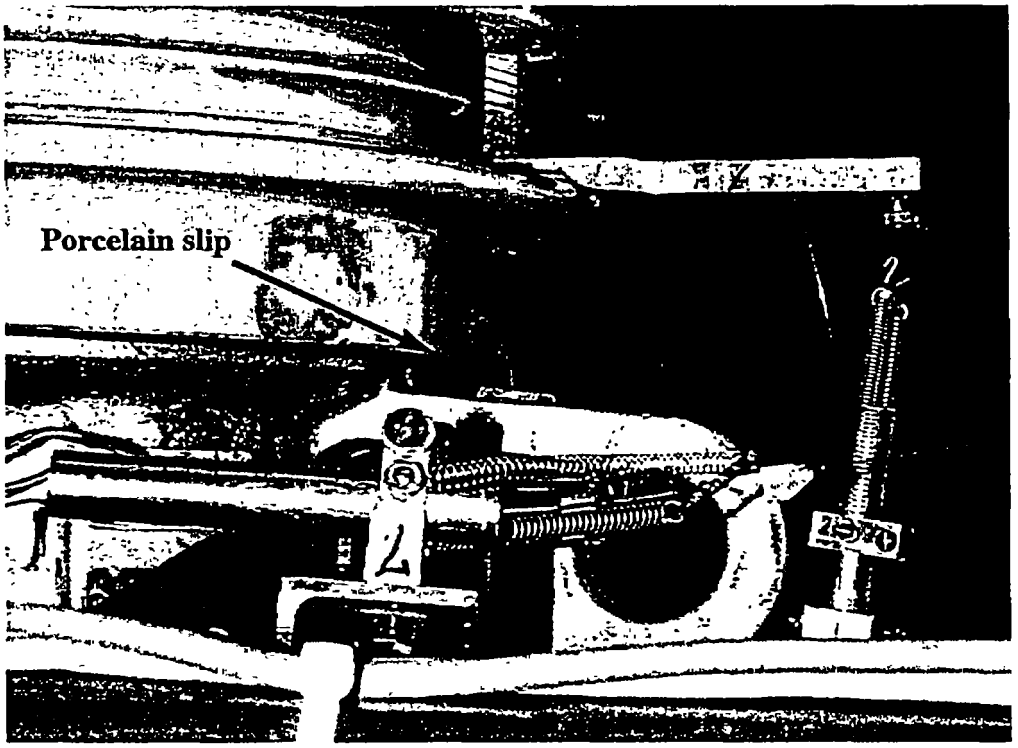

Figure 7-13 Bushing-2 after Test No 17 (target PGA=1.8g) showing slip of porcelain

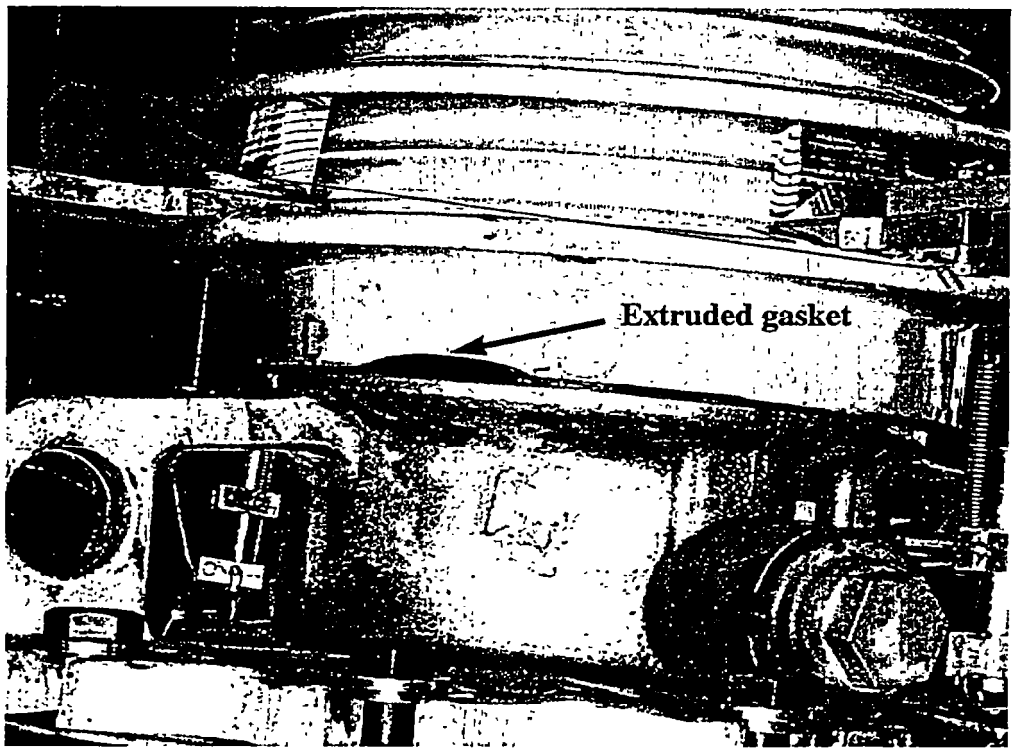

Figure 7-14 Bushing-2 after Test No 18 (target PGA=2.0g) showing extruded gasket

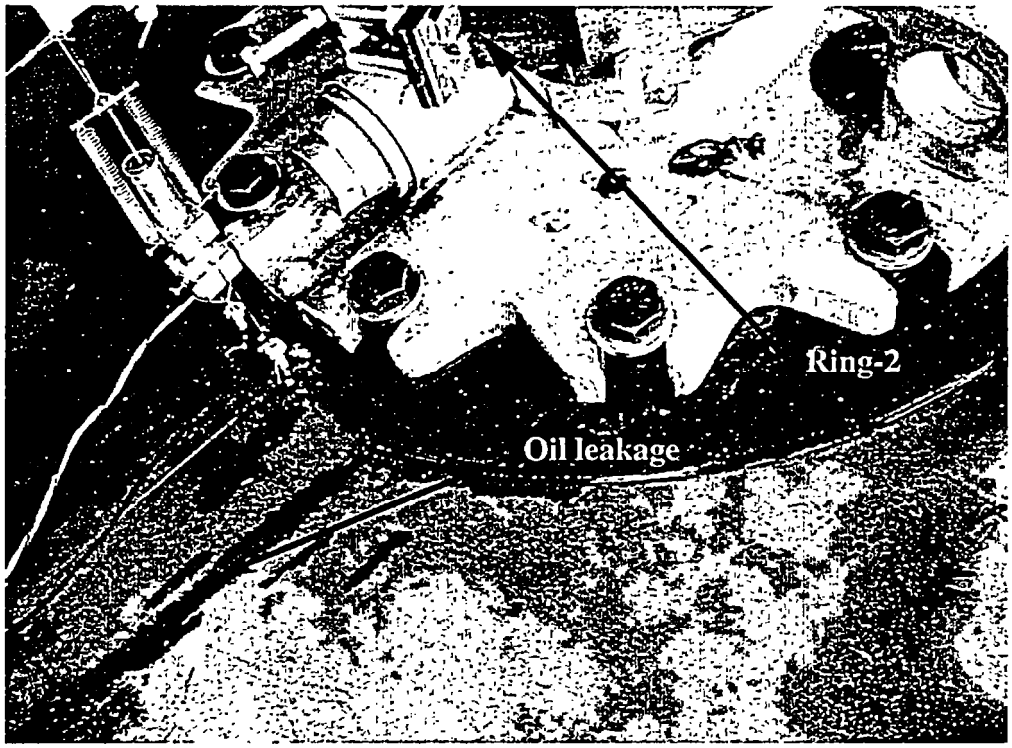

Figure 7-15 Retrofitted Bushing-2 after Test No 23 (target PGA=2.8g) showing oil leakage

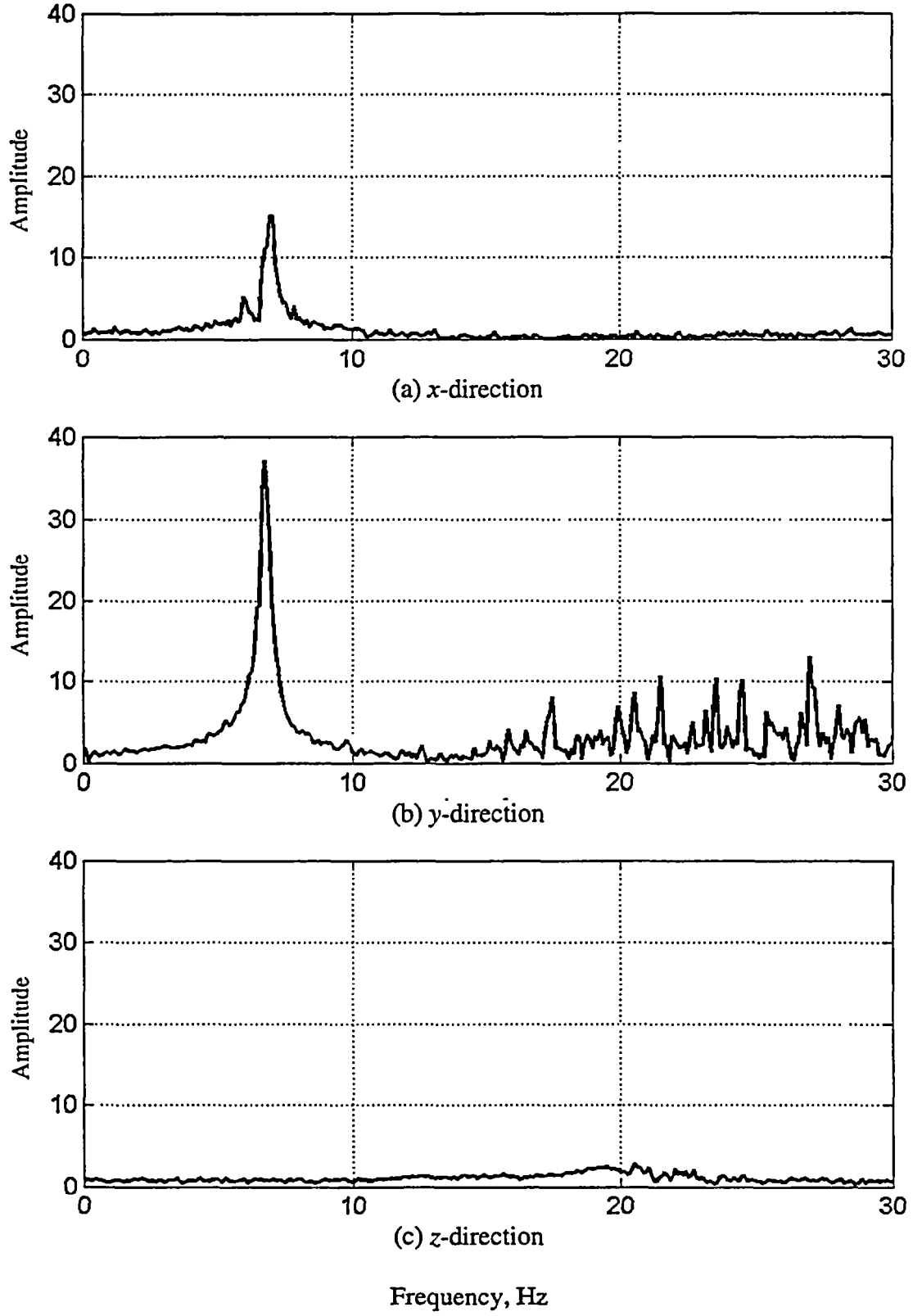

Figure 7-16 Transfer function amplitudes between the top of Bushing-2 and the flexible plate

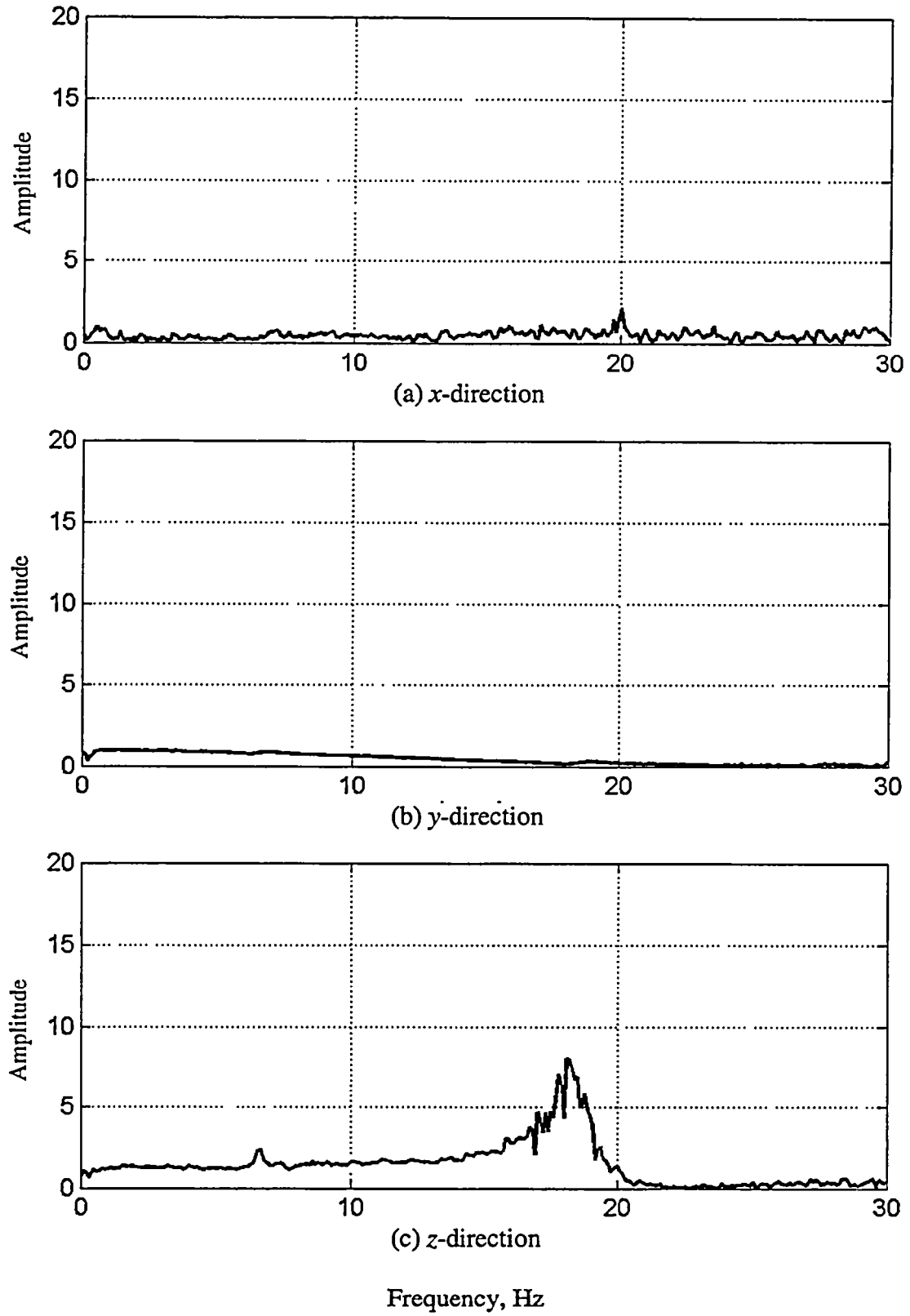

Figure 7-17 Transfer function amplitudes between the flexible plate and the rigid support

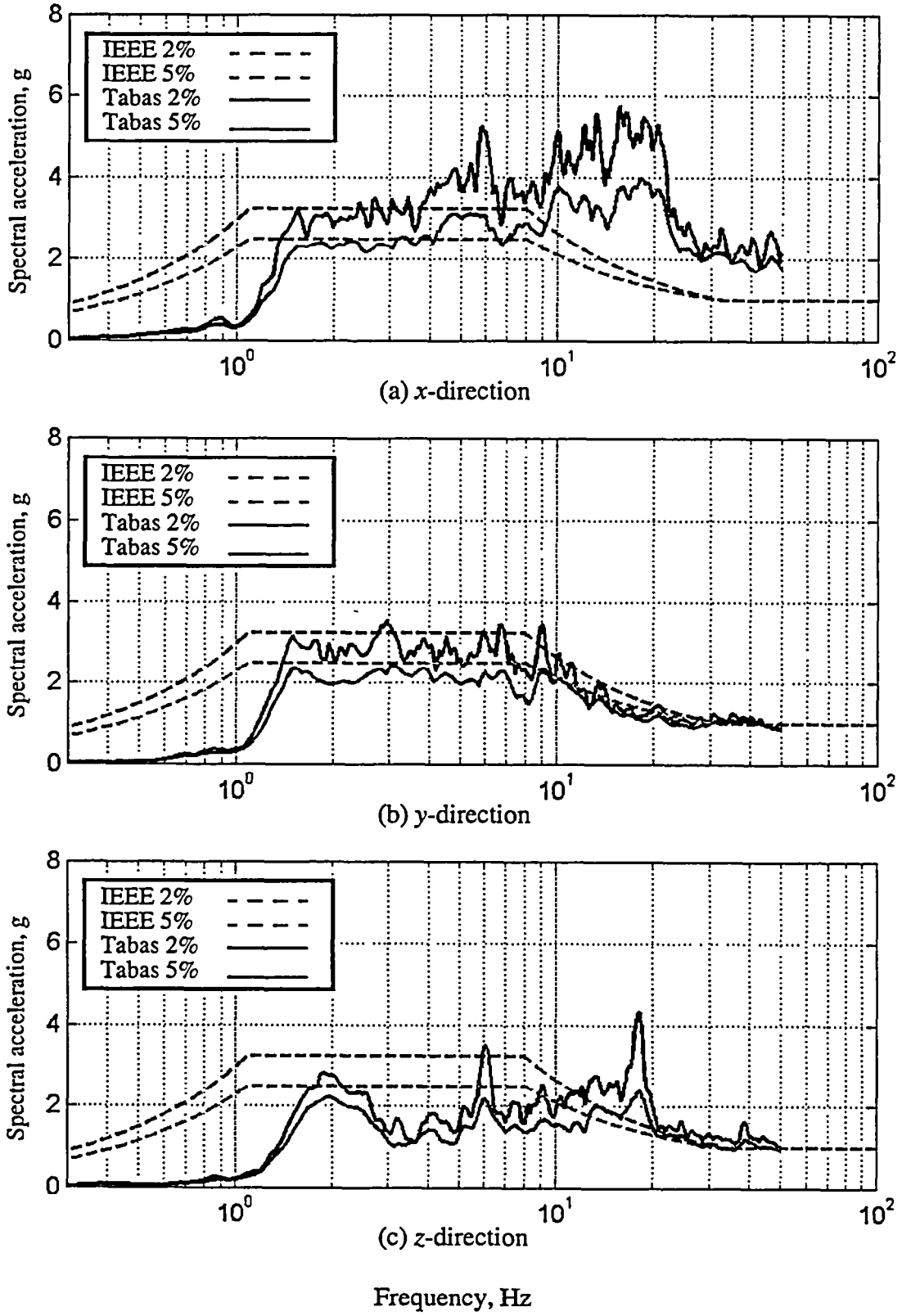

Figure 7-18 Response spectrum for Bushing-2 without Ring-2; Test No 13, Tabas-A, target PGA=1.0g

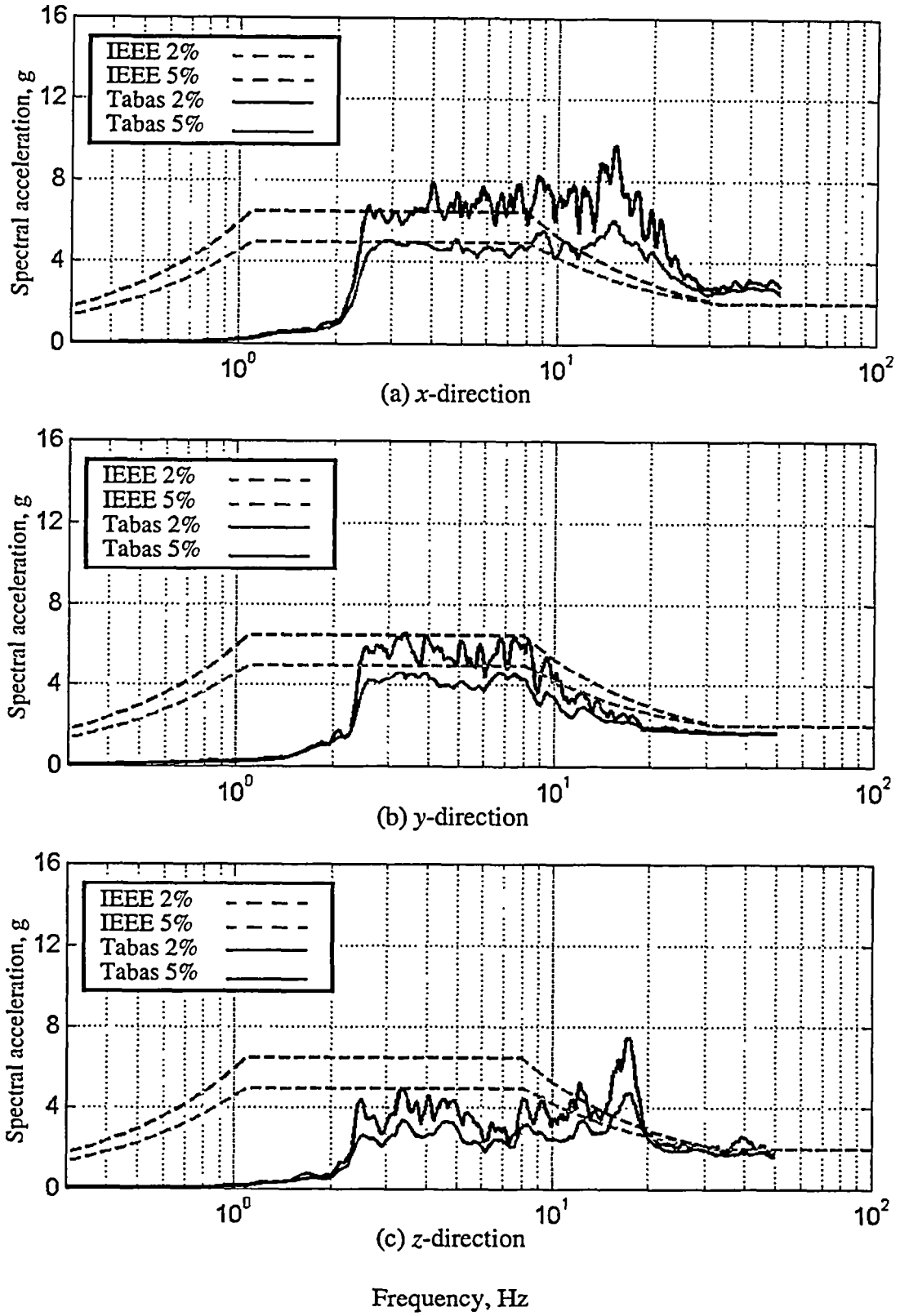

Figure 7-19 Response spectrum for Bushing-2 without Ring-2; Test No 18, Tabas-A, target PGA=2.0g

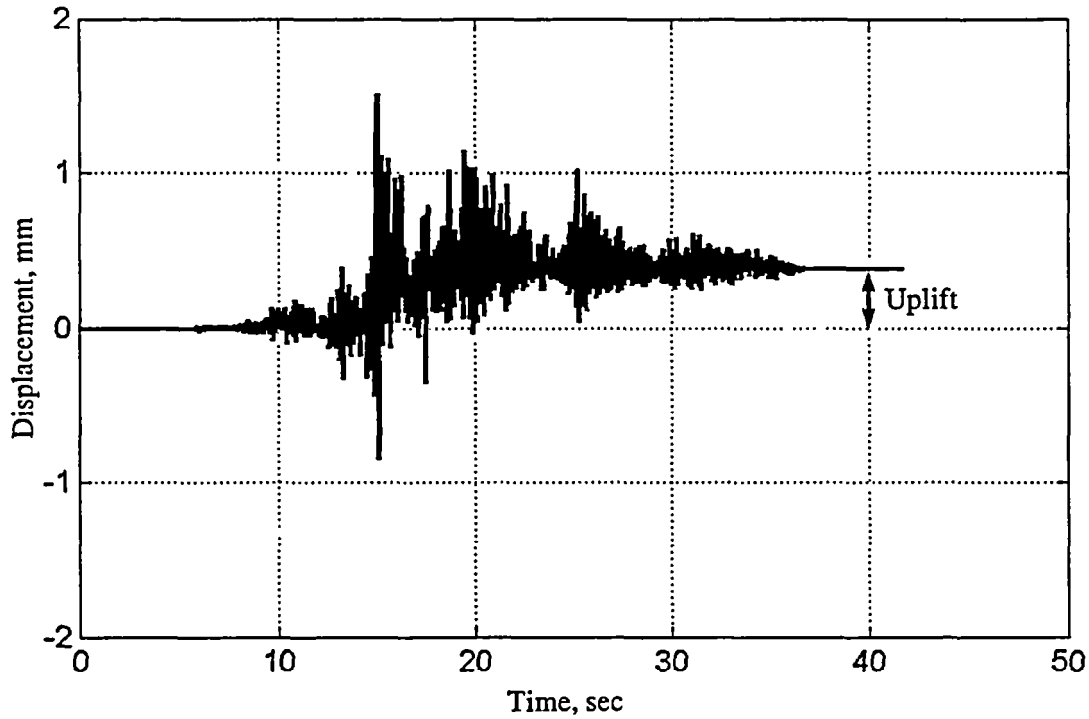

(a) Along y-axis (Channel 49)

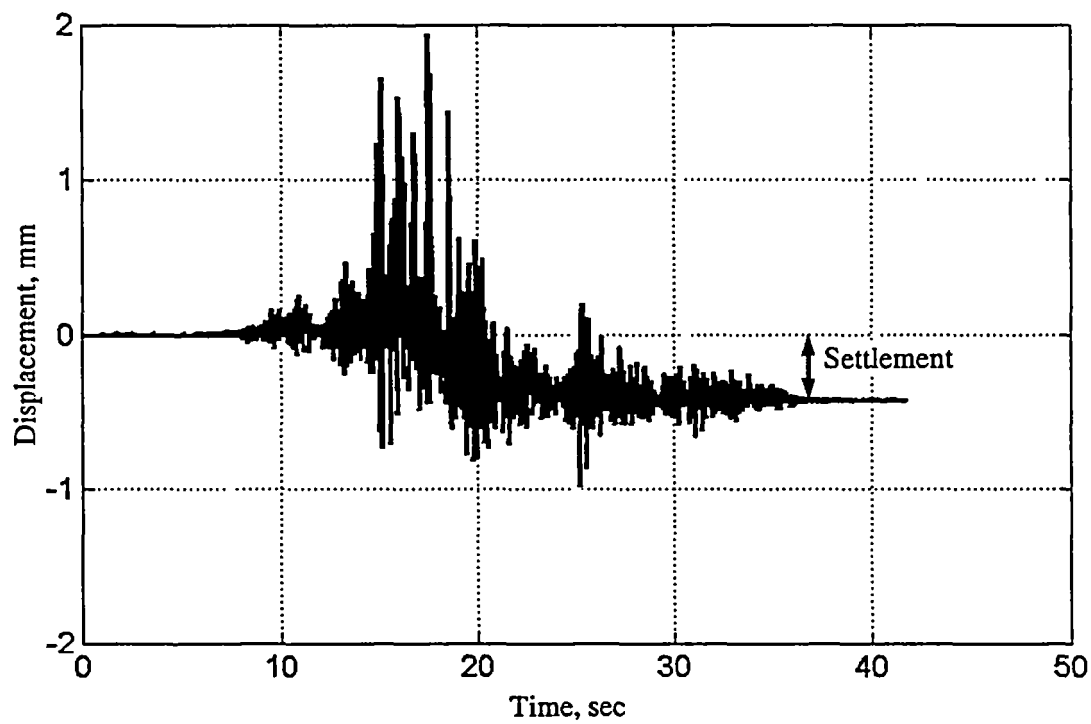

(b) Along y-axis (channel 51)

Figure 7-20 Components of vertical motion for Bushing-2 without Ring-2; Test No 18, Tabas-B, target PGA=2.0g

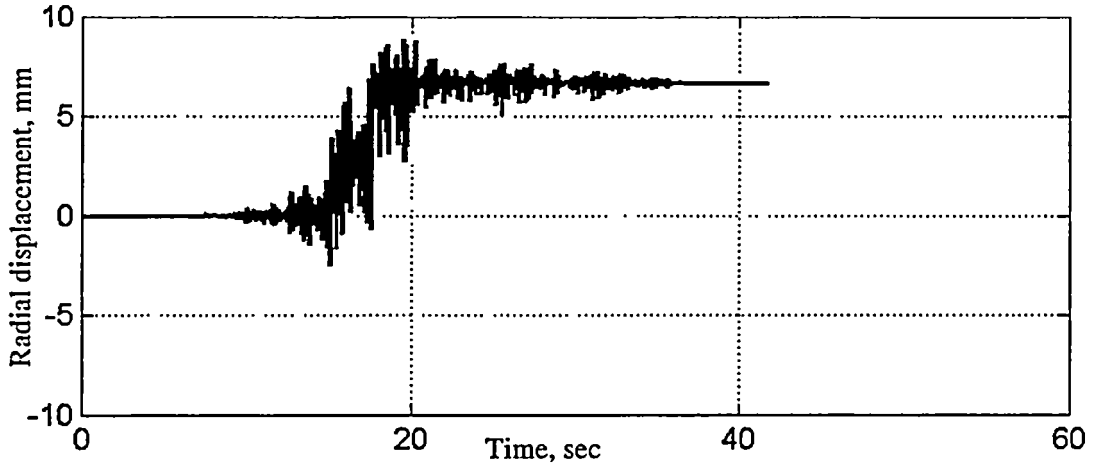

(a) Slip of the UPPER-1 porcelain in the *x*- direction

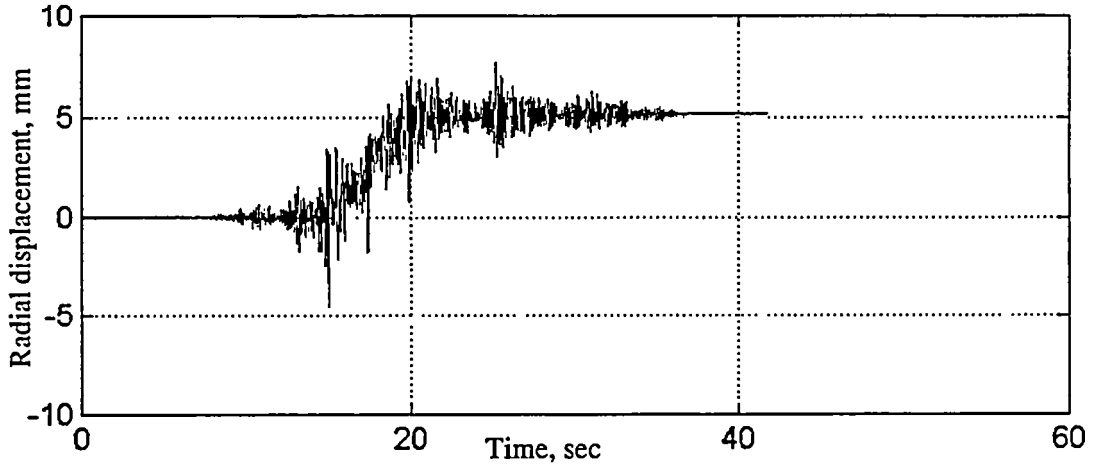

(b) Slip of the UPPER-1 porcelain in the *y*- direction

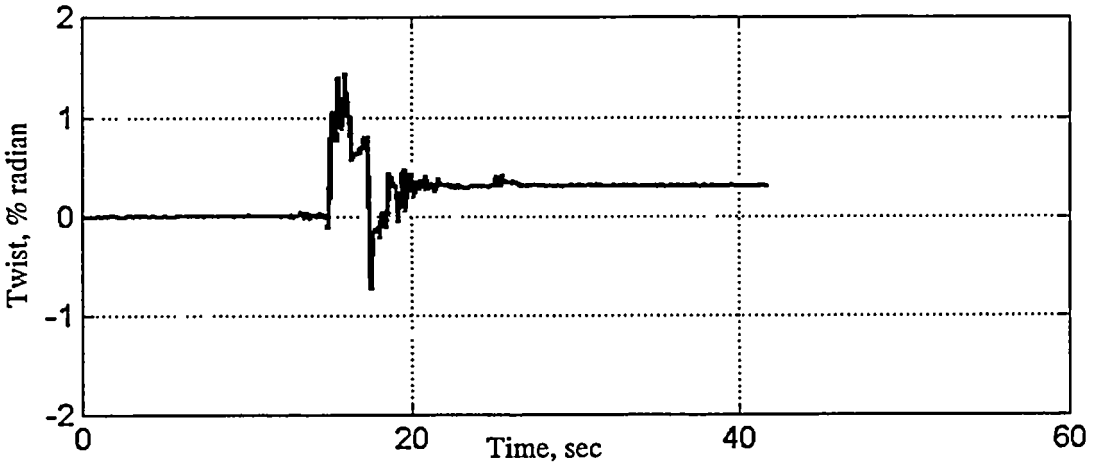

(c) Twist of the UPPER-1 porcelain unit about the *z*- axis

Figure 7-21 Components of horizontal motion for Bushing-2 without Ring-2; Test No 18, Tabas-B, target PGA=2.0g

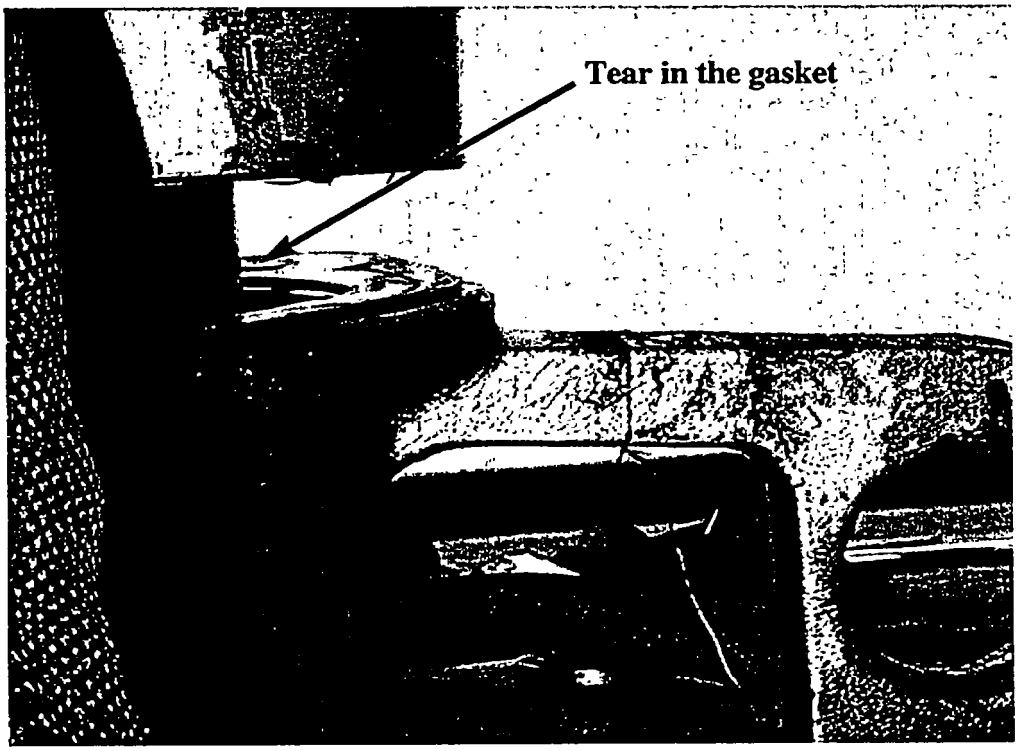

Figure 7-22 Bushing-2 after earthquake testing showing the largest tear in the gasket

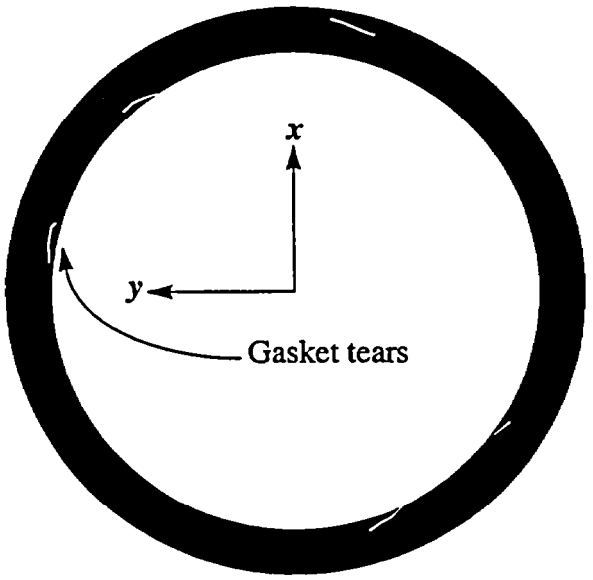

Figure 7-23 Drawing of the gasket locating tears

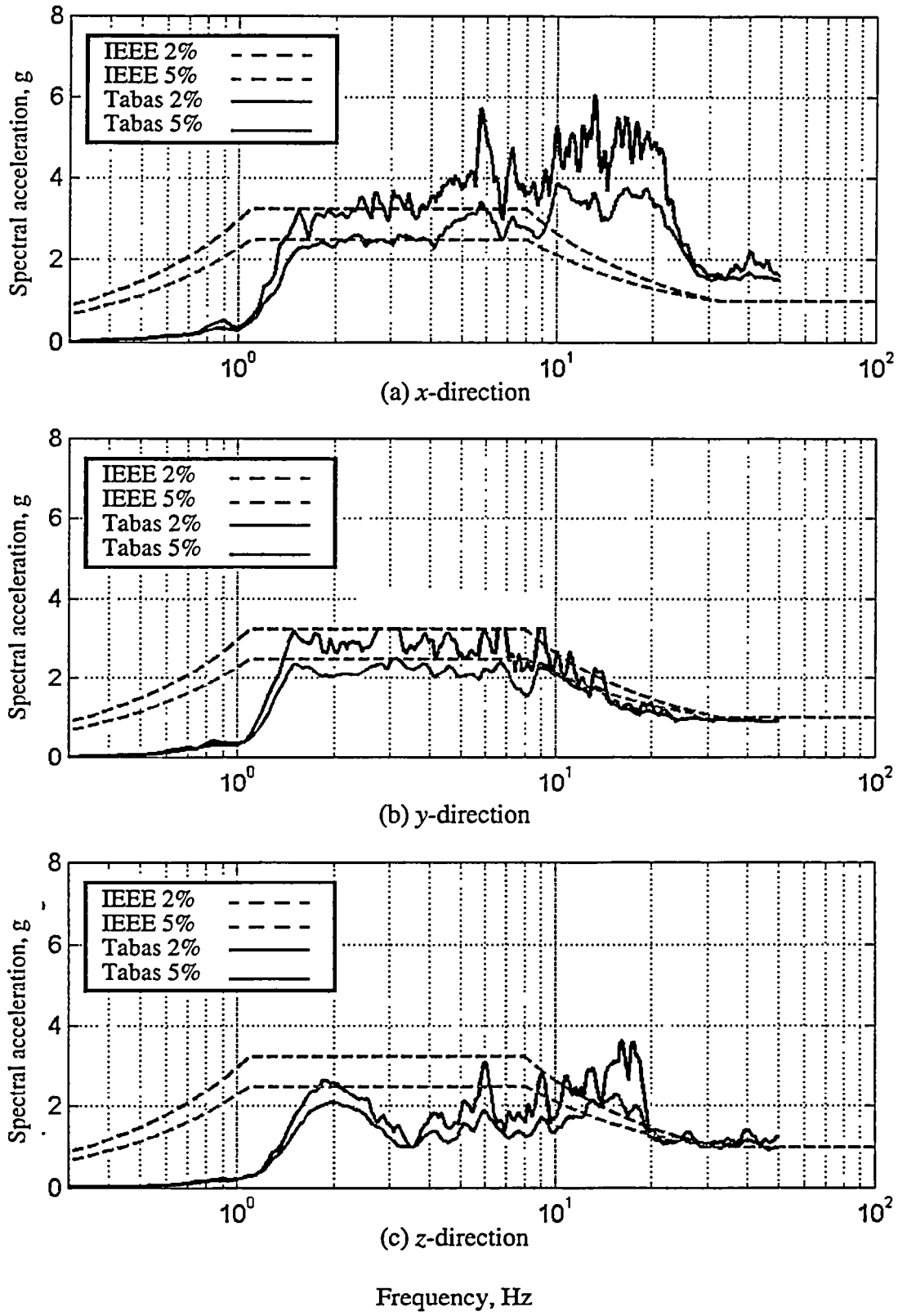

Figure 7-24 Response spectrum for Bushing-2 retrofitted with Ring-2; Test No 13, Tabas-A, target PGA=1.0g

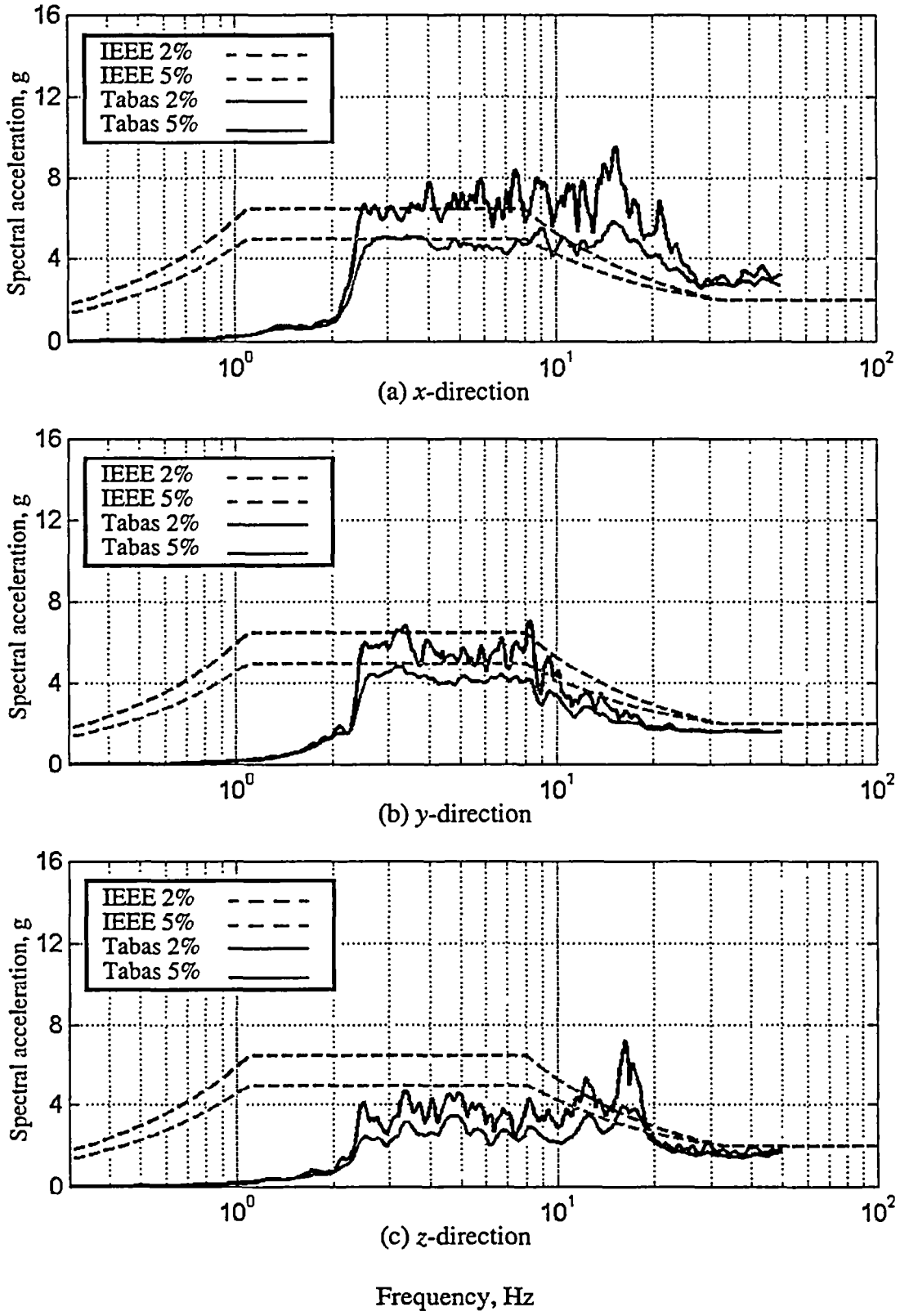

Figure 7-25 Response spectrum for Bushing-2 retrofitted with Ring-2; Test No 18, Tabas-B, target PGA=2.0g

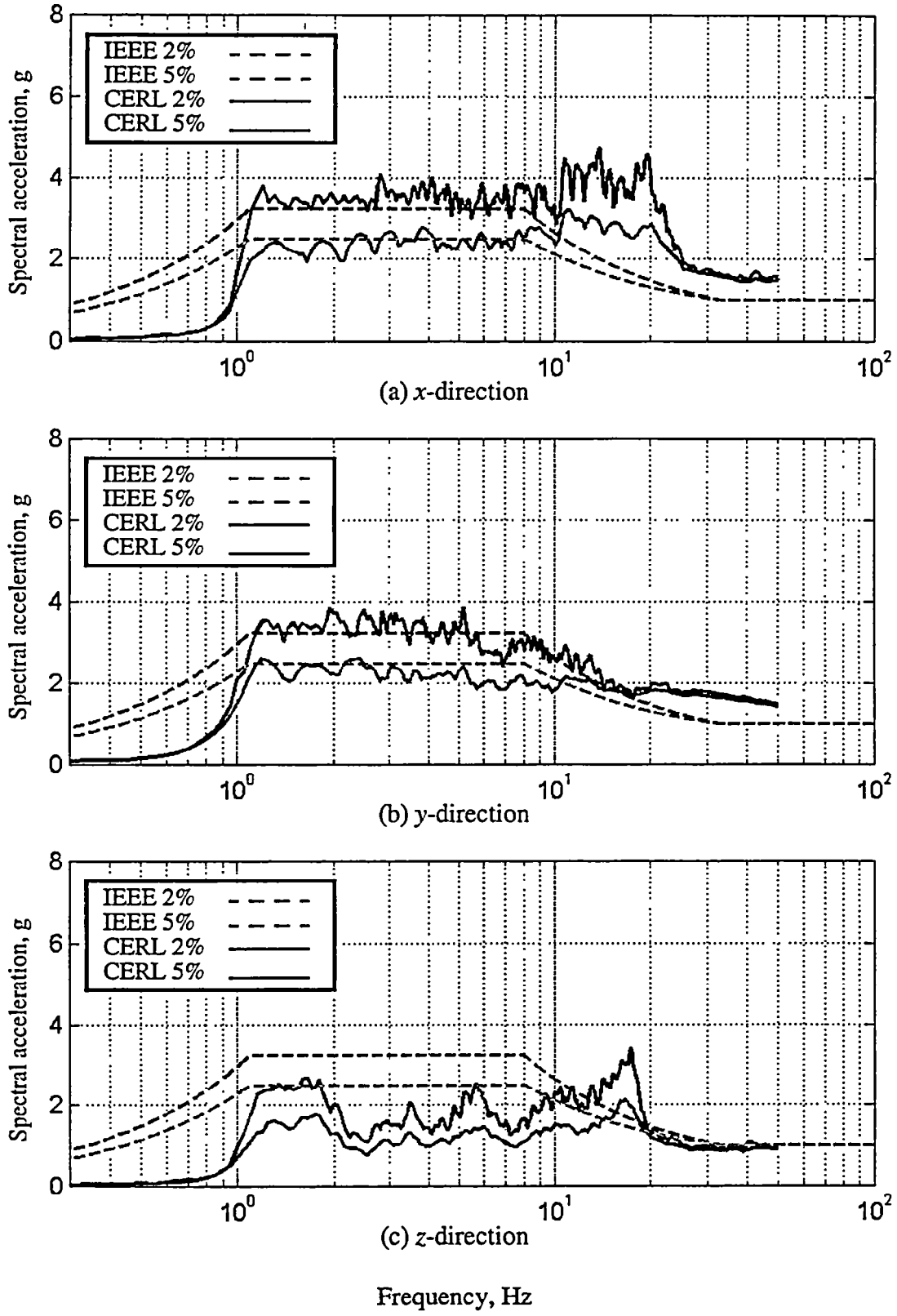

Figure 7-26 Response spectrum for Bushing-2 retrofitted with Ring-2; Test No 19, CERL, target PGA=1.0g

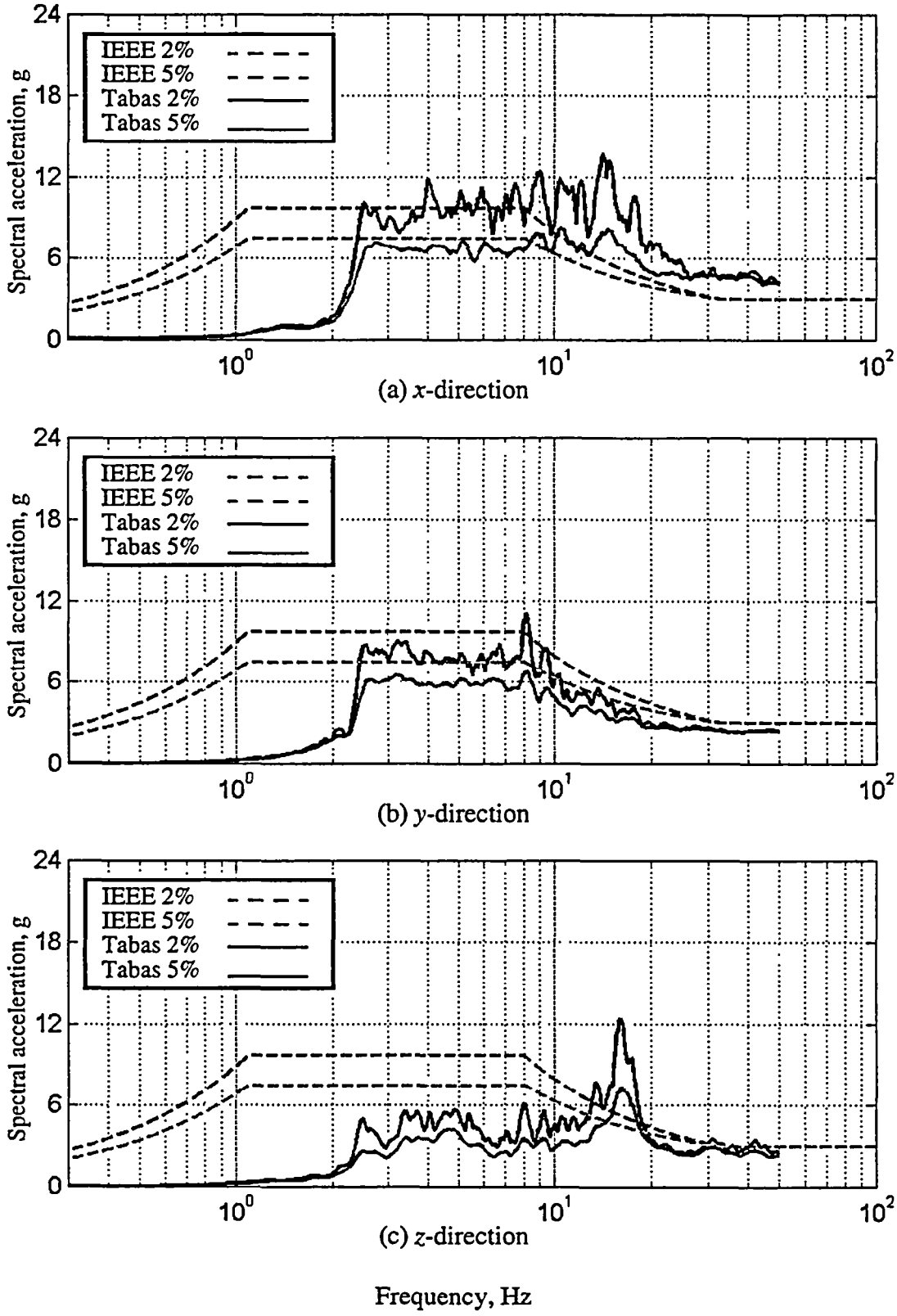

Figure 7-27 Response spectrum for Bushing-2 retrofitted with Ring-2; Test No 24, Tabas-B, target PGA=3.0g

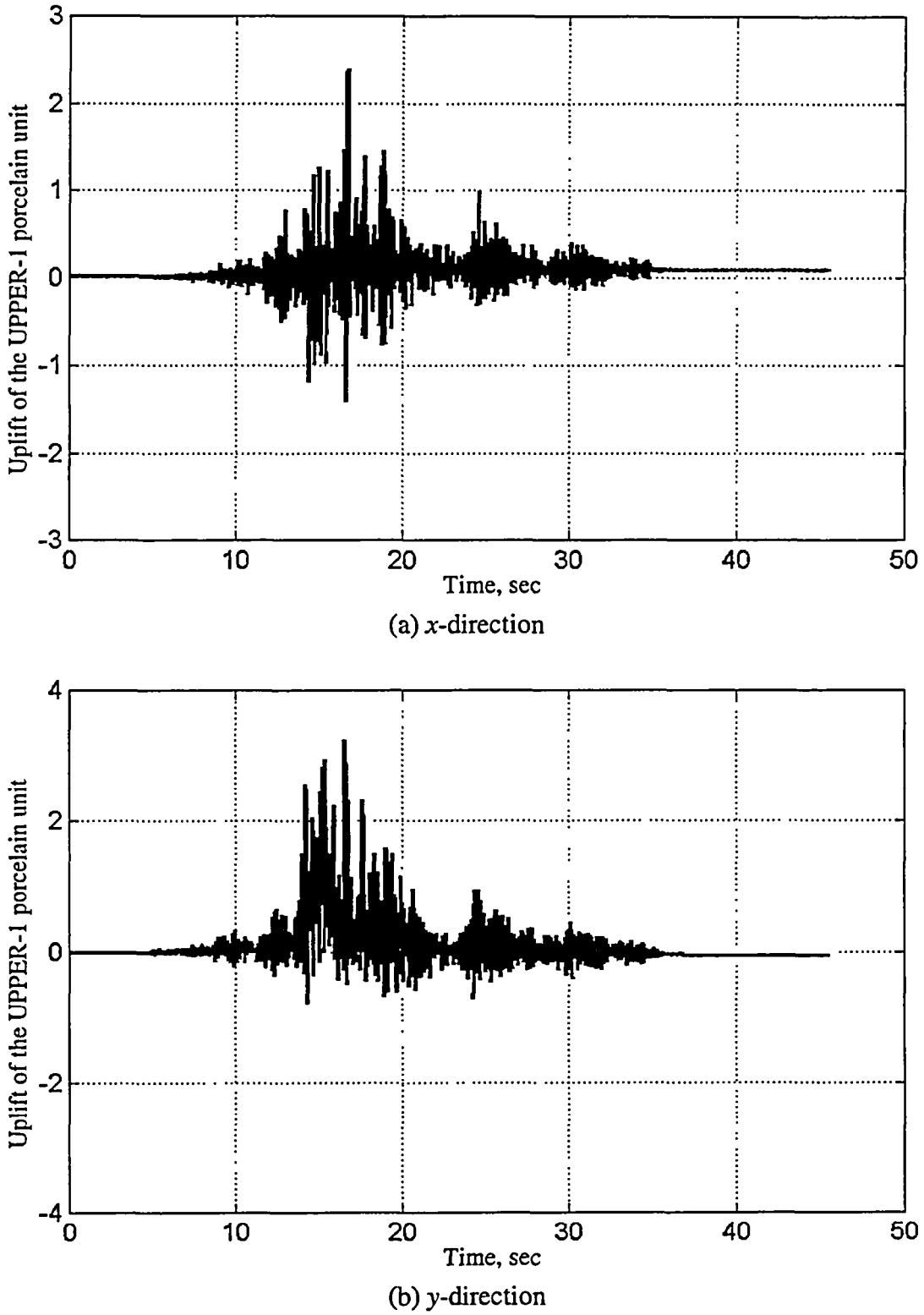

Figure 7-28 Components of vertical motion for Bushing-2 retrofitted with Ring-2; Test No 24, Tabas-B, target PGA=3.0g

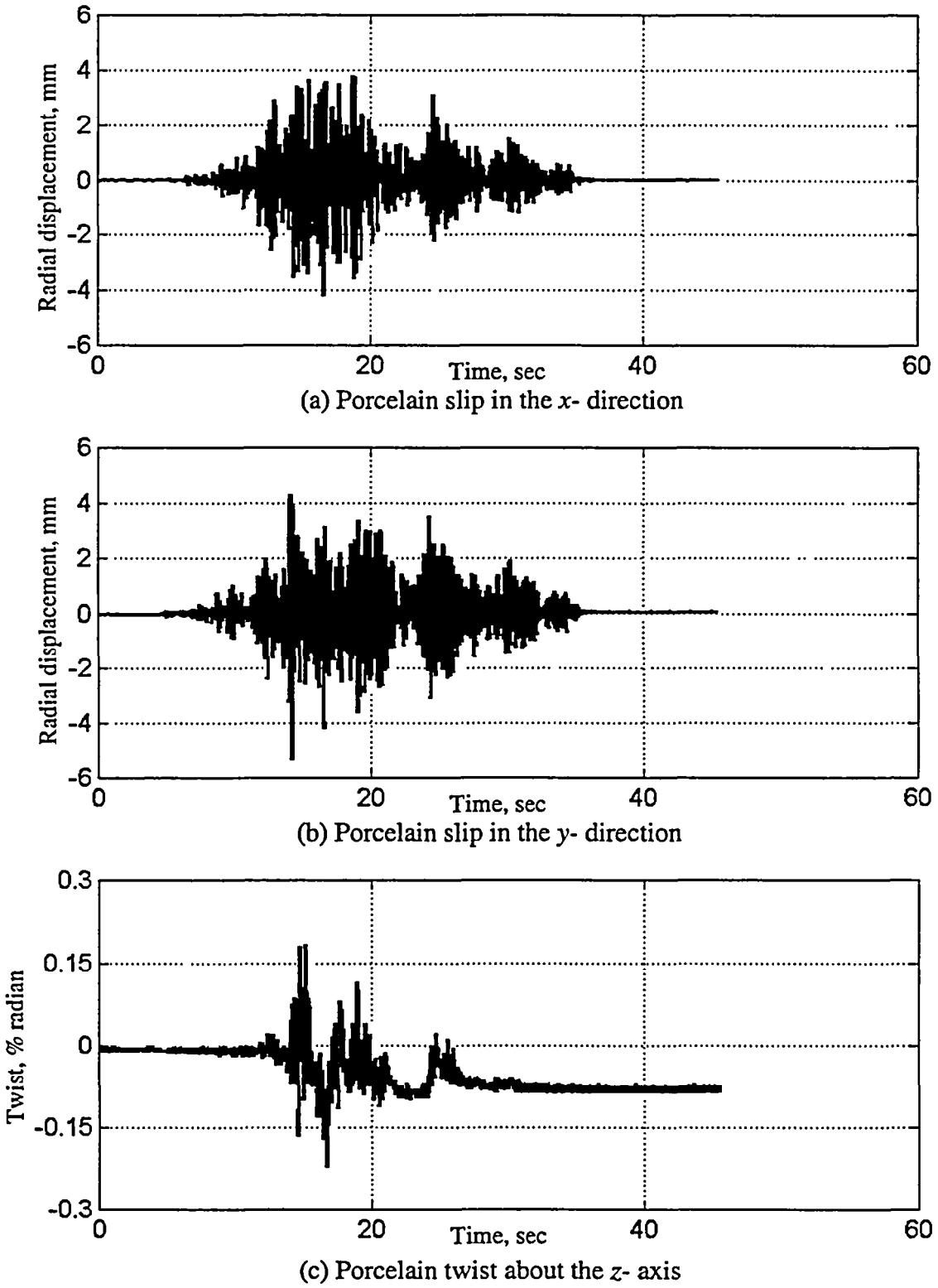

Figure 7-29 Components of horizontal motion for Bushing-2 retrofitted with Ring-2; Test No 24, Tabas-B, target PGA=3.0g

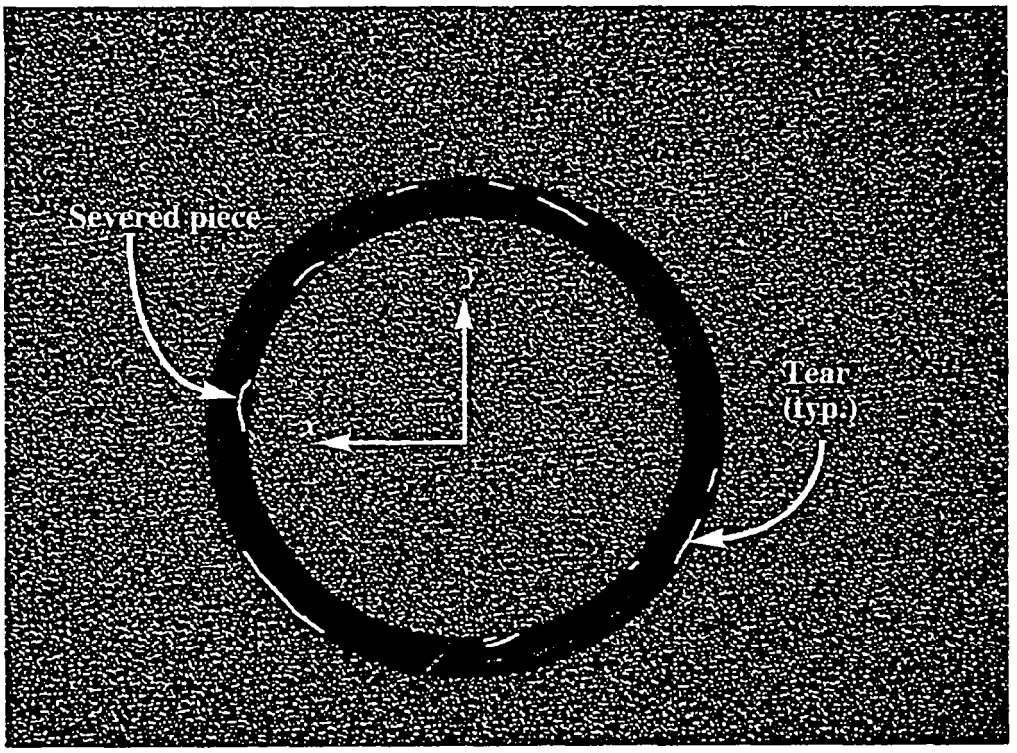

Figure 7-30 Post-test photograph of gasket locating tears and lacerations

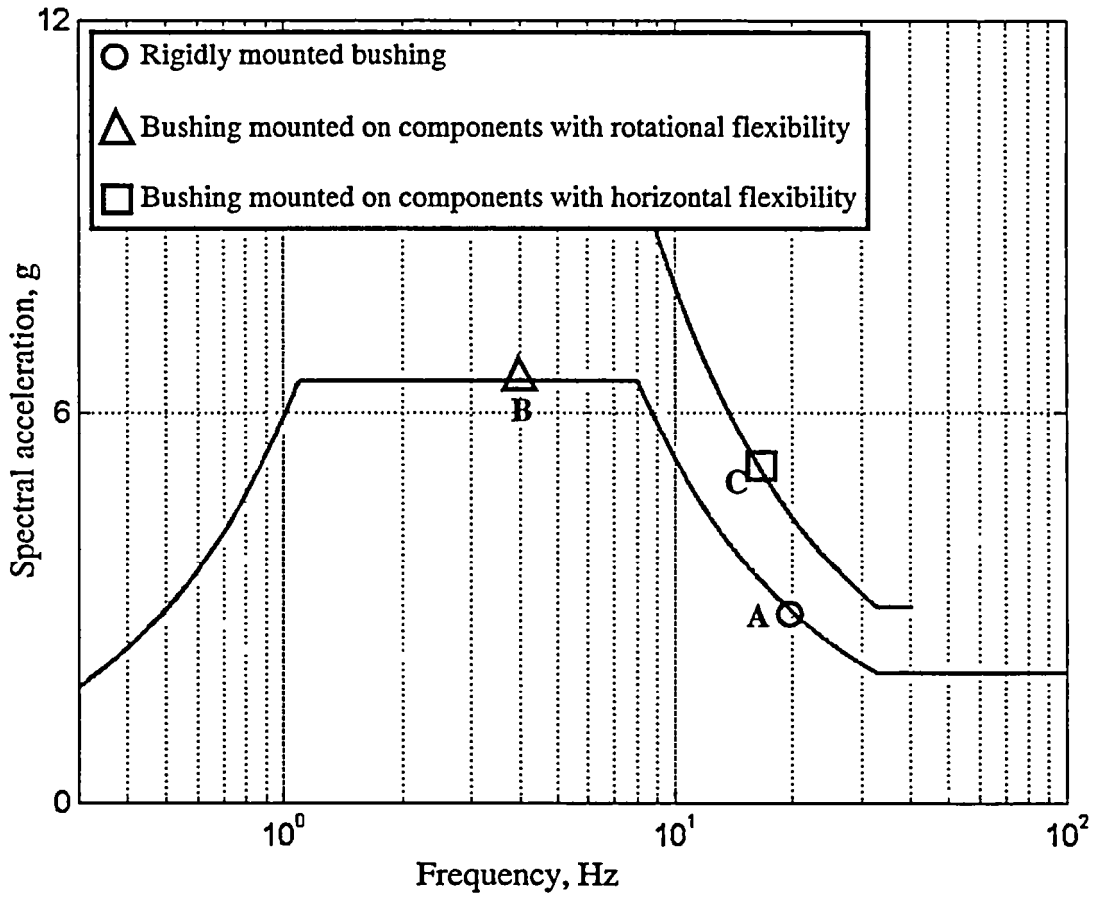

Figure 7-31 Effects of support flexibility on the spectral acceleration response of a bushing

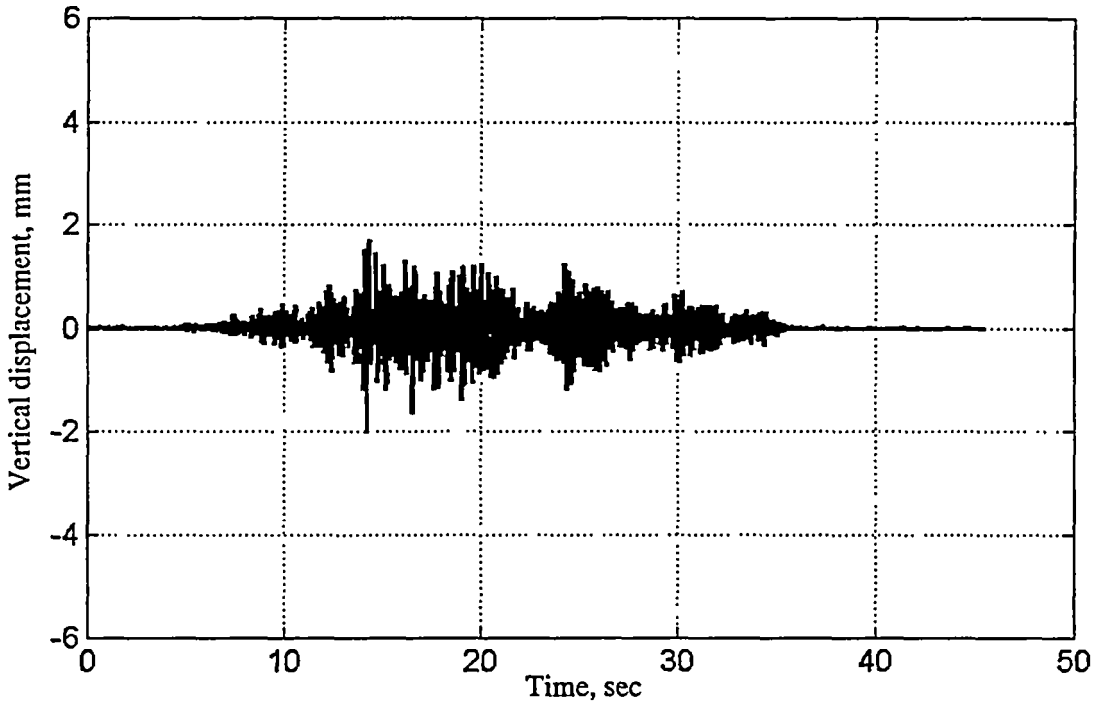

(a) At mid-circle of *flexible* plate (channel 60)

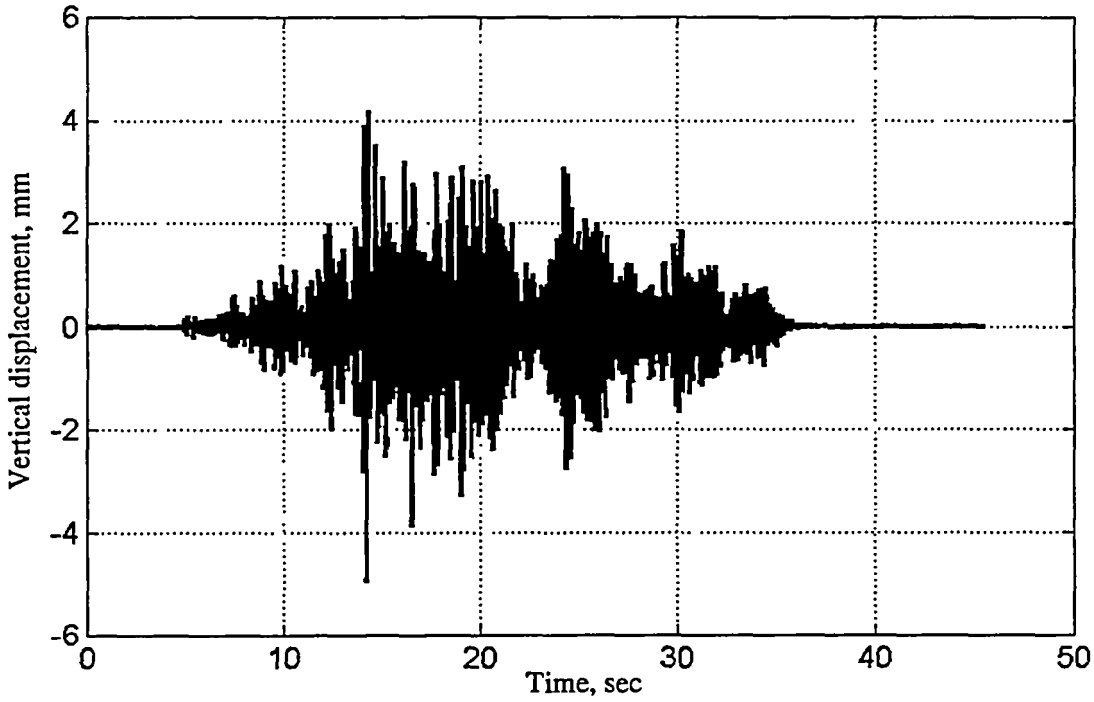

(b) At the bushing flange (channel 61)

Figure 7-32 Displacement response of flexible plate in *z*- direction; Test No 24, Tabas-B, target PGA=3.0g

8 Summary and Conclusions

8.1 Summary

8.1.1 Overview

The reliability and functionality of electrical transmission and distribution (T&D) systems after an earthquake depend on the seismic response of individual substation components. Porcelain transformer bushings (insulated conductors used to provide electrical connection between a high-voltage line) are a key component of power transmission and distribution (T&D) systems. Bushings are typically mounted on the top of an oil-filled transformer or on a turret attached to the transformer. High-voltage bushings (bushings rated at 196 kV and higher) have sustained major damage during recent severe ground shaking. For these bushings, because of their size and mass, earthquake motions can generate large shear forces and bending moments at the gasket connection (interface between the flange and porcelain), which can lead to failure. Four major failure modes have been documented: oil leakage, porcelain slip, gasket extrusion, and porcelain fracture.

Since transformer bushings form an integral part of power T&D systems, their structural and electrical integrity are critical to maintaining power transmission. To mitigate the vulnerability of new bushings and other electrical substation equipment, representatives from electrical utilities and equipment manufacturers in North America, consulting engineers, and members of the academic community jointly developed a new national standard, IEEE 693-1997. Both IEEE 693-1997 and IEC 61463 (a code similar to IEEE 693-1997 that is used in Europe) state that new equipment rated for high voltage (typically 161 kV and higher) must be qualified by triaxial earthquake simulator testing. These requirements are expected to improve the seismic capability of new equipment. However, electrical utilities will continue to maintain substantial inventories of the older equipment that were procured to specifications less stringent than current seismic standards.

The investigation reported in this document was sponsored by the California Electric Commission and a consortium of utilities (Pacific Gas & Electric Company, Bonneville Power Administration, Southern California Edison, and British Columbia Hydro) for the purpose of characterizing the response of older bushings and developing retrofit details to improve the seismic performance of such equipment. The key objectives of the project were: (a) identify vulnerable bushings, (b) develop a testing program that incorporated both dynamic and static testing, and both flexible and rigid support frames, (c) develop the appropriate earthquake ground motion records suitable for

the seismic evaluation and fragility testing, (d) develop a practical and cost-effective retrofit detail, and (e) draw conclusions regarding the seismic performance of the vulnerable porcelain transformer bushings, the influence of support condition on the bushing response, and the efficacy of the retrofit detail.

8.1.2 Test bushings

Two criteria were used to select the candidate bushing. First, the bushing had to be widely used in practice, and second, there had to be tangible evidence that the candidate bushing had sustained earthquake-induced damage. A survey of electrical substations by the utilities indicated that 230-kV type-U bushings manufactured by General Electric (GE) Company are widely used in electrical substations and have been damaged in past earthquakes.

Two identical 230-kV, 3,000-A, type-U transformer bushings manufactured in the mid-1980s by GE were used for testing and evaluation. The two bushings were identified by serial numbers 1795450 and 1795451 and were designated Bushing-1 and Bushing-2, respectively. The overall length of the transformer bushing was 144.5 in. (3.7 m). The segment of the bushing above the cast aluminum flange was 85 in. (2.2 m) long and included two porcelain insulator units or stacks (UPPER-1 and UPPER-2), and a metallic dome at the top of the bushing (above porcelain unit UPPER-2). The porcelain units, the cast aluminum flange, and the metallic dome were separated by nitrile-rubber gaskets. The gasket between the flange and porcelain unit UPPER-1 was a flat annular strip of rubber. The segment of the bushing below the flange included an extension of the cast aluminum flange, one porcelain insulator, and a cast aluminum lower support. Flat annular gaskets separate these components. The flange plate, which was used to connect the bushing to the transformer, was cast with two lifting lugs to facilitate movement and installation of the bushing.

In cross section, the bushing had an aluminum core that provided the electrical connection; a multilayered oil-impregnated kraft paper condenser wrapped around the core; an annular gap between the porcelain and condenser that was filled with oil to provide electrical insulation; and a porcelain insulator. The weight of the bushing was approximately 920 lbs (4.1 kN), and its center of mass was located approximately 18 in. (0.45 m) above the flange plate. The portion of the bushing extending from the top of flange to the top of the bushing, weighed approximately 560 lbs (2.5 kN), with its center of mass located 44 in. (1.1 m) above the flange plate. The bushing was post-tensioned along its longitudinal axis through its core. The main physical and electrical characteristics of the bushings are summarize in Table 8-1.

8.1.3 Experimental program

8.1.3.1 Introduction

The seismic characterization and fragility testing of the test bushings consisted of three parts: (1) fragility testing of two *rigidly* mounted bushings; (2) static testing of Bushing-1 (with and without retrofit detail); and (3) fragility testing of *flexibly* mounted Bushing-2, (with and without retrofit detail). The earthquake testing was performed on the earthquake simulator at the PEER Center, which is headquartered at the University of California at Berkeley. The 20 ft by 20 ft (6.1 by 6.1 m) simulator can accommodate models up to 140 kips (623 kN) in weight and 40 ft (12.2 m) in height.

Table 8-1 Characteristics of the 230-kV type-U bushings manufactured by GE

Property	*Parameter*	*Value*
Electrical properties	Voltage rating	230 kV
	Amperage	3,000 A
	BIL[1]	900 kV
Physical properties	Weight	4.1 kN
	Total length	3.7 m
	Initial PT force	98 kN
Component material	insulator	porcelain
	bushing oil	mineral oil
	condenser	kraft paper
	core	aluminum
	gasket	nitrile rubber
Identification plate	Model No.	11B802BB G10
	Serial No.: Bushing-1; Bushing-2	1795450; 1795451

1. Basic Impulse level (BIL) designates the impulse voltage the bushing can withstand.

8.1.3.2 Mounting frames

A stiff frame previously used for the qualification and fragility testing of 196-kV and 550-kV bushings was re-used for the earthquake testing of the *rigidly* mounted bushings. For earthquake testing of the *flexibly* mounted bushings, a *flexible* plate was attached to the top of the stiff frame. The mounting plates for both setups were sloped at 20 degrees measured to the vertical; since a bushing qualified at this angle is deemed by IEEE 693-1997 to be qualified for all angles between vertical and 20 degrees measured to the vertical.

8.1.3.3 Test program

The testing program consisted of three components: (1) resonant-search tests, (2) static tests, and (3) triaxial earthquake tests. The resonant-search (white-noise, sine-sweep, pull-back and free-vibration) tests were conducted to determine the dynamic properties of the bushings. Static tests (unidirectional, unidirectional with offset, and bidirectional) were conducted to characterize the response of Bushing-1 and to evaluate the effectiveness of the first retrofit detail (Ring-1). Triaxial earthquake tests were used to evaluate the response of the bushings, to examine the effect of support flexibility, and to evaluate the efficacy of the second retrofit detail (Ring-2).

8.1.3.4 Development of ground motions for triaxial earthquake testing

Recorded earthquake ground motion histories were used to evaluate the seismic response of the two 230-kV transformer bushings. The earthquake histories used for the fragility testing of the 230-kV bushings were developed using the three-component set of near-fault earthquake motions recorded during the 1978 Tabas earthquake. The power spectrum for each history has moderate bandwidth. To obtain IEEE 693-1997 spectrum-compatible normalized histories, a three-step process was utilized combining time-domain spectrum-matching algorithm and frequency-domain high-pass filtering. First, the original earthquake history was high-pass filtered to remove low-frequency content such that the maximum displacement and velocity of the filtered history were approximately equal to 5 in. (127 mm) and 25 in./sec (635 mm/sec), respectively. The cut-off frequencies (1 to 2.2 Hz) were much smaller than the resonant frequency of the 230-kV bushings (known to range between 16 to 20 Hz for *rigidly* mounted bushings and between 6 to 8 Hz for *flexibly* mounted bushings). Removal of such low-frequency components from the input signals to the simulator was known to have a negligible impact on the dynamic response of the bushings. Second, the filtered earthquake histories from step one were matched to the target spectrum for frequencies greater than the corner frequency of the trapezoidal filter using the Abrahamson (Abrahamson, 1996) algorithm. Third, the spectrum-compatible motions from step two were high-pass filtered to exactly limit the maximum displacement and velocity to 5 in. (127 mm) and 25 in./sec (635 mm/sec), respectively.

8.1.4 Retrofit details

A cost-effective external retrofit detail for the gasket connection of 230-kV bushings was developed by Dr. Schiff and utility representatives. The retrofit detail consisted of two semicircular rings clamped around the gasket connection. A two-compound filler material was used to grout the space between the detail and the bushing. Two retrofit rings were developed for the purpose of testing and evaluation. Ring-1 was placed around the gasket connection of Bushing-1. During the static tests, Ring-1 was not effective in improving the response of Bushing-1. A modified version of Ring-1 was developed for further evaluation. Ring-2 was similar to Ring-1 with the addition of steel tabs; these tabs were bolted to the ring and clipped under the bushing flange to delay uplift and rotation of the ring.

8.1.5 Summary of experimental results

8.1.5.1 Introduction

The following sections present a summary of experimental results and findings from the resonant-search tests, seismic testing of two *rigidly* mounted bushings, static tests of Bushing-1 (without and with Ring-1), and seismic tests of *flexibly* mounted Bushing-2 (without and with Ring-2).

8.1.5.2 Experimental results from resonant-search tests

Experimental data from resonant-search tests were used to calculate the dynamic properties of the bushings and to evaluate the effects of the bushing post-tensioning force, the flexibility of the mounting frame, and the addition of terminal mass at the top of the bushing on the dynamic properties of the bushings.

The vibration frequency of the *rigidly* mounted bushings in the x- and y-directions (measured at the top of bushings) were 20 Hz and 18 Hz, respectively. The lateral stiffness and damping ratios of bushing were approximately 6 kips/in. (0.9 kN/mm) and between 2 to 3 percent of critical, respectively. The fundamental frequency and the lateral stiffness of the bushing were slightly larger in the x- direction due to the presence of the lifting lugs on the bushing flange. The effective weight of the bushing (at the top) of 140 lbs (0.6 kN) was computed assuming that the bushing was a single-degree-of-freedom system with a lumped mass at its top. This weight was only 25 percent of the weight of the segment of the bushing between the flange and the top. The frequency and damping ratio in the x-direction of the bushing (measured at the bottom) were 52 Hz and 3 percent of critical, respectively.

The modal properties of the bushing where unchanged when the bushing preload was reduced from 27 kips (120 kN) to 20 kips (89 kN), when the gasket at the gasket connection was lubricated (coated with oil), or when the retrofit ring was added to the gasket connection. The attachment of the terminal (to simulate equipment interconnection jumper weight) at the top of the bushing reduced the frequency of the bushing significantly, (from 20 Hz to 14 Hz) and introduced a second vibration mode to the response. When the bushing was mounted on a *flexible* plate, the frequency of the bushing-support system was approximately 7.5 Hz. When a 1/4-in. (6-mm) thick gasket was placed between the bushing flange and the mounting plate, the frequency of the bushing-support system dropped to 6.5 Hz. The measured dynamic properties of the 230-kV bushings in the different test configurations are presented in Table 8-2.

8.1.5.3 Experimental results from rigidly mounted bushings

Seismic testing of *rigidly* mounted Bushing-1 and Bushing-2 included fragility testing of the bushings up to a test with the spectrum equal to the IEEE 693-1997 spectrum for High Level qualification (Tabas-B, target PGA equal to 2.0g). At the request of the utilities, Bushing-2 was also subjected to a 5-Hz constant amplitude unidirectional motion along the x-axis.

At the level of shaking consistent with Moderate Level qualification (target PGA equal to 1.0g), the maximum acceleration and displacement relative to the mounting frame (recorded at the top of the bushing) were approximately 4g and 0.17 in. (4 mm), respectively.

Table 8-2 Modal properties of 230 kV bushings[1]

			Stiffness (kN/mm)		*Frequency (Hz)*		*Damping Ratio (% critical)*	
Mounting Frame[2]	*Top Terminal Attached*[3]	*Mounting Gasket Attached*[4]	*x-dir*	*y-dir*	*x-dir*	*y-dir*	*x-dir*	*y-dir*
Rigid	No	No	0.9	0.9	20	18	3	2
Rigid	Yes	No	0.9	-	14	13	3	3
Rigid	No	Yes	0.8	-	18	-	3	-
Rigid	Yes	Yes	0.8	-	13	-	4	-
Flexible	No	No	0.2	0.2	7.5	7.5	2	2
Flexible	Yes	No	0.2	-	6.5	-	3	-
Flexible	No	Yes	0.1	0.1	6.5	6.5	4	4
Flexible	Yes	Yes	0.1	-	5.5	-	5	-

1. Data reported only for the top of the bushing.
2. Rigid mounting frame is shown in Figure 4.1; flexible mounting plate is shown in Figure 7.1.
3. Terminal, shown in Figure 4.6, weighs 280 N; the threaded attachment weighs 50 N.
4. Mounting gasket: 6-mm thick annular rubber.

At the level of shaking consistent with High Level qualification (target PGA equal to 2.0g), the maximum acceleration and displacement relative to the mounting frame (recorded at the top of the bushing) were approximately 6g and 0.4 in. (10 mm), respectively. In the range of the bushing frequency (18 to 20 Hz), the 2-percent and 5-percent damped acceleration response spectra for the bushings generated using measured acceleration histories at the flange plate exceeded the IEEE 693-1997 acceleration ordinates for High Level qualification: There was no oil leakage or evidence of structural damage, and porcelain stresses were well below the ultimate value.

Although neither Bushing-1 nor Bushing-2 were originally designated for qualification, given that the measured spectral amplitudes in the range of the measured bushing frequency exceeded the IEEE 693 1997 high-level spectrum, there was no oil leakage, and the measured porcelain stresses were less than the ultimate stress, Bushing-1 and Bushing-2 *were qualified by test to the high-level.*

Bushing-2 was subjected to a constant-amplitude, single-frequency harmonic motion with an input frequency equal to 5 Hz. During this tests, oil leaked from the gasket connection and the UPPER-1 porcelain unit slipped over the flange. Examination of the simulator input data showed that due to the dynamics of the earthquake simulator, harmonics of the input motion at 15, 20, and

25 Hz were present in the translational and rotational simulator accelerations. Examination of the response spectrum for the input signal showed that because of these higher harmonics, the bushing was subjected to spectral accelerations which significantly exceeded those of the IEEE 693-1997 spectrum for High Level qualification.

8.1.5.4 Experimental results from static tests of Bushing-1

Static testing of Bushing-1 mounted on a stiff frame included cyclic testing of Bushing-1 without Ring-1 and cyclic and monotonic testing of Bushing-1 with Ring-1.

During the unidirectional tests (Test Set 1) of Bushing-1 without Ring-1, during the cycles to a target displacement of 0.35 in. (8.75 mm) and 0.4 in. (10 mm), the bushing leaked oil and the UPPER-1 porcelain unit slipped over the gasket connection. When the gasket at the gasket connection was lubricated (Test Set 5), the bushing leaked oil at the gasket connection during displacement cycles to 0.3 in. (7.5 mm). When the post-tensioning force was reduced from 27 kips (120 kN) to 20 kips (90 kN), the bushing leaked oil during the cycles to a target displacement of 0.3 in. (7.5 mm). During the bidirectional tests (Test Set 4), the bushing leaked oil during displacement cycles to 0.3 in. (7.5 mm).

During the unidirectional tests (Test Set 12) of Bushing-1 with Ring-1, the bushing leaked oil and the UPPER-1 porcelain unit slipped over the gasket connection during the cycles to a target displacement of 0.4 in. (10 mm) and 0.45 in. (11.25 mm). During the cycles to a target displacement of 0.5 (12.5 mm), Ring-1 rotated with respect to the longitudinal axis of the bushing. During the bidirectional tests (Test Set 13), the bushing leaked oil, Ring-1 rotated, and the UPPER-1 porcelain unit twisted above the flange during the cycles to a target displacement of 0.45 in. (11.25 mm).

During the monotonic test (Test Set 14), the bushing leaked oil at the gasket connection at a displacement of approximately 0.4 in. (10 mm). When the actuator displacement exceeded approximately 1.5 in. (38 mm), the oil leak became continuous. At a displacement of approximately 5.5 in. (140 mm), the cast aluminum flange fractured. At a displacement of approximately 6 in. (152 mm), the displacement limit of the actuator was reached. As the actuator was retracted, the rotated Ring-1 made contact with and fractured the bottom shed of the UPPER-1 porcelain unit.

8.1.5.5 Experimental results from flexibly mounted Bushing-2

Seismic fragility testing of the *flexibly* mounted Bushing-2 included fragility testing of Bushing-2 without Ring-2 up to a test with the spectrum equivalent to the IEEE 693-1997 spectrum for the High Level qualification (Tabas-B, target PGA equal to 2.0g), and fragility testing of Bushing-2 with Ring-2 up to a test with the spectrum equivalent to the 150 percent of IEEE 693-1997 spectrum for High Level qualification (Tabas-B, target PGA equal to 3.0g). At the request of the utilities, Bushing-2 was also subjected to a single test using a three-component input motion developed at CERL with spectrum equivalent to the IEEE 693-1997 spectrum for Moderate Level qualification (CERL, target PGA equal to 1.0g).

At a level of shaking consistent with the moderate-level qualification test per IEEE 693-1997 (target PGA equal to 1.0g), the maximum acceleration and displacement relative to the mounting frame (recorded at the top of the bushing) of Bushing-2 without Ring-2 were approximately 3g and 0.7 in. (17 mm), respectively. During the tests with target PGAs equal to 1.4g and 1.6g, the bushing leaked oil. During the tests with target PGAs equal to 1.8g and 2.0g, the bushing leaked oil from the gasket connection, the UPPER-1 porcelain unit slipped over the gasket connection, and the gasket extruded from the gasket connection. At the conclusion of the testing, the bushing was de-stressed and partially disassembled. The value of post-tensioning load was measured at 9 kips (40 kN) — approximately one third of the original value. Examination of the gasket at the gasket connection revealed that the gasket had several shallow tears.

At a level of shaking consistent with the IEEE 693-1997 Moderate Level qualification spectrum (target PGA equal to 1.0g), the maximum acceleration and displacement relative to the mounting frame (recorded at the top of the bushing) of Bushing-2 with Ring-2 were approximately 3.4g and 0.8 in. (21 mm), respectively. At a level of shaking consistent with the IEEE 693-1997 High Level qualification spectrum (target PGA equal to 1.0g), the maximum acceleration and displacement relative to the mounting frame (recorded at the top of the bushing) of Bushing-2 with Ring-2 were 6.4g and 1.8 in. (45 mm), respectively. During the tests with target PGAs equal to 2.6g and 2.8g, oil leaked from around Ring-2. During the test with a target PGA of 3.0g, the bushing leaked oil and the UPPER-1 porcelain unit uplifted over the gasket connection. At the conclusion of the testing, Ring-2 was removed. A small segment of the gasket had extruded from the gasket connection. The bushing was de-stressed and disassembled. The value of the post-tensioning load was measured at 22 kips (98 kN). Examination of the gasket at the gasket connection revealed that the gasket had additional tears and a small portion of the gasket had severed.

Table 8-3 presents selected peak response values gasket connection for Bushing-2 with and without Ring-2.

Table 8-3 Response of flexibly mounted Bushing-2 at the gasket connection

Ring-2 Installed	*Target PGA (g)*	*Maximum Slip (mm)*	*Maximum Uplift (mm)*	*Comments*
No	1.2	2	0.8	
	1.4	4	1	First test with oil leakage.
	2.0	9	2	Spectrum equivalent to high-level qualification.
Yes	1.2	2	0.8	No *visible* oil leakage or porcelain slip[1].
	1.4	3	1	
	2.0	4	2	

1. Presence of Ring-2 made visual identification of small slip and uplift impossible.

8.2 Conclusions

8.2.1 Seismic response of 230-kV transformer bushings

Two 230-kV transformer bushings were undamaged by severe earthquake shaking when mounted on a *rigid* frame. Bushing-1 and Bushing-2 passed the IEEE 693-1997 requirements for High Level qualification. Both bushings were subjected to six earthquake simulations with input accelerations exceeding 1.0g and suffered no visible damage. When mounted on a *flexible* support, Bushing-2 passed the IEEE 693-197 requirements for Moderate Level qualification.

Bushing-1 was subjected to a series of static tests using four displacement orbits. Oil leakage and slip of the UPPER-1 porcelain unit was only observed when the imposed actuator loads exceeded 1.5 kips (6.7 kN)—approximately three times the weight of the portion of the bushing above the flange.

Field reconnaissance and observations from past earthquakes suggest that failures (oil leakage and slip of porcelain units) of similar bushings occurred at levels of ground shaking significantly lower than those to which the two bushings were subjected. The reason for this discrepancy in performance is somewhat unclear. However, it is likely that the IEEE procedures do not adequately capture the critical loading environment for bushings because the electrical equipment attached at the top of the bushing in the field (termed interconnected equipment elsewhere in this report) are not included in the qualification and fragility testing.

8.2.2 Effect of support flexibility

For bushings mounted on transformers, the flexibilities of the turret and top plate of the transformer have two effects on the *horizontal* response of the bushing-transformer system. First, the *rotational* flexibility of turrets or transformer-tank tops will reduce the frequency of the bushing-transformer system and generally result in larger spectral accelerations. Second, the *horizontal* flexibility of turrets or transformer-tank tops can amplify the shaking effects at the bushing flange plate with respect to the ground. Only the first effect was simulated in the studies reported herein. A two-fold increase in maximum bushing acceleration was observed for similar ground-motion inputs when the bushing was installed on a mounting plate with rotational flexibility.

8.2.3 Effect of post-tensioning force

Previous analytical studies (Gilani et al., 1998) have indicated that the dynamic properties of a bushing are highly dependent upon the axial stiffness of the rubber gasket that is routinely placed immediately above the bushing flange plate. The gasket in the bushings tested in this study was placed in an annular groove or pocket that rendered it substantially incompressible. Changes in the bushing post-tensioning force therefore had little effect on the dynamic properties of the bushing. However, reductions in the post-tensioning force from the value typically used by the manufacturer did reduce the uplift displacement at which the oil leaked from the gasket connection.

8.2.4 Efficacy of retrofit design

The two retrofit details (Ring-1 and Ring-2) described in this report were detailed primarily to limit the slip of the UPPER-1 porcelain unit over the bushing flange. Both details utilized semicircular rings and epoxy filler material. Neither ring was engineered and the test results cannot be extrapolated to other bushings. Ring-1 was not effective. Ring-2, similar in design to Ring-1 but with steel tabs to attach the ring to the bushing flange, was effective in reducing the slip of the UPPER-1 porcelain unit and preventing oil leakage for earthquake inputs with PGAs less than 2.6g.

8.3 Recommendations for future study

8.3.1 Procedures for seismic qualification and fragility testing

The 230-kV bushings were installed in a *rigid* and a *flexible* mounting frame without electrical connections for earthquake testing. It was noted that when the bushing was mounted on the *flexible* plate, the fundamental frequency of the bushing-support system was reduced, however, the horizontal accelerations were not amplified. For qualification of equipment attached to a foundation, IEEE 693-1997 specifies a response spectrum for earthquake-simulator testing. The amplitude of the input motion for qualification of bushings is doubled to account for flexibility and ground-motion amplification in the transformer or support equipment. It is not known whether the IEEE 693 assumptions are reasonable, conservative, or non-conservative. Numerical (finite element) studies of transformer bushings and other turret structures should be undertaken to review the current specifications for equipment qualification. At a minimum, such studies should identify: (a) the stiffness characteristics of typical bushing support structures, (b) stiffness and damping properties of the mounting gasket(s) used to connect the bushing to the turret and to the transformer top plate, (c) the damping effects of the oil contained in the support structure, if any, (d) the amplification of earthquake shaking effects, if any, through the support structure to the base of a bushing, and (d) the importance of rotational input to a bushing resulting from flexibility in the upper plate of the transformer to which bushings are attached. Answers to these questions will provide valuable guidance to those tasked with revising the IEEE 693-1997 *Recommended Practices for Seismic Design of Substations.*

8.3.2 Development of fragility curves for substation equipment

Currently adopted procedures for reporting fragility data for substation equipment such as transformer bushings are neither appropriate nor conservative. Fragility data presented in the form of peak ground (input) acceleration are of limited value because peak input acceleration is a poor descriptor of damage. Fragility data based on spectral acceleration at the frequency of the bushing provides an improved estimate of damage but cannot account for substructure flexibility and damping, both of which will profoundly affect bushing response. Mean spectral acceleration over a range of frequencies provides a means by which to account for substructure flexibility. Mean-minus-one-standard-deviation spectral acceleration *fragility* data over a range of frequencies

could account for variations in spectral acceleration over a frequency range. Improved, rational procedures are needed to analyze and interpret fragility test data. Such procedures must both better reflect the field installation of equipment and account for substructure flexibility, installation of terminals (for bushings), and the effects of interconnected equipment.

8.3.3 Interconnected equipment

Although IEEE 693-1997 acknowledges that physical (electrical) connections between substation equipment may detrimentally affect the seismic response of individual pieces of equipment, the testing procedures described in IEEE 693-1997 do not adequately account for the effects of such connectivity. These physical connections can vary widely in flexibility and strength. There is substantial evidence from past earthquakes that such electrical connections may have precipitated bushing failures because of dynamic interaction between the interconnected equipment. The analytical and experimental studies completed so far have identified several important parameters affecting dynamic interaction between interconnected equipment. An experimental program should be pursued to investigate both the characteristics of standard interconnections and strategies to mitigate the effects of dynamic interaction.

8.3.4 Behavioral studies of porcelain transformer bushings

Future experimental work will be useful to attain a better understanding of the properties of the components of the bushings. In particular, tests of the nitrile rubber gaskets will provide valuable information regarding the stiffness properties of the gasket and the relation between the post-tensioning force, gasket stiffness, and the dynamic properties of bushings.

8.3.5 Mathematical modeling of porcelain transformer bushings

A three-dimensional finite element model of the bushing incorporating all the critical components is needed to gain a better understanding into the bushing response. The model need to incorporate nonlinear springs developed to simulate the nitrile rubber gaskets (detailed mechanical characteristics of the gaskets will be needed); variation in the post-tensioning force during the analysis; fluid elements to model the bushing oil and the constraint to relative lateral movement of the aluminum core and the perimeter porcelain units offered by the this oil; boundary conditions (support flexibility and mounting gaskets) of the bushing flange; and attachments at the bushing tip (terminals, cables, connections to other equipment). Accurate models of porcelain bushings that would be suitable for rigorous vulnerability (fragility and parametric) studies could be developed with such information.

References

Abrahamson, N. 1996. "Nonstationary response-spectrum matching." Unpublished paper.

Elder, L. 1999. *Personal communications*, ABB Power T&D Company, Inc., Components Division of Alamo, Tennessee.

Schiff, A. J., ed. 1997. *Guide to post-earthquake investigation of lifelines.* Technical Council on Lifeline Earthquake Engineering, Monograph No. 11. Reston, Va.: ASCE.

Bellorini, S., Bettinali, F., Salvetti, M., and Zafferani, G. 1997. *Seismic qualification of transformer high voltage bushings*, IEEE Transactions on Power Delivery.

Bellorini, S., Bettinali, F., Salvetti, M., Gatti, F., Zafferani, G., and Monzari, O. 1998. *Mechanical seismic behavior of power transformers.* IEEE Transactions on Power Delivery.

Villaverde, R., Pardoen, G., and Carnella, S. 1999. *Ground motion amplification at the base of bushings mounted on electronic substation transformers.* A technical report of research supported by PEER/PG&E. Irvine: Dept. of Civil Engineering, University of California.

Wilcoski, J., and Smith S. J. 1997. *Fragility testing of a power transformer bushing.* USACERL Technical Report 97/57. Champaign, Ill.: US Army Corps of Engineers Construction Engineering Research Laboratories.

IEEE. 1998. *IEEE Standard 693-1997, Recommended practices for seismic design of substations.* Piscataway, N.J.: IEEE Standards Department. [New York].

IEC. 1996. *Bushings, seismic qualification.* IEC technical report 61463-1996. Luglio, Italy: IEC.

Gilani, A. S., Whittaker, A. S., Fenves, G. L., and Fujisaki, E. 1999. *Seismic evaluation of 550 kV porcelain transformer bushings.* PEER 1999/05. Berkeley, Calif.: Pacific Earthquake Engineering Research Center, University of California.

Gilani, A. S., Chavez, J. W., Fenves, G. L., and Whittaker, A. S. 1998. *Seismic evaluation of 196 kV porcelain transformer bushings.* PEER 1998/02. Berkeley, Calif.: Pacific Earthquake Engineering Research Center, University of California.

Mathworks. 1999. *The language of technical computing.* Natick, Mass.: The Mathworks, Inc.

Computers and Structures, Inc., *SAP 2000 Integrated finite element analysis and design of structures*, Version 6.1. Berkeley, California, 1997.

Roberts, A. D., 1988. *Natural rubber science and technology.* Oxford science publications. New York: Oxford University Press.

Lindley, P. B. 1978. *Engineering design with natural rubber.* The Malaysian Rubber Producers' Research Association, Hertford Offset Ltd., U.K.

Lilhanand, K., and Tseng, W. S. 1988. "Development and application of realistic earthquake time histories compatible with multiple-damping design spectra." *Proceedings of Ninth World Conference on Earthquake Engineering, Tokyo, Japan.* [Tokyo]: 9WCEE Organizing Committee, Japan Association for Earthquake Disaster Prevention.

Clough R. W., and Penzien J. 1993. *Dynamics of structures.* New York: McGraw-Hill, Inc.

Appendix A IEEE Practice for Earthquake Testing of Transformer Bushings

A.1 Introduction

The document IEEE 693-1997 (IEEE 1998) entitled "Recommended Practices for Seismic Design of Substations" is used in the United States for the seismic qualification and fragility testing of electrical equipment such as transformer bushings. This document provides qualification requirements for substation equipment and supports manufactured from steel, aluminum, porcelain, and composites. Procedures for equipment qualification using analytical studies (static analysis, static coefficient analysis, and response-spectrum analysis) and experimental methods (response-history testing, sine-beat testing, and static pull testing) are described. The objective of the document is "... to secure equipment such that it performs acceptably under reasonably anticipated strong ground motion."

IEEE 693-1997 identifies eleven methods for experimental testing. The most rigorous method is earthquake-response analysis using earthquake ground motion records, the spectral ordinates of which equal or exceed those of a Required Response Spectrum (RRS). Categories of earthquake simulator testing include (a) single-axis, (b) biaxial (i.e., horizontal and vertical), (c) multiaxis, and (d) triaxial.

Section 9 of IEEE 693-1997 describes seismic performance criteria for electrical substation equipment. Information on three seismic qualification levels (Low, Moderate, and High), Performance Levels, the Required Response Spectrum (RRS), the relation between PL and RRS, and acceptance criteria are provided.

The studies described in the body of this report employed triaxial earthquake simulator testing for the qualification and fragility testing of 230-kV bushings. IEEE 693-1997 writes text on six key topics related to the seismic qualification of transformer bushings:

- Performance level and performance factor
- Performance level qualification
- Support frame and mounting configuration

- Testing procedures
- Instrumentation
- Acceptance criteria

Each of these topics are elaborated upon in the following sections. For fragility testing, the amplitude of the seismic excitation is increased in small increments to determine the level of shaking that causes damage to the bushing, thereby establishing a point on a fragility curve.

A.2 Performance Level and Performance Factor

A Performance Level (PL) for substation equipment is represented in IEEE 693-1997 by a response spectrum. The shape of this spectrum represents a broadband response that envelopes earthquake effects in different areas considering site conditions that range from soft soil to rock. Three values of equivalent viscous damping are specified: 2 percent, 5 percent, and 10 percent. IEEE 693-1997 states that very soft sites and hill sites might not be adequately covered by the PL shapes.

Three seismic performance levels are identified in IEEE 693-1997: High, Moderate, and Low. In California, the relevant performance levels are High and Moderate. Equipment that is shown to perform acceptably in ground shaking consistent with the High Seismic Performance Level (see Figure A-1) is said to be seismically qualified to the High Level. Equipment that is shown to perform acceptably in ground shaking consistent with the Moderate Seismic Performance Level (see Figure A-2) is said to be seismically qualified to the Moderate Level.

IEEE 693-1997 states that it is often impractical or not cost effective to test to the High or Moderate PL because (a) laboratory testing equipment might be unable to attain the necessary high accelerations, and/or (b) damage to ductile components at the PL, although acceptable in terms of component qualification, would result in the component being discarded following testing. For these reasons, equipment may be tested using accelerations that are one-half of the PL. The reduced level of shaking is called the Required Response Spectrum (RRS). The ratio of PL to RRS, termed the performance factor in IEEE 693-1997, is equal to 2. The High and Moderate RRSs are shown in Figures A-3 and A-4, respectively. The shapes of the RRS and the PL are identical, but the ordinates of the RRS are one-half of the PL.

Equipment tested or analyzed using the RRS is expected to have acceptable performance at the PL. This assumption is checked by measuring the stresses obtained from testing at the RRS, and a) comparing the stresses to 50 percent (equal to the inverse of the performance factor) of the ultimate strength of the porcelain (assumed to be brittle) or cast aluminum components, and b) using a lower factor of safety against yield combined with an allowance for ductility of steel and other ductile materials.

A.3 Performance Level Qualification

Procedures for selecting the appropriate seismic qualification level for a site are presented in IEEE 693-1997. Qualification levels are directly related to site-specific peak acceleration values

calculated using a 2-percent probability of exceedance in 50 years. If the peak ground acceleration is less than 0.1g, the site is classified as Low. If the peak ground acceleration exceeds 0.5g, the site is classified as High. If the peak ground acceleration ranges in value between 0.1g and 0.5g, the site is classified as Moderate. Sites in California are classified as either Moderate or High.

A.4 Support Frame and Mounting Configuration

IEEE 693-1997 writes that bushings 161 kV and larger must be qualified using earthquake-simulator testing. Recognizing that it is impractical to test bushings mounted on a transformer, IEEE requires bushings to be mounted on a rigid stand during testing. To account for the amplification of earthquake motion due to the influence of the transformer body and local flexibility of the transformer near the bushing mount, the input motion measured at the bushing flange shall match a spectrum with ordinates twice that of the Required Response Spectrum. The resulting spectra, termed the Test Response Spectra (TRS), for Moderate Level qualification are shown in Figure A-5.

A transformer bushing must be tested at no less than its in-service slope, which is defined as the slope angle measured from the vertical. IEEE 693-1997 recommends that a bushing be tested at 20 degrees measured from the vertical. If so tested, a bushing is assumed to be qualified for use on all transformers with angles from vertical to 20 degrees. (A bushing installed at an angle greater than 20 degrees must be tested at its in-service angle.)

A.5 Testing Procedures for Transformer Bushings

Three types of earthquake-simulator testing are identified in IEEE 693-1997 for the seismic qualification of transformer bushings: (a) earthquake ground motions, (b) resonant frequency search, and (c) sine-beat testing. Earthquake ground motion tests (termed *time-history shake table tests* in IEEE 693-1997) and resonant frequency tests are mandatory; additional information on these two types of tests follow.

A.5.1 Resonant search tests

Sine-sweep or broadband white noise tests are used to establish the dynamic characteristics (natural frequencies and damping ratios) of a bushing. These so-called *resonant search* tests are undertaken using uni-directional excitation along each principal axis of the earthquake simulator platform. If broadband white noise tests are performed, the amplitude of the white noise must not be less than 0.25g.

If sine-sweep tests are used, IEEE 693-1997 specifies that the resonant search be conducted at a rate not exceeding one octave per minute in the range for which the equipment has resonant frequencies, but at least at 1 Hz. Frequency searching above 33 Hz is not required. Modal damping is calculated using the half-power bandwidth method.

A.5.2 Earthquake ground motion tests

Triaxial earthquake simulator testing is mandated for the seismic qualification of bushings rated at or above 161 kV. The Test Response Spectrum (TRS) for each horizontal earthquake motion must

match or exceed the target spectrum. The TRS for the vertical earthquake motion shall be no less than 80 percent of target spectrum. Earthquake motions can be established using either synthetic or recorded histories. IEEE 693-1997 recommends that 2-percent damping be used for spectral matching and requires at least 20 seconds of strong motion shaking be present in each earthquake record.

A.6 Instrumentation of Transformer Bushings

IEEE 693-1997 states that porcelain bushings must be instrumented to record the following response quantities:

1. maximum vertical and horizontal accelerations at the top of the bushing, at the bushing flange, and at the top of the earthquake-simulator platform

2. maximum displacement of the top of the bushing relative to the flange

3. maximum porcelain stresses at the base of the bushing near the flange

A.7 Acceptance Criteria for Transformer Bushings

IEEE 693-1997 writes that a bushing is considered to have passed the qualification tests if all the criteria tabulated below related to general performance, allowable stresses, and leakage are met. The data obtained from testing using ground motions compatible with the Test Response Spectrum (see Figure A-5) are used to assess general performance and allowable stresses. Oil leakage is checked for a higher level of earthquake shaking.

General Performance:	No evidence of damage such as broken, shifted, or dislodged insulators. No visible leakage of oil or broken support flanges.
Allowable Stresses:	The stresses in components are below the limiting values. (See Section A.2. For example, the stresses in the porcelain components associated with earthquake shaking characterized by the spectrum presented in Figure A-5 must be less than 50 percent of the ultimate value.)
Leakage:	Bushings qualified by earthquake simulator testing shall have a minimum factor of safety of two against gasket leaks for loads imposed during application of the Test Response Spectrum. IEEE 693-1997 states that an acceptable method to demonstrate this factor of safety is to have no leaks after shaking characterized by twice the Test Response Spectrum. (Such shaking corresponds to a Performance Factor equal to 1.0.)

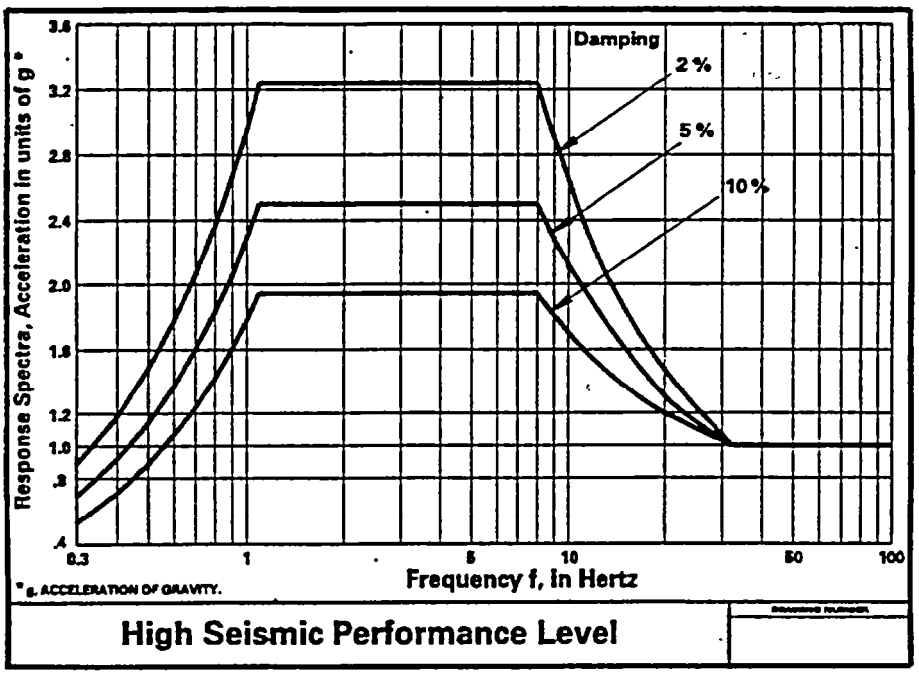

Figure A-1 Spectra for High Seismic Performance Level (IEEE, 1998)

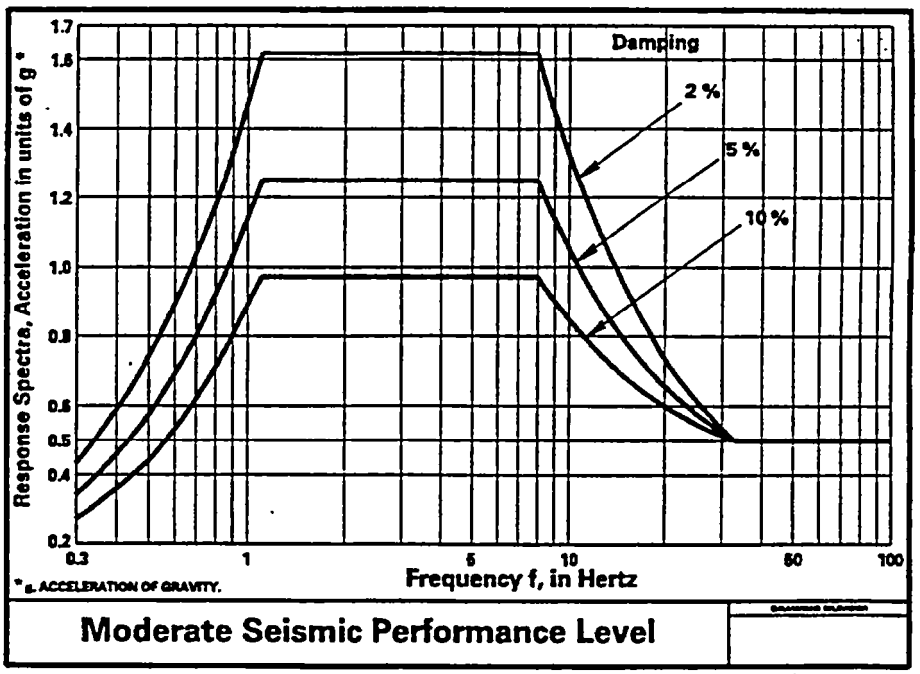

Figure A-2 Spectra for Moderate Seismic Performance Level (IEEE, 1998)

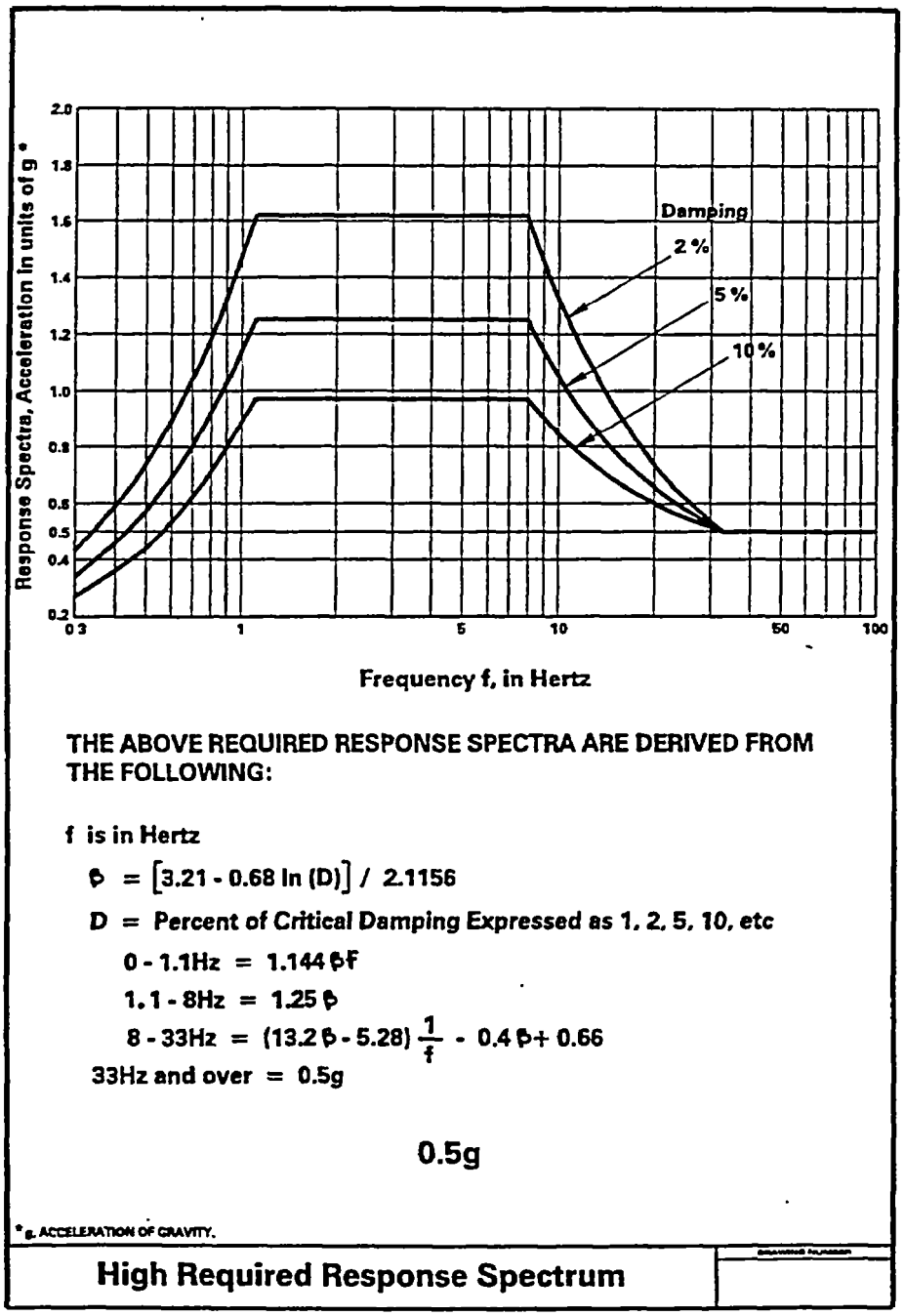

Figure A-3 Spectra for High Level Required Response Spectrum (IEEE, 1998)

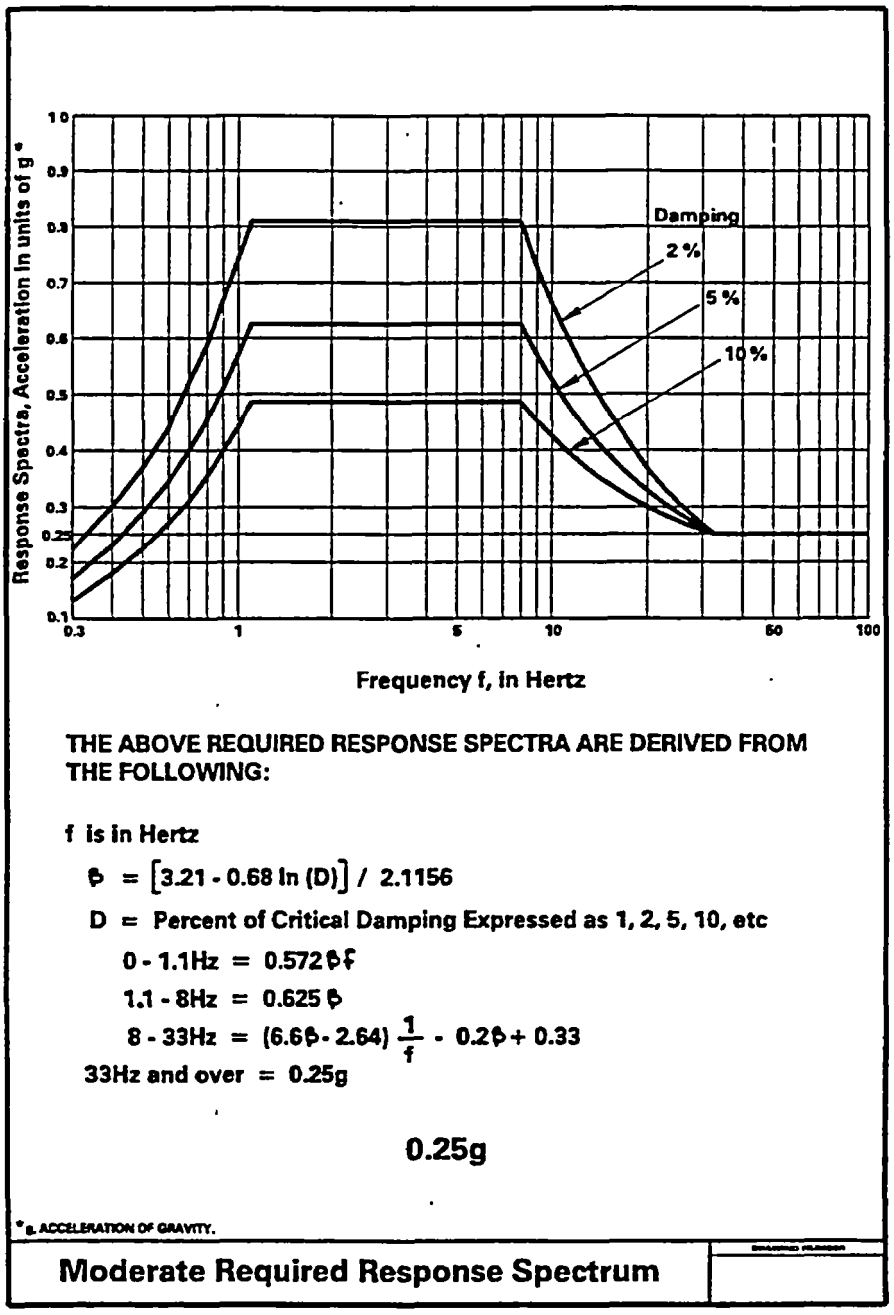

Figure A-4 Spectra for Moderate Level Required Response Spectrum (IEEE, 1998)

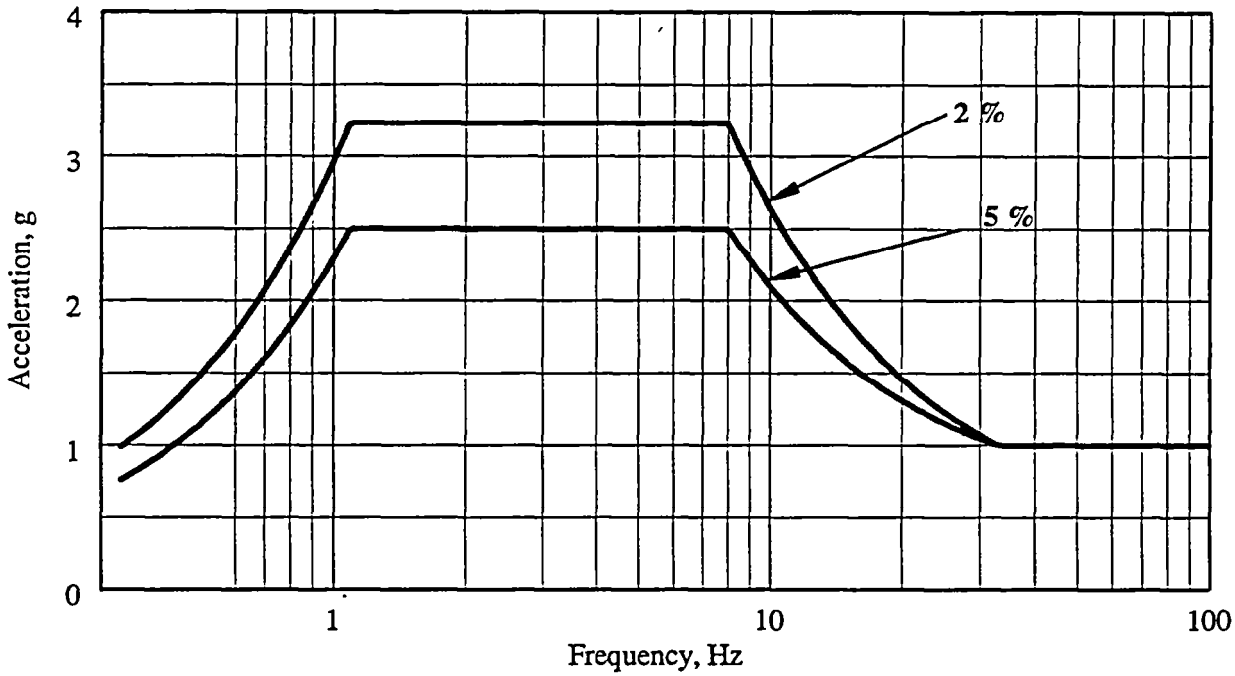

Figure A-5 Test Response Spectra for Moderate Level qualification of a transformer-mounted Bushing

PEER REPORTS

PEER reports are available from the National Information Service for Earthquake Engineering (NISEE). To order PEER reports, please contact the Pacific Earthquake Engineering Research Center, 1301 South 46th Street, Richmond, California 94804-4698. Tel.: (510) 231-9468; Fax: (510) 231-9461.

PEER 2000/01 *Further Studies on Seismic Interaction in Interconnected Electrical Substation Equipment.* Armen Der Kiureghian, Kee-Jeung Hong, and Jerome L. Sackman. November 1999. $20.00

PEER 1999/14 *Seismic Evaluation and Retrofit of 230-kV Porcelain Transformer Bushings.* Amir S. Gilani, Andrew S. Whittaker, Gregory L. Fenves, and Eric Fujisaki. December 1999. $26.00

PEER 1999/11 *Performance Evaluation Database for Concrete Bridge Components and Systems under Simulated Seismic Loads.* Yael D. Hose and Frieder Seible. November 1999. $20.00

PEER 1999/08 *Envelopes for Seismic Response Vectors.* Charles Menun and Armen Der Kiureghian. July 1999. $26.00

PEER 1999/07 *Documentation of Strengths and Weaknesses of Current Computer Analysis Methods for Seismic Performance of Reinforced Concrete Members.* William F. Cofer. November 1999. $15.00

PEER 1999/06 *Rocking Response and Overturning of Anchored Equipment under Seismic Excitations.* Nicos Makris and Jian Zhang. November 1999. $15.00

PEER 1999/05 *Seismic Evaluation of 550 kV Porcelain Transformer Bushings.* Amir S. Gilani, Andrew S. Whittaker, Gregory L. Fenves, and Eric Fujisaki. October 1999. $15.00

PEER 1999/04 *Adoption and Enforcement of Earthquake Risk-Reduction Measures.* Peter J. May, Raymond J. Burby, T. Jens Feeley, and Robert Wood. $15.00

PEER 1999/03 *Task 3 Characterization of Site Response General Site Categories.* Adrian Rodriguez-Marek, Jonathan D. Bray, and Norman Abrahamson. February 1999. $20.00

PEER 1999/02 *Capacity-Demand-Diagram Methods for Estimating Seismic Deformation of Inelastic Structures: SDF Systems.* Anil K. Chopra and Rakesh Goel. April 1999. $15.00

PEER 1999/01 *Interaction in Interconnected Electrical Substation Equipment Subjected to Earthquake Ground Motions.* Armen Der Kiureghian, Jerome L. Sackman, and Kee-Jeung Hong. February 1999. $20.00

PEER 1998/08 *Behavior and Failure Analysis of a Multiple-Frame Highway Bridge in the 1994 Northridge Earthquake.* Gregory L. Fenves and Michael Ellery. December 1998. $20.00

PEER 1998/07 *Empirical Evaluation of Inertial Soil-Structure Interaction Effects.* Jonathan P. Stewart, Raymond B. Seed, and Gregory L. Fenves. November 1998. $26.00

PEER 1998/06 *Effect of Damping Mechanisms on the Response of Seismic Isolated Structures.* Nicos Makris and Shih-Po Chang. November 1998. $15.00

PEER 1998/05 *Rocking Response and Overturning of Equipment under Horizontal Pulse-Type Motions.* Nicos Makris and Yiannis Roussos. October 1998. $15.00

PEER 1998/04 *Pacific Earthquake Engineering Research Invitational Workshop Proceedings, May 14–15, 1998: Defining the Links between Planning, Policy Analysis, Economics and Earthquake Engineering.* Mary Comerio and Peter Gordon. September 1998. $15.00

PEER 1998/03 *Repair/Upgrade Procedures for Welded Beam to Column Connections.* James C. Anderson and Xiaojing Duan. May 1998. $33.00

PEER 1998/02 *Seismic Evaluation of 196 kV Porcelain Transformer Bushings.* Amir S. Gilani, Juan W. Chavez, Gregory L. Fenves, and Andrew S. Whittaker. May 1998. $20.00

PEER 1998/01 Unassigned.

The Pacific Earthquake Engineering Research Center (PEER) is a consortium of western U.S. universities working in partnership with business, industry, and government to identify and reduce the risks from major earthquakes to life safety and to the economy.

PEER achieves its objectives of earthquake risk reduction through a coordinated program of research, education, and partnerships with users of research results. PEER's research program includes basic and applied components of seismology, engineering, architecture, urban planning, and economics.

PEER is headquartered at UC Berkeley.

PEER reports are available individually or by yearly subscription from the National Information Service for Earthquake Engineering (NISEE).

To order PEER Reports, contact the Pacific Earthquake Engineering Research Center, 1301 S. 46th St., Richmond, California 94804-4698, Tel: 510-231-9468, Fax: 510-231-9461.